

Investigating the Tectonic Significance of Spiral Garnets from the Betic-Rif Arc of Southern Spain and Northern Morocco Using Sm-Nd Garnet Geochronology:

Author: Thomas Farrell

Persistent link: <http://hdl.handle.net/2345/bc-ir:108592>

This work is posted on [eScholarship@BC](#),
Boston College University Libraries.

Boston College Electronic Thesis or Dissertation, 2019

Copyright is held by the author, with all rights reserved, unless otherwise noted.

INVESTIGATING THE TECTONIC
SIGNIFICANCE OF SPIRAL GARNETS
FROM THE BETIC-RIF ARC OF
SOUTHERN SPAIN AND NORTHERN
MOROCCO USING SM-ND GARNET
GEOCHRONOLOGY

Thomas P. Farrell

A thesis

submitted to the Faculty of

the department of Earth and Environmental Sciences

in partial fulfillment

of the requirements for the degree of

Master of Science

Boston College
Morrissey College of Arts and Sciences
Graduate School

August 2019

INVESTIGATING THE TECTONIC SIGNIFICANCE OF SPIRAL GARNETS FROM THE BETIC-RIF ARC OF SOUTHERN SPAIN AND NORTHERN MOROCCO USING SM-ND GARNET GEOCHRONOLOGY

Thomas P. Farrell

Advisor: Ethan F. Baxter, Ph.D.

Abstract

Spiral garnets are well-documented metamorphic microstructures that have been observed in orogens throughout the world. The preferred orientation of spiral garnet axes has been proposed (Bell and Johnson, 1989) to record and preserve information about the timing, rate, and orientation of the tectonic-scale processes. Using the model of Bell and Johnson (1989), Aerden et al. (2013) proposed a link between the preferred orientation of spiral garnets and changes in relative plate motion between Iberia and Africa. The goal of this thesis is to test this relationship by absolutely dating, eight samples from the Betic-Rif arc with measurable spiral axis orientations were chosen for Sm-Nd garnet geochronology. Chapter one is a detailed literature review of prior work on the formation and interpretation of spiral garnets. In chapter two we present 11 bulk Sm-Nd garnet ages from eight samples, these ages range from 35.6 ± 2.8 to 13.62 ± 0.69 Ma. The results from the obtained bulk garnet ages reveal a more complex relationship between FIA orientations and plate motion that originally hypothesized in Aerden et al. (2013). Large-scale rigid block rotations that

postdate garnet growth may have influenced the current orientation of FIA from the western Betic-Rif. In chapter three, zoned geochronology was conducted on a single sample from the Nevado-Filabride Complex. This study revealed spiral garnet formation occurring on a rapid timescale, just $0.45^{+0.51}_{-0.32}$ Myr. While other zoned garnet studies have shown similar rapid growth in subduction zone setting (Dragovic et al., 2012), this is the first such documentation of such rapid growth from a garnet hosting spiral inclusion trails in a regional metamorphic setting. We calculated strain rates considering different genetic models for the spiral inclusion trails either by garnet rotation in simple shear, or by episodic overgrowth of suborthogonal crenulation cleavages due to switching stress axes. In both cases a similar fast strain rate of ca. 10^{-13} s^{-1} was obtained, which is an order of magnitude faster than typical regional strain rates and faster than previous spiral garnet studies regardless of the method used to calculate strain-rate.

TABLE OF CONTENTS

Table of contents	v
List of tables	vii
List of figures	viii
Acknowledgements	xi
Introduction	1
1.0 Models of Spiral Garnet Formation	2
1.1 Introduction	2
1.2 Background	4
1.2.1 Rotational model	6
1.2.2 Non-rotational model	7
1.2.3 Contemporary research	9
1.2.4 Numerical models	12
1.2.5 Foliation Intersection Axes (FIAs).....	12
1.2.6 Techniques for Measuring FIAs	14
1.3 Tectonic Interpretations of Inclusion Trails	15
1.3.1 Geochronological Constraints on Strain-Rate.....	18
2.0 Sm-Nd Garnet Geochronology on Oriented Samples from the Betic-Rif Arc	20
2.1 Introduction	20
2.2 Geologic Setting	20
2.2.1 Alborán Domain	21
2.2.2 Alpujarride Complex.....	21
2.2.3 Nevado-Filbride Complex	22
2.2.4 Plate Reconstructions in the Betic-Rif	23
2.2.5 Previous Geochronology in the Betic-Rif	24
2.3 Existing Structural Data	25
2.3.1 Macrostructural Sequence in the Field.....	25
2.3.2 FIA Data	26
2.4 Previous Geochronology	26
2.5 Sample Description	27
2.5.1 Alpujarride-Sebtide Samples	27
2.5.2 Nevado-Filabride Samples	29
2.6 Geochronological Methods	30
2.6.1 Bulk Mineral Separation	30
2.6.2 Sample Digestion	31
2.6.3 Column Chromatography	32
2.6.4 Isotopic Analysis	33
2.7 Results	33
2.7.1 Alpujarride-Sebtide Ages.....	34

2.7.2	Nevado-Filabride Ages	37
2.7.3	Timing of Inclusion Trail Formation in the Betic-Rif.....	38
2.8	Discussion	39
2.8.1	New Sm-Nd garnet ages vs. model of Aerden et al. (2013).....	39
2.8.2	Rigid block rotations in the western Betic-Rif	42
2.9	Conclusion	44
3.0	Rapid Spiral Garnet Growth in the Nevado-Filabride Complex	45
3.1	Introduction.....	46
3.2	Geologic Setting	47
3.3	Microstructural Analysis	48
3.4	Methods	48
3.5	Zoned Geochronology	49
3.6	Discussion	50
3.6.1	Duration of Garnet Growth	50
3.6.2	Strain-rate	51
3.7	Interpretation.....	52
3.7.1	The case for non-rotation	53
3.7.2	The case for rotation.....	54
3.8	Conclusion	55
3.9	Supplementary Material for Chapter 3.....	55
4.0	Data Tables.....	61
4.1	Data tables from Chpater 2	62
4.2	Data tables from Chapter 3	71
5.0	Figures.....	74
5.1	Figures from Chapter 1	75
5.2	Figures from Chapter 2	81
5.3	Figures from Chapter 3	115
6.0	Bibliography	132
Appendix A: Standards and Nd blanks		141
Appendix B: GPS sample locations		147
Appendix C: Calculations of shear strain-rate		148
Appendix D: Nd spike reduction sheets.....		149

LIST OF TABLES

Table 2.1 Isotopic data for sample A7	62
Table 2.2 Isotopic data for sample B5	63
Table 2.3 Isotopic data for sample F8	64
Table 2.4 Isotopic data for sample F16	65
Table 2.5 Isotopic data for sample MT8	66
Table 2.6 Isotopic data for sample 27.1.2	67
Table 2.7 Isotopic data for sample 27.2.1	68
Table 2.8 Isotopic data for sample 53.10.1	69
Table 2.9 Summary of bulk garnet ages	70
Table 3.1 Summary of zoned garnet weights	71
Table 3.2 Summary of zoned garnet ages	72
Table 3.3 All isotopic data for zoned garnets from sample 27.1.2	73
Table A.1 Summary of Nd blanks	142
Table A.2 Summary of Ames NdO Standards	144
Table A.3 Summary of Ames Sm Standards	146
Table B.1 GPS sample locations	147

LIST OF FIGURES

Figure 1.1.1	75
Figure 1.2.1	76
Figure 1.2.2	77
Figure 1.2.3	78
Figure 1.2.4	79
Figure 1.3.1	80
Figure 2.2.1	81
Figure 2.2.2	82
Figure 2.2.3	83
Figure 2.3.1	84
Figure 2.3.2	85
Figure 2.5.1	86
Figure 2.5.2	87
Figure 2.5.3	88
Figure 2.5.4	89
Figure 2.5.5	90
Figure 2.5.6	91
Figure 2.5.7	92
Figure 2.7.1	93
Figure 2.7.2	94
Figure 2.7.3	95

Figure 2.7.4	96
Figure 2.7.5	97
Figure 2.7.6	98
Figure 2.7.7	99
Figure 2.7.8	100
Figure 2.7.9	101
Figure 2.7.10	102
Figure 2.7.11	103
Figure 2.7.12	104
Figure 2.7.13	105
Figure 2.7.14	106
Figure 2.7.15	107
Figure 2.7.16	108
Figure 2.7.17	109
Figure 2.7.18	110
Figure 2.8.1	111
Figure 2.8.2	112
Figure 2.8.3	113
Figure 2.8.4	114
Figure 3.2.1	115
Figure 3.3.1	116
Figure 3.3.2	117
Figure 3.4.1	118

Figure 3.5.1	119
Figure 3.6.1	120
Figure 3.6.2	121
Figure 3.9.1	122
Figure 3.9.2	123
Figure 3.9.3	124
Figure 3.9.4	125
Figure 3.9.5	126
Figure 3.9.6	127
Figure 3.9.7	128
Figure 3.9.8	129
Figure 3.9.9	130
Figure 3.9.10	131
Figure A.1	143
Figure A.2	145

ACKNOWLEDGEMENTS

I would like to thank my committee members, Noah Snyder and Seth Kruckenberg, and my lab mates, Paul Starr, Katie Maneiro, Steph Walker, and Anna Gerrits. A special thanks to my collaborator, Domingo Aerden for all of his knowledge and support during my research, and through our collaboration has become more like a friend. I would like to thank Alex Ronan for his help in picking garnets, while providing some comic relief in the clean lab. I would like to thank my advisor Ethan Baxter for all of his support and guidance. Special thanks to my parents for quiet listening to me as I describe Sm-Nd garnet geochronology, and to Sam Dow for proof reading and editing this thesis. Finally, I would like to thank Mike Tappa for all of his mentorship in and out of the clean lab, and without whose help I would still most likely be calibrating my first bottle of MLA. This thesis was funded in part by the Morrissey College Graduate School.

INTRODUCTION

This thesis is divided into three chapters. Chapter one details the key hypotheses and questions that motivated this study, as well as a detailed literature review of some of the seminal work on the processes and mechanisms of spiral garnet formation. This includes a summary of the key concepts and assumptions behind both the rotational and non-rotational models, as well as the interpretations that can be made assuming a certain model. Chapter two details bulk Sm-Nd garnet ages from eight samples from around the Betic-Rif arc conducted by the author of this thesis. The main body of chapter two focuses on the geochronological methods used and bulk Sm-Nd garnet ages obtained during this study. The discussion portion of chapter two focuses on comparing the obtained bulk Sm-Nd garnet ages to the ages in the model proposed by Aerden et al. (2013). The fundamental ideas behind the model of Aerden et al. (2013) are detailed in chapter one. Chapter three is a draft of a manuscript for publication that is focused on zoned Sm-Nd garnet geochronology conducted on a single sample from the Nevado-Filabride Complex of the Betic Cordillera. The goal of this zoned chronology is to investigate the rate of spiral garnet formation and how this relates to either the rotational or non-rotations models of formation.

CHAPTER 1

MODELS OF SPIRAL INCLUSION TRAIL FORMATION

1.1 INTRODUCTION

Spiral inclusion trails within rigid porphyroblasts are well-documented metamorphic microstructures that have been observed in many orogens throughout the world (e.g. Rosenfeld, 1968; Hayward, 1990; Sayab, 2005; Bell and Sapkota, 2012; Sayab *et al.*, 2016; Aerden, 1994; Robyr *et al.*, 2008; Aerden *et al.*, 2013). These unique metamorphic microstructures are tools with which interpretations of past phases of metamorphism and deformation can be made. Unlike other metamorphic microstructures and indicators of shear-sense such as mica fish, S-C fabrics, and asymmetric folds that form in the surrounding matrix, inclusion trails form within rigid porphyroblasts and are protected by the rigid nature of the porphyroblast from subsequent overprinting or modification. Therefore, the study of spiral inclusion trail orientations offers a unique opportunity to interpret a more complete tectonic evolution for a given region. In 1968 John Rosenfeld wrote the seminal paper on the mechanics of spiral inclusion trail formation; in the half century since, a massive body of research has emerged greatly advancing our understanding of these microstructural features and what interpretations can be made about past phases of deformation (Passchier and Trouw, 2005). These inclusions often form patterns known as “inclusion trails,” which regularly form sigmoidal to spiral geometries, and commonly have orientations at high angles to that of the surrounding

matrix and in many cases are completely orthogonal (Johnson, 1993) (Figure 1.1.1). These contrasting orientations suggest the porphyroblast grew syn-kinematic with more than one phase of deformation (Passchier and Trouw, 2005).

Currently, two mutually exclusive hypotheses attempt to explain the formation of spiral inclusion trails and their relationship to the surrounding matrix. One hypothesis states that inclusion trails form within a rotating porphyroblast in a ductile deforming matrix as the result of progressive simple shear induced rotation (Rosenfeld, 1968). Assuming the rotational model, the inclusion trail orientation would be controlled by the orientation of localized shear zones. The second hypothesis states that the porphyroblast does not rotate. Inclusion trails in this model form from porphyroblastic overgrowths of episodic overprinting of suborthogonal crenulation cleavages that form from compression-collapse cycles during orogenesis (Bell, 1985; Bell and Johnson, 1989). Any apparent rotation is a consequence of the intersection between the inclusion trails and the matrix foliation. Where two or more inclusion trails meet within a porphyroblast, a feature known as a foliation intersection axis (FIA) is formed (Bell and Johnson, 1989; Hayward, 1990; Bell *et al.*, 1995). Assuming the stationary model, inclusion trail orientations can be directly linked to regional scale tectonic processes. Over the past several decades, numerous studies using the stationary model of Bell and Johnson (1989) (e.g. Bell and Kim, 2004; Bell and Sapkota, 2012; Aerden *et al.*, 2013; Sayab *et al.*, 2016) have proposed a link between the preferred orientation of inclusion trails within a population of garnet porphyroblasts and the orientation of relative plate motion.

In order to understand to what extent the preferred orientation of inclusion trails can be used to reconstruct terrane-wide tectonic processes we first must understand how

regionally-variable inclusion trail orientations relate to one another both spatially and temporally. It is from this that I propose to use bulk and zoned Sm-Nd garnet geochronology on microstructurally-characterized samples from the Betic Cordillera in southern Spain and the Rif Cordillera in northern Morocco. Through the combination of microstructural and geochronologic data sets we aim to test the following hypotheses.

***Hypothesis 1:** The preferred orientation of micro-scale foliation intersection axes (FIA) preserved within a representative population of porphyroblasts is temporally consistent within a given cohesive tectonic block.*

***Hypothesis 2:** Changes in the preferred orientation of FIA within garnet porphyroblasts from the Betic-Rif are recording and preserving changes in the plate motion of Africa relative to Iberia.*

The Betic-Rif Arc provides an excellent location to address the above mentioned hypotheses relating to correlation between FIA orientations and regional-scale tectonic processes. The Betic-Rif orogen has been the site of extensive microstructural research that has found evidence for five distinct FIA orientations compiled from thousands of measurements (Aerden and Sayab, 2008; Aerden *et al.*, 2013; Ruiz-Fuentes and Aerden, 2018), and multiple, complementary macrostructural reconstructions of plate motion (Rosenbaum *et al.*, 2002; Handy *et al.*, 2010; Macchiavelli *et al.*, 2017).

1.2 BACKGROUND

Garnet, being a common rock-forming mineral within metapelitic rocks, can often record valuable information about temperature, pressure, and deformational conditions

present during growth. The growth of garnet is principally controlled by the process of diffusion, either via solid-state, or through the movement of chemically active fluids along grain boundaries. Other mineral phases adjacent to the porphyroblast-matrix interface not participating in growth must be removed by means of dissolution or diffusion. During high-grade metamorphism, rates of diffusion and dissolution can often be high enough to necessitate complete removal of non-participating phases; however, during low-to-medium-grade metamorphism these rates are commonly inefficient in completely removing non-participating phases. Any non-participating phases will become enclosed by porphyroblastic overgrowth as passive inclusions in equilibrium with the porphyroblast at the time of overgrowth. The mechanisms controlling porphyroblastic growth are up for some debate, but this is beyond the scope of this thesis and the reader is referred to references herein (Gaidies *et al.*, 2011; Pattison *et al.*, 2011; Carlson, 2011).

If garnet growth and deformation are synchronous, these inclusions may form features known as “inclusion trails,” which regularly exhibit orientations that differ from the surrounding matrix. These contrasting foliation orientations suggest the porphyroblast grew syn-kinematic with one or more deformational event. The geometries of inclusion trails can reflect the structure of the matrix during porphyroblastic growth (Passchier and Trouw, 2005). Spiral inclusion trails have been observed for over a century; Peach *et al.* (1912) and Schmidt (1918) were among the first to document them. However, due to the lack of adequate methods and instrumentation, it was not until the late 1960s and 1970s that significant and comprehensive research was conducted to elucidate the mechanisms of inclusion trail formation. Spry (1963), Rosenfeld (1968), and Schoneveld (1979) did much of the early pioneering work on the mechanics of spiral inclusion trail formation. Their

investigations concluded that spiral inclusion trails form in porphyroblasts that have rotated in response to progressive simple shear (non-coaxial) deformation. This interpretation has become known as the “rotational model” of spiral inclusion trail formation.

A radically different interpretation of inclusion trail formation came to the forefront in the mid-to late 1980s. Bell (1985) and Bell and Johnson (1989) were the first to publish on the hypothesis that porphyroblasts do not rotate, but are stationary, and the matrix rotates around the porphyroblast in response to changes in the distribution and orientation of stress. Although Bell (1985) was the first to publish specifically on what has become known as the “non-rotational” model, the idea of stationary porphyroblasts was first alluded to by Ramsey (1962). For several decades both models have been invoked to interpret the formation of spiral inclusion trails. Each of the inclusion trail geometries described earlier can be explained by slight modifications to either model (Johnson, 1993). The following section will attempt to summarize the evidence presented to date that supports or refutes each model.

1.2.1 Rotational model

The classical theory of fluid dynamics states: “a rigid spheroidal object suspended in a homogeneously deforming medium is expected, under a specific set of conditions to rotate with respect to a fixed point” (Jeffery, 1922). In the rotational models proposed by Rosenfeld (1968, 1970) and Schoneveld (1977, 1979), only one foliation is present and no bulk shortening perpendicular to the foliation occurs. The deformation is simple progressive, non-coaxial shearing strain parallel to the foliation. Shearing of material around the porphyroblasts initiates rotation with respect to a geographically fixed reference point; as the porphyroblast continues to grow it overgrows the foliation, preserving the

inclusion trails (Rosenfeld, 1968; Schoneveld, 1979; Johnson, 1993). This situation is idealized and over simplified, with several inherent assumptions related to garnet growth: (1) porphyroblasts are equidimensional and spherical in shape; (2) a continuous growth rate with a linear increase in radius; (3) constant rotation during deformation; and (4) homogeneously distributed deformation throughout the system. Schoneveld (1979) admits these assumptions for the sake of simplicity, but argues parameters more representative of the real world would not seriously affect the model's validity (Johnson, 1993).

Rosenfeld (1968) was the first to employ the rotational model for determining magnitude, direction, and sequence of deformation in southeast Vermont. The hypothesis proposed by Thompson (1950) suggested porphyroblast rotation was caused by drag-folding during deformation; however, porphyroblasts showed two distinct stages of rotation: an inner, earlier counterclockwise rotation and an outer, later clockwise rotation. Thus rotation due to drag-folding was not a complete hypothesis. From this finding, Rosenfeld (1968) determined that a single porphyroblast could be rotated about more than one axis, and therefore could record evidence of more than one deformational event. The determination of the amount of rotation on each axis can infer qualitative information about the relative rates and duration of each deformational event. Rosenfeld (1968) novel approach to measuring multiple rotational axes in a single 'rotated' garnet porphyroblast would lay the groundwork for future work to progress the use of inclusion trail orientation to elucidate the tectonic processes responsible for their formation.

1.2.2 Non-rotational model

The fundamental principle of the non-rotational model states that inclusion trails are formed from sequential near-orthogonal foliation and crenulation cleavage overprinting

caused by episodic changes from progressive shortening to gravitational collapse during orogenesis (Figure 1.2.1) (Bell, 1985; Bell and Johnson, 1989; Johnson, 1993). This successive orthogonal overprinting will cause the apparent rotation to cluster in multiples of 90° (Johnson, 1993). There are however, as with the rotation model, several inherent assumptions: (1) continuous porphyroblastic growth during prograde metamorphism; (2) deformation partitioning is efficient enough to inhibit rotation; and (3) the deformation experienced by the porphyroblast is not progressive, homogeneous, simple shear. However, unlike the rotation model there are no assumptions needed for porphyroblast shape or growth rate (Johnson, 1993).

In order to fully understand the non-rotational model, an understanding of deformation partitioning and its effect on the development of crenulated cleavage is paramount. Deformation partitioning (Figure 1.2.2) is dependent on primary or secondary heterogeneities present in the rock. It can occur on a variety of length-scales from thin section, to outcrop, to entire terranes (Bell, 1985). As a result of these heterogeneities, different minerals, rock-types, and individual beds can experience four different types of strain during stages of deformation: (1) no strain; (2) progressive shortening strain (i.e. coaxial deformation); (3) progressive shortening plus shearing strain; and (4) progressive shearing strain (types 3 and 4 are examples of non-coaxial deformation) (Bell, 1981; Bell, 1985; Bell and Bruce, 2007). According to Bell (1985) when observing larger length-scale features, both 3 and 4 can essentially be considered coaxial in nature.

In addition to controlling the distribution of strain, deformation partitioning can also control the growth and distribution of porphyroblasts within the matrix. Porphyroblasts can only nucleate and grow in zones of low strain (type 1) (Figure 1.2.2b).

As demonstrated in Figure 1.2.2c, the non-coaxial (types 3 and 4) component of deformation is partitioned around the porphyroblast, which thus protects an ellipsoidal zone of matrix from the effect of progressive, non-coaxial shearing (Bell, 1985). Furthermore, once porphyroblastic growth has occurred, the relatively large grain-size compared to the surrounding matrix allows porphyroblasts to control the localized partitioning of the deformation and strain. Consequently, as a result of deformation partitioning, the non-rotational model states that porphyroblasts do not rotate during deformation. The intense shearing (non-coaxial) component of deformation is partitioned around the porphyroblast causing them to become isolated from the shearing component (type 1), which is accommodated in the surrounding matrix (type 3 and 4) (Bell, 1985; Aerden, 2008; Fay *et al.*, 2009). Therefore, whether or not porphyroblasts experience rotation is a direct function of the deformation partitioning.

1.2.3 Contemporary Research

Jiang and Williams (2004) present three arguments against the non-rotational model of Bell (1985) and Bell and Johnson (1989). Their arguments are based on geometry, reference frame, and the law of angular momentum. Three-dimensional inclusion trails geometries, they contend, are too geometrically complex to be used to reconstruct past deformational histories. Secondly, the required deformational path to produce the 3-D geometries present in porphyroblasts via non-rotation with respect to the earth are highly unlikely (Jiang and Williams, 2004). Thirdly, to state that rigid porphyroblasts in a ductile deforming medium generally do not rotate with respect to the earth violates the fundamental law of balance of angular momentum. If an external foliation is rotating, then the porphyroblast must be subject to a torque force from the surrounding matrix, and

therefore the porphyroblast rotates to eliminate the force. According to Jiang and Williams (2004), in order for porphyroblast non-rotation to occur, some other force must be counteracting the external torque applied by the deforming matrix. They see no such source for this force in nature, and therefore find the concept of porphyroblast non-rotation to be unfounded based on the laws of physics (Jiang and Williams, 2004).

Aerden (2005) refutes the interpretation proposed by Jiang and Williams (2004) and their conclusion that non-rotation is invalid. Modelling ductile deformation in metamorphic rocks based on fluid dynamics or continuum mechanics greatly simplifies rock to a homogeneous isotropic material, which is a gross oversimplification (Aerden, 2005). Rocks are heterogeneous anisotropic materials composed of minerals and rock-types of differing mechanical properties, these intense heterogeneities can lead to strong partitioning of strain with major consequences on the vorticity induced rotation model described in Jiang and Williams (2004) (Bell, 1985; Aerden, 2005). The matrix induce torque force cited by Jiang and Williams (2004) can be neutralized by the strain shadow created during deformation partitioning. The torque force is sufficiently small enough to be resisted by a reaction torque exerted by the quartz-rich strain shadow (Aerden, 2005).

In a paper by Trouw *et al.* (2008), the authors contradict the conclusion stated earlier that apparent rotation of porphyroblasts clustering about 90, 180, and 270 degrees is best explained by the non-rotation model (Bell, 1985; Bell and Johnson, 1989; Johnson, 1993a). Although it is assumed that most garnet porphyroblasts are spherical, many observed garnet porphyroblasts have an elongate shape. This elongate shape is thought to result from garnet's tendency to grow into the mica-rich strain caps orthogonal to the foliation rather than the quartz-rich strain shadow parallel to the foliation (Trouw *et al.*,

2008; Passchier and Trouw, 2005). While spherical objects would rotate at a consistent rate, producing no clustering about any degree of rotation, an elongate object would have a variable rotation rate which would cluster about multiples of 90 degrees.

In a study of rotated porphyroblasts from Lukmanier Pass in the Swiss Alps, Robyr *et al.* (2009) analyzed two populations of garnet porphyroblasts containing spiral inclusion trails, one population from the fold hinge and the other population from the fold limb. Robyr *et al.* (2009) employed a novel approach to the problem of distinguishing between rotation and non-rotation, by combining microstructural, geochemical, and crystallographic-orientation analysis. Their results showed garnets from the fold hinge exhibited an apparent rotation of 360 degrees, whereas the garnets from the fold limb only had an apparent rotation of 270 degrees. Therefore, the amount of apparent rotation could be a function of the location of the porphyroblast within the fold structure (Robyr *et al.*, 2009). The porphyroblasts from the fold hinge showed a discernable change in inclusion trail geometry from smoothly-curved in the core, to crenulated in the outer spiral arms, at an apparent rotation of 270 degrees, suggesting a sudden change in deformation conditions. As shown earlier, a smoothly-curving geometry is best explained by non-coaxial flow, while a crenulated geometry is strongly suggestive of coaxial flow. The discontinuity in inclusion trail geometry is also accompanied by changes in compositional zoning and crystallographic-orientation.

Their data suggests that the end-member models proposed by Rosenfeld (1968) and Bell (1985) can operate in succession during porphyroblast growth. The first 270 degrees of apparent rotation is best explained by rotation, whereas the last 90 degrees of apparent rotation is more consistent with non-rotation (Robyr *et al.*, 2009). The results of this study

strongly suggest that perhaps no single pure end-member model is present in nature, and most likely a combination of rotation and non-rotation is the norm.

1.2.4 Numerical Models

Numerous theoretical, analog, and numerical models have been developed to determine whether or not porphyroblasts rotate during deformation (e.g. Jeffery, 1922; Jiang and Williams, 2004; Griera et al, 2013; Fay *et al.*, 2008; Bons *et al.*, 2009). The majority of these studies have determined that rigid porphyroblasts in a ductile deforming matrix are likely to rotate, conflicting with the non-rotation model of Bell (1985). However, several numerical modelling studies have shown evidence for non-rotation during deformation. The model of Fay *et al.* (2008) demonstrates that if an anastomosing strain field is present, then porphyroblasts not likely to rotate. This anastomosing geometry causes the matrix to deform around the porphyroblasts, significantly reducing the vorticity induced by the deformation around them, and can be thought of as processes of deformation partitioning (Fay *et al.*, 2008, 2009). It must be noted that models predicting the behavior of rigid porphyroblasts in an anisotropic matrix need further development to fully address the debate. Improvements in analytical techniques have increased the availability of 2D and 3D models. Additionally, current advances in SEM, EBSD, and XRT have made these techniques useful in determining the dynamics of porphyroblasts growth during deformation (Robyr *et al.*, 2009; Huddle-Holmes and Ketcham, 2010; Griera *et al.*, 2013).

1.2.5 Foliation Intersection Axes (FIAs)

In the simplest terms, a foliation intersection axis (FIA) is the intersection of near orthogonal foliations preserved within a porphyroblast (Bell and Sapkota, 2012); however,

FIA can also be thought of as an axis of relative matrix-porphyroblast rotation (Aerden, 2003). Sigmoidal and spiral inclusion trails are considered to have axes that define the axis of porphyroblast rotation as it grew over an actively developing foliation; however, the orientation of such axes were rarely measured, with the notable exception of Rosenfeld (1968) in the Chester Dome area of southeast Vermont (Bell *et al.*, 1998). The effect of younger deformational events rotating previously-formed rotational axes could have a large effect on the validity of the interpretation. The effect of younger apparent rotations of the porphyroblast would have to be removed before the earlier rotation axis orientation could be studied (Rosenfeld, 1968; Bell *et al.*, 1998). The advantage of FIA as compared to apparent rotational axes is their ability to preserve foliations without alteration from subsequent deformation.

If the non-rotational model of inclusion trail formation is correct, then FIA orientations in garnet porphyroblasts can be records of complex tectonic history. The porphyroblasts are therefore recording and protecting the orientations of the intersection of overprinting foliations from destruction by subsequent deformation (See figure 1.2.3). Foliation intersection axes either relate to bulk shearing (assuming the rotational model), or bulk shortening (assuming the non-rotational model), therefore, in both models they are important kinematic indicators (Bell *et al.*, 1995; Aerden *et al.*, 2013). These microstructures may be related to bulk motion on the scale of orogenesis, or even entire tectonic plates. The rotational model suggests changes in FIA orientation are the result of heterogeneities in the distribution of deformation (small-length scale), whereas the non-rotational model suggest that changes in FIA orientation are the result of much longer

length-scale tectonic processes (Bell *et al.*, 1998; Bell, 1985; Bell and Johnson, 1989; Rosenfeld, 1968).

1.2.6 Techniques for Measuring FIA Orientations

There are currently two techniques for measuring and determining the strike, trend and plunge of foliation intersection axes: (1) the asymmetry technique, devised by Hayward (1990) and (2) the FitPitch technique developed by Aerden (2003), both of which are often with one another in the same study (e.g. Aerden *et al.*, 2013; Sayab *et al.*, 2016).

Asymmetry Technique of Hayward (1990), refined by Bell *et al.* (1995), applies the geometric principle that the observed cross-sectional asymmetry of folds, crenulations, or inclusion trails switches in thin sections as the axis is crossed (Figure 1.2.4). This change in asymmetry allows FIA orientations to be determined from radial sets of vertical and horizontal thin sections. FIA trends are constrained between the strikes of two adjacent thin sections that mark the switch in curvature asymmetry. The plunge of the FIA can be constrained similarly by cutting thin section radially about a horizontal axis oriented orthogonal the FIA trend. Where the asymmetry flips between adjacent thin sections, a FIA must pass between them. However, uncertainty in FIA orientation is on the order of $\pm 20^\circ$ (Aerden, 2003; Aerden *et al.*, 2013).

FitPitch Program, an improvement on the asymmetry technique of Hayward (1990) and Bell *et al.* (1995), was developed by Aerden (2003). It is a statistical best fit computer model to determine the preferred orientation of planar microstructures within porphyroblasts. This allows for a more quantitative characterization of the spatially

preferred orientation of inclusion trails which can have unimodal, bimodal, or trimodal preferred orientation patterns.

Fitpitch, written in FORTRAN programming language, fits inclusion trails orientations gathered from differently oriented thin sections to one, two or three planes. Inclusion trails are treated as intersection lines of one or more foliation planes. The data is then compared to a large number of uniformly spaced model (i.e. theoretical) planes; a best fit model plane or a best combination of two or three model planes can be identified by reducing the deviation between the natural data (i.e. inclusion trails) and the modeled (i.e. theoretical) data. The difficulty in this method is the vast number of combinations that can be formed with only a limited number of known variables. To circumvent this problem, a three-step strategy is implemented: (STEP-1) reduce the number of model planes; (STEP-2) refine the solution from step 1 through iteration; and (STEP-3) evaluate the results (Aerden, 2003). The advantage of this method over more qualitative methods (i.e. asymmetry) of fitting data are that subjective correlation of multimodal orientation maxima between different thin section planes is eliminated, and that the solutions are based on every single datum rather than on selected modal maxima. The degree of fit (i.e. uncertainty) is quantified in terms of the deviation between the natural and model intersection lines (Aerden, 2003). The results from FIA analysis are often displayed in the form of stereonet or rose diagrams. The advantage of the rose diagrams, is the ability to see in one diagram the evolution of several FIA generations.

1.3 TECTONIC INTERPRETATIONS OF INCLUSION TRAILS

The model used to reconstruct orogenesis from inclusion trail geometries shown in Figure 1.3.1 was proposed by Bell and Johnson (1989), and further revised by Aerden and

Malavieille (1999). The model is centered on the hypothesis of cyclic sub-vertical and sub-horizontal foliation development resulting from changes in the state of stress, from compressional to extensional. At mid-to upper crustal pressures sub-vertical foliations develop as a result of crustal shortening (compression), initiating a thickening of the continental crust (Figure 1.3.1), a sub-horizontal foliation then forms by gravitational collapse caused by the over-thickening of the orogen (extension; figure 1.3.1). Because of a “space” problem, an asymmetry develops in the orogen between the upper crust and the lower crust (red line in figure, 1.3.1). Extension does not extend below the average depth of the upper crust (Bell and Johnson, 1989), creating a basal detachment (red line in figure 1.3.1). This detachment allows gravitational collapse to continue in the upper portion of the orogen, while compression continues in the lower portion. Once the orogen has become gravitationally stable again, horizontal compression continues above the basal detachment, deforming the basal detachment and the rocks above. This shortening-collapsing cycle can repeat several times during orogenesis (Johnson and Bell, 1989; Bell and Sapkota, 2012).

According to Bell and Johnson (1989) porphyroblasts growing during this deformation will record these changes in foliation orientation as foliation intersection axes. The FIA orientations, in combination with macroscale fold orientations, can be used to track the location of material in a mountain belt during orogenesis. This data, in combination with P-T-t path determination from compositional zoning of porphyroblasts can allow a more refined understanding of the relationship between deformation and metamorphism during orogenesis (Welch, 2003; Kim and Bell, 2005; Aerden *et al.*, 2013; Sayab *et al.*, 2016).

Recent work has modified and improved upon the reconstruction model of Bell and Johnson (1989) and Aerden and Malavieille (1999) and has been applied to many orogens throughout the world (Aerden, 2004; Bell and Newman, 2006; Aerden et al., 2013; Sayab et al., 2016). The reconstruction of tectonic events requires careful observations and analysis of multiple inclusion trail geometries preserved within porphyroblasts from deformed and metamorphosed terranes. As described in previous sections, foliation intersection axes are intersections of near orthogonal foliations preserved within porphyroblasts, and are theorized to form in preferred orientations, thereby preserving a deformational history (Bell and Johnson, 1989; Aerden, 1995; Bell and Sapkota, 2012). Multiple FIA trend generations in metamorphic terranes, having a geographically consistent preferred orientation have been observed and used to reconstruct past tectonic histories (e.g. Aerden *et al.*, 2013; Aerden and Sayab, 2008; Shah *et al.*, 2011; Sayab *et al.*, 2016; Sayab, 2005; Bell *et al.*, 1998; Aerden, 1995; Bell and Sapkota, 2012). Bell and Kim (2004) and Kim and Bell (2005) detected garnet porphyroblasts with distinct FIA trends associated with the Acadian Orogeny, despite the presence of strong Alleghenian metamorphic and deformational overprinting. Similar studies have found evidence for porphyroblasts recording FIAs from multiple orogenies (Cihan *et al.*, 2006; Sayab, 2008, 2009). Consequently, FIA trends can not only be records of single orogenic event, but also record the tectonic evolution of a terrane over multiple orogenic events.

A novel hypothesis of preferred FIA orientations is that they are records of past plate movement (Shah *et al.*, 2011; Bell and Sapkota, 2012; Aerden *et al.*, 2013; Sayab *et al.*, 2016) Recent work as shown a strong correlation between FIA orientation and the known orientations of plate motion from paleomagnetic data (Bell and Sapkota, 2012;

Aerden *et al.*, 2013; Sayab *et al.*, 2016). FIA lie parallel to the intersection between alternating sub-vertical and sub-horizontal dipping foliations; their trend is close to, and controlled by the strike of the sub-vertical foliation (Bell and Sapkota, 2012). FIA trend, being controlled by the orientation of the vertical foliation suggests that changes in FIA trend are independent of geographic location within the orogen and are only dependent on changes in bulk shortening, responsible for the development of vertical foliations. Therefore, FIA should form perpendicular to the direction of maximum compressional stress (i.e. plate motion) (Bell *et al.*, 1995; Bell and Sapkota, 2012; Sayab *et al.*, 2016).

1.3.1 Geochronological Constraints on Strain Rate

Garnet, having the ability to both record and preserve deformational fabrics in the form spiral inclusion trails, while also being a robust geochronometer using several isotopes systems has made garnet a target mineral for assessing and calculating regional metamorphic strain and strain-rates. Previous studies have used spiral inclusion trails within garnet to calculate strain-rates in deformed metamorphic terranes (Biermeier and Stüwe, 2003; Baxter and DePaolo, 2004; Berg *et al.*, 2013). Christensen *et al.* (1989, 1994) and Vance and O’Nions (1992) combined their calculations of shear-strain with zoned garnet chronology to obtain regional metamorphic strain-rates. Christensen *et al.* (1989, 1994) analyzed garnet porphyroblasts from the core to rim using Rb-Sr geochronology to quantify a growth rate. This growth rate was combined with data from spiral inclusion trails (assuming the rotational model) to determine a regional metamorphic strain rates of $2.4^{+1.6}_{-0.7} \times 10^{-14}$ and $2.7^{+1.2}_{-0.7} \times 10^{-14}$, second^{-1} respectively. Vance and O’Nions (1992) conducted a similar study using garnet geochronology to quantify rates of prograde metamorphism and deformation, calculating a regional metamorphic strain rate of

$1.9_{-0.9}^{+0.9} \times 10^{-14}$ second⁻¹. Muller *et al.* (2000) employed a novel technique of using Rb-Sr dating to quantify a strain rates of 1.1×10^{-15} to 7.7×10^{-15} second⁻¹ from syntectonic fibrous strain fringes around pyrite porphyroblasts. More Recent work by Berg et al. (2013) calculated strain-rates from spiral garnets assuming both the rotational model of Rosenfeld (1968) and the non-rotational model of Bell (1985). In both cases, they found that the strain-rates were in near agreement.

CHAPTER 2

BULK SM-ND GARNET GEOCHRONOLOGY ON GEOGRAPHICALLY-ORIENTED SAMPLES FROM THE NEVADO-FILABRIDE AND THE ALPUJÁRRIDE-SEBTIDE COMPLEXES IN THE BETIC-RIF ARC

2.1 INTRODUCTION

This chapter details bulk Sm-Nd garnet ages from the Betic-Rif arc that will be a part of a publication in preparation by our collaborator Domingo Aerden at the University of Granada. The main body of this chapter describes in detail the geochronological methods used and bulk Sm-Nd garnet ages obtained during this study. The discussion portion of this chapter is largely focused on comparing the obtained garnet ages to the model as originally proposed in Aerden et al. (2013). The fundamental ideas behind the model proposed by Aerden et al. (2013) are described in the introduction section of this thesis. All of the bulk garnet geochronology outlined in this thesis was conducted by the author (Thomas Farrell), and all of the FIA and microstructural analysis was conducted by Domingo Aerden.

2.2 GEOLOGIC AND TECTONIC SETTING

The Betic-Rif Arc is an oroclinal fold and thrust belt orogen encompassing the Betic Cordillera in southern Spain and the Rif Cordillera in northern Morocco and represents westernmost extent of the Alpine orogenic system (Figure 2.2.1) (Monie *et al.*, 1991). It is comprised of a foreland of strongly shortened and unmetamorphosed Mesozoic to Tertiary

passive margin sediments known as the “External Zones,” and a hinterland of metamorphic complexes comprised of thrust nappe sequences of Paleozoic basement and Mesozoic sediments known as the “Internal Zones,” or “Alborán Domain.” The complexity of the Betic-Rif orogenic system has resulted in many remaining unanswered questions about its origin and evolution; however, most models agree that the Betic-Rif Arc formed during the closure of the western Tethys Ocean basin resulting from the early Tertiary convergence of Africa, Iberia, and several micro-plates. While strong convergence continued in the External Zones, the Alborán Domain has experienced intense inter-orogenic extension and high pressure-low temperature metamorphism during the Miocene which ultimately led to the opening of the western Mediterranean basins (Platt et al., 2013).

2.2.1 Alborán Domain

The “Internal Zones” or “Alborán Domain” has traditionally been divided into three major complexes based upon lithology and metamorphic grade. From top to bottom, they are the Maláguide, Alpujárride, and the Nevado-Filabride. The Maláguide is the least metamorphosed complex, with some areas preserving Variscan-aged deformational textures (Aerden *et al.*, 2013; Kirchner *et al.*, 2016). The metamorphic grade increase dramatically in the lower two complexes. It is from these two lower complexes that the samples for this study were collected. Figure 2.2.2 is a geologic map of the Alborán Domain and shows the geographic extent of the three metamorphic complexes.

2.2.2. Alpujárride Complex (AC)

The Alpujárride Complex, known as the Sebide Complex in the Rif Cordillera, volumetrically represents the bulk of the Alborán Domain (Soto and Platt, 1999; Comas *et*

*al.*1999). The history of this complex is crucial to understanding the evolution of the Alborán Domain (hinterland) and its interaction with the External Zones (foreland). In the Alpujarride, early compressional deformation was accompanied by HP-LT metamorphism which produced assemblages of garnet, staurolite and kyanite. This HP-LT metamorphism was then followed by lower pressure and localized higher temperature metamorphism that resulted from extensional tectonics in the region, which produced assemblages of andalusite and sillimanite (Gracia-Casco *et al.*, 1996; Platt *et al.*, 2013). Deformation in this complex is characterized by intense ductile deformation that completely penetrates the entire complex with multiple generations of tight to isoclinal folding and associated crenulation cleavage development (Vissars, 2012; Aerden *et al.*, 2013; Platt *et al.*, 2013).

2.2.3. Nevado-Filabride Complex (NFC)

The Nevado-Filabride Complex (NFC) represents structurally lowest and most metamorphosed complex in the Alborán Domain. It is only exposed in the central and eastern portions of the Betic Cordillera; no outcroppings of the NFC have been found the Rif Cordillera. Although the NFC is the lowest unit structurally in the Betic-Rif, it outcrops at the highest elevations in the entire region (3746 m; Figure 2.2.3), where it forms two broadly east-west trending anticlinorium mountain ranges known as the Sierra Nevadas and the Sierra Los Filabrides. Similar to the Alpujarride, the NFC exhibits evidence for a long and complex metamorphic and deformational history.

The Nevado-Filabride is divided in several subunits, there is some debate as to the number of subunits and the location of the contacts (Ruiz-Fuentes and Aerden, 2018). Traditionally, the NFC has been divided into the lower Veleta Complex (VC) and the upper Mulhacén Complex (MC), the latter of which is subdivided again into the lower Caldera

unit, the upper Sabinas unit, and the middle Ophiolite unit. The VC is composed of graphitic-schists several kilometers thick and outcrops as a tectonic window through the overlying complex. The MC is composed of thrust nappe sequences comprised of a Paleozoic basement and Mesozoic sedimentary cover, between these, a Mesozoic ophiolite nappe is tectonically intercalated (Puga *et al.*, 2002). Martinez *et al.* (2002) mapped new tectonic boundaries and renamed the units as the Ragua unit (lower part of Veleta), Calar-Alto unit (upper part of Veleta and lower part of Mulhacén), and the Bedar-Macael unit (upper Mulhacén). Ruiz-Fuentes and Aerden (2018) in their recent mapping found no evidence for the new contacts described by Martinez *et al.* (2002). For this study, I will use the traditional subdivision nomenclature of the Veleta and Mulhacén Complexes by Puga *et al.* (2002).

2.2.4 Plate Reconstructions in the Betic-Rif

Paleomagnetism has been used in the region to constrain the relative movements of the Iberian, Eurasian, and African plates, as well as several associated microplates, the Adrian, Alcapian, and Alkapecian (Roest and Srivastava, 1991; Rosenbaum *et al.*, 2002; Handy *et al.*, 2010; Macchiavelli *et al.*, 2017). Beginning in the Early to Mid-Cretaceous (120–80 Ma) seafloor spreading began in the Bay of Biscay, which drastically changed the kinematics between Iberia and Eurasia. The plate boundary which had predominantly been strike-slip during the Jurassic began to become transpressional, and became completely convergent by the beginning of the Cenozoic (~65 Ma), resulting in the formation of the Pyrenees Mountains. Starting in the Paleogene, convergence began between Africa and Iberia, the Betic-Rif Arc straddles this convergent zone. From the early Eocene to present, the region has accommodated anywhere from 140 to 500 km of northward movement of

Africa relative to Iberia (Vissars and Meijer, 2012; Behr and Platt, 2013). It has proven difficult to delineate a distinct plate boundary between Iberia and Africa, instead the present-day seismicity is scattered over the whole region (Bufom and Udias, 1991; Vissars, 2012).

2.2.5 Previous Geochronology in the Betic-Rif

Geochronological studies in the Betic-Rif has been conducted by in different studies using different isotopic systems. Below is a review of a selection of these studies.

Lu-Hf Garnet Dating – Platt *et al.* (2006) conducted Lu-Hf geochronology on bulk garnet eclogite and kyanite schist samples from the Nevado-Filabride to constrain the timing and rate of high pressure metamorphism and subduction of the Nevado-Filabride Complex. The four garnet ages from this study were 13.6 ± 0.4 , 16.8 ± 0.3 , 16.9 ± 1.2 , and 18.2 ± 0.8 Ma. All four samples give a Miocene age for subduction of continental crust in the Betics.

Rb-Sr Multimineral Dating – Kirchner *et al.* (2016) conducted Rb-Sr geochronology on samples from the Nevado-Filabride to constrain high-pressure metamorphism and subduction in the Betic Cordillera. The three ages published in their study were 20.1 ± 1.1 , 16.0 ± 0.3 , and 13.3 ± 1.3 Ma. These ages strongly agree with the Lu-Hf garnet ages of Platt *et al.* (2006) suggesting early Miocene subduction in the Betic Cordillera.

U-Pb Dating – Li and Massone (2017) conducted in situ U-Pb monazite dating of phengite-garnet-bearing metapelites from the Nevado-Filabride Complex. Their study yielded ages between 14 to 48 Ma. Based on monazite composition two age populations

with mean ages of 40.2 ± 1.7 and 24.1 ± 0.8 (1σ) Ma were defined. Based on the Y_2O_3 content the older population of monazite age was assigned to the formation of garnet cores and an earlier P-T loop, while the younger population of monazite ages was related to a second younger P-T loop. Li and Massone (2018) propose a model of Eocene subduction of continental crust followed by Early Miocene reheating caused by nappe thrust stacking.

Sm-Nd Dating – Stewart (2015) conducted both bulk and zoned Sm-Nd garnet geochronology on structurally characterized samples from the Nevado-Filabride Complex. The goal of this work was to address the hypothesis of Aerden *et al.* (2013) that FIA orientations within garnets from the NFC are recording changes in relative plate motion between Africa and Iberia. Garnet ages from that work ranged from 10 to 36 Ma.

2.3 EXISTING STRUCTURAL DATA

2.3.1. Macrostructural Sequence in the Field

Macrostructural studies have concluded the Betic-Rif Arc was affected by five different phases of penetrative deformation (Bakker *et al.*, 1989; Aerden and Sayab, 2008; Ruiz-Fuentes and Aerden, 2018). These phases of deformation have manifested as large-scale folds, matrix foliations, stretching lineations, and inclusion trails within garnet and staurolite porphyroblasts. The first two phases of deformation (D_{1-2}) created the dominate fabric in the region, a composite S_1 - S_2 penetrative cleavage, termed the “regional foliation” or “main-phase foliation,” it is associated with isoclinal folds reaching kilometer in scale. The third phase (D_3) is characterized by NW to WNW trending anticlines and synclines with a steeply NE dipping crenulation cleavage. The fourth (D_4) phases saw the roof detachment of the NFC, this fault is delineated by a thick sequence of mylonites and

breccias. This detachment clearly crosscuts the older phases of ductile deformation. The fifth phase (D₅) refers to sets of upright folds that weakly fold the D₄ detachment (Martinez-Martinez *et al.*, 2002; Aerden and Sayab, 2008; Ruiz-Fuentes and Aerden, 2018).

2.3.2. FIA Data

Detailed microstructural and petrologic work by Aerden *et al.* (2013) attempts to link the FIA orientations within garnet porphyroblasts to the five distinct phases of deformation and ultimately to the vectors of relative plate motion in the region (Figure 2.3.1). FIA orientations were determined from 93 garnet schist samples using the Asymmetry technique (Hayward, 1990; Bell *et al.*, 1995). The relative timing of these FIA is based on their crosscutting relationships, oldest to youngest: (1) NE-SW, (2) NW-SE, (3) W-E, (4) NNW-SSE, and (5) NE-SW (Ruiz-Fuentes and Aerden, 2018). The geographic extent and proposed ages of FIA orientations are shown in Figure 2.3.2.

2.4. PREVIOUS GARNET GEOCHRONOLOGY

Stewart (2015; unpublished) conducted a similar project, using bulk and zoned Sm-Nd garnet geochronology to test the hypothesis of Aerden *et al.* (2013). The results of her study were predominately inconclusive, this was primarily due to poor age precision. Stewart's (2015) most precise obtained bulk Sm-Nd ages were 35.5 ± 2.1 , 18.6 ± 7.4 , 15.8 ± 3.5 Ma. Stewart (2015) also conducted zoned Sm-Nd ages on sample 27.1.2 (the focus of chapter three): however due to small sample size, the zoned analysis of this sample was ultimately unsuccessful. Of these data, sample B13c, which gave the most robust age of 35.5 ± 2.1 Ma supported the hypothesis of Aerden *et al.* (2013). The other ages from her

study were not precise enough to adequately test the hypothesis. For detailed discussion on these ages the reader is referred to Stewart (2015).

2.5. SAMPLE DESCRIPTION

Eight structurally characterized samples were selected for bulk Sm-Nd garnet chronology. Four were from the Sebtime Complex of the Rif Cordillera, one was from the Alpujarride Complex of the Betic Cordillera, and three were from the Nevado-Filabride Complex of the Betic Cordillera (Figure 2.5.1). In general, samples from the Alpujarride/Sebtime are predominantly fine-grained and graphite-rich, whereas the samples from the Nevado-Filabride are coarser-grained with a quartz-rich matrix.

2.5.1. Alpujarride-Sebtime Samples

Sample A7 is a fine-grained garnet-bearing graphitic schist from the Almuñecar-Torrex Schist. The matrix is composed of quartz, biotite, muscovite, graphite, staurolite, and amphibole. The garnet porphyroblasts are small subeuhedral grains, approximately 500 μ m in diameter and sparsely distributed, accounting for a small percentage of the whole rock (Figure 2.5.2). Structurally, the inclusion trails within these garnets have a well constrained FIA orientation striking north-west to south-east, which according to Aerden *et al.* (2013), should correspond to FIA 2. The hypothesized age for this sample is between 33 – 39 Ma.

Sample B5 is a fine-grained garnet-bearing graphitic schist from the Biznou Schist. The matrix is composed of quartz, muscovite, graphite, and opaques. The matrix is heterogeneous with alternating mica-graphite rich and quartz rich layers. The garnet porphyroblasts are small euhedral grains, approximately 1 mm in diameter, equally

distributed throughout the matrix (Figure 2.5.3). The inclusion trails within these garnets have a broadly east-west trend. According to the model proposed by Aerden *et al.* (2013), this sample should host FIA 3. The hypothesized age, assuming the model of Aerden *et al.* (2013) for B5 is between 19 – 33 Ma.

Sample F8 is a garnet-bearing graphitic micaschist belonging to the Filali Schist which directly overlies the Beni-Bousera peridotite in the Rif Mountains of Morocco. The matrix is composed of quartz, plagioclase, white mica, biotite, and graphite. The garnet porphyroblasts are small, approximately 1 mm in diameter and equally distributed throughout the matrix. The inclusion trails within these garnets have bimodal orientations, one populations trending broadly east-west and another trending northwest-southeast. According to the model proposed by Aerden *et al.* (2013) these orientations belong to FIA generations 3 and 2 respectively. The hypothesized age, assuming the model of Aerden *et al.* (2013) is between 19 – 33 Ma for FIA 3 and between 33 – 39 Ma for FIA 2.

Sample F16 is a garnet-bearing graphitic micaschist belonging to the Filali Schist. The matrix is composed of muscovite, biotite, quartz, graphite, and other opaque minerals. The garnet porphyroblasts are small, only several mm in diameter and are distributed into densely populated discrete bands approximately 1 – 2 cm in width (Figure 2.5.4). Structurally, the garnet porphyroblasts in this sample have a bimodal distribution of inclusion trail orientations, a rather broad east-west orientation and a narrow northeast-southwest orientation. The broad east-west trend would correlate with FIA 3 and the northeast-southwest trend would correlate more with FIA 5. The hypothesized age, assuming the model of Aerden *et al.* (2013) is between 19 – 33 Ma.

Sample MT8 is a fine-grained graphitic garnet-bearing micaschist from the Filali Schist. Garnet porphyroblasts in this sample are smaller (≤ 1 mm in diameter) and account for a smaller proportion of the rock as a whole (Figure 2.5.5). The matrix is composed of muscovite, biotite, quartz, graphite, and other opaque minerals. The inclusion population in these garnets are distinctly zoned with cores dominated by quartz inclusions and rims dominated by graphite inclusions. The preferred inclusion trail orientations within these garnets exhibit a north-northeast to south-southwest trend, which correlations spatially with FIA 5. The hypothesized age, assuming the model of Aerden *et al.* (2013) is between 10 – 15 Ma.

2.5.2. Nevado-Filabride Samples

Sample 27.2.1 is a garnet-bearing quartz-rich micaschist from the lower Mulhacén unit. The matrix is predominately quartz, muscovite, and opaques with some chlorite found primarily in the fringe shadows along garnet porphyroblasts. The garnet porphyroblasts are quite large, approximately 1 – 5 mm in diameter and account for a considerable amount of the whole rock (Figure 2.5.6). Inclusion trail in these garnet show simple geometries with a well constrained orientation striking north-south. The north-south trend should correlate with FIA 4. The hypothesized age, assuming the model of Aerden *et al.* (2013) should lie between 10 – 19 Ma.

Sample 27.1.2 is a quartz-rich garnet micaschist with abundant kyanite, chloritoid and rutile from the Mulhacén unit. The garnet porphyroblasts from this sample are large, with some up to 1.5 cm in diameter. The matrix is composed of muscovite, quartz, and chloritoid with apatite, rutile, zircon and minor amounts of alunite (Figure 2.5.7). The orientation of inclusion trails within these garnets is well-constrained, trending N-075, or

broadly east-west. This orientation belongs to FIA generation 3; therefore the model of Aerden et al. (2013) would proposed a garnet age of 19 to 33 Ma. This sample was the target of both bulk and zoned analysis by Stewart (2015). The obtained bulk age from that study was 15.8 ± 3.5 Ma. The zoned chronology of 1 cm garnets from this sample yielded ages ranging from 21 ± 26 Ma to 318 ± 130 Ma. The zoned chronology conducted on this sample during this study is the subject of chapter three.

Sample 53.10.1 is a garnet-bearing quartz-rich graphitic micaschist from the Mulhacén unit. The matrix is composed of quartz, white mica, biotite and chlorite. The garnet prophyroblasts are quite large, 1 – 5 mm in diameter. The inclusion trails within these garnets trend broadly north-south, the hypothesized age, assuming the model of Aerden *et al.* (2013) is between 10 – 19 Ma.

2.6. GEOCHRONOLOGICAL METHODS

The geochronological methods employed during this study fall into four categories: (1) bulk mineral extraction, (2) partial and full sample dissolution, (3) column chemistry and sample purification, and (4) isotopic analysis. Each step is described in detail during this section.

2.6.1. Bulk Mineral Separation

The seven samples chosen for bulk analysis were crushed to a fine gravel using a large tungsten-carbide mortar and pestle. After this initial crushing a portion (approximately 20-25%) representing homogeneous whole rock fraction was set aside for isotopic analysis with care taken not to fractionate based on grain-size. The whole rock separate was powdered in an agate mortar and pestle and sieved to ≤ 75 μm grain-size (200

sieve size). The remaining coarse-grained material (approximately 75-80%) was processed to obtain a representative bulk garnet separate. The extraction of garnets from the surrounding matrix was accomplished through a combination of crushing, sieving, magnetic Franz separation, and hand-picking. Once ≥ 50 mg of visibly clean garnet was obtained, it was crushed using a small tungsten-carbide mortar and pestle until the grain-size was between 75 and 150 μm to obtain a garnet separate; anything finer than 75 μm was collected as a garnet powder separate. The 75 – 150 μm grain-size was determined by Pollington and Baxter (2011) to be the ideal grain-size to maximize exposure of inclusion phases while minimizing sample loss. Both garnet and garnet powder separates were put through a partial dissolution process.

2.6.2. Sample Digestion

All Sm and Nd isotope analyses were performed at the Boston College Center for Isotope Geochemistry. In the clean lab, garnet and garnet powder separates were put through a partial dissolution procedure consisting of alternating 7N HNO_3 and dilute HF acid steps in an enclosed 7mL beaker at 120 °C for ~2 hours. The purpose of these steps was to leach out contaminating inclusion phases. Separates were first put in 2mL of 7N nitric to dissolve any exposed non-silicate inclusions present. Next, separates were put in anywhere from 20 - 100 μL of concentrated HF + 1mL Milli-Q H_2O to partially dissolve the sample to further access inclusions and to dissolve any silicate inclusions present. The separates were then put back in 7N nitric to dissolve any buildup of secondary fluorides that accumulated during the HF step. These steps were continued until the separates were deemed clean, this was approximately 75 – 95% sample loss. Following partial dissolution each separate was fully dissolved over several days in a combination of concentrated HF,

nitric, and 6N HCl. All whole rack separates were fully dissolved using the same procedure as garnet and powder separates. After full dissolution samples were stored in an 8:1 aqua regia solution. Prior to column chromatography sample aliquots were spiked with a mixed spike enriched in ^{150}Nd and ^{147}Sm .

For a majority of garnet and garnet powder separates leachate, representing a combined HF + nitric step, was collected during the partial dissolution process. Each leachate collected should represent a different stage of samples loss during the partial dissolution procedure, and thus should represent an intermediate step between the cleaned and uncleaned separate. If the garnet and inclusion phases grew in equilibrium the leachates should still fall along the isochron, however if the inclusions have an inherited isotopic signature then the leachate will not fall along the isochron.

2.6.3. Column Chromatography

The isolation of Sm and Nd was accomplished using the three column procedure described in Harvey and Baxter (2009). The procedure consists of (1) a Fe clean-up column using AG50w-X4 resin, rinsed with 1.5 N HCl to remove iron, and sample eluted with 6 N HCl, (2) TRU-spec resin column, rinsed with 2N HNO₃ to remove major cations, and REEs eluted with 0.05 N HNO₃, and (3) a 2-methyl-lactic acid (MLA) column using AG50w-X4 resin conditioned with 10 mL of 0.2 M MLA was used to separate Sm from Nd and remove isobaric interferences, predominately Pr and Gd. To track Nd contamination, a three column blank was run with each set of columns. All spike weights, isotopic ratios, and blank weights from all three-column and full procedural blanks from this study are summarized in appendix A.

2.6.4. Isotopic Analysis

Sm and Nd isotopic ratios were analyzed on an Isotopx Phoenix Thermal Ionization Mass Spectrometer (TIMS). Nd isotopes were loaded with 2 μ L of 2N nitric onto Re filaments and run in dynamic mode as the oxide species (NdO⁺) with 2 μ L of tantalum oxide (Ta₂O₅) activator slurry added to facilitate greater sample ionization. Instrumental induced mass fractionation was normalized to $^{146}\text{Nd}/^{144}\text{Nd} = 0.7219$ using an exponential correction factor. Sm isotopes were loaded with 2 μ L of 2N nitric onto Ta filaments and run in static mode as metal species. Instrumental induced mass fractionation was normalized to $^{149}\text{Sm}/^{152}\text{Sm} = 0.516860$ using an exponential correction factor. Both Sm and Nd samples, as well as standards were loaded using parafilm dams to decrease sample spread across the filament. Two 4ng Ames NdO standards and two 20ng Ames Sm standards were run with every barrel to track the external reproducibility. Over the period of analysis from this study the $^{143}\text{Nd}/^{144}\text{Nd}$ long-term value was 0.512152 ± 13.25 ppm 2σ (n=32) and $^{147}\text{Sm}/^{152}\text{Sm}$ long-term value was 0.560870 ± 49.88 ppm 2σ (n=34). All data from standard runs can be found in appendix A.

2.7 RESULTS

All Sm and Nd isotopic data from samples A7, B5, F8, F16, MT8, 27.2.1, 53.10.1, and preliminary bulk analysis of 27.1.2 are summarized in Tables 2.1 – 2.8. Selected isotopic data for final age calculations can be found in Table 2.9. Raw isotope data was reduced using Tripoli (Bowring *et al.*, 2011). All isotopic and age errors are reported at 2σ standard error. In cases where the internal precision for a given analysis was better than the external precision, the external precision was reported. All garnet isochron ages were calculated using Isoplot 4.15 software program (Ludwig, 2003).

2.7.1 Alpujarride-Sebtide Garnet Ages

Sample A7

Figure 2.7.1 is a five point isochron including all of the analyzed data for sample A7, which consists of a garnet, garnet leachate, garnet powder, garnet powder leachate and whole rock separates. The calculated age of 21.0 ± 3.9 Ma is made less precise by a single data point, the garnet fraction that slightly lies off the isochron resulting in a MSWD of 6.3. The high MSWD suggests considerable geologic scatter in the data, however, with a high $^{147}\text{Sm}/^{144}\text{Nd}$ ratio of 1.89 this data point cannot be explained merely by contamination of inclusion phases. We propose this scatter to be the result of unintentional grain-size fractionation during mineral separation that potentially fractionated garnet cores from rims, or fractionated a younger population of garnets from an older population. This scatter either represents two populations of garnet growth, or the duration of garnet growth within this sample. Therefore, perhaps it is more geologically meaningful to separate sample A7 into two different age groups, a core dominated older age and a rim dominated younger age. The calculated older age is a four point isochron yielding an age of 21.98 ± 0.86 Ma (MSWD = 0.90) (Figure 2.7.2), and the younger age is a two point isochron yielding an age of 19.2 ± 1.2 Ma (Figure 2.7.3). Both of these ages have high $^{147}\text{Sm}/^{144}\text{Nd}$ ratios of 2.73 and 1.89 respectively, therefore we have high confidence both of these ages are accurate and not affected by contamination of inherited inclusions.

Sample B5

Figure 2.7.4 is a five point isochron including all of the analyzed data for sample B5, which consists of two garnet, garnet leachate, garnet powder, garnet powder leachate,

and whole rock separates. The calculated age from these data of 21 ± 17 Ma (MSWD = 6.0) is made significantly less precise by the large error from several of the measurements and. However, two of the data can be dismissed due to poor TIMS analysis resulting in very large uncertainty in the $^{143}\text{Nd}/^{144}\text{Nd}$ ratio. The omission of these data results in an age of 26.2 ± 2.5 Ma (MSWD = 2.0) from a three point isochron with a highest $^{147}\text{Sm}/^{144}\text{Nd}$ ratio of 2.17 (Figure 2.7.5).

Sample F8

Figure 2.7.6 is a five point isochron containing all of the analysis data for sample F8 which consists of three garnet, garnet leachate, and whole rock separates. The calculated age from these data of 30 ± 16 Ma is made less precise by a single data point, a garnet fraction that lies off the isochron resulting in a MSWD of 15. The high MSWD suggests considerable geologic scatter in the data, however, with a high $^{147}\text{Sm}/^{144}\text{Nd}$ ratio of 1.513 this data point cannot be explained simply by contamination of inclusion phases. We propose this scatter to be the result of unintentional fractionation during mineral separation. Franz magnetic separation created two garnet separates, one with a higher magnetism, and one with a lower magnetism. This difference in magnetism possibly preferred a garnet core enriched with magnetite or ilmenite inclusions, thus fractionating garnet cores from rims. Therefore, perhaps it is more geologically meaningful to separate sample F8 to two different age groups, a core dominated older age and a rim dominated younger age. The separating of this sample into two ages resulted in a younger a four point isochron age of 26.1 ± 1.4 Ma (MSWD = 1.6) (Figure 2.7.7), and an older two point isochron age of 35.6 ± 2.8 Ma (Figure 2.7.8). Both of these ages have relatively high $^{147}\text{Sm}/^{144}\text{Nd}$ ratios of 1.513

and 1.823 respectively, therefore we have high confidence both of these ages are accurate and are not affected by contamination of inherited inclusions.

Sample F16

Figure 2.7.9 is a six point isochron containing all of the analysis data for sample F16 which consists of two garnet, garnet leachate, garnet powder, garnet powder leachate, and whole rock separates. The calculated age from all these data is 24.95 ± 0.61 Ma (MSWD = 1.8). One data point, a garnet separate has very high uncertainty on the $^{143}\text{Nd}/^{144}\text{Nd}$ ratio of 1458.4 ppm 2σ , omitting this data point from the age calculation does not change the obtained age or age uncertainty of 24.95 ± 0.61 Ma, but does raise the MSWD from 1.8 to 2.4 (Figure. 2.7.10).

Sample MT8

Figure 2.7.11 is a seven point isochron containing all of the analyzed data for sample MT8, which consists of two garnet, two garnet leachate, two garnet powder, and whole rock separates. The calculated age from these data of 26.2 ± 3.7 Ma is made significantly less precise by a single data point, the garnet leachate separate that slightly falls off the isochron resulting in a high MSWD of 3.4. The garnet leachate separate has a $^{147}\text{Sm}/^{144}\text{Nd}$ ratio of 0.489, this relatively low ratio suggests this data point is most likely not pure garnet, but rather a mix between the clean garnet isotopic signature and an older inherited isotopic signature from contaminating inclusion phases. Therefore, we can reasonably omit this data point from the age calculation. The resulting six point isochron (Figure 2.7.12) yields an age of 26.9 ± 1.5 Ma (MSWD = 0.95). Note, the omission of this data point does not significantly change the absolute age.

2.7.2 Nevado-Filabride Garnet Ages

Sample 27.1.2

Figure 2.7.18 is a four point isochron containing a selection of preliminary bulk data for sample 27.1.2 which consists of three garnets and a whole rock separate. The calculated age from these data is 13.62 ± 0.69 Ma (MSWD = 1.7). A detailed zoned geochronology study of four garnets from this sample is the focus of chapter three.

Sample 27.2.1

Figure 2.7.13 is a ten point isochron containing all of the analyzed data for sample 27.2.1, which consists of five garnet, one garnet leachate, three garnet powder, and two whole rock separates. The calculated age from these data is 13.0 ± 1.9 Ma. The high MSWD of 5.3 suggests considerable scatter among data points, especially data points with low $^{147}\text{Sm}/^{144}\text{Nd}$ ratios. Omitting three data points from the age calculation, two with low $^{147}\text{Sm}/^{144}\text{Nd}$, a garnet and a garnet powder, and one with a high $^{147}\text{Sm}/^{144}\text{Nd}$, of 1.75, but with very large uncertainty in the $^{143}\text{Nd}/^{144}\text{Nd}$ ratio. From these factor, we can reasonably omit these data points from the age calculation, the resulting seven point isochron (Figure 2.7.14) yields an age of 12.9 ± 1.6 Ma (MSWD = 3.5). The omission of this data point does not significantly change the absolute age, but does lower the MSWD.

Sample 53.10.1

Figure 2.7.15 is a six point isochron containing all of the analysis data for sample 53.10.1 which consists of three garnet, two garnet powder, and whole rock separates. The calculated age from these data of 16.3 ± 8.4 Ma is made less precise by scatter in the data resulting in a MSWD of 5.4 Due to this high scatter in the data it may be more geologically

meaningful to separate sample 53.10.1 into two different age groups. This results in an older four point isochron age of 21.8 ± 2.4 Ma (MSWD = 0.49; Figure 2.7.16), and a younger three point isochron age of 16.5 ± 2.5 Ma (MSWD = 2.29; Figure 2.7.17). Both of these ages have relatively high $^{147}\text{Sm}/^{144}\text{Nd}$ ratios of 0.923 and 1.193 respectively, therefore, we have confidence both of these age are accurate and not affected by contamination of inherited inclusions.

2.7.3. Timing of Spiral Inclusion Trail Formation in the Betic-Rif arc

This study produced eleven statistically valid Sm-Nd isochron garnet ages that range from 12.9 to 35.6 Ma with 2σ uncertainties ranging from 0.69 to 2.8 Ma. The four Rif Cordillera samples have inclusion trail orientations that broadly trend from northeast-southwest (samples F16 and MT8) in the southern Rif near the Beni Bousera peridotites, to a trend becomes more east-west (sample B5) near Ceuta. The garnet ages from these samples are for as follows, MT8: 26.9 ± 1.5 Ma, F16: 24.95 ± 0.61 Ma and B5: 26.2 ± 2.5 Ma. Note, these samples have varying inclusion trail orientations, but the same garnet ages are within uncertainty.

The four Betic Cordillera samples come from the Nevado-Filabride and overlying Alpujarride complexes. The Alpujarride sample has inclusion trails trending northwest-southeast (sample A7), garnet ages indicate this deformation occurred 21.98 ± 0.86 Ma. The samples from the Nevado-Filabride have inclusion trails trending north-south (Samples 27.2.1 and 53.10.1) and east-west (27.1.2). The samples trending north-south were dated to 12.9 ± 1.6 Ma and 16.4 ± 2.8 Ma. The sample (27.1.2) with inclusion trails trending east-west was dated to 13.62 ± 0.69 Ma. Samples 27.1.2 and 27.2.1 in this complex have different inclusion trail orientations, but are the same age within uncertainty.

2.8. DISCUSSION OF BULK GARNET AGES

2.8.1. *New Sm-Nd Garnet Ages vs. Model of Aerden et al. (2013)*

The overarching motivation behind this study was to use high precision bulk Sm-Nd garnet geochronology on samples with well-defined and characterized inclusion trail orientations to test the hypothesis proposed in Aerden *et al.* (2013) which states tectonic-scale plate motions control FIA orientation. If we recall from section 2.3.2, the proposed ages of FIA generations from Aerden *et al.* (2013) are, FIA 2, 33 – 39 Ma; FIA 3, 19 – 33 Ma; FIA 4, 10 – 19 Ma; and FIA 5, < 15 Ma. A first order test of this hypothesis would be to strictly compare the obtained garnet ages to the proposed FIA ages. Figure 2.8.1 shows this first order comparison of the ten ages obtained during this study and the hypothesis of Aerden *et al.* (2013).

Sample A7 has a FIA orientation trending northeast-southwest, this orientation belongs to FIA generation 2; therefore the garnet age from this sample should fall between 33 to 39 Ma. The obtained garnet age from this sample of 21.98 ± 0.86 Ma is in disagreement with Aerden *et al.* (2013) This high precision of this age leaves no doubt that the FIA orientation in this sample cannot be recording NE directed plate motion.

Sample MT8 has a FIA orientation trending north-northeast to south-southwest, this orientation belongs to FIA generation 5; garnet ages from this generation should be < 15 Ma. The obtained age from this sample 26.9 ± 1.5 Ma, is in disagreement with the predicted age for FIA generation 5. The age of this sample falls into the range for FIA generation 3 rather than FIA generation 4. This sample refutes the hypothesis of Aerden *et al.* (2013).

Both the structural and geochronologic characterizations of sample F8 are less precisely constrained than the other samples from this study. The geochronology revealed the presence of two potential populations of garnet ages, an age at 26.1 ± 1.4 Ma and a less robust age at 35.6 ± 2.8 Ma (see previous section for discussion on these ages). The younger age is constant with the other garnet ages from the Rif. The FIA orientations also appear to be bimodal, with an orientation trending northwest-southeast, which corresponds to FIA 2, and another trending broadly east-west, which correspond to FIA 3. Unfortunately, this bimodal distribution of FIA populations wasn't discovered until after the mineral separation had begun on this sample. Therefore we cannot say definitively which age belonged to which FIA orientation.

Sample F16 has a FIA orientation trending east-northeast to west-southwest, this orientation is on the edge of being either FIA generation 3 or 5. Our age result of 24.95 ± 0.61 Ma is in agreement with the predicted age of 19 to 33 Ma for FIA generation 3. This agreement supports Aerden *et al.* (2013). However, we cannot unequivocally say if this sample truly belongs to FIA generation 3.

Sample B5 has a FIA orientation trending broadly E-W, this orientation belongs to FIA generation 3; therefore the garnet ages from this sample should lie between 19 to 33 Ma. The obtained garnet age from this sample of 26.2 ± 2.5 Ma agrees with the predicted age. This agreement supports the hypothesis proposed by Aerden *et al.* (2013).

Three samples (27.1.2, 27.2.1, and 53.10.1) were dated from the Nevado-Filabride Complex, of these, one supported, one refuted, and one was not precise enough to confirm and refute the model proposed by Aerden *et al.* (2013). Sample 27.2.1 has a FIA orientation trending N-S, this orientation belongs to FIA generation 4; therefore the garnet age from

this sample should lie between 10 to 19 Ma. The obtained garnet age from this sample of 12.9 ± 1.6 Ma agrees with the predicted age. This age supports the hypothesis proposed by Aerden *et al.* (2013).

Sample 27.1.2 has a FIA orientation trending N-075, this orientation belongs to FIA generation 3; garnet ages from this generation should range from 19 to 33 Ma. The obtained age from this sample of 13.62 ± 0.69 Ma is in disagreement with the predicted age of FIA generation 3. The age of this sample falls into the range for FIA generation 4 rather than FIA generation 3. This sample strongly refutes the hypothesis of Aerden *et al.* (2013).

The geochronologic characterization of sample 53.10.1 is not as well-constrained as the other samples from this study (see previous section for discussion on this age). The geochronology revealed the presence of two potential populations of garnet ages, a younger age at 16.5 ± 2.5 Ma and an older age at 21.8 ± 2.4 Ma. This sample belongs to FIA generation 4 with inclusion trail orientations trending north-south. The garnet age from this sample should lie between 10 to 19 Ma. The younger age falls within this age range, but the older age lies just outside of this age range. Given this sample's bimodal age distribution and relatively poor age precision this sample can neither refute nor support the hypothesis of Aerden *et al.* (2013). Future geochronology to better the age precision is necessary.

Of the nine samples discussed herein to address the hypothesis of Aerden *et al.* (2013), eight from this study and one from the study of Stewart (2015), four samples fell within the accepted age range to support the hypothesis, three samples fell outside the accepted age range, and as a result refute the hypothesis, and two samples due to poor constraints on either FIA orientation or garnet age could not adequately refute nor support

the hypothesis. In general the fact that a sample fell within the appropriate age range to support the hypothesis does not signify a strong confirmation. The proposed ages of FIA generations range many millions of years, consequently the fact that some samples support the hypothesis would be expected. Therefore, just a first order comparison of obtained Sm-Nd bulk garnet ages and FIA orientations does not support the initial hypothesis as outlined in Aerden *et al.* (2013). However, this does not fully refute the possible connection between FIA orientations and regional-scale tectonics.

2.8.2. Aerden et al. (2013) in the Context of Post Metamorphic Rigid-Block Rotations

Many studies have found evidence for large-scale rigid-block rotations in the Betic-Rif arc (Villalain *et al.*, 1996; Villasante-Marcos *et al.*, 2003; Mattei *et al.*, 2006; Cifelli *et al.*, 2008; Platt *et al.*, 2013; Brendt *et al.*, 2015). These rotations are characterized by clockwise rotations in the Betics and anticlockwise rotations in the Rif. The most recent work by Brendt *et al.* (2015) indicates the Ronda peridotite in the Betics recorded clockwise rotations of $46.8 \pm 8^\circ$, and the Ceuta and Beni Bousera peridotites in the Rif recorded anticlockwise rotations of $19.7 \pm 5.9^\circ$ and $72.3 \pm 12.1^\circ$, respectively. Figure 2.8.2 from Brendt *et al.* (2015) is cartoon diagram that show the orientation of exposed peridotites before and after rigid block rotations. All three of these large exposed peridotite bodies are hosted in the Alpujarride-Sebtide complex. The timing of these rotations was most likely younger than 20 Ma (Brendt *et al.*, 2015), post-dating the age of garnet grade metamorphism obtained in this study for the Alpujarride and Sebtide complexes.

These post-metamorphic rigid-block rotations are intriguing in the context of Aerden *et al.* (2013) and the obtained Sm-Nd garnet ages. If rigid block rotation does indeed post-date garnet growth, then the FIA orientations would have also been affected

by these rotations (personal communication, Domingo Aerden). These rotations, however only appear to have affected FIA orientations in the western portions of the Alpujarride-Sebtide; the Nevado-Filabride and eastern Betics were most likely unaffected. The obtained garnet ages from the Alpujarride-Sebtide range from 21.9 to 26.9 Ma, this range lies within the proposed age range for FIA generation 3. Reconstructing the blocks to their positions prior to rotation reorients the FIA orientations of samples B5, F8, F16, and MT8 in the Rif clockwise and sample A7 in the Betics anticlockwise. This reorientation brings all of the FIA orientations to a broadly east-west trend, aligning them all into the accepted orientation range for FIA generation 3 (Figure 2.8.3). However, there is not complete agreement between the rigid-block rotations obtained from Brendt et al. (2015) and rotations obtained from FIA orientations in the area of Beni Bousera. A rotation of $72.3 \pm 12.1^\circ$ over rotates the FIA orientations of samples F8, F16 and MT8; using the FIA orientations from these samples alone would suggest an anticlockwise rotation of approximately 30° (Fig. 2.33). Though this result is compelling, it requires more robust and detailed research to determine the affect these large-scale rigid-block rotations had on reorienting the FIA in the western Betic-Rif Arc. Figure 2.8.4 summarizes the new comparison of FIA orientations and ages assuming 30 degrees clockwise rotation in the Beni Bousera, southern Rif, with plate motion studies from Rosenbaum et al. (2003) and Macchiavelli et al. (2017).

2.9 CONCLUSION

Twelve bulk Sm-Nd garnet isochron ages were obtained from nine garnet-bearing samples from across the Betic-Rif arc. These data constitute new robust constraints on the timing of microscale deformation and garnet grade metamorphism in a region that has

witnessed a complex tectonometamorphic evolution. The potential effects of post-metamorphic rigid block rotations on the preferred orientation of FIA from the Sebide-Alpujárride Complex, in combination with newly obtained garnet ages, has prompted a refining of the original model proposed by Aerden et al. (2013).

CHAPTER 3

A RAPID PULSE OF SPIRAL GARNET FORMATION REVEALED FROM ZONED SM-ND GARNET GEOCHRONOLOGY IN THE NEVADO-FILABRIDE COMPLEX, BETIC CORDILLERA, SPAIN

ABSTRACT

Multiple studies have used zoned garnet geochronology to place temporal constraints on rates and durations of metamorphism and deformation (Christensen et al., 1989; Pollington and Baxter, 2010). Here, we report new high resolution Sm-Nd isochron ages on individual growth zones from structurally-characterized garnets from the Nevado-Filabride Complex, the lowest and most metamorphosed unit in the Betic Cordillera of Spain. Four 1 cm garnets hosting spectacular spiral inclusions were micro-drilled to isolate concentric growth zones based upon Mn concentration contours and inclusion trail truncations. Cores were found to have nucleated at 13.60 ± 0.31 Ma, median domains at 13.37 ± 0.36 Ma, and garnet rims at 13.28 ± 0.48 Ma. The age of these garnets is consistent with Lu-Hf garnet ages from the same complex (Platt et al., 2006). The core to rim duration of growth was constrained using a Monte Carlo style analysis to $0.45^{+0.51}_{-0.32}$ Myr. While other zoned garnet studies have shown similar rapid growth in subduction zone setting (Dragovic et al., 2012), this is the first such documentation of such rapid growth from a garnet hosting spiral inclusion trails in a regional metamorphic setting. We calculated strain rates considering different genetic models for the spiral inclusion trails either by garnet

rotation in simple shear, or by episodic overgrowth of suborthogonal crenulation cleavages due to switching stress axes. In both cases a similar fast strain rate of ca. 10^{-13} s^{-1} was obtained, which is an order of magnitude faster than typical regional strain rates and faster than previous spiral garnet studies regardless of the method used to calculate strain-rate.

3.1 INTRODUCTION

Spiral garnets are well-documented metamorphic microstructures that have been observed in numerous orogens throughout the world (e.g. Rosenfeld, 1968; Bell et al., 1992; Robyr et al., 2008; Aerden et al., 2013; Sayab et al., 2016). The canonical origin of spiral garnets by shearing induced porphyroblast rotation (Rosenfeld, 1968; Schoneveld, 1979) went unquestioned until Bell and Johnson (1989) discovered that in many orogens, the internal truncation surfaces typically associated with these microstructures, systematically align along vertical and horizontal axes. They explained this preferred orientation by invoking a model in which porphyroblasts do not rotate but rather episodically overgrow multiple suborthogonal crenulation cleavages forming around them, perhaps as the result of compression-collapse cycles during orogenesis. Determining which microstructural model is responsible for the formation of spiral garnets is vital for interpreting the tectonic significance of these important microtectonic fabrics. The ubiquity of garnet in metamorphic rocks, in combination with its ability to record P-T-d-t conditions has made it a primary target phase for investigating timing, rates, and duration of metamorphic and deformational processes. (Baxter et al., 2017). Christensen *et al.* (1989, 1994) and Vance and O'nions (1992) pioneered zoned garnet geochronology as a tool for placing temporal constraints on rates and duration of garnet growth and deformation in metamorphic terranes. These studies found that spiral inclusion trails develop on multi-

million year timescales in the regional metamorphic schists they explored. More recent work (e.g. Pollington and Baxter, 2010; Dragovic *et al.*, 2012, 2015) has shown evidence for rapid pulses of garnet growth over much shorter timescales (i.e. < 1 Myr) in subducted blueschists. To further explore the nature, tectonic significance, and origin of spiral garnets, we have combined detailed microstructural analysis with high resolution zoned Sm-Nd garnet geochronology to spiral garnets from the Nevado-Filabride Complex of the Betic Cordillera, Spain.

3.2 GEOLOGIC SETTING

The Betic-Rif arc orogenic belt is one of the world's smallest and tightest oroclines located at the western termination of the Mediterranean Alpine orogenic system. Its metamorphic hinterland, or Internal Zones, comprises three nappe complexes, the lowest of which is the Nevado-Filabride Complex (NFC) from where the sample from this study was collected. The NFC outcrops as a tectonic window in the central and eastern Betics where it forms a broadly east-west trending anticlinorium including the Sierra Nevada and Sierra de los Filabres (Figure 3.2.1). The NFC has been subdivided into the lower Veleta Complex (VC) and the upper Mulhacén Complex (MC). The VC is composed of polymetamorphic Paleozoic graphitic-schists and quartzites several kilometers in thickness. The MC comprises similar Paleozoic basement rocks overlain by a Permo-Triassic and possibly younger metasedimentary sequences, which from bottom to top, are composed of light colored schists, calcschists and marbles. Eclogitized mafic and ultramafic lenses in this cover sequence have been interpreted as remains of a narrow branch of the Alpine Tethys (Puga et al, 2008) that originally separated the Iberian

paleomargin (including most of the NFC) from a microcontinent to the east that included the overlying Alpujarride and Maláguide complexes (e.g. Platt et al. 2013).

3.3 MICROSTRUCTURAL ANALYSIS

The sample (27.1.2) studied herein is a quartz-rich micaschist with garnets up to 15 mm in diameter. The sample was collected from the cover sequence of the MC in the western Sierra de los Filabres (Lat. -2.82784° , Long. 37.30270°). Abundant kyanite, chloritoid, and rutile suggest a higher pressure origin (see figure 3.3.1). Using the asymmetry technique of Hayward (1992), multiple vertical and horizontal cuts of the oriented sample revealed inclusion trails spiraling up to 180° with vertical truncations trending predominantly E-W. The 3D geometry of the inclusion trails was studied further with X-ray Tomography (XRT) applied to a companion sample (46.8.1) taken less than 2 meters away from sample 27.1.2. XRT allows for the measurement of spiral axes within individual garnets by applying the technique of Hayward (1992) to sets of virtual radial slices through the garnet centers, a similar approach was used by Hudlestone-Holmes and Ketcham (2010). XRT scans of large garnets from 46.8.1 show an ENE-WSW maximum trend (see figure 3.3.2a). This orientation agrees well with the E-W maximum trend from 27.1.2 (see figure 3.3.2b). Similar orientation maxima are defined by fold axes measured in a larger region extending up to 3 km east of the sample location (see figure 3.3.2c-d). All microstructural analyses and field measurements were conducted by Domingo Aerden.

3.4 METHODS

Preliminary geochronology on bulk garnet separates from sample 27.1.2 yields an age of 13.62 ± 0.62 Ma (MSWD = 1.7; n=4). This age agrees with the lower bound of Lu-

Hf garnet ages from the MC (Platt et al., 2006). From this same hand sample, four (~ 1 cm) garnets with representative inclusion geometries were chosen for zoned chronology. Garnets were cut through their geometric centers into 1 mm thick sections. Using Mn zonation maps and inclusion trail truncations, three discernable growth zones for garnets B8, B9, and E2, and two for garnet D1 were chosen for micro-sampling following the procedure of Pollington and Baxter (2011) (Figure 3.4.1). Due to small sample volume, the core and median zones from garnets B8, B9, and E2, and the rims from B8 and E2 were combined to ensure sufficient material for a successful analysis. The six separates were crushed, hand-picked, and sieved forming a coarser (75 – 150 μm) garnet separate and finer (< 75 μm) garnet powder separate. The resulting twelve separates were put through a partial dissolution procedure modified after Pollington and Baxter (2010) consisting of multiple alternating nitric and HF steps to dissolve out contaminating inclusion phases. The isolation of samarium (Sm) and neodymium (Nd) was accomplished using the three column procedure of Harvey and Baxter (2009). All isotopic ratios were analyzed on an Isotopx Phoenix (TIMS). Nd was loaded on single Re filaments with Ta₂O₅ activator, and Sm was loaded on single Ta filaments with a H₃PO₄ binder added. During the period of the analysis the long-term average Ames 4ng NdO ¹⁴³Nd/¹⁴⁴Nd value was 0.512152 ± 13.28 ppm (2 σ) (n=32). All sample preparation and isotope analyses were performed at the Boston College Center for Isotope Geochemistry.

3.5 ZONED GEOCHRONOLOGY

Eight of the twelve prepared zone separates were successfully analyzed. Four failed to produce acceptable data, two due to sample loading errors, and two were deemed dirty with low (< 0.34) ¹⁴⁷Sm/¹⁴⁴Nd ratios, likely reflecting contamination from Nd-rich mineral

inclusions. For comparison, clean garnet separates from this study yielded $^{147}\text{Sm}/^{144}\text{Nd}$ ratios ranging from 1.00 to 3.89. As a result, these four separates are not included in age calculations. All zone separates are paired with four matrix and one whole rock separate from which it is assumed they grew in isotopic equilibrium. Isotope and concentration data for garnet zones are shown in Table 3.1. Raw isotope data was reduced using Tripoli 4.9 data processing software (Bowring et al., 2011). All isotopic and age errors are reported at 2σ standard error. In cases where the internal precision for a given analysis was better than the external precision (13.28 ppm), the external is reported. Figure 3.5.1 shows isochron diagrams for each zone analyzed; all isochron ages were calculated using Isoplot 4.15 (Ludwig, 2003). The cores yielded an age of 13.60 ± 0.31 Ma (MSWD = 0.98; n=7). The medians yielded an age of 13.37 ± 0.36 Ma (MSWD = 1.4; n=8). The rims yielded an age of 13.28 ± 0.48 Ma (MSWD = 0.98; n=8).

3.6 DISCUSSION

3.6.1 Duration of Garnet Growth

The most significant aspect of the geochronologic results presented herein is the similarity in the obtained age between all three zones; they are identical within 2σ uncertainty. The difference in age between the core and rim is 0.32 Myr; propagating the 2σ age uncertainty provides a 95% confidence interval of garnet growth that spans from instantaneous to 0.97 Myr. Because of the simple geometric constraint of core-to-rim growth (assuming no disturbance or re-equilibration of initial garnet growth (Whitney, 1996), as indicated by the simple concentric chemical zonation seen in figure 3.4.1), the decrease in age from core-to-rim is absolute. To utilize this geometric constraint, a Monte Carlo application of a Bayesian statistical approach was used to better constrain the

duration of garnet growth. Using the obtained isochron ages for each zone as input values in the Isoplot function “Calculate age limits for a sequence of stratigraphically-constrained units,” the duration of garnet growth was constrained to $0.45_{-0.32}^{+0.51}$ Myr (2σ) (Figure 3.6.1). From this, we conclude that garnet growth occurred in less than 1 Myr, and most likely spanned only a few 100 kyrs. Combining the growth duration with an average radius from the four garnets of 5 mm, a radial growth rate of $1.34_{-0.62}^{+3.03}$ cm/Myr, and a volumetric growth rate of $1.19_{-0.65}^{+3.17}$ cm³/Myr were calculated. While other zoned garnet studies have shown similar rapid rates in garnet growth (Dragovic et al., 2012, 2015), this is the first documentation of rapid growth from garnet porphyroblasts hosting spiral inclusion trails.

3.6.2 Calculations of Strain-Rate

Whatever process led to the formation of the observed spiral inclusion trails in these garnets from the NFC, it occurred on a timescale spanning just a few hundred thousand years. Christensen et al. (1989, 1994) and Vance and O’inions (1992) applied zoned Rb-Sr garnet chronology to calculate shear-strain rates ($\dot{\gamma}$) from spiral garnets by analogy to a rigid sphere embedded in a simple shear flow, rotating at half the shear-strain rate (Jeffery, 1922; Rosenfeld, 1970). The shear-strain rates they obtained were $2.4_{-0.7}^{+1.6} \times 10^{-14}$, $2.7_{-0.7}^{+1.2} \times 10^{-14}$, and $1.9_{-0.9}^{+0.9} \times 10^{-14}$ per second (s^{-1}) respectively. These workers assumed their spiral garnets to have formed by rotation in simple shear. Their strain rates are therefore minimum values, because any component of pure shear would have lowered the rotation rate of garnets and implies larger finite strain before the same amount of inclusion-trail curvature is reached. Adopting the same kinematic model, Biermeier and Stüwe (2003) and Berg et al. (2013) calculated shear-strain rates of $6.6 \times 10^{-14} s^{-1}$ and $3.2_{-1.0}^{+0.9} \times 10^{-14} s^{-1}$. These two studies, although useful do not directly date the duration of garnet growth, but

rather use thermodynamic modeling of garnet growth zoning under the assumption of reasonable regional heating rates to constrain the duration of garnet growth. Interestingly, Berg et al. (2013) also considered the alternative origin of spiral inclusion trails through overgrowth of successive orthogonal foliations in non-rotating garnets (Bell and Johnson, 1989; Fay et al., 2008). Every 90° increment of inclusion-trail curvature corresponds to a new foliation in this model. Assuming 60% shortening associated with the development of each subsequent foliation, Berg et al. (2013) obtained very similar axial strain rates $\dot{\epsilon} = 7.9_{-2.4}^{+2.4} \times 10^{-15} \text{ s}^{-1}$. Following the same approach as Berg et al. (2013), but substituting their (heating-rate)/(change in temperature) with our directly measured growth duration, we obtain strain-rates an order of magnitude faster, $\dot{\gamma} = 4.2_{-2.4}^{+10.9} \times 10^{-13} \text{ s}^{-1}$ in the rotational model, or $\dot{\epsilon} = 1.9_{-1.0}^{+4.8} \times 10^{-13} \text{ s}^{-1}$ in the non-rotation model. For a direct comparison of strain-rates from the above mentioned studies, we have plotted apparent garnet rotation (ω) from inclusion trails against the directly obtained garnet growth chronologies, and for the studies of Biermeier and Stüwe (2003) and Berg et al. (2013) their thermodynamically derivate growth durations. Figure 3.6.2 clearly shows that our spiral garnets from the NFC recorded strain-rates an order of magnitude faster than previous studies regardless of the method used to calculate strain-rate.

3.7 INTERPRETATION

A comparison of the above-reported strain rates from spiral garnets shows that they are largely independent of the genetic model that is chosen involving either porphyroblast rotation or non-rotation. However, the tectonic implications of both models are quite different. If our garnets developed by rotation in simple shear, then high strain rates could simply reflect strain partitioning over several orders of magnitude within a shear zone (e.g.

Fagereng and Biggs, 2018). A non-rotation origin on the other hand, implies that three foliations formed within less than one million years by alternating horizontal and vertical shortening related to cyclic stress permutations. Bell and Newman (2006) concluded a succession of numerous individual foliations and related compression-collapse cycles as short as 100,000 to 500,000 years from inclusion-trail data and monazite ages in the New England Appalachians. The general lack of evidence for such complex histories in the matrix of porphyroblastic rocks has been attributed to several factors including reactivation of pre-existing foliations, strain intensification against porphyroblasts where the matrix may only experience weak deformation, spatially heterogeneous development of foliations, and local transposition of foliations by new ones in zones of intense deformation (Aerden, 2005). These factors hamper the extrapolation of strain rates deduced from porphyroblasts to outcrop, let alone regional scales.

3.7.1 The Case for Non-Rotation

A porphyroblast rotation of approximately 170° in simple shear flow is theoretically reached at a shear strain of 5.94, or a maximum stretch of 6.10. In a simple shear dominated system, a strain of this magnitude would be expected to produce well-developed stretching lineations aligning (N-S) normal to the spiral axes that strike predominately E-W. However, there is no evidence of stretching lineations with this orientation. Instead, spiral axes are subparallel to intersection- or crenulation-lineations and fold-axes as predicted by the non-rotation model. Secondly, the inclusion trails exhibit similar vertical and horizontal preferred orientations as documented previously in other metamorphic rocks (e.g. Bell et al., 1992; Hayward, 1992; Stallard and Hickey, 2001; Aerden et al. 2013; Bell and Sapkota; 2012) as evidence for a polyphase origin of these

microstructures. Viete et al. (2018), in their recent study show evidence for four pulses in hydrostatic pore pressure recorded by oscillations in garnet growth zonation occurring within 300,000 years. This hundred thousand year timescale lies between the 10 kyr cycle of mega earthquakes, and the 1 Myr cycle of burial-exhumation cycles or “yo-yo” tectonics (Rubato et al., 2011). However, this is similar to the 100 kyr timescale for three stress permutations indicated by our zoned garnet chronology. Therefore, changes in the magnitude of the mean stress revealed by Viete et al. (2018) could be closely related to changes in the orientation of the principal stress axes recorded by spiral garnets, reflecting the dynamics of an orogenic wedge.

3.7.2 The Case for Rotation

For a rotational origin of sample 27.1.2, the garnets overgrew a progressively deforming matrix, where the simple shear component of deformation induced porphyroblast rotation forming the observed spiral inclusion trails. In a simple shear dominated system, the calculated shear strain of 5.94 would be expected to produce stretching lineations oriented normal to the axes of rotation (i.e. the axis of kinematic vorticity), which is not observed in 27.1.2. However, during wrench dominated transpression, where shortening occurs across a shear zone, stretching lineations can flip orientation to become parallel with the axis of kinematic vorticity (i.e. the porphyroblast rotation axis) (Teyssier et al., 1995; Tikoff and Fossen, 1999). A wrench transpressional dominated system could therefore produce the observed relationships between the orientation of spiral axes within garnets and the orientation of macroscopic structural fabrics such as lineations and fold-axes in the surrounding matrix from sample 27.1.2,

without the need to develop multiple foliations by invoking the model of Bell and Johnson (1989).

3.8 CONCLUSION

The rapid 100,000 year timescale over which these microstructures formed is the novel result of this study. These are some of the fastest growing spiral garnets ever documented outside of a subduction zone setting, where such fast growth rates are more likely to occur (e.g. Dragovic, 2012). In addition, figure 3.6.2 clearly illustrates, however calculated, these spiral garnets record strain rates about an order magnitude faster than any directly measured by geochronological methods. Whichever process is chosen for the formation of the spiral garnets from the NFC, either via shear inducted rotation, or by the episodic overgrowth of successive suborthogonal foliations, it occurred on a timescale far faster than the conventional thinking about this microstructures would suggest. For that reason, the results of this study may require a reassessment of the timescales of deformational and metamorphic processes during orogenesis.

3.9 SUPPLEMENTRY MATERIAL FOR CHAPTER 3

Sample Description

Sample 27.1.2 is a garnet-bearing, kyanite, chloritoid, quartz micaschist with abundant rutile and minor apatite, zircon, and allentite. Garnet porphyroblasts range up to 15 mm in diameter with spiral inclusion trails curving up to 180 degrees. This sample was collected by Domingo Aerden in the summer of 2014 from the cover sequence of the Ophiolite unit of the Mulhacén Complex. This unit is interpreted as metamorphosed oceanic sediments from the Mesozoic Iberian paleomargin (Puga et al., 2011). Eclogitized

mafic lenses associated with these metamorphosed sediments have been dated using Lu-Hf and Rb-Sr dating to between 20 and 14 Ma (e.g. Platt et al., 2013; Kirchner et al., 2016).

Microstructural Analysis

Multiple horizontal and vertical slabs were cut from the sample, coarsely polished and photographed. Line tracings of all inclusion-trail patterns visible in these photographs highlight the presence of predominately E-W trending truncations that separate quartz inclusion-rich garnet cores from more pure-garnet rims. Various vertical N-S cuts show inclusion trails curving up to 180°. The 3D geometry of the inclusion-trails was studied further with X-ray Tomography (XRT) in a companion sample (46.8.1) taken less than 2 meter away from sample 27.1.2. The XRT data allowed us to measure the axes of spiral inclusion trails in individual garnets by applying the technique of Hayward (1992) to sets of radial virtual slices passing through garnet centers. The XRT scan of spiral axes from 18 large garnet from sample 46.8.1 show an ENE-WSW trend maximum that agrees with the broad E-W maximum defined by the strikes of truncations that were measured on horizontal slabs of 27.1.2 (Figure 3.9.1). The spiral axes are also subparallel to the axes of meter-scale folds present in the outcrop with south vergence and steeply north dipping axial planes. A similar maxima is defined by fold axes measured in a larger region extending up to 3 km east of the outcrop.

Chemical Mapping and Micro-Drilling of sample 27.1.2

Four microstructurally-characterized garnets ranging from 8 to 10 mm in diameter exhibiting clear and representative inclusion trails were chosen for zoned Sm-Nd geochronology. Each garnet was cut through its geometric center and polished to form 1

mm thick sections. Garnets were analyzed on the electron microprobe at the University of Granada to make elemental zonation maps of Mn, Ca, Fe, and Mg. In addition, electron microprobe point transect were made across all four garnets (Figure 3.9.2 and 3.9.3). These point transects will be used for future thermodynamic modelling. Using the Mn zonation maps and inclusion trail truncations, three distinct growth zones were discernable from garnets B8 (Figure 3.9.4), B9 (Figure 3.9.5), and E2 (Figure 3.9.6), and two distinct growth zones from garnet D1 (Figure 3.9.7). Based upon Mn concentration and inclusion trail geometry, the core of garnet D1 was interpreted to be contemporaneous with the median zones of garnets B8, B9, and E2. Upon arrival at Boston College garnet wafers were prepared for micro-drilling by removing them from the glass slide and gluing them to a carbon block using Crystalbond™. Growth zones from within a single garnet were individually isolated for Sn-Nd dating using the Micromill drilling system from New Wave. After drilling, each garnet zone was removed from the carbon block and ultrasonicated in acetone to remove any residual Crystalbond™. Once cleaned, the zones were crushed and handpicked to obtain a visibly pure garnet separate.

Due to the small sample volume available, zones from multiple garnets were combined together to ensure there was sufficient material to ensure a successful analysis. The garnet zones were combined as follows. Cores (zone 1) and medians (zone 2) from garnets B8, B9, and E2 were combined together. Rims (zone 3) from garnets B8 and E2 were combined; however, there was sufficient sample material to analyze the rim (zone 3) from B9 separately. The core and rim zones from garnet D1 were analyzed separately. The combination of garnet zones is detailed in Table 3.1. Once combined, the zones were crushed and picked to mechanically remove any inclusions, once the zone separates

deemed visibly clean they were crushed and sieved to obtain two grain-size populations, a coarser (garnet) fraction with a grain-size of 75 – 150 μm and a finer (garnet powder) fraction with a grain-size of $\leq 75 \mu\text{m}$. The 75 – 150 μm grain-size has been shown by Pollington and Baxter (2010) to be the ideal grain-size to both maximize access to inclusion phases while mitigating the amount of sample loss during the partial dissolution procedure. All micro-drilling and mineral extraction was conducted at the Boston College Mineral Separation Laboratory.

Clean Lab Procedures and Isotopic Analysis

In the clean lab, the resulting twelve separates were put through a partial dissolution procedure consisting of alternating nitric and HF steps to dissolve contaminating inclusion phases. All separates were initially put in 2 mL of 7N nitric for a least 2 hours at 120°C, this processes was used to dissolve any exposed inclusion phases. Next the separates where combined with anywhere from 15 - 100 μL of concentrated HF + 1 mL of MQ H₂O for an additional 2+ hours on the hot plate. The goal of this step was to dissolve any silicate inclusion phases, as well as, dissolve a percentage of garnet material to access deeper inclusions. Following the HF step, the separates were put back in the 7N nitric to break up any accumulation of secondary fluorides. These alternating nitric – HF steps were continued until the separate was deemed “clean”. In cases with sufficient starting sample mass, separates were deemed clean after approximately 75 – 95% sample loss. However, with a limited sample mass available, as was the case with garnet zones from 27.1.2, the garnet and garnet powder separates were deemed clean after enough sample mass was dissolved, so that assuming a clean garnet concentration of 0.3 ppm Nd would result in no less than 1-2 ng of Nd remaining for TIMS analysis. Following full dissolution, the

isolation of samarium and neodymium was accomplished using the three column procedure of Harvey and Baxter (2009). All isotopic ratios were analyzed on an Isotopx Phoenix Thermal Ionization Mass Spectrometer (TIMS); over the period of the analysis the Ames 4ng NdO $^{143}\text{Nd}/^{144}\text{Nd}$ value was 0.512152 ± 13.28 ppm (2σ) ($n=32$). Nd samples and standards was loaded onto single Re filaments with a Ta₂O₅ activator added to facilitate greater sample ionization. Sm samples and standards was loaded onto single Ta filaments with a H₃PO₄ binder added. All sample preparation and isotope analyses were performed at the Boston College Center for Isotope Geochemistry.

Isotope Data

Table 3.3 shows all of the obtained isotope ratios and concentrations from this study. Eight of the twelve prepared zone separates were successfully analyzed. Two failed to produce acceptable data due to sample loading errors, the sample flipped underneath the filament, and two were deemed dirty due to low (< 0.34) $^{147}\text{Sm}/^{144}\text{Nd}$ ratios, reflecting likely contamination from mineral inclusions. For comparison clean garnets from this study had $^{147}\text{Sm}/^{144}\text{Nd}$ ratios ranging from 1.00 to 4.47. As a result, these four separates were not included in the age calculations. All zone separates was paired with four matrix separates and one whole rock separate from which it is assumed the garnets grew in isotopic equilibrium. Raw isotope data was reduced using Tripoli 4.9 data processing software (Bowring *et al.*, 2011). All isotopic and age errors are reported at 2σ standard error. In cases where the internal precision for a given analysis was better than the external precision, the external is reported. All isochron ages were calculated using Isoplot 4.15 (Ludwig, 2003). Excluding the unacceptable data, the combined cores (zone 1) yielded an age of 13.60 ± 0.31 Ma (MSWD = 0.98; $n=7$), the combined medians (zone 2) yielded an

age of 13.37 ± 0.36 Ma (MSWD = 1.4; n=8), and the rims (zone 3) yielded an age of 13.28 ± 0.48 Ma (MSWD = 0.98; n=8). Isochron diagrams for these zones are shown in figures 3.9.8– 3.9.10.

4. DATA TABLES

This section compiles all of the data tables referenced in chapters two and three.

Lch. = leachate separate

Gt. = garnet separate with sieved grain-size between 75 – 150 microns

Pwd. = garnet powder separate with a sieved grain-size less than 75 microns

Alq. = aliquot taken from a larger storage volume

4.1 DATA TABLES FROM CHAPTER 2

Table 2.1 Summary of isotopic data for bulk garnet analysis of sample A7

Sample	Nd loaded (ng)	Nd ppm	Sm ppm	¹⁴⁷Sm/ ¹⁴⁴Nd	± 2 S.E.	¹⁴³Nd/ ¹⁴⁴Nd	± 2 S.E.	¹⁵⁰Nd/ ¹⁴⁴Nd
whole rock alq1	9.589	31.388	5.882	0.113362	0.000010	0.512017	0.000005	1.044
whole rock alq2	31.178	31.361	5.897	0.113740	0.000013	0.512024	0.000010	1.056
Gt. pwd. alq1	1.457	0.523	2.316	2.680296	0.003866	0.512421	0.000043	2.203
Gt. pwd. alq2	2.514	0.510	2.297	2.725160	0.000438	0.512414	0.000022	1.682
Gt. pwd. lch 2	2.596	0.819	2.251	1.663106	0.000209	0.512246	0.000013	1.575
Gt. A alq 1	5.329	1.026	3.209	1.892517	0.000734	0.512241	0.000013	0.649
Gt. A alq 2	5.167	1.020	3.192	1.893075	0.000315	0.512247	0.000024	1.378
Gt. A lch 3	6.289	1.749	2.621	0.906284	0.000250	0.512141	0.000028	0.670
Gt. A lch 3 alq2	11.556	1.736	2.602	0.906427	0.000112	0.512134	0.000011	0.986

Table 2.2 Summary of isotopic data for bulk garnet analysis of sample B5

Sample	Nd loaded (ng)	Nd ppm	Sm ppm	¹⁴⁷Sm/ ¹⁴⁴Nd	± 2 S.E.	¹⁴³Nd/ ¹⁴⁴Nd	± 2 S.E.	¹⁵⁰Nd/ ¹⁴⁴Nd
whole rock alq1	62.969	45.125	8.636	0.115771	0.000015	0.512006	0.000005	0.787
Gt. A	0.721	0.215	0.771	2.174158	0.000489	0.512344	0.000039	5.119
Gt. A lch 1	2.936	0.440	0.740	0.735762	0.000285	0.512049	0.000014	1.785
Gt. B	1.535	0.213	0.741	0.2099291	0.001167	0.512167	0.000126	1.013
Gt. pwd 1	1.854	0.731	0.741	0.612982	0.000064	0.512100	0.000014	1.785

Table 2.3 Summary of isotopic data for bulk garnet analysis of sample F8

Sample	Nd loaded (ng)	Nd ppm	Sm ppm	¹⁴⁷Sm/ ¹⁴⁴Nd	± 2 S.E.	¹⁴³Nd/ ¹⁴⁴Nd	± 2 S.E.	¹⁵⁰Nd/ ¹⁴⁴Nd
whole rock alq1	49.641	35.593	6.8	0.116307	0.000014	0.511935	0.000008	0.913
Gt. Cl	1.329	0.151	0.377	1.512787	0.004852	0.512260	0.000025	1.787
Gt. Cl lch2	0.833	0.197	0.361	1.110684	0.000194	0.512088	0.000021	1.726
Gt. Dr	0.416	0.132	0.398	1.823000	0.000188	0.512243	0.000042	3.094
Gt. a	3.497	0.199	0.427	1.296198	0.000217	0.512137	0.000009	1.009

Table 2.4 Summary of isotopic data for bulk garnet analysis of sample F16

Sample	Nd loaded (ng)	Nd ppm	Sm ppm	¹⁴⁷Sm/ ¹⁴⁴Nd	± 2 S.E.	¹⁴³Nd/ ¹⁴⁴Nd	± 2 S.E.	¹⁵⁰Nd/ ¹⁴⁴Nd
whole rock alq1	11.490	37.16 6	7.535	0.119815	0.000026	0.511992	0.000013	0.846
whole rock alq3	9.602	37.40 4	7.387	0.119471	0.000013	0.512003	0.000005	0.947
Gt. pwd.	2.742	0.590	2.049	2.101898	0.000300	0.512322	0.000008	1.556
Gt. pwd. lch	5.156	0.893	2.035	1.378931	0.000168	0.512204	0.000010	1.271
Gt. D lch	2.144	0.529	1.752	2.005170	0.000234	0.512322	0.000011	1.944
Gt. B	5.124	0.724	2.552	2.133227	0.001611	0.512199	0.000747	0.585
Gt. C	0.827	1.103	2.812	1.543676	0.000776	0.512269	0.000071	0.532

Table 2.5 Summary of isotopic data for bulk garnet analysis of sample MT8

Sample	Nd loaded (ng)	Nd ppm	Sm ppm	¹⁴⁷Sm/ ¹⁴⁴Nd	± 2 S.E.	¹⁴³Nd/ ¹⁴⁴Nd	± 2 S.E.	¹⁵⁰Nd/ ¹⁴⁴Nd
whole rock alq1	2.753	2.981	0.775	0.157095	0.000043	0.511985	0.000020	8.181
whole rock alq2	2.861	3.106	0.841	0.163731	0.000104	0.511999	0.000013	7.900
whole rock alq4	16.074	3.123	0.802	0.155420	0.000018	0.122993	0.000008	1.029
Gt. pwd alq1	0.450	0.182	0.408	1.356609	0.000658	0.511958	0.000099	7.607
Gt. pwd alq2	1.989	0.177	0.402	1.377123	0.000238	0.512210	0.000010	1.201
Gt. A alq1	1.825	0.341	0.539	0.955476	0.000152	0.512139	0.000021	2.286
Gt. A alq2	3.160	0.336	0.528	0.950350	0.000137	0.512113	0.000019	1.006
Gt. A lch 3 alq2	9.2739	0.631	0.511	0.489618	0.000076	0.512070	0.000010	0.738
Gt. UC	11.169	0.439	0.770	1.061256	0.000512	0.512151	0.000012	0.425
Gt. UC lch 2	5.644	0.799	0.984	0.744498	0.000126	0.512098	0.000008	0.668
Gt. pwd. UC	8.342	0.526	0.713	0.820384	0.000280	0.512104	0.000006	0.449

Table 2.6 Summary of isotopic data for bulk garnet analysis of sample 27.2.1

Sample	Nd loaded (ng)	Nd ppm	Sm ppm	¹⁴⁷Sm/ ¹⁴⁴Nd	± 2 S.E.	¹⁴³Nd/ ¹⁴⁴Nd	± 2 S.E.	¹⁵⁰Nd/ ¹⁴⁴Nd
whole rock 1 aq1	60.592	42.088	8.197	0.117807	0.000015	0.512017	0.000005	0.785
whole rock 2 aq2	58.665	45.472	8.828	0.117443	0.000017	0.512009	0.000005	0.735
Gt. A	84.051	4.563	3.020	0.400369	0.000176	0.512048	0.000005	0.333
Gt. A lch 1	165.993	21.642	5.595	0.156389	0.000100	0.512009	0.000011	0.267
Gt. B	5.207	0.576	1.666	1.750130	0.001331	0.512208	0.000057	0.731
Gt. B lch 3	2.503	0.462	1.599	2.102950	0.000328	0.512191	0.000012	1.451
Gt. D	6.472	1.032	2.559	1.499316	0.000533	0.512118	0.000017	0.615
Gt. E	6.270	0.854	2.261	1.600732	0.000695	0.512127	0.000008	0.677
Gt. pwd 2	24.124	2.273	1.370	0.304393	0.000046	0.512038	0.000017	0.556
Gt. pwd 3	36.666	5.758	2.854	0.299869	0.000065	0.512027	0.000007	0.446

Table 2.7 Summary of isotopic data for bulk garnet analysis of sample 27.1.2

Sample	Nd loaded (ng)	Nd ppm	Sm ppm	¹⁴⁷Sm/ ¹⁴⁴Nd	± 2 S.E.	¹⁴³Nd/ ¹⁴⁴Nd	± 2 S.E.	¹⁵⁰Nd/ ¹⁴⁴Nd
Whole rock 1	10.327	34.165	6.570	0.11632	0.000088	0.511997	0.000021	0.987
Gt. A	2.235	0.419	0.232	0.33562	0.000049	0.512035	0.000005	0.511
Gt. B	11.476	1.957	3.467	1.07171	0.000268	0.512055	0.000012	0.631
Gt. C	11.48	1.089	2.631	1.46163	0.001771	0.512131	0.000009	0.718
Gt. pwd 1	6.731	1.267	4.430	2.1148	0.000558	0.512193	0.000007	0.909

Table 2.8 Summary of isotopic data for bulk garnet analysis of sample 53.10.1

Sample	Nd loaded (ng)	Nd ppm	Sm ppm	¹⁴⁷Sm/ ¹⁴⁴Nd	± 2 S.E.	¹⁴³Nd/ ¹⁴⁴Nd	± 2 S.E.	¹⁵⁰Nd/ ¹⁴⁴Nd
whole rock alq1	56.653	41.018	8.152	0.120213	0.000014	0.512005	0.000008	0.989
Gt. A	9.883	1.220	1.181	0.585535	0.000141	0.512074	0.000008	0.485
Gt. B	11.102	1.109	1.160	0.632932	0.000059	0.512081	0.000008	0.926
Gt. C	5.062	1.256	1.550	0.746413	0.00014	0.512079	0.000010	0.611
Gt. Pwd. 1	2.574	0.631	1.245	1.193458	0.000044	0.512107	0.000023	0.813
Gt. Pwd. 2	2.271	0.738	1.125	0.922553	0.00014	0.512116	0.000012	0.867

Table 2.9 Summary of Sm and Nd concentrations and isotopic ratios from bulk samples analyzed in this study

Sample	Material	ng Nd loaded	Nd ppm	Sm ppm	$^{147}\text{Sm}/^{144}\text{Nd}$	$\pm 2 \text{ S.E.}$	$^{143}\text{Nd}/^{144}\text{Nd}$	$\pm 2 \text{ S.E.}$
A7 age 1 = 21.89 \pm 0.86 Ma, MSWD = 0.90; age 2 = 19.2 \pm 1.2 Ma, MSWD = 0								
	Whole rock	9.589	31.388	5.882	0.113362	0.000010	0.512017	0.000005
	Garnet powder	2.514	0.510	2.297	2.725160	0.000438	0.512414	0.000022
	Garnet powder leachate	2.596	0.819	2.251	1.663106	0.000209	0.512246	0.000013
	Garnet	5.329	1.026	3.209	1.892517	0.000734	0.512237	0.000013
	Garnet leachate	11.556	1.749	2.621	0.906284	0.000250	0.512141	0.000028
B5 age = 26.2 \pm 2.5 Ma, MSWD = 2.9								
	Whole rock	62.969	45.125	8.636	0.115771	0.000015	0.512006	0.000005
	Garnet	0.721	0.215	0.771	2.174158	0.000489	0.512344	0.000039
	Garnet powder	1.854	0.731	0.741	0.612982	0.000064	0.512100	0.000014
F8 age 1 = 26.1 \pm 1.4 Ma, MSWD = 1.6; age 2 = 35.6 \pm 2.8 Ma, MSWD = 0								
	Whole rock	49.641	35.593	6.800	0.116307	0.000014	0.511935	0.000008
	Garnet	1.329	0.151	0.377	1.512787	0.004852	0.512260	0.000025
	Garnet	0.416	0.132	0.398	1.823000	0.000188	0.512243	0.000042
	Garnet	3.497	0.199	0.427	1.296198	0.000217	0.512137	0.000009
	Garnet leachate	0.833	0.197	0.362	1.110684	0.000194	0.512088	0.000021
F16 age = 24.95 \pm 0.61 Ma, MSWD = 2.4								
	Whole rock	9.602	37.404	7.387	0.119471	0.000013	0.512003	0.000005
	Garnet	0.827	1.103	2.812	1.543676	0.000776	0.512269	0.000071
	Garnet leachate	2.144	0.529	1.752	2.005170	0.000234	0.512322	0.000011
	Garnet powder	2.742	0.590	2.049	2/101898	0.003000	0.512322	0.000008
	Garnet powder leachate	5.156	0.893	2.035	1.378931	0.000168	0.512204	0.000010
MT8 age = 26.9 \pm 1.5 Ma, MSWD = 0.95								
	whole rock	16.074	3.123	0.802	0.155420	0.000018	0.511993	0.000008
	Garnet powder	1.989	0.177	0.402	1.377123	0.000238	0.512210	0.000010
	Garnet	1.825	0.341	0.539	0.955476	0.000152	0.512139	0.000021
	Garnet	11.169	0.439	0.770	1.061256	0.000512	0.512151	0.000012
	Garnet powder	8.342	0.526	0.713	0.820384	0.000280	0.512104	0.000006
	Garnet leachate	5.644	0.799	0.984	0.744498	0.000126	0.512098	0.000008
27.2.1 age = 12.9 \pm 1.6 Ma, MSWD = 3.5								
	whole rock	60.592	42.088	8.197	0.117807	0.000015	0.512017	0.000005
	whole rock	58.665	45.472	8.828	0.117443	0.000017	0.512009	0.000005
	Garnet	6.472	1.032	2.559	1.499316	0.000533	0.512118	0.000017
	Garnet	6.270	0.854	2.261	1.600732	0.000695	0.512127	0.000008
	Garnet leachate	2.503	0.462	1.599	2.102950	0.000328	0.512191	0.000012
	Garnet powder	36.666	5.758	2.854	0.299869	0.000065	0.512027	0.000007
	Garnet leachate	165.993	21.642	5.595	0.156389	0.000100	0.512009	0.000011
53.10.1 age 1 = 21.8 \pm 2.4 Ma, MSWD = 0.49; age 2 = 16.5 \pm 2.5 Ma, MSWD = 2.9								
	Whole rock	56.653	41.018	8.152	0.120213	0.000014	0.512005	0.000008
	Garnet	9.883	1.220	1.181	0.585535	0.000141	0.512074	0.000008
	Garnet	11.102	1.109	1.160	0.632932	0.000059	0.512081	0.000008
	Garnet	5.062	1.256	1.550	0.746413	0.000140	0.512079	0.000010
	Garnet powder	2.547	0.631	1.245	1.193458	0.000428	0.512107	0.000023
	Garnet powder	2.271	0.738	1.125	0.922553	0.000140	0.512116	0.000012

4.2 DATA TABLES FROM CHAPTER 3

Table 3.1 Summary of individual and combined garnet zone weights throughout the sample preparation process for garnets B8, B9, D1, and E2 from sample 27.1.2. All weights are in mg.

Garnet Zones	Before Combining	Combined Zones	Before crushing	Obtained separate	Before partial dissolution	After partial dissolution	Sample loss (%)
B8 Zone 3	37.0	B8E2 Zone 3	87.0	Garnet	28.77	8.27	71.3%
E2 Zone 3	50.0			Powder	16.50	5.29	67.9%
B8 Zone 1	16.0	B8B9E2 Zone 1	68.5	Garnet	20.1	6.26	68.8%
B9 Zone 1	26.5			Powder	16.00	5.30	66.9%
E2 Zone 1	26.0						
B8 Zone 2	26.0	B8B9E2 Zone 2	90.0	Garnet	27.10	6.25	76.9%
B9 Zone 2	47.5			Powder	17.88	5.25	70.6%
E2 Zone 2	16.5						
B9 Zone 3	101.5	n/a	101.5	Garnet	16.63	6.46	61.2%
				Powder	16.68	3.19	80.9%
D1 Zone 1	29.5	n/a	29.5	Garnet	12.25	5.83	52.4%
				Powder	8.07	3.87	52.0%
D1 Zone 2	108.0	n/a	108.0	Garnet	32.12	9.17	71.5%
				Powder	23.43	4.34	81.5%

Table 3.2 Summary of selected Sm and Nd concentrations and ratios from zoned garnet chronology of sample 27.1.2 used in final age calculations.

Sample	Material	ng Nd loaded	Nd ppm	Sm ppm	$^{147}\text{Sm}/^{144}\text{Nd}$	$\pm 2 \text{ S.E.}$	$^{143}\text{Nd}/^{144}\text{Nd}$	$\pm 2 \text{ S.E.}$
Each of the zones below is matched with these five matrix and whole rock separates								
	Whole rock	40.457	39.453	7.662	0.117473	0.000013	0.512027	0.000007
	Matrix B8	57.456	38.359	7.427	0.116958	0.000013	0.512020	0.000007
	Matrix B9	47.545	30.253	5.732	0.114616	0.000010	0.512025	0.000007
	Matrix D1	66.448	41.486	7.748	0.116046	0.000015	0.512031	0.000007
	Matrix E2	47.931	30.760	5.384	0.116177	0.000013	0.512025	0.000007
Zone 1 (core): age = 13.60 \pm 0.31 Ma, MSWD = 0.98								
	Garnet	2.770	0.442	2.639	3.608321	0.001321	0.512337	0.000008
	Garnet powder	1.869	0.374	2.291	3.707553	0.001079	0.512344	0.000011
Zone 2 (median): age = 13.37 \pm 0.36 Ma, MSWD = 1.40								
	Garnet	3.349	0.536	3.159	3.566838	0.001547	0.512329	0.000008
	Garnet	3.639	0.624	3.549	3.441135	0.002694	0.512310	0.000027
	Garnet powder	10.414	1.984	3.283	1.001238	0.000424	0.512096	0.000008
Zone 3 (rim): age = 13.28 \pm 0.48 Ma, MSWD = 0.98								
	Garnet	3.637	2.655	1.557	0.354775	0.000043	0.512047	0.000007
	Garnet	2.575	0.281	1.808	3.894910	0.001221	0.512347	0.000018
	Garnet powder	1.667	0.431	2.666	3.743721	0.001315	0.512346	0.000016

Table 3.3 Summary of all isotopic data for zoned garnet analysis of sample 27.1.2

Sample	Nd loaded (ng)	Nd ppm	Sm ppm	¹⁴⁷Sm/ ¹⁴⁴Nd	± 2 S.E.	¹⁴³Nd/ ¹⁴⁴Nd	± 2 S.E.	¹⁵⁰Nd/ ¹⁴⁴Nd
Matrix B8	57.456	38.359	7.417	0.116958	0.000013	0.512020	0.000008	0.951
Matrix B9	47.545	30.253	5.732	0.114616	0.000010	0.512025	0.000008	1.142
Matrix D1	66.448	41.489	7.748	0.116046	0.000015	0.512031	0.000008	0.883
Matrix E2	47.931	30.760	5.384	0.116177	0.000013	0.512025	0.000008	1.115
Matrix B6	40.457	39.453	7.662	0.117473	0.000013	0.512027	0.000005	0.873
B6 zone 3 gt	3.637	2.655	1.557	0.354775	0.000043	0.512047	0.000007	0.586
B6 zone 3 gt pwd	16.263	14.785	5.588	0.207827	0.000078	0.512037	0.000005	0.320
B8B9E2 Zone 1 gt	2.670	0.442	2.639	3.608321	0.001321	0.512337	0.000008	1.045
B8B9E2 Zone 1 gt pwd	1.869	0.374	2.291	3.707553	0.001079	0.512344	0.000011	1.369
B8B9E2 Zone 2 Gt	3.349	0.536	3.159	3.566838	0.001547	0.512329	0.000008	0.914
B8B9E2 Zone 2 gt pwd	10.414	1.984	3.283	1.001238	0.000424	0.512096	0.000006	0.441
B8E2 Zone 3 Gt	3.505	0.424	2.287	3.264274	0.001058	0.512332	0.000018	1.113
B8E2 Zone 3 gt pwd	29.916	5.655	3.129	0.334750	0.000180	0.512029	0.000004	0.307
B9 Zone 3 Gt	1.310	0.204	1.511	4.477093	0.001446	0.512490	0.000037	2.048
B9 Zone 3 gt pwd	37.538	11.767	3.054	0.180014	0.000153	0.512015	0.000006	0.269
D1 zone 1 Gt	3.639	0.624	3.549	3.441135	0.002694	0.512310	0.000027	0.605
D1 zone 1 gt pwd	1.003	0.259	1.456	3.397723	0.000887	0.512348	0.000037	1.737
D1 zone 2 Gt	2.575	0.281	1.808	3.894910	0.001221	0.512347	0.000018	1.317
D1 zone 2 gt pwd	1.667	0.431	2.666	3.743721	0.001315	0.512346	0.000016	1.144

5. FIGURES

This section compiles all of the figures referenced in the above three chapters

5.1 FIGURES FROM INTRODUCTION

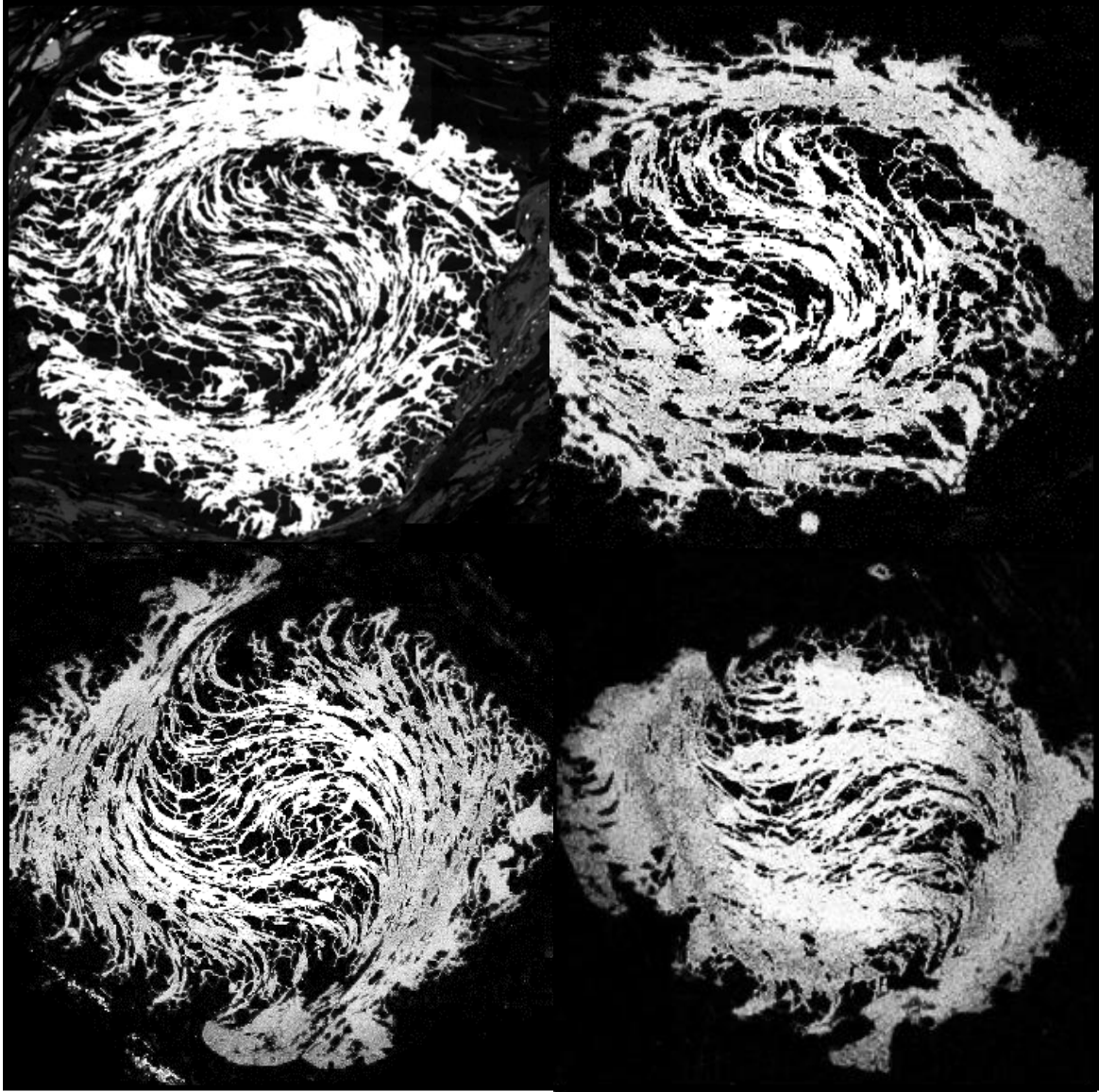


Figure 1.1.1 SEM photos of garnet porphyroblasts from the Nevado-Filabride Complex of the Betic Cordillera hosting spectacular spiral inclusion trails. Each photo is approximately 1 cm across.

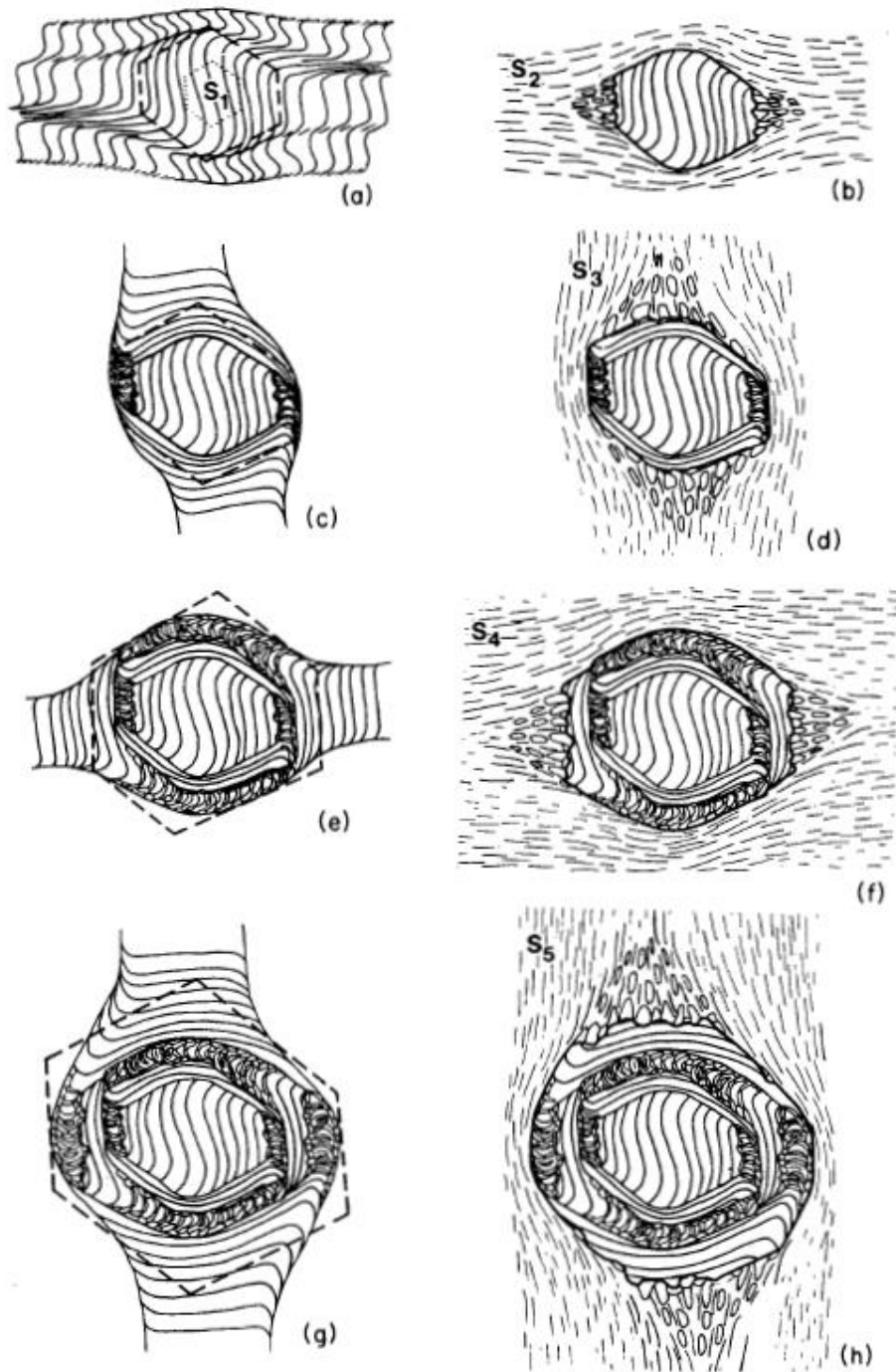


Figure 1.2.1 Model of Bell and Johnson (1989). In this model the inclusion trails represent relicts of multi-generational overprinting of orthogonal foliations (five generations from S_1 - S_5), where no rotation of the porphyroblast occurs. This differs fundamentally from the rotation model of Schoneveld (1979) where only a single foliation is present (Jiang and Williams, 2004).

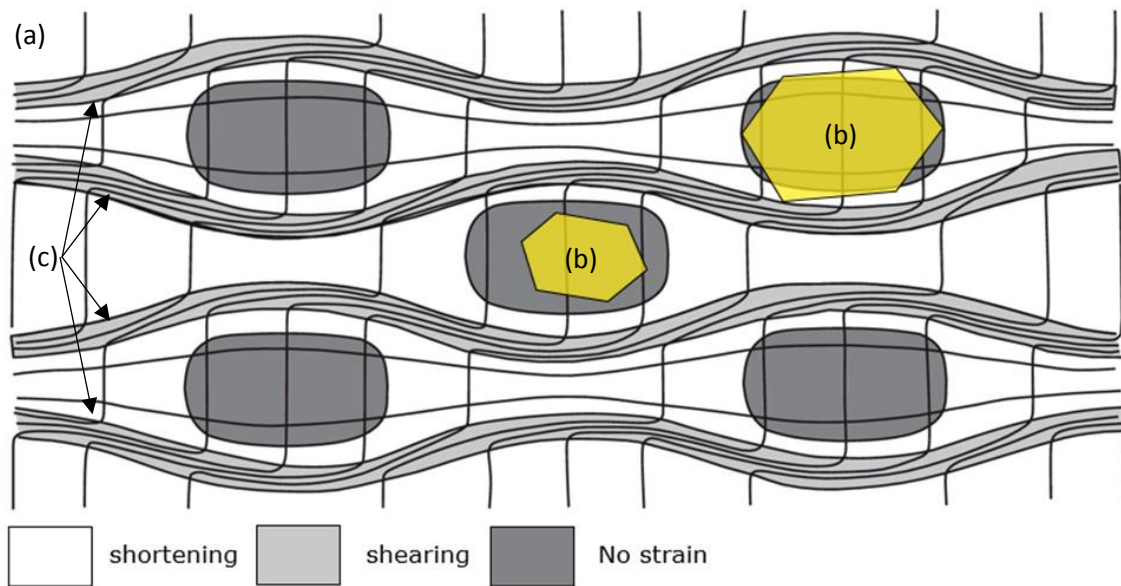


Figure 1.2.2 (Modified after Bell and Bruce (2007)). (a) Shows the partitioning of deformation into zones of no strain, progressive shortening strain, progressive shearing plus shortening strain, and progressive shearing only strain that results from a history of deformation involving progressive bulk inhomogeneous shortening with a component of shear. (b) Yellow hexagons denote porphyroblastic growth in lens of low strain (type 1). (c) The partitioning of non-coaxial deformation around the porphyroblasts.

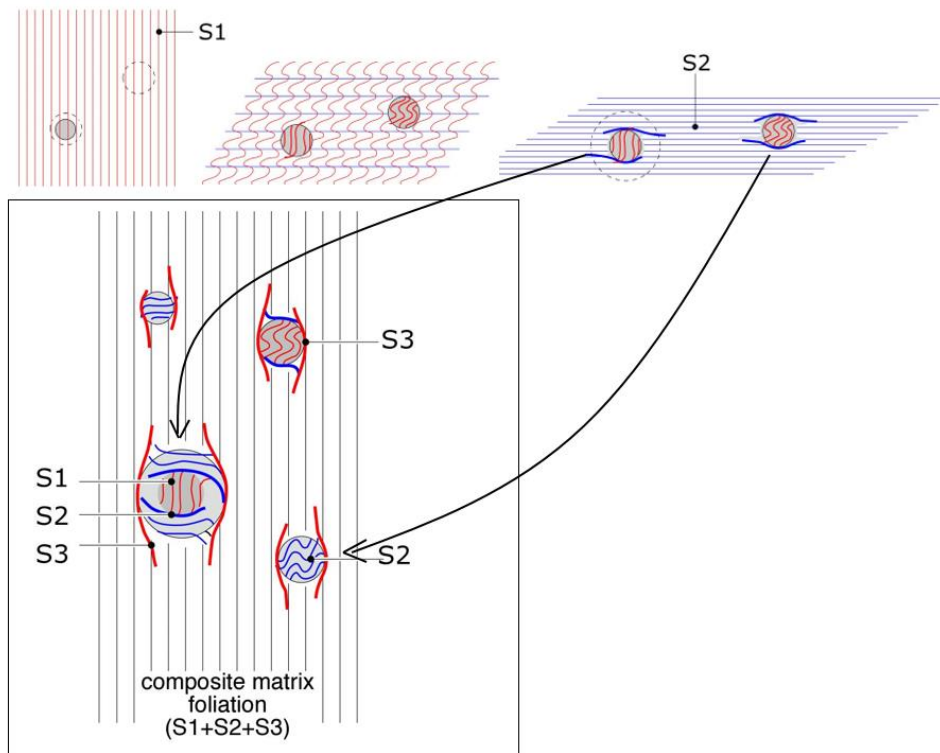


Figure 1.2.3 Modified after Aerden (2004). A conceptual model of progressive porphyroblast overgrowth preserving successive orthogonal crenulations. Porphyroblasts (a) and (b) nucleate during D₂ and preserve the S₁ foliation. During D₃, porphyroblast (b) does not grow, (a) has further growth, and (c) and (d) nucleate and overgrow S₂ foliation.

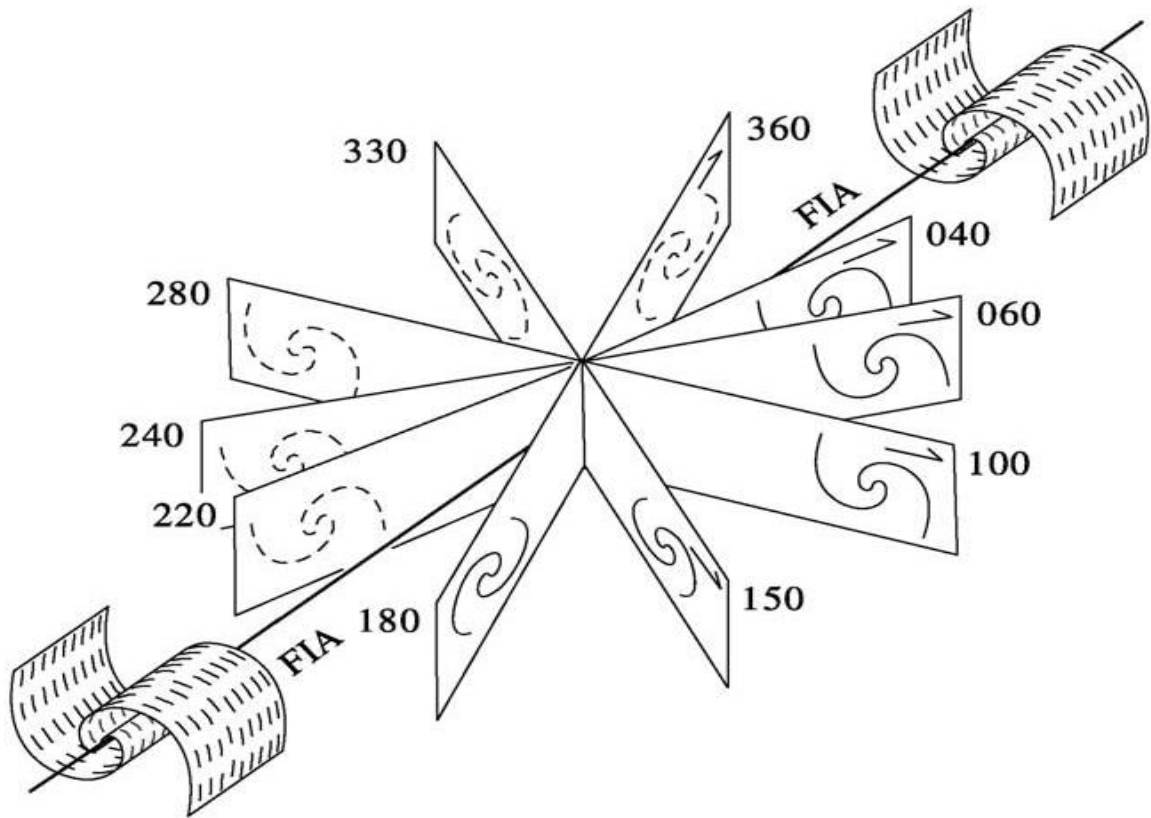


Figure 1.2.4 from Hayward (1992) demonstrates geometrically how the asymmetry of inclusion trail curvature flips as the strike of the FIA is crossed.

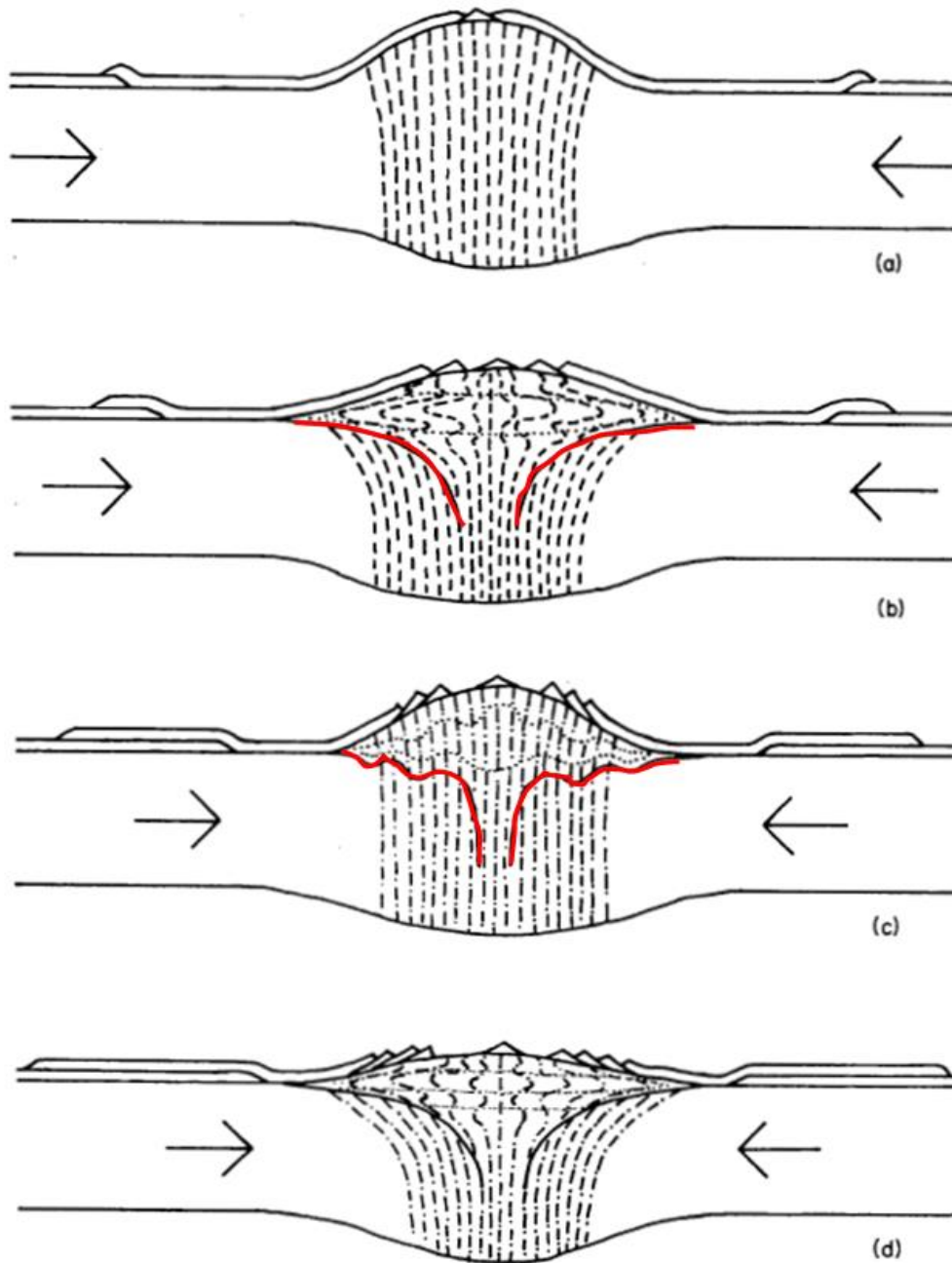


Figure 1.3.1 Modified from Bell and Johnson (1989). A series of conceptual drawing (a-d) showing the tectonic model necessary to explain the orthogonal overprinting foliation preserved as inclusion trails in porphyroblasts (Bell and Johnson, 1989), and development the basal detachment during cyclic crustal shortening and gravitational collapse (see text for further discussion). (a) On set of Crustal shortening. (b) Gravitational collapse and development of basal detachment (red line). (c) Continued Crustal shortening and deformation of basal detachment (red line). (d) Continued gravitational collapse.

5.2 FIGURES FROM CHAPTER 2

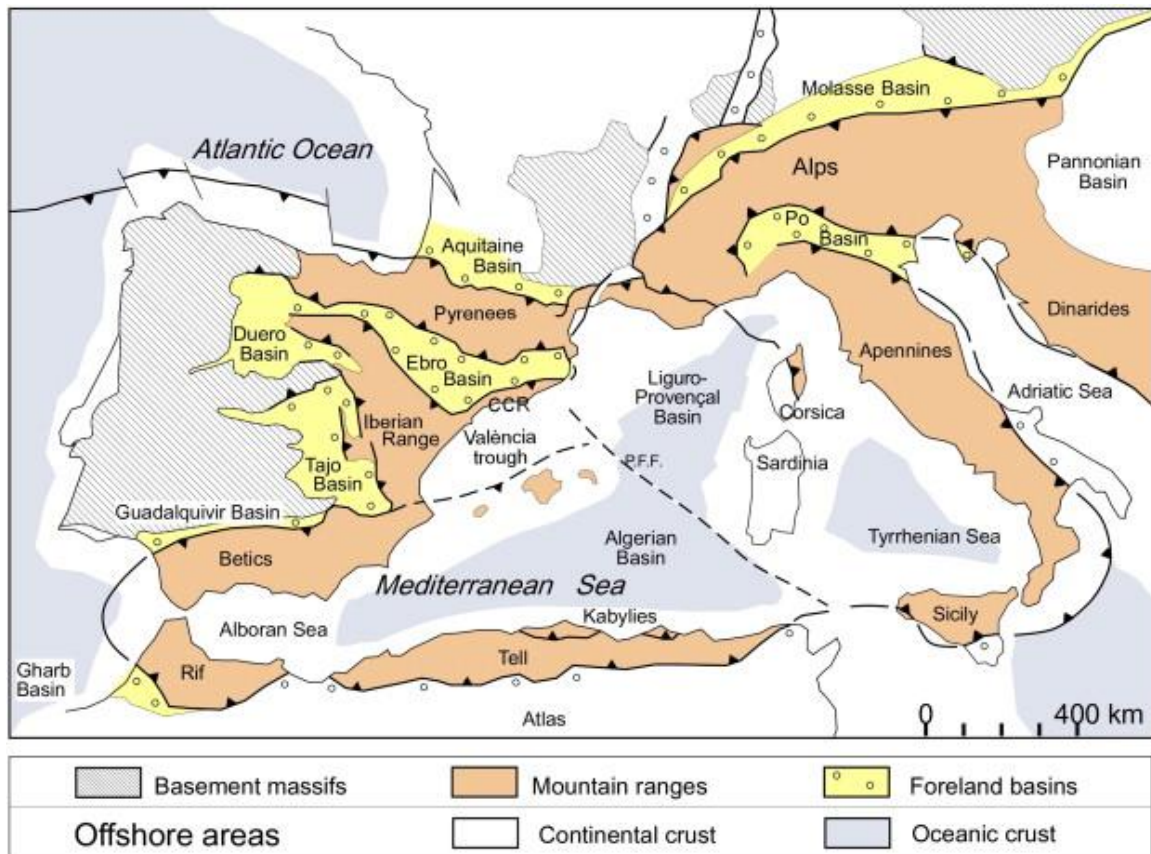


Figure 2.2.1 Tectonic map from Vergés and Sàbat (1999) of the western Mediterranean, highlighting the major orogenic belts and foreland basins.

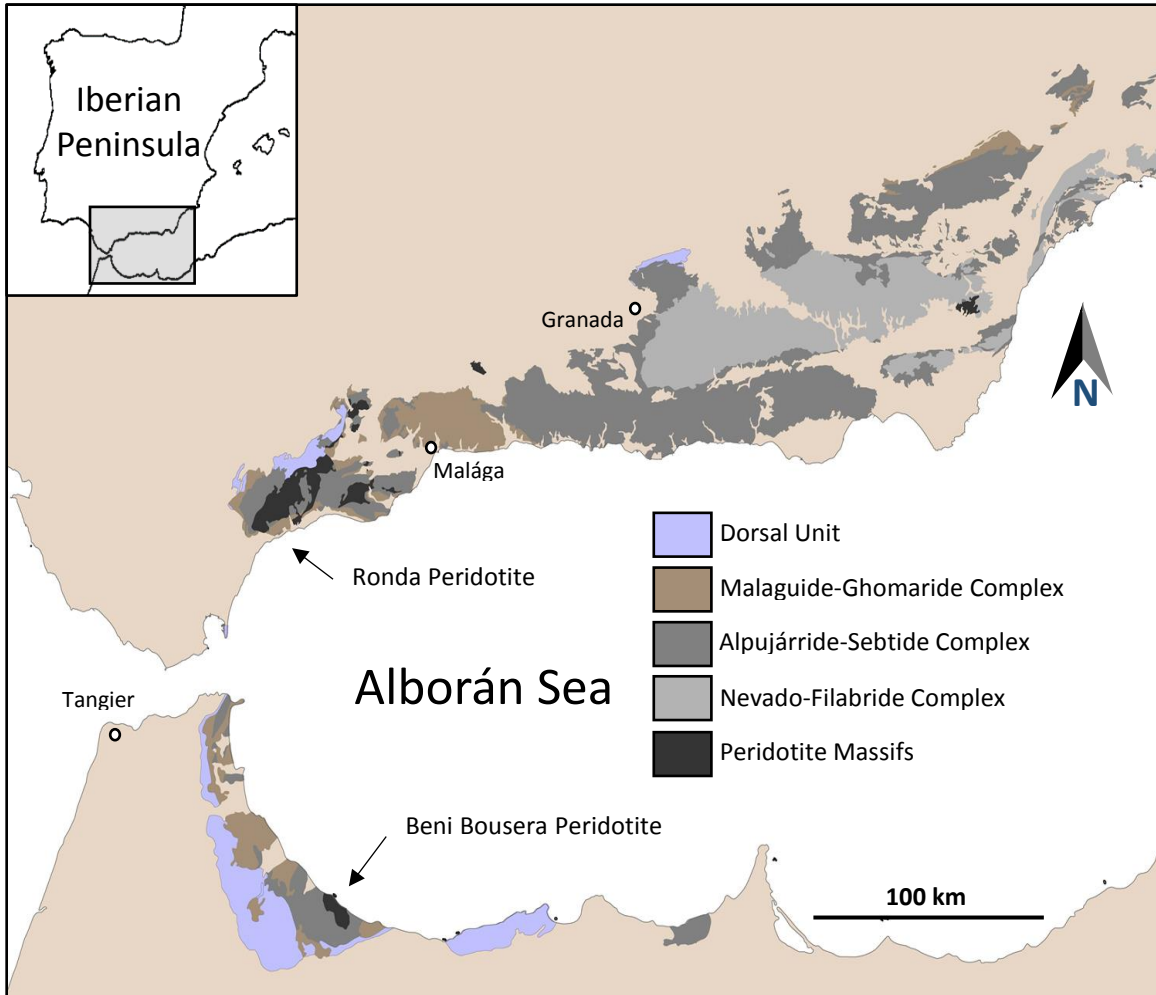


Figure 2.2.2 Geologic map of Internal Zones (Alborán Domain) of the Betic-Rif Arc. Courtesy of Domingo Aerden.



Figure 2.2.3 Photos of Nevado-Filabride Complex. Top photo of Mulhácen Peak (highest point in the Betics) looking north along strike of the anticlinorium from Veleta Peak. Bottom photo showing regional-scale macro foliation. Both photos by author.

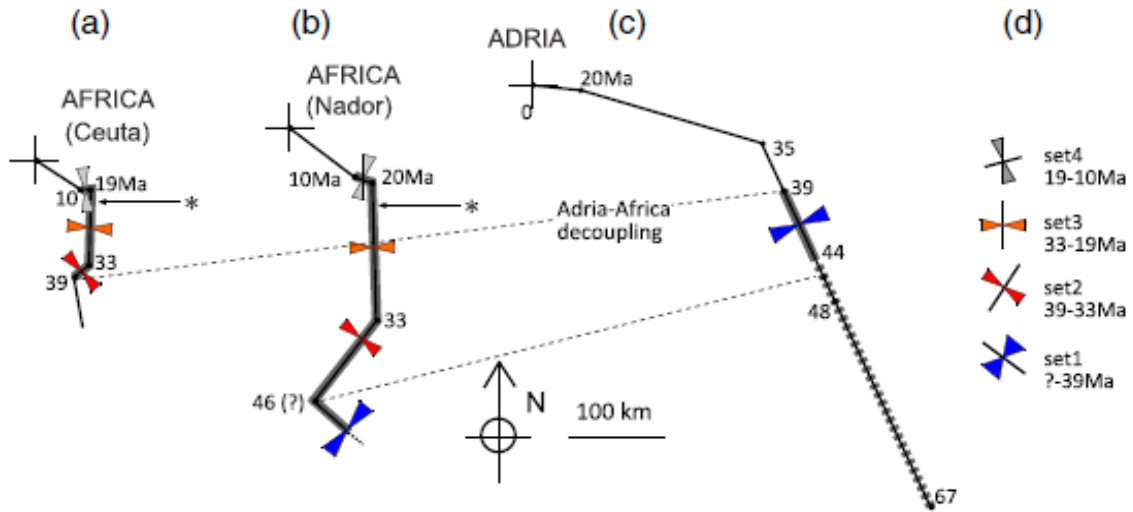


Figure 2.3.1 from Aerden *et al.*, 2013. Correlation of FIA orientations with plate motion in the Betic Cordillera. (a – c) Correlation of FIA orientations to different plate motion reconstruction studies. (d) Proposed FIA ages from Aerden *et al.* (2013).

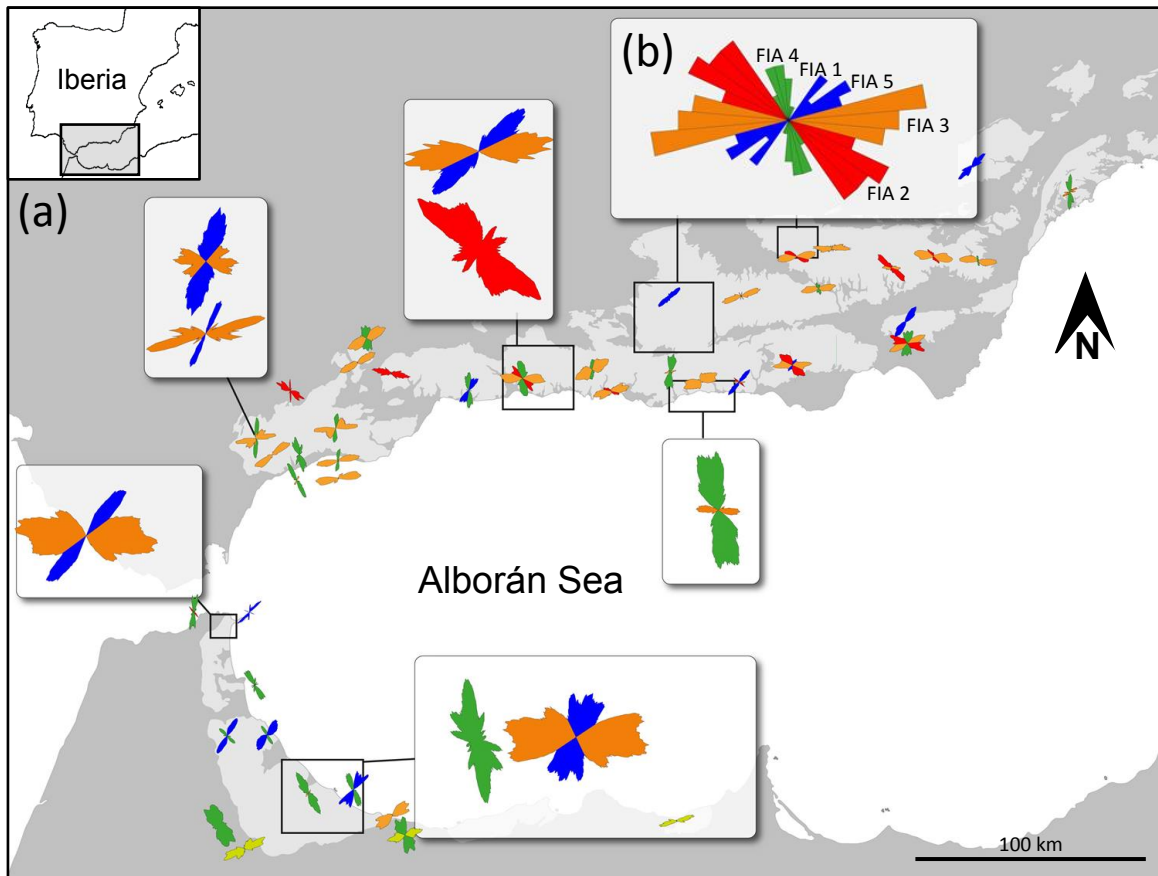


Figure 2.3.2 (a) Map showing location of over 10,000 FIA orientation measurements throughout the Betic-Rif Arc (Courtesy of Domingo Aerden). (b) Rose diagram showing the orientations of the 5 FIA generations, as defined by Aerden et al. (2013) and Ruiz-Fuentes and Aerden (2018).

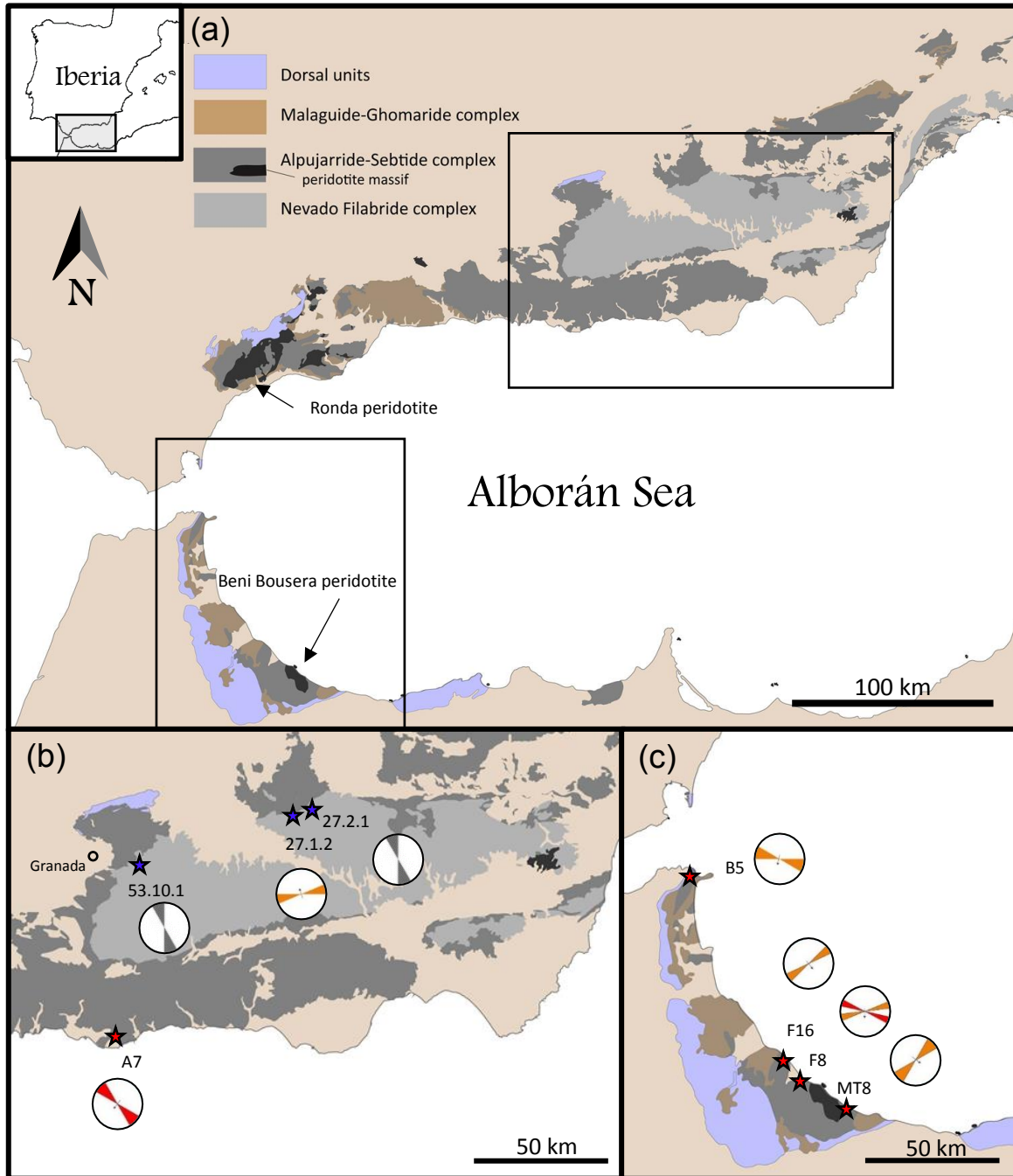


Figure 2.5.1 (a) Geological map of Betic-Rif Arc showing the three metamorphic complexes of the Internal Zones. (b) Location of samples from the Betic Cordillera. (c) Location of samples from the Rif Cordillera. Stars denote location of samples from this study. Blues stars; Nevado-Filabride samples, and red stars; Alpujarride-Sebtide samples.

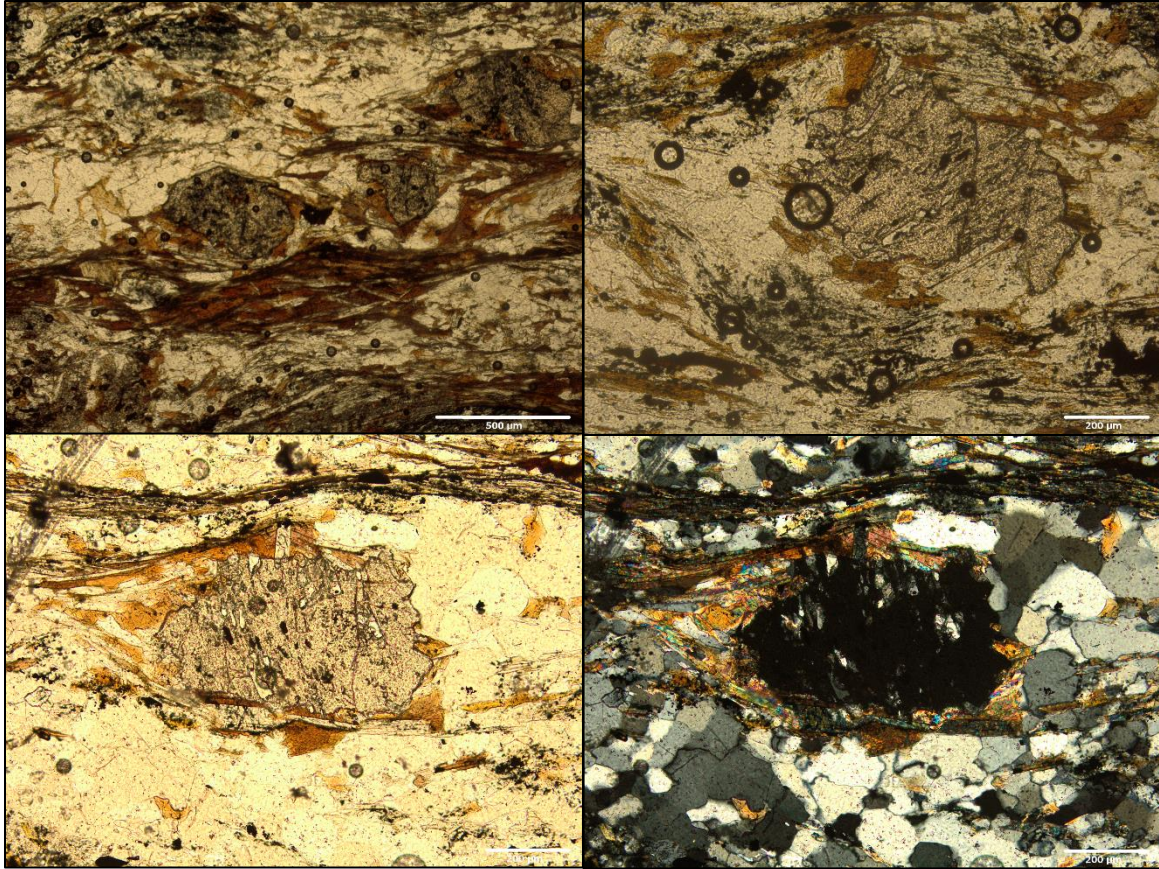


Figure 2.5.2 thin section photos of sample A7

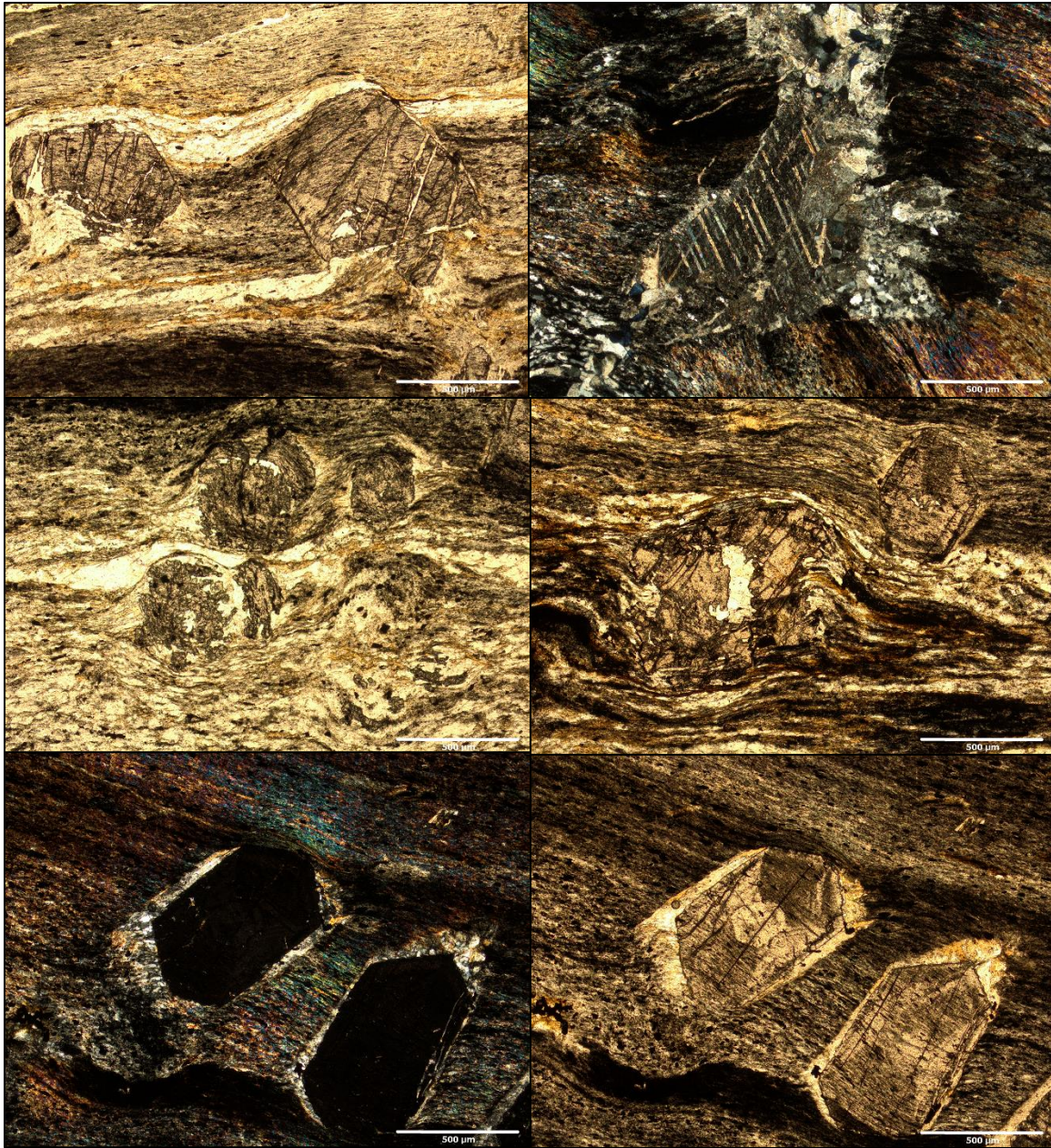


Figure 2.5.3 thin section photos of sample B5

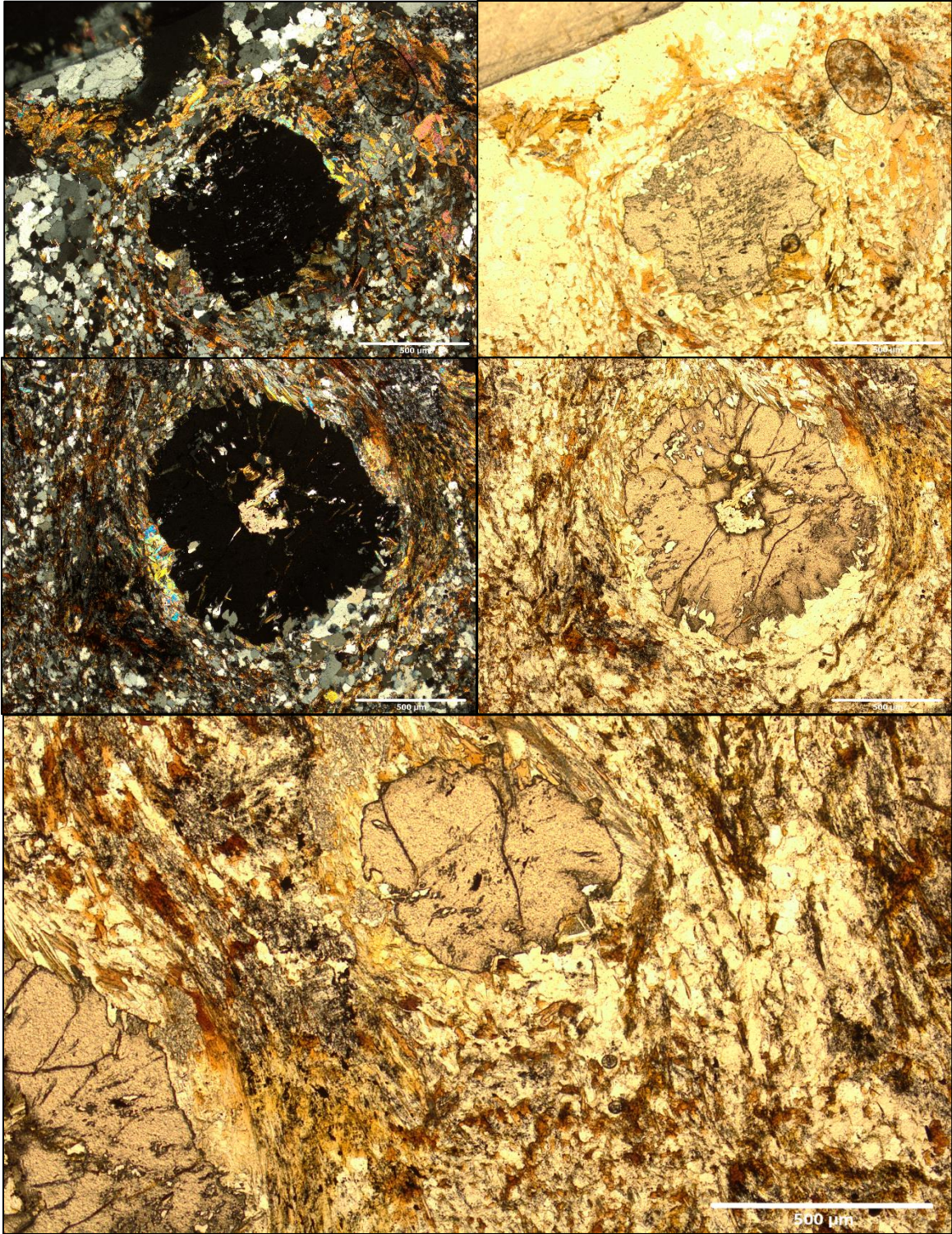


Figure 2.5.4 thin section photos of sample F16

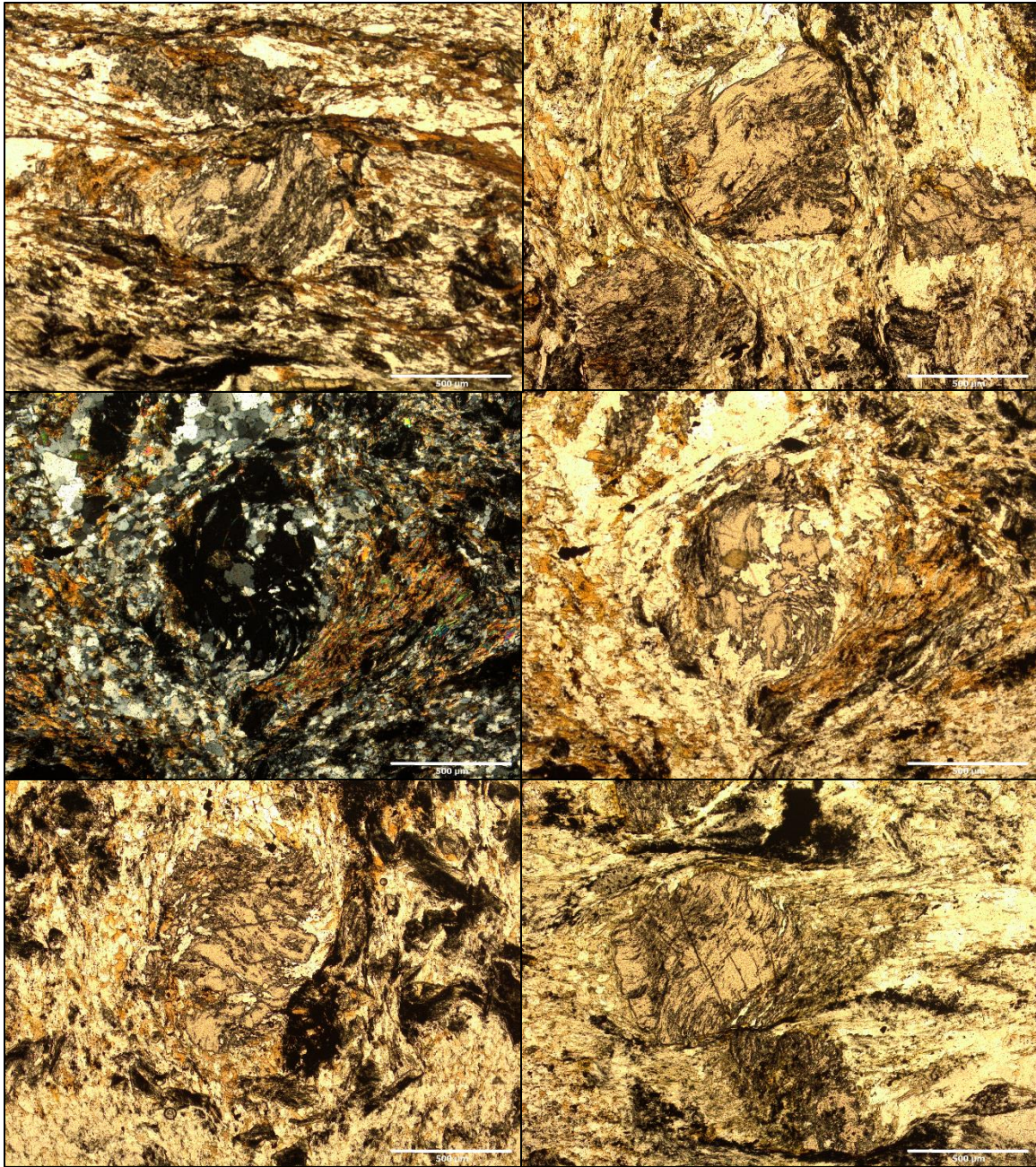


Figure 2.5.5 thin section photos of sample MT8

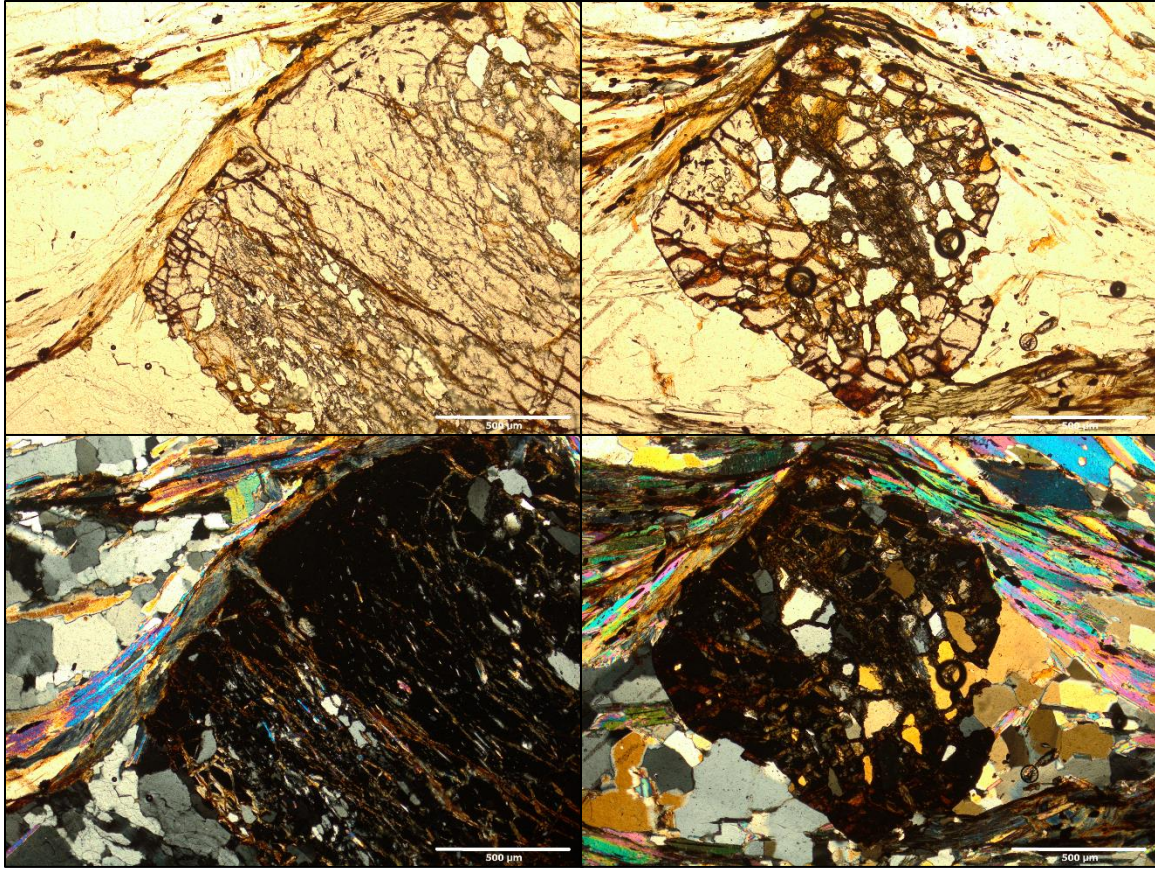


Figure 2.5.6 thin section photos of sample 27.2.1

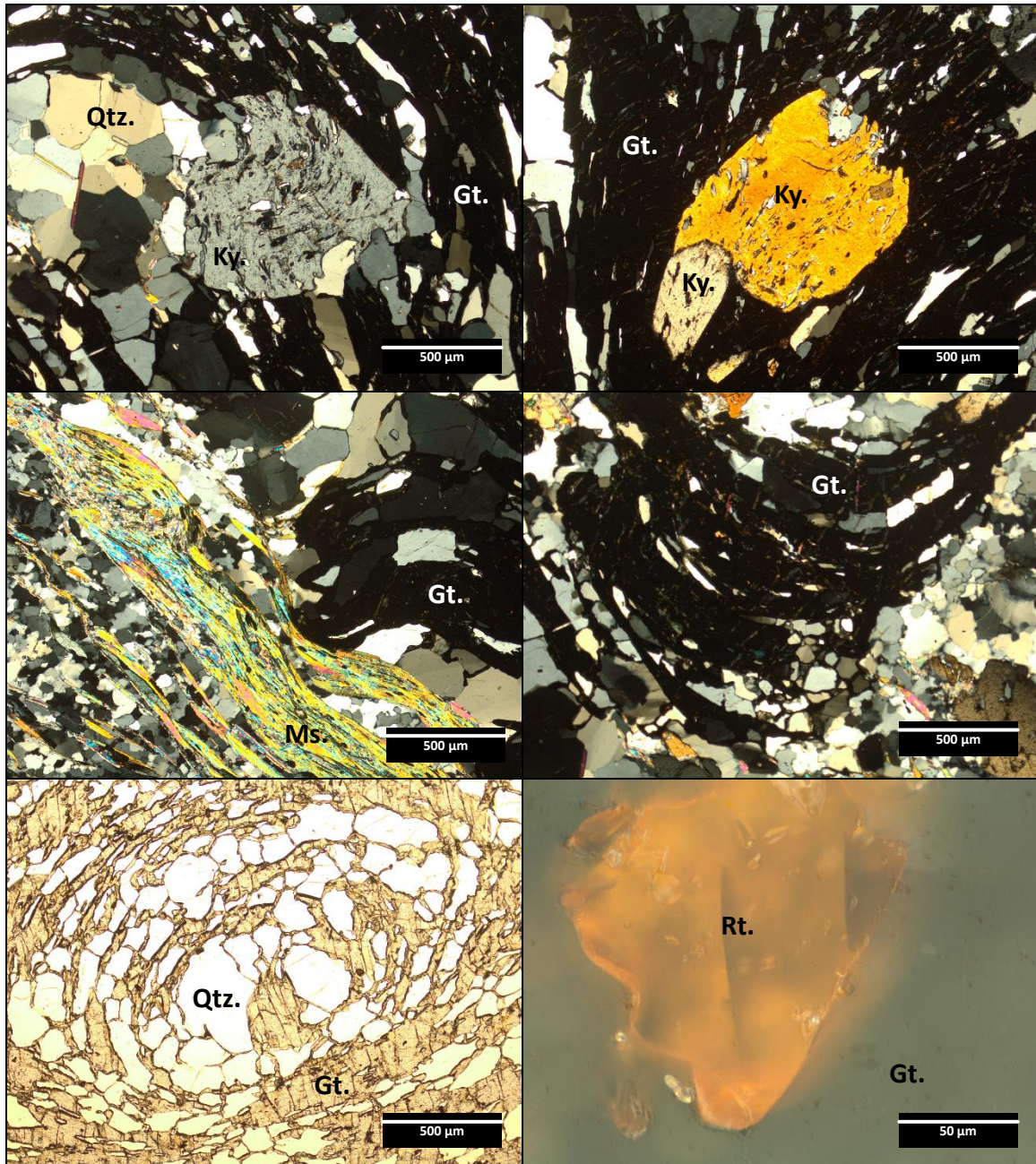


Figure 2.5.7 Thin Section photo of sample 27.1.2. Top left and right XPL photos showing kyanite inclusions within a large garnet porphyroblasts. Middle left photo shows the micaceous foliation against the garnet. Middle right photo shows the spiral nature of the inclusion trails. Bottom left photo in PPL showing garnet core rich in quartz inclusions. Bottom right photo in reflected light showing rutile inclusion in garnet. Gt. = garnet, Ky. = kyanite, Ms. = Muscovite, Qtz = quartz, Rt. = rutile.

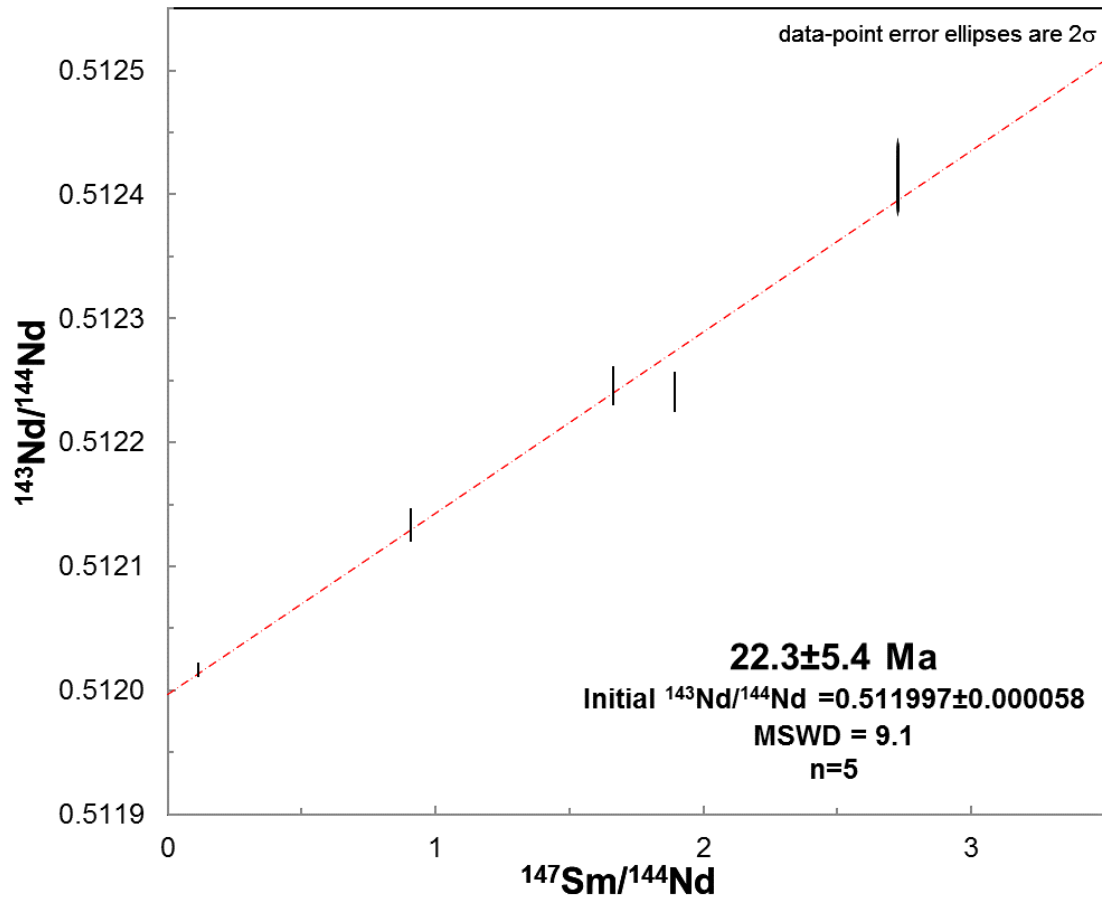


Figure 2.7.1 Five-point isochron including all analyzed data for sample A7

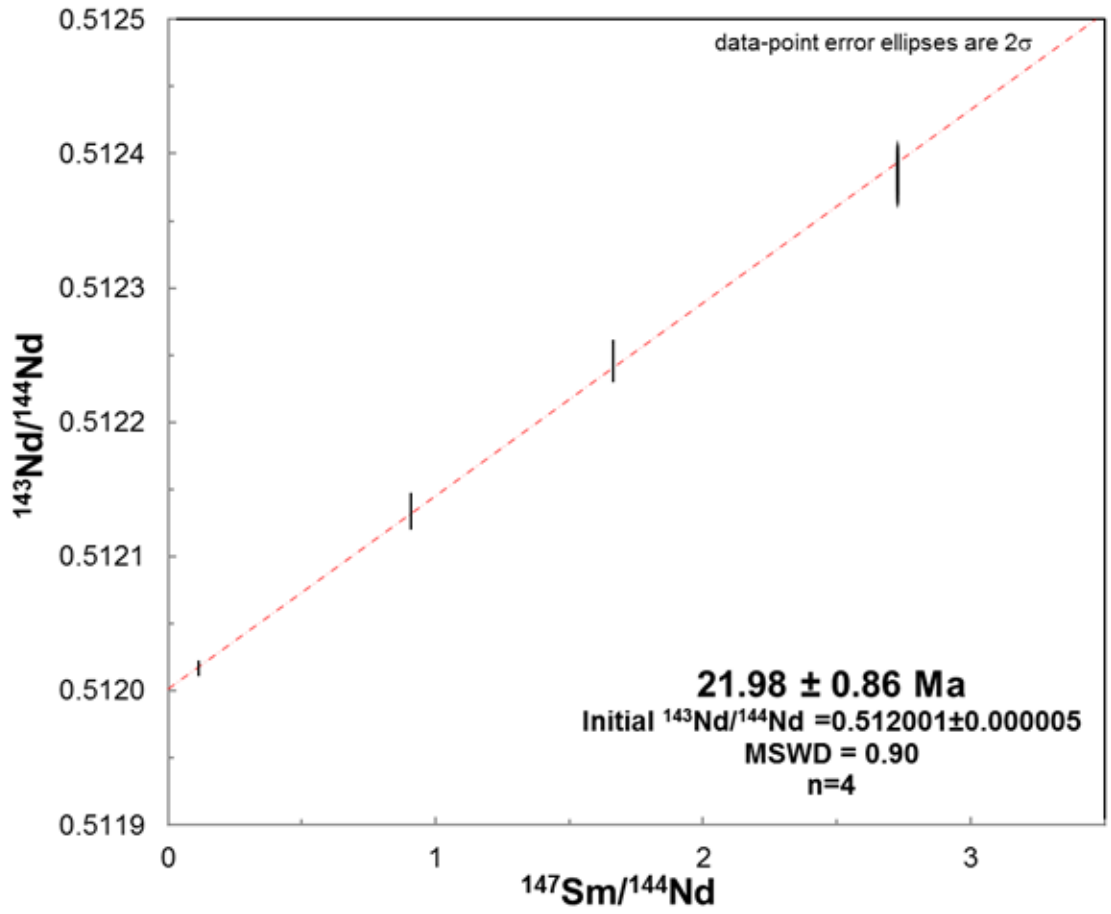


Figure 2.7.2 Four-point isochron of selected data for sample A7

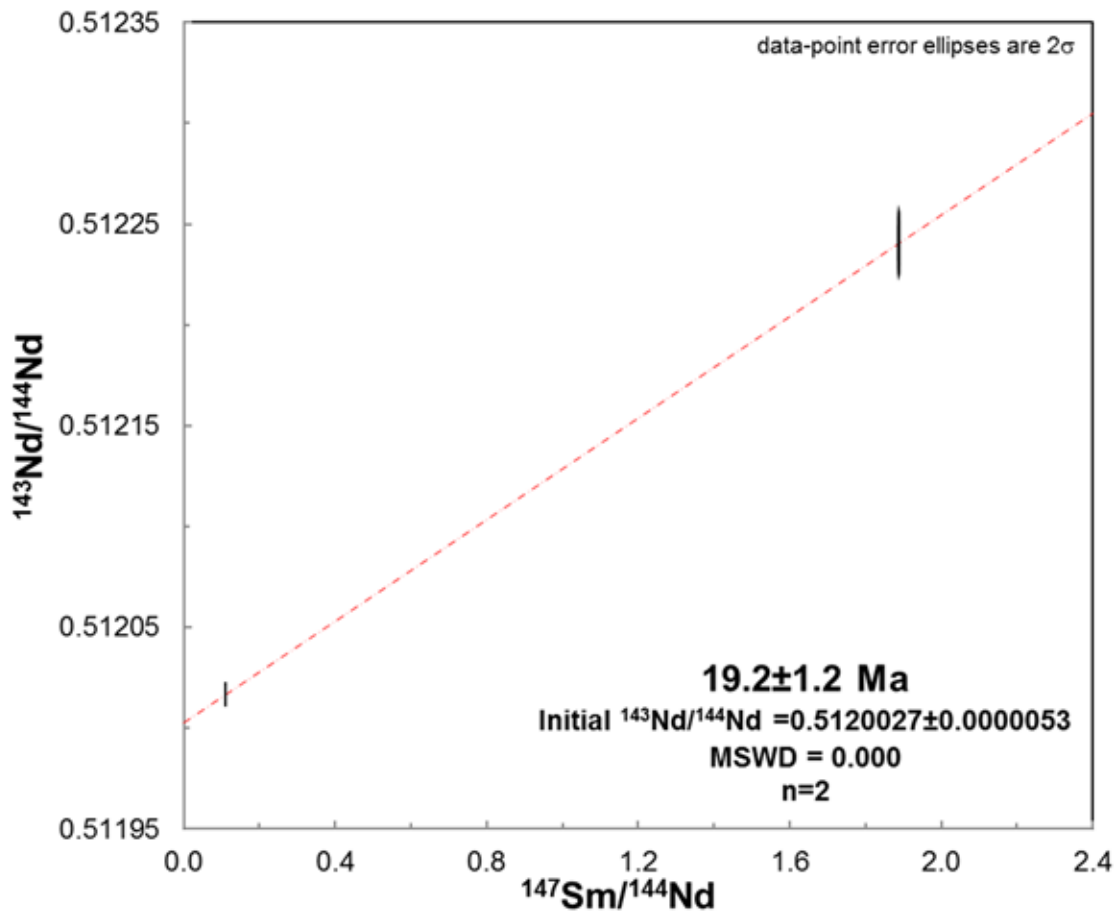


Figure 2.7.3 Two-point isochron of selected data for sample A7

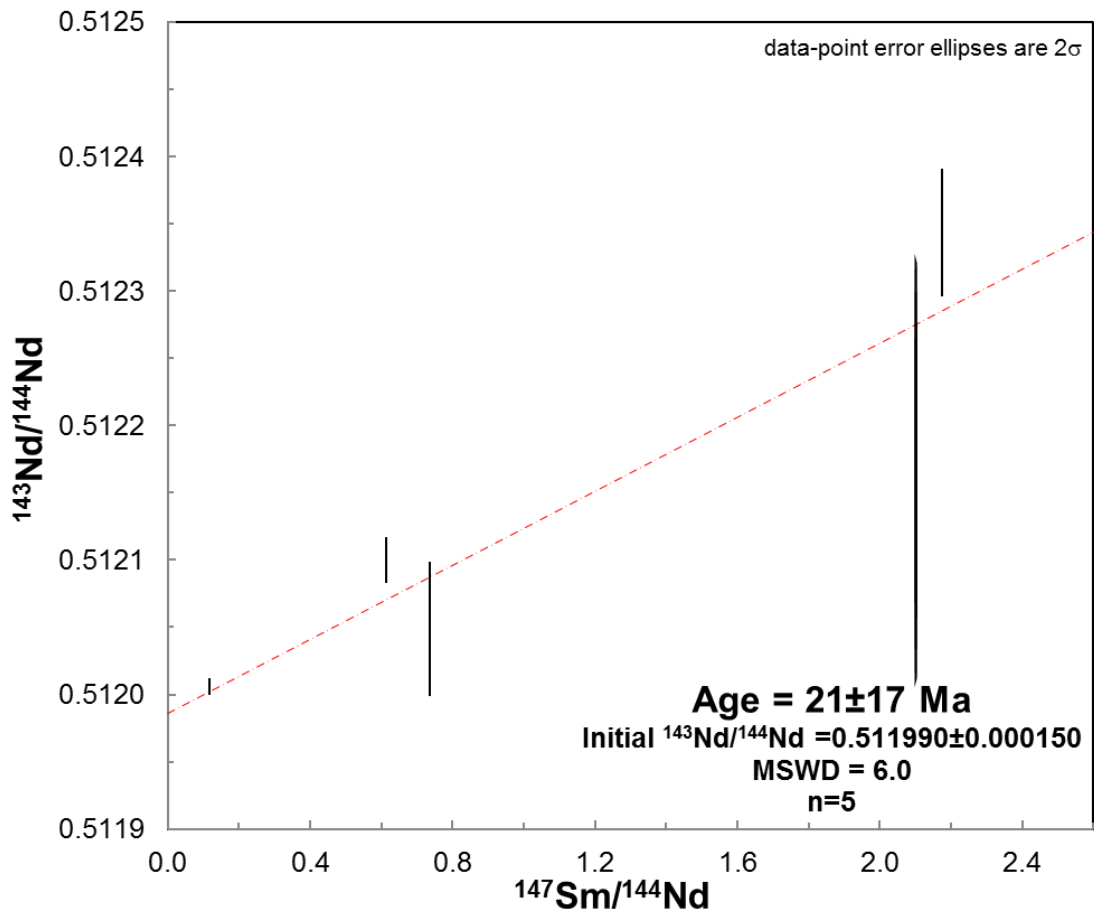


Figure 2.7.4 Five-point isochron including all analyzed data for sample B5

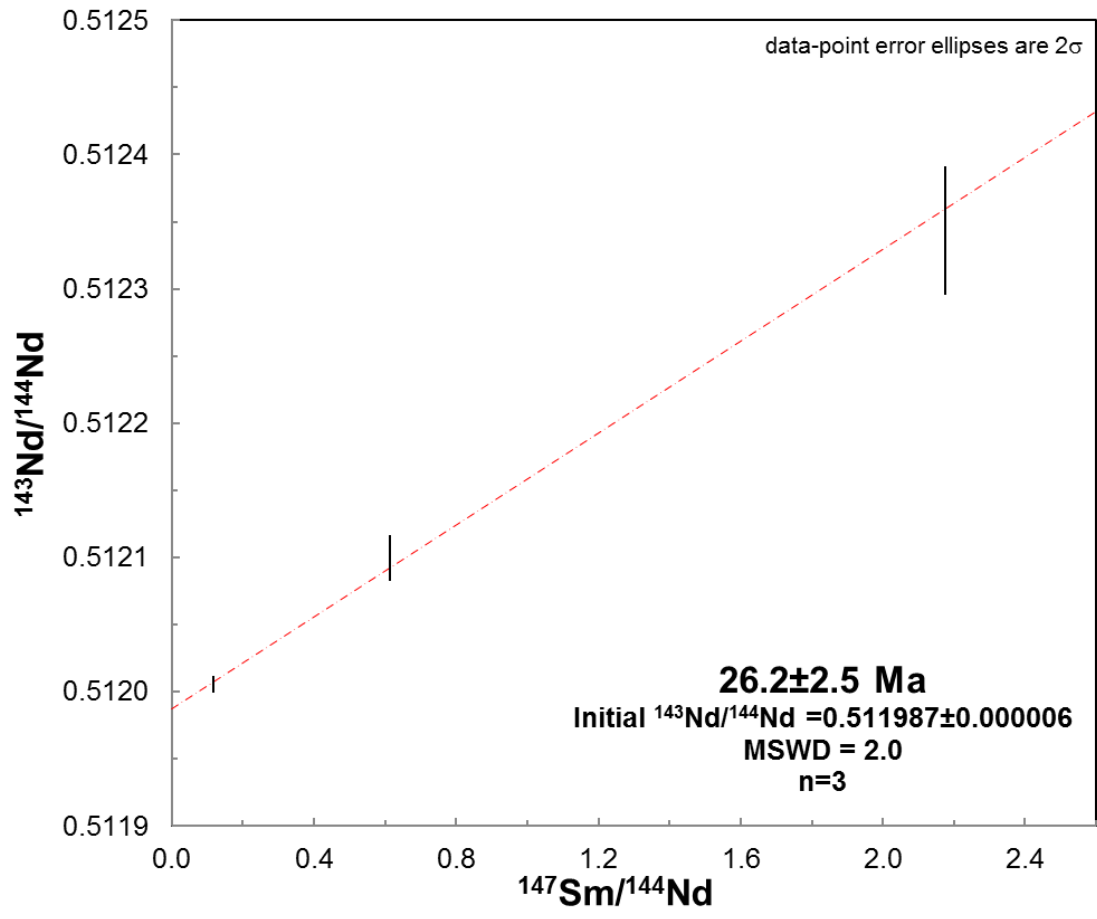


Figure 2.7.5 Three-point isochron of selected data for sample B5

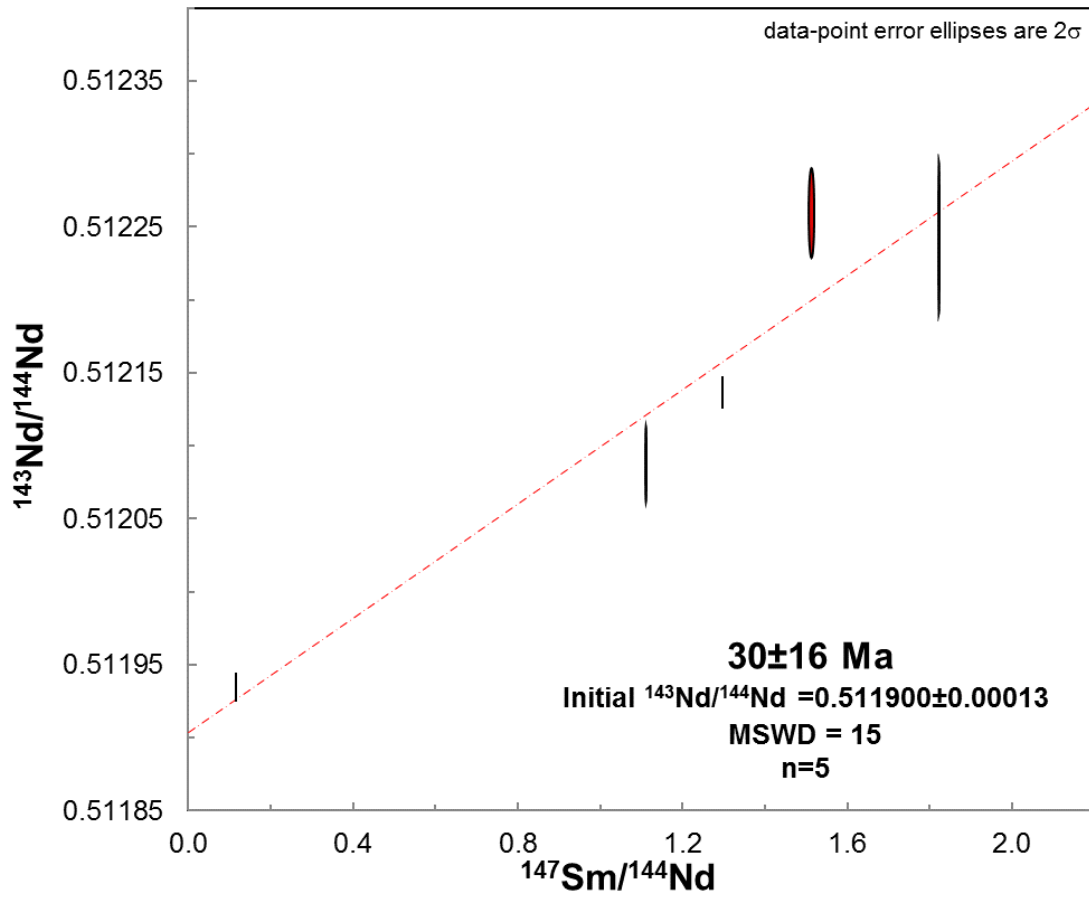


Figure 2.7.6 Five-point isochron including all analyzed data for sample F8

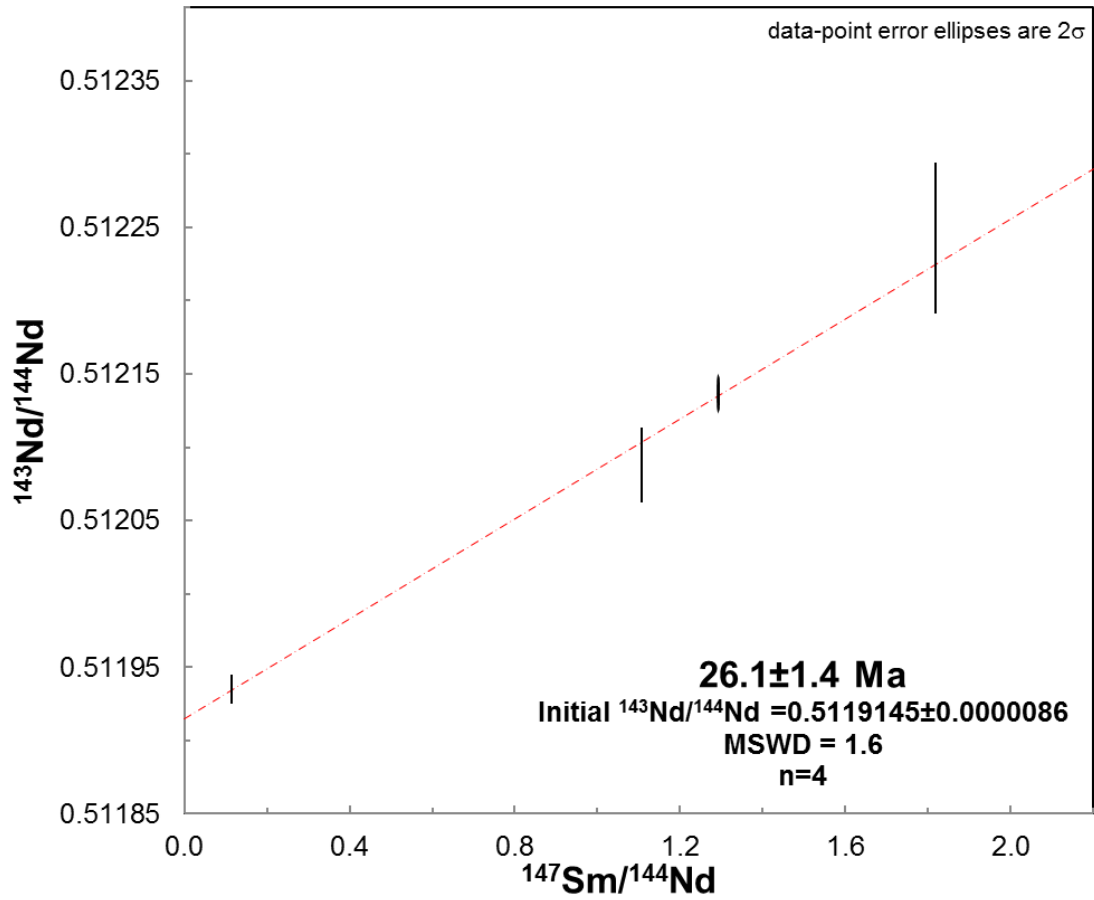


Figure 2.7.7 Four-point isochron of selected data for sample F8

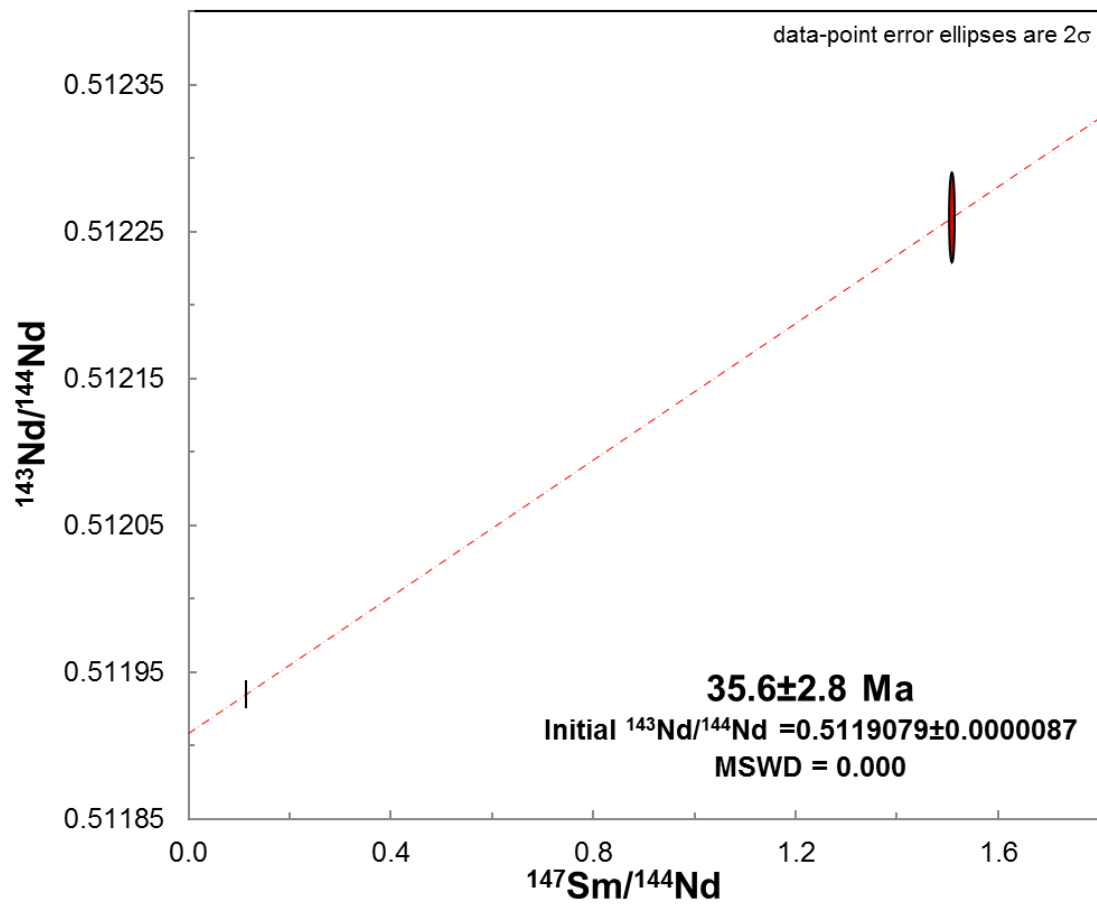


Figure 2.7.8 Two-point isochron of selected data for sample F8

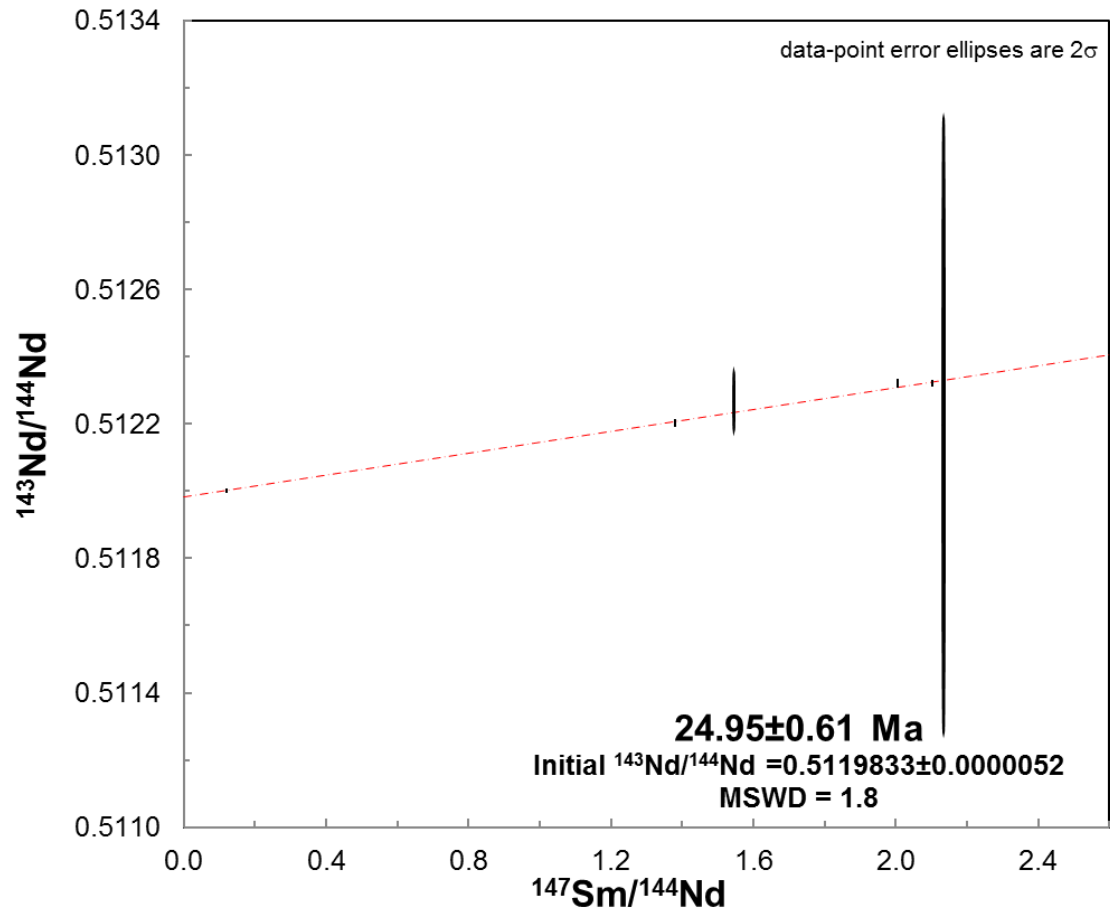


Figure 2.7.9 Six-point isochron including all analyzed data for sample F16

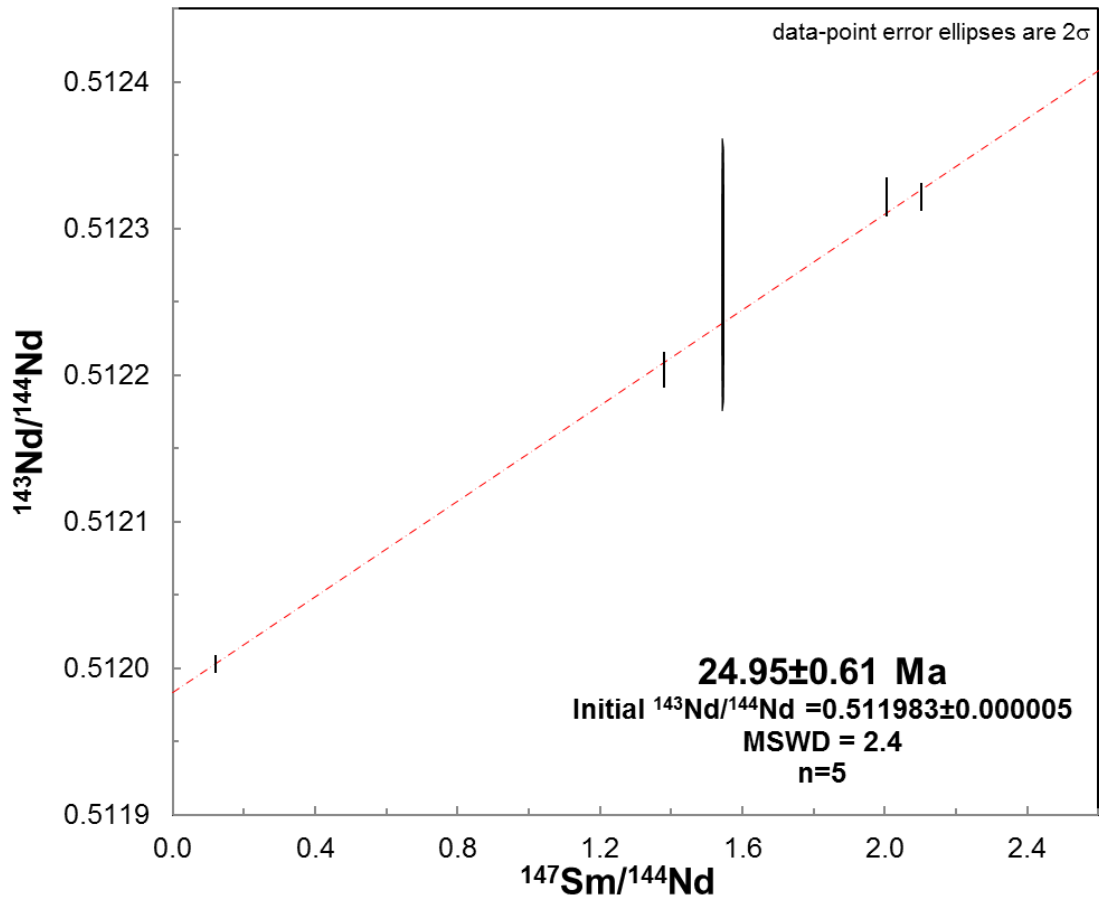


Figure 2.7.10 Five-point isochron of selected data for sample F16

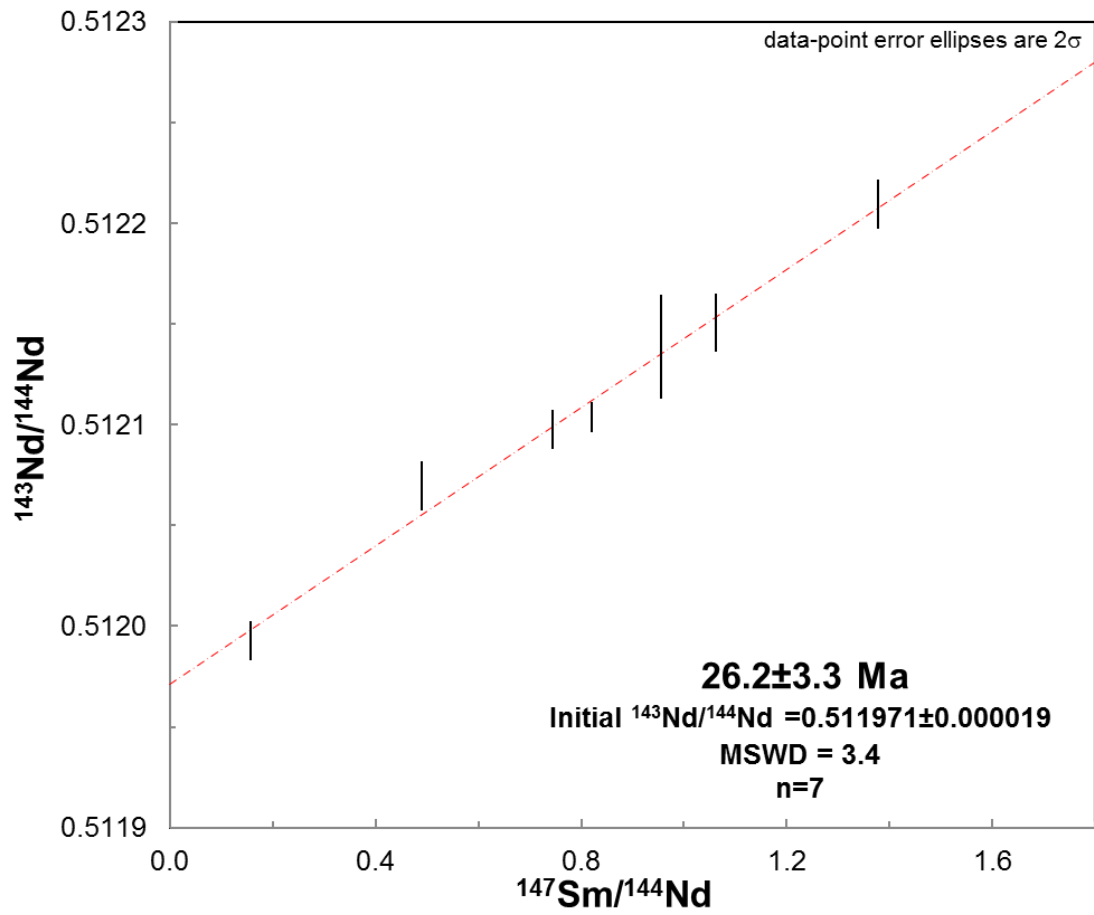


Figure 2.7.11 Seven-point isochron including all analyzed data for sample MT8

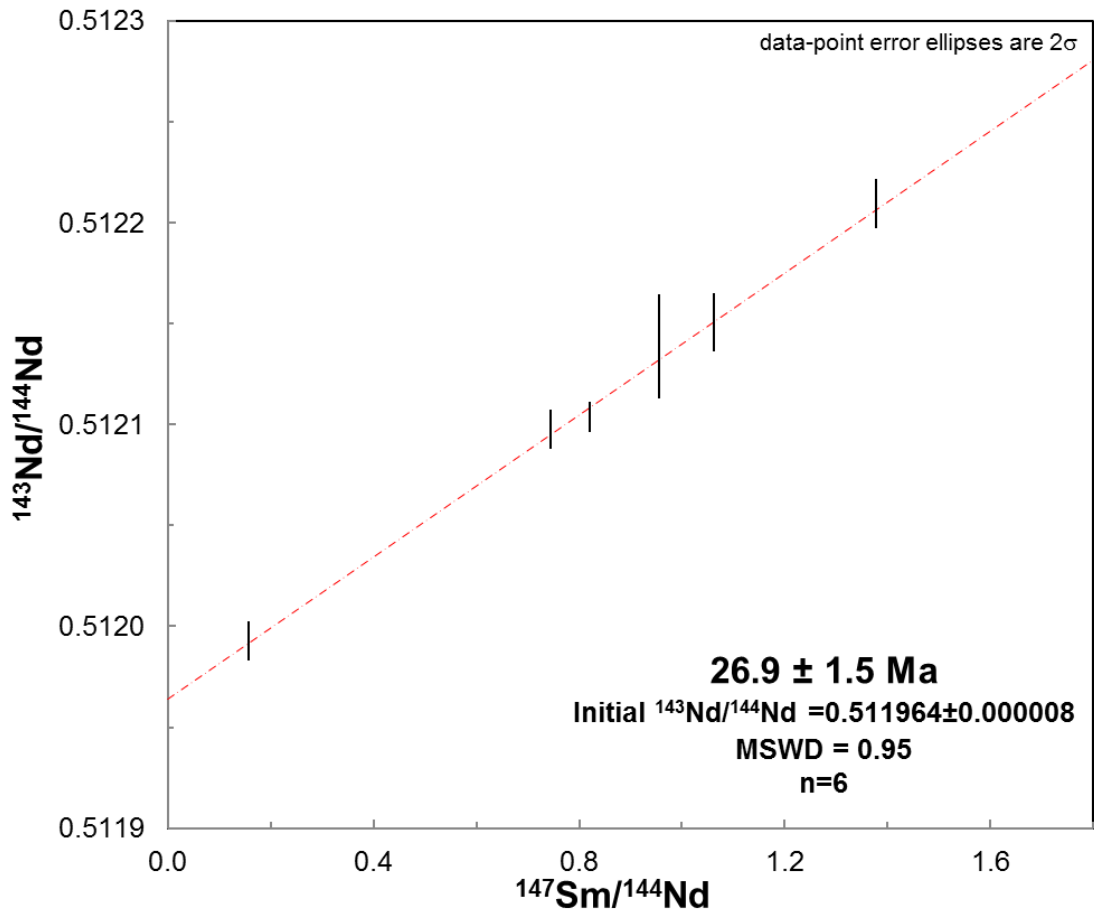


Figure 2.7.12 Six-point isochron of selected data for sample MT8

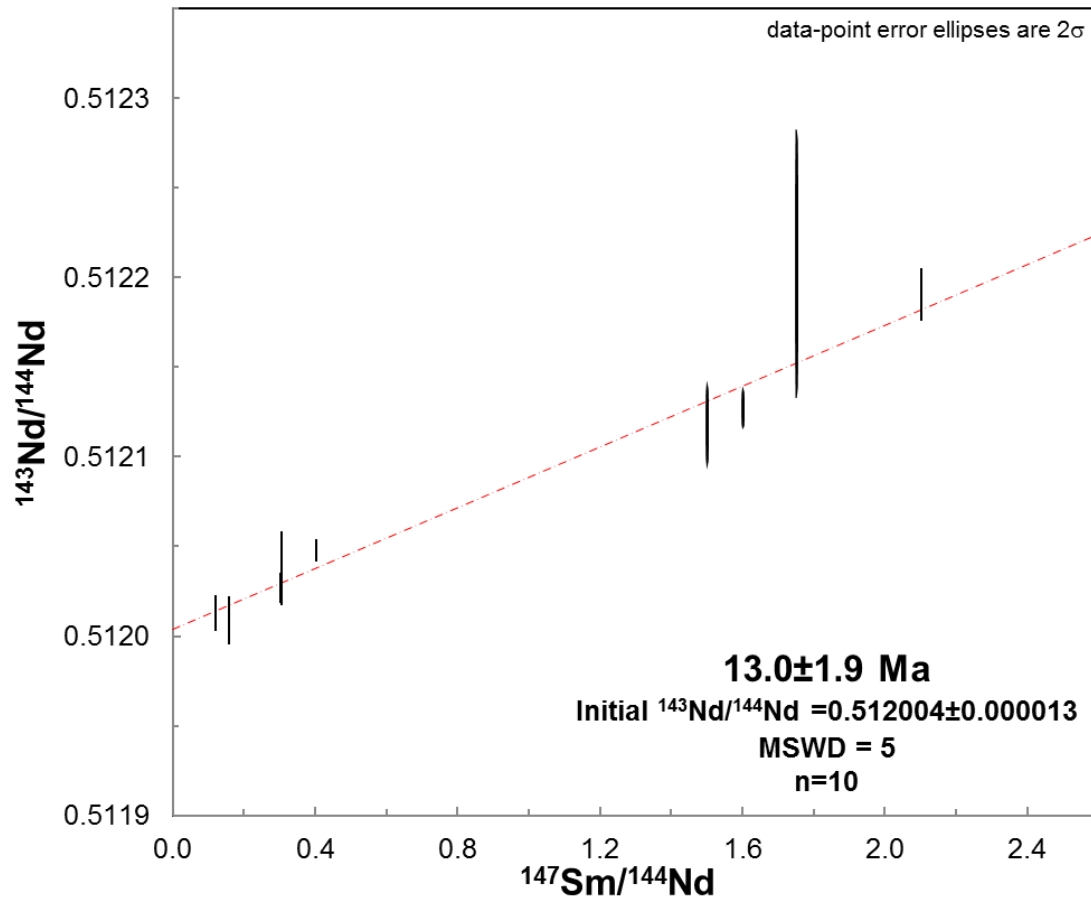


Figure 2.7.13 Ten-point isochron including all analyzed data for sample 27.2.1

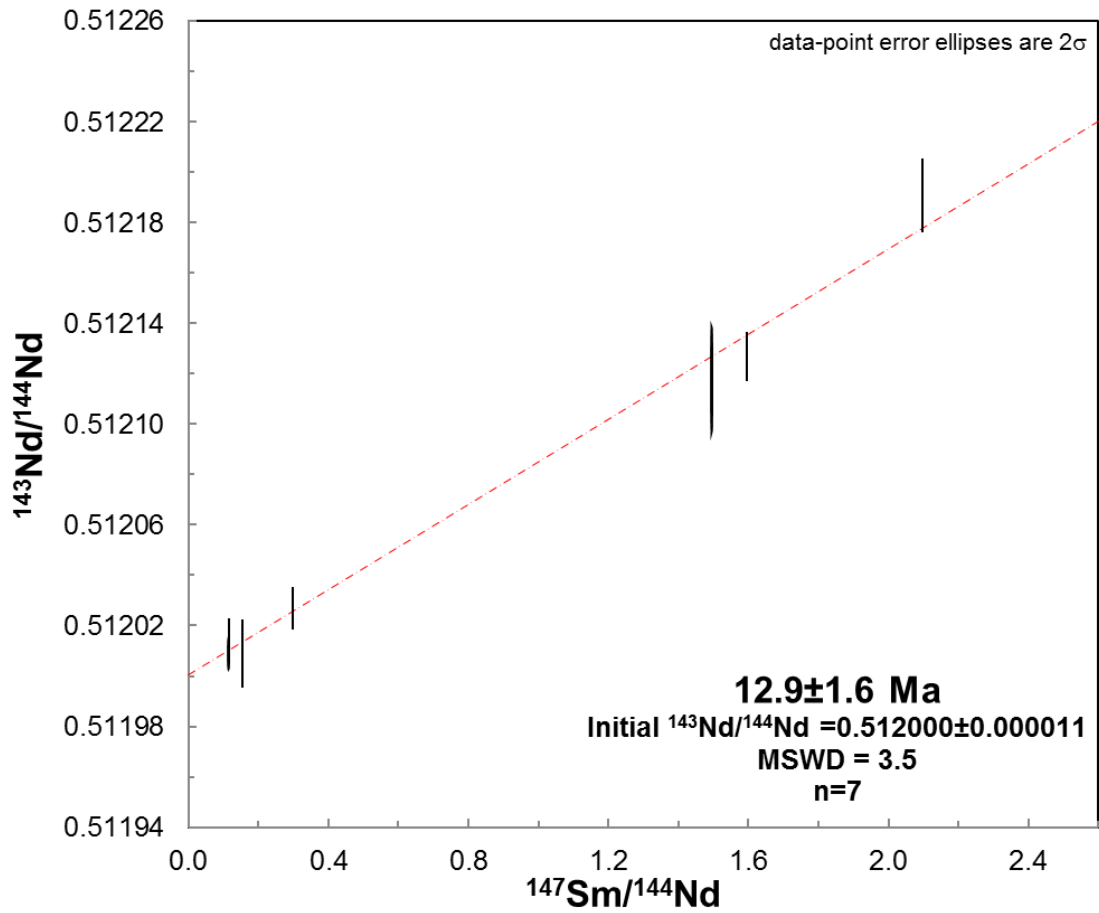


Figure 2.7.14 Seven-point isochron of selected data for sample 27.2.1

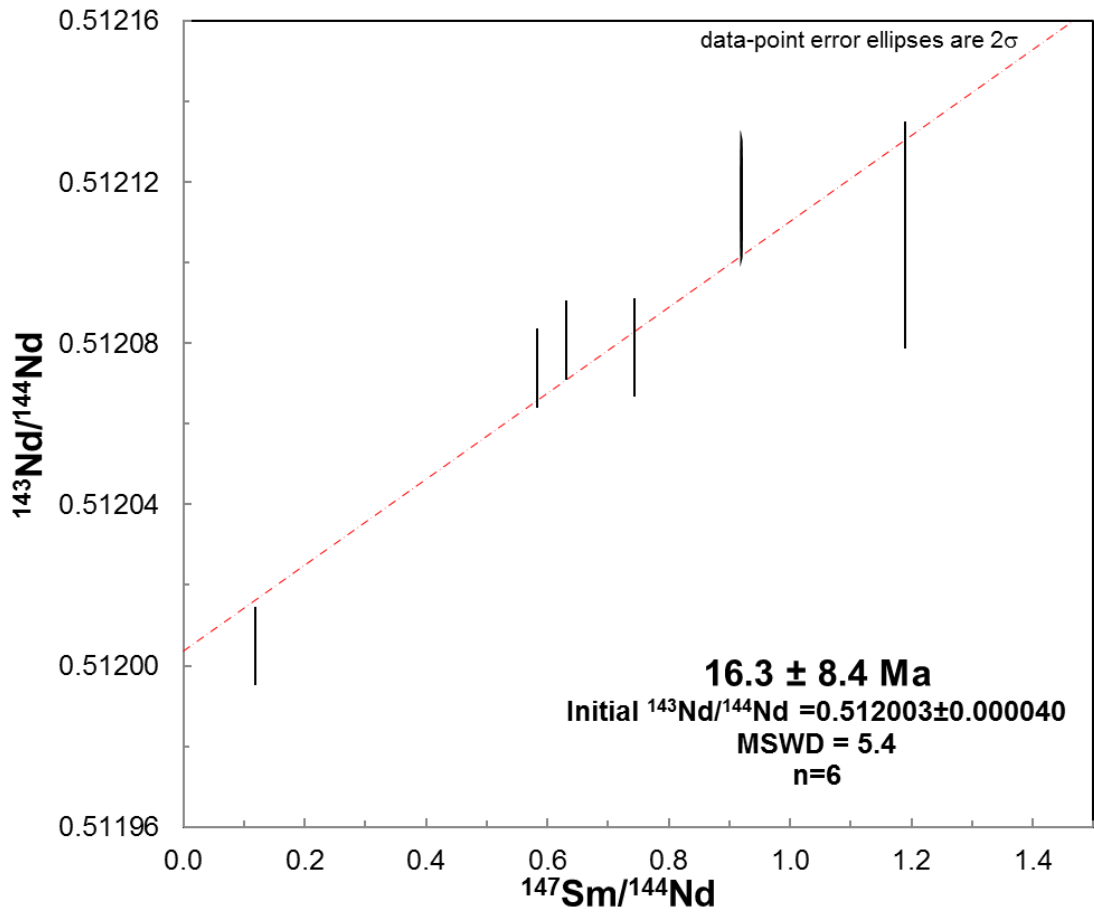


Figure 2.7.15 Six-point isochron including all analyzed data for sample 53.10.1

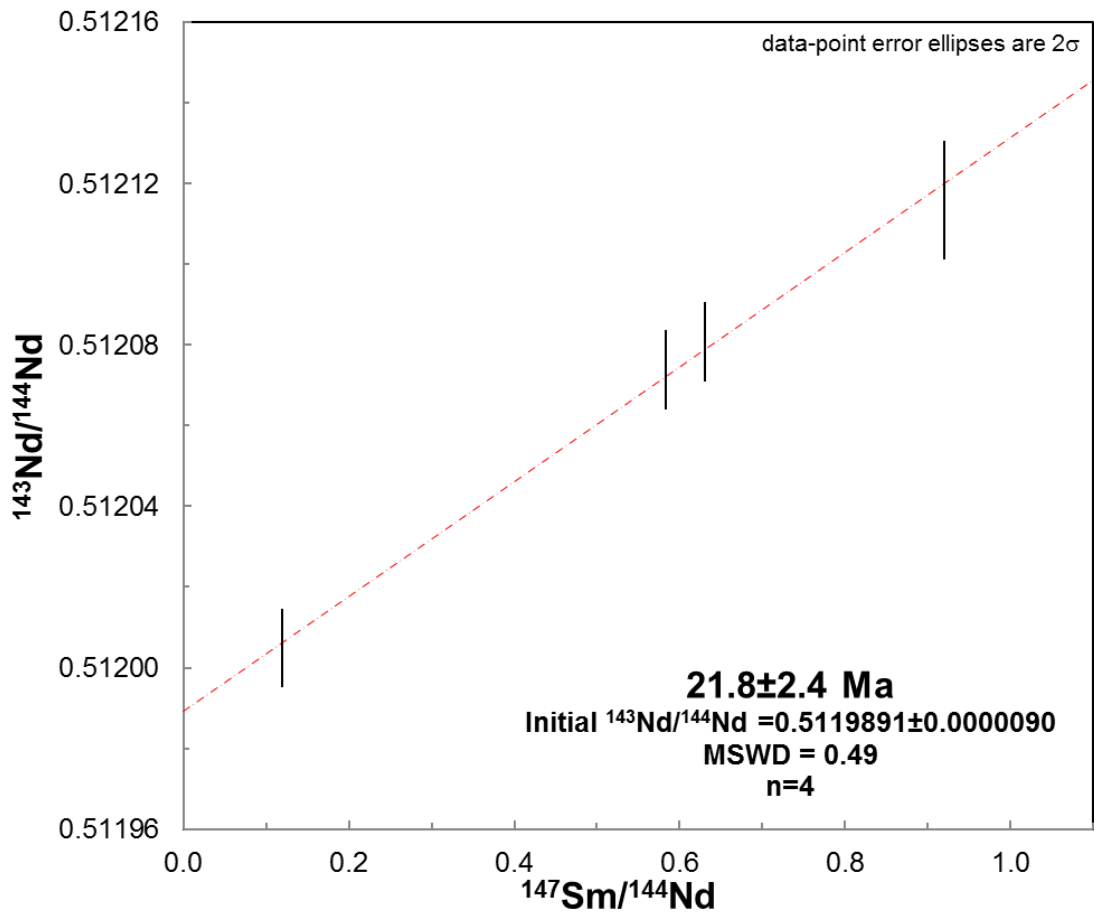


Figure 2.7.16 Four-point isochron of selected data for sample 53.10.1

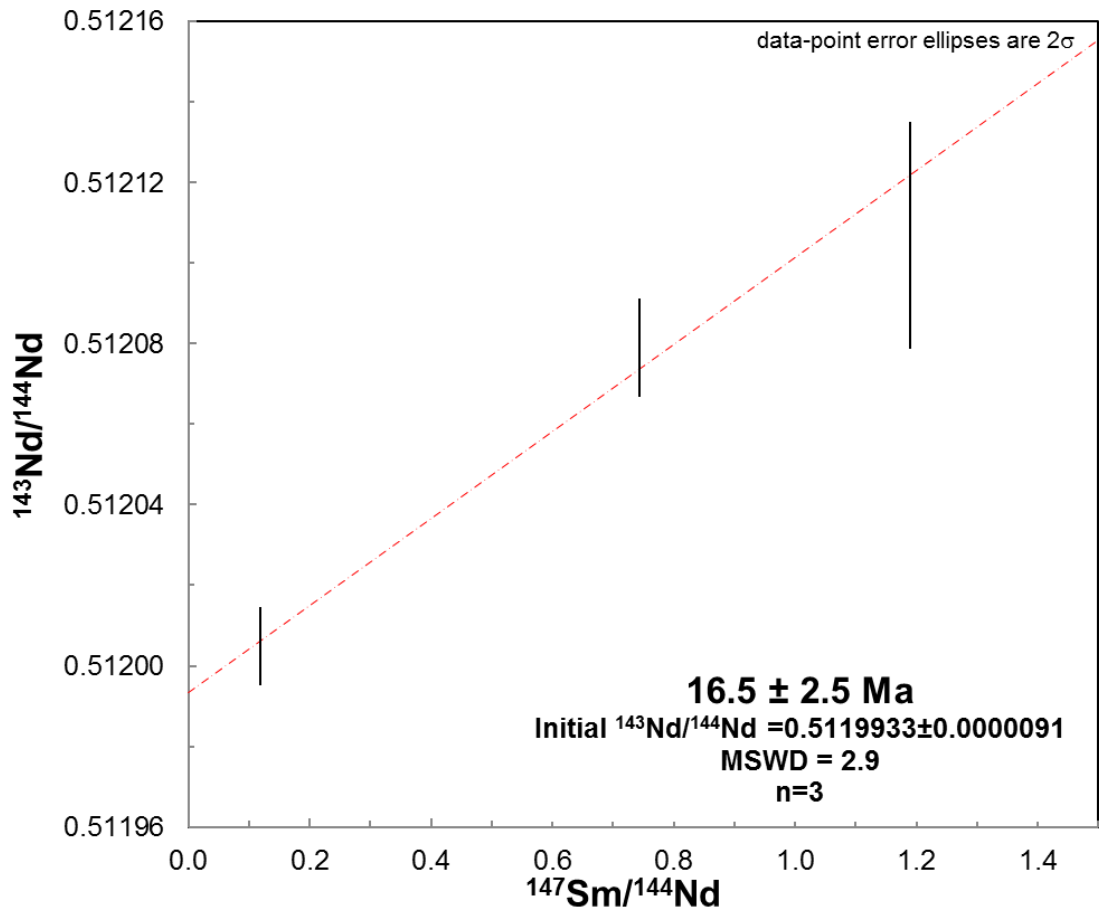


Figure 2.7.17 Three-point isochron of selected data for sample 53.10.1

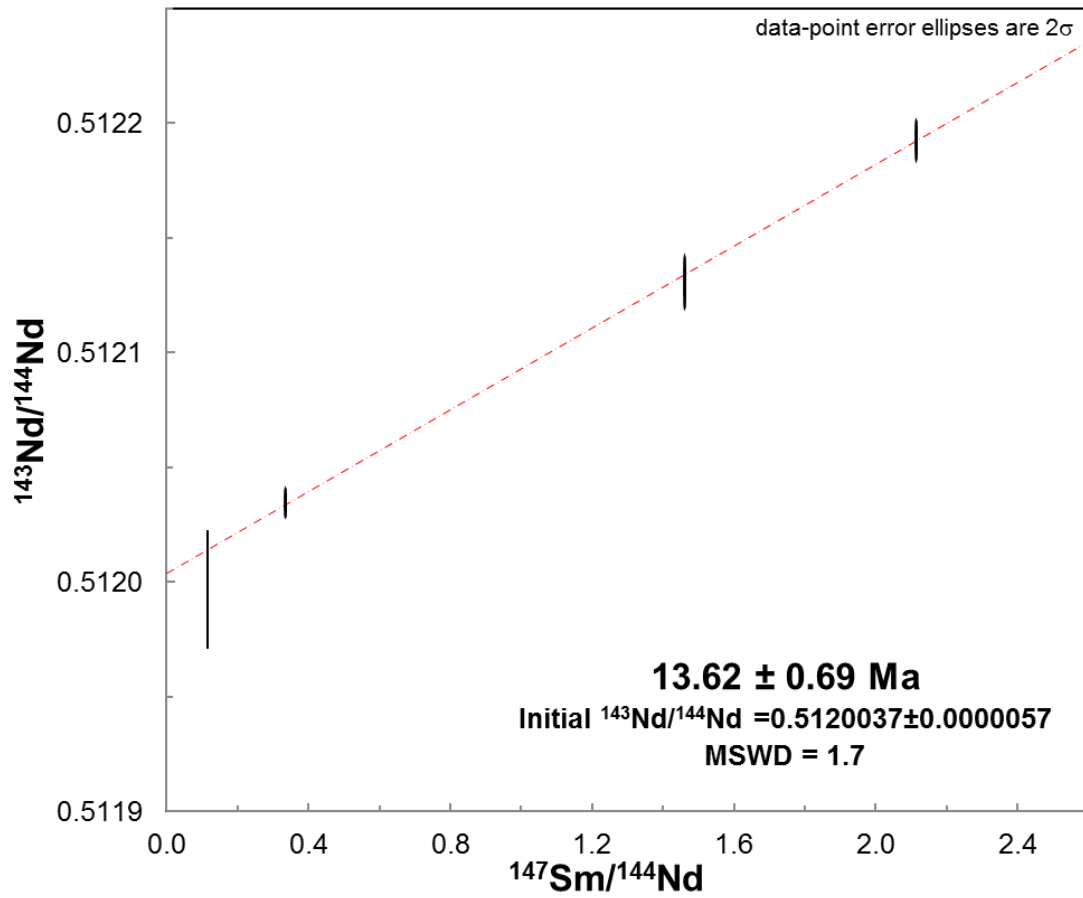


Figure 2.7.18 Four-point isochron for bulk analysis of sample 27.1.2

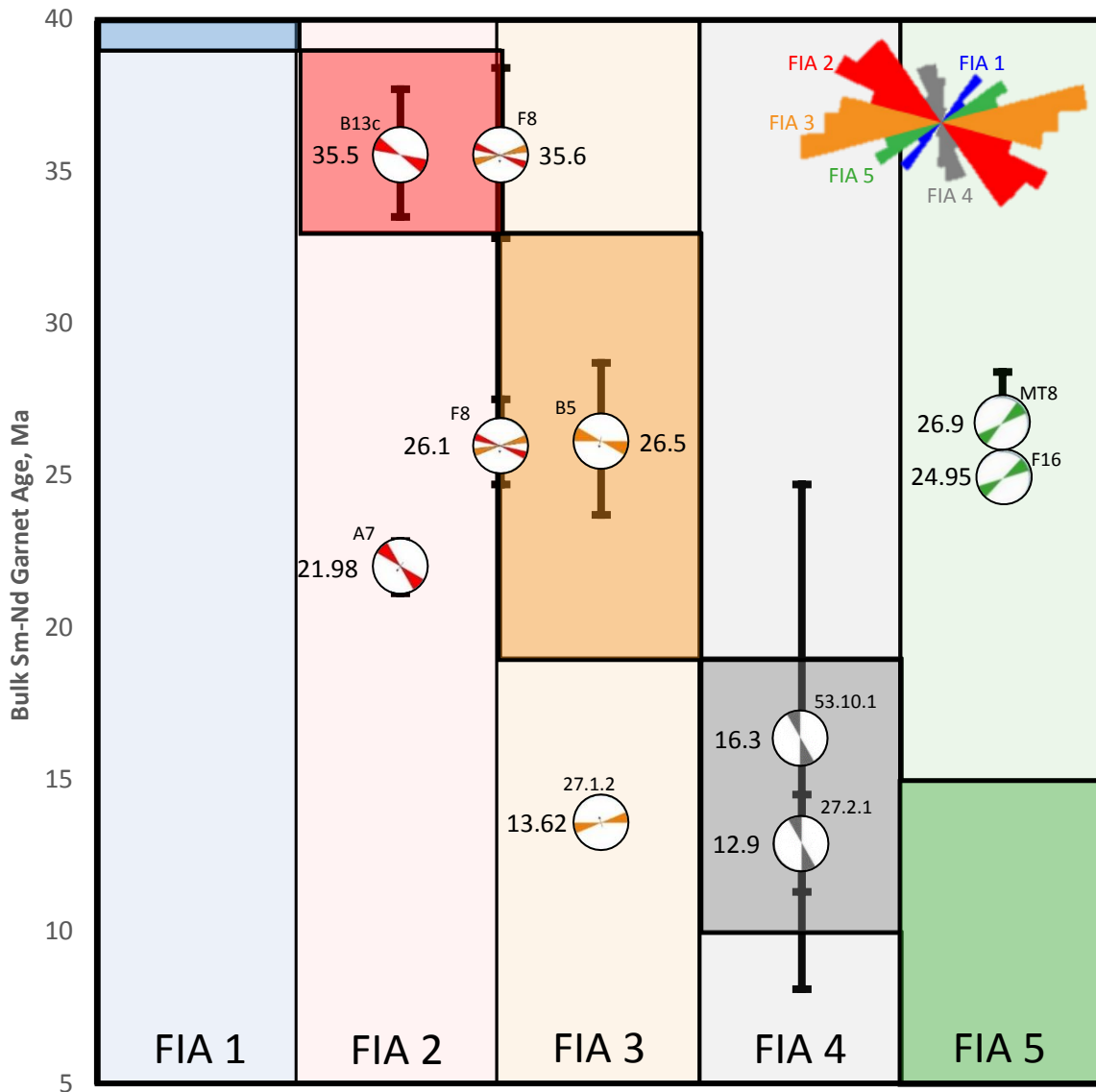


Figure 2.8.1 Comparison of obtained Sm-Nd bulk garnet ages to the range of FIA generation ages as proposed in Aerden et al. (2013). All garnet ages are from this study except for sample B13c which is from Stewart (2015). Light shade regions denote each FIA generations, darker shaded regions denote the proposed age range from Aerden et al. (2013) for each FIA generation. The individual FIA orientations for each sample are shown by a rose diagrams. Rose diagram in top right corner is from Ruiz-Fuentes and Aerden (2018) showing the range of each FIA generation. All age uncertainties are reported at (2 σ) 95% confidence. Samples that lie within the darker shaded region support the hypothesis of Aerden et al. (2013).

Reorientations of FIA in the Alpujarride-Sebide

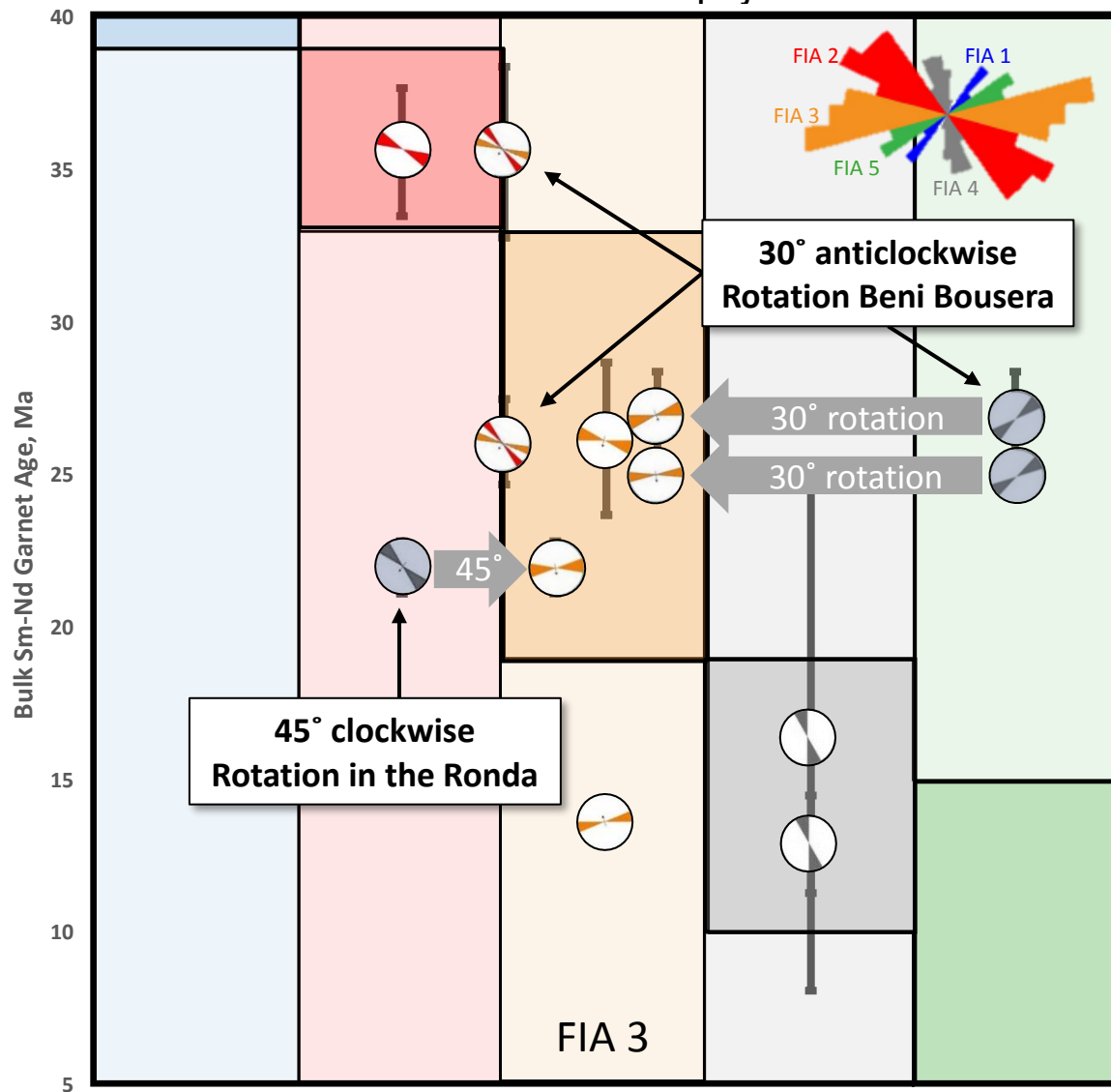


Figure 2.8.2 Modification of figure 2.8.1, comparison of obtained Sm-Nd bulk garnet ages to the range of FIA generation ages as proposed in Aerden et al. (2013) when rigid block rotation is considered. Note samples A7, F16 and MT8 all fall within the accepted age for FIA 3.

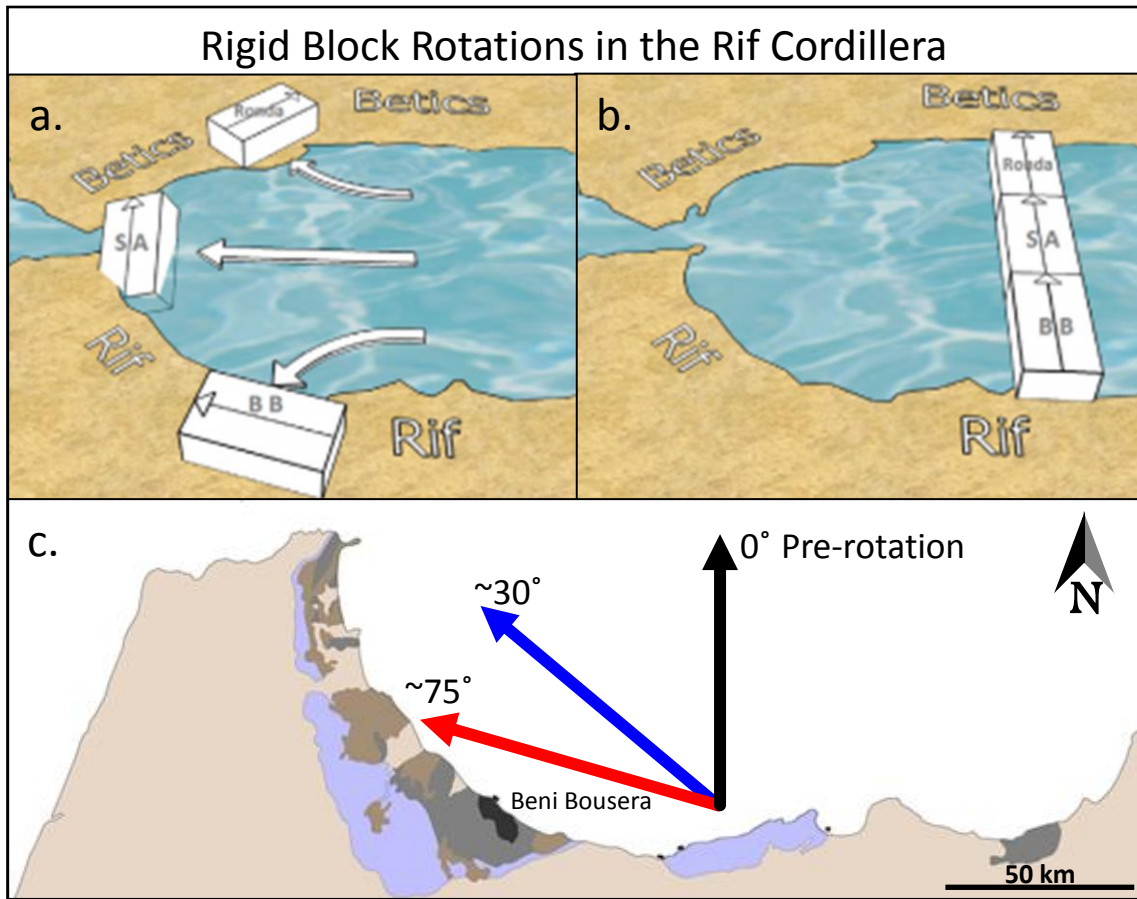


Figure 2.8.3 Post metamorphic rigid block rotations in the Rif Cordillera. (a-b) figures from Brendt et al. (2015), (a) blocks in the current position, (b) blocks in their position before rigid block rotations (SA=Ceuta peridotite; BB=Beni Bousera peridotite; Ronda=Ronda peridotite). (c) Black arrow = orientation of Beni Bousera prior to rotations, red arrow = rotation angle defined by Brendt et al. (2015), blue arrow = indicates block rotations defined by FIA orientations from this study.

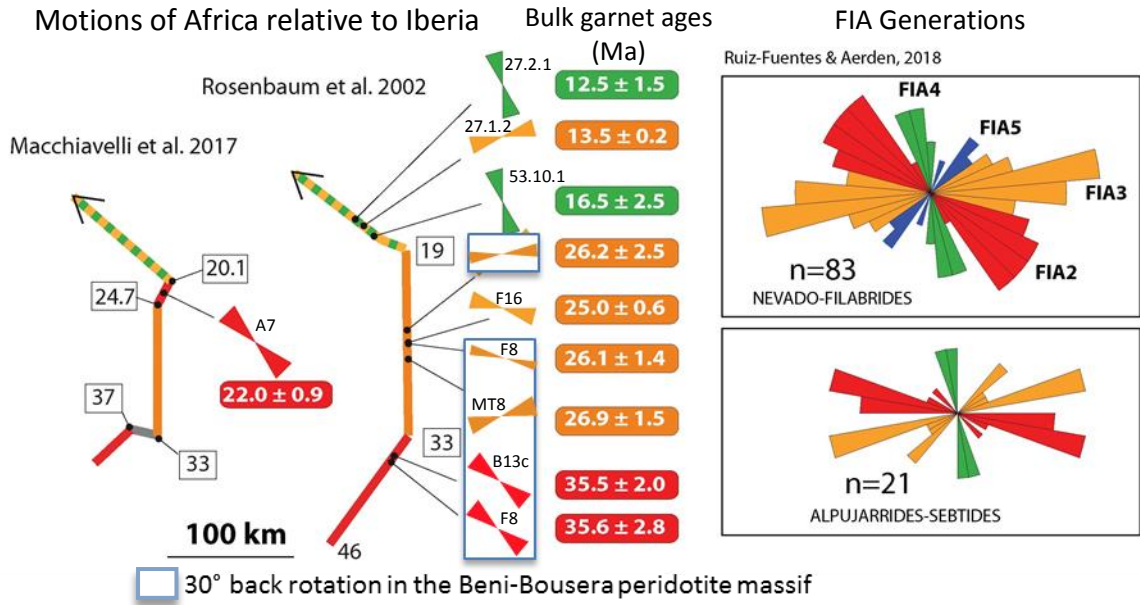


Figure 2.8.4 Correlation of obtained bulk garnet ages from this study and FIA orientations from Aerden et al. (2013) and Ruiz-Fuentes and Aerden (2018) with plate motions of Africa relative to Iberia. Courtesy of Domingo Aerden.

5.3 FIGURES FROM CHAPTER 3

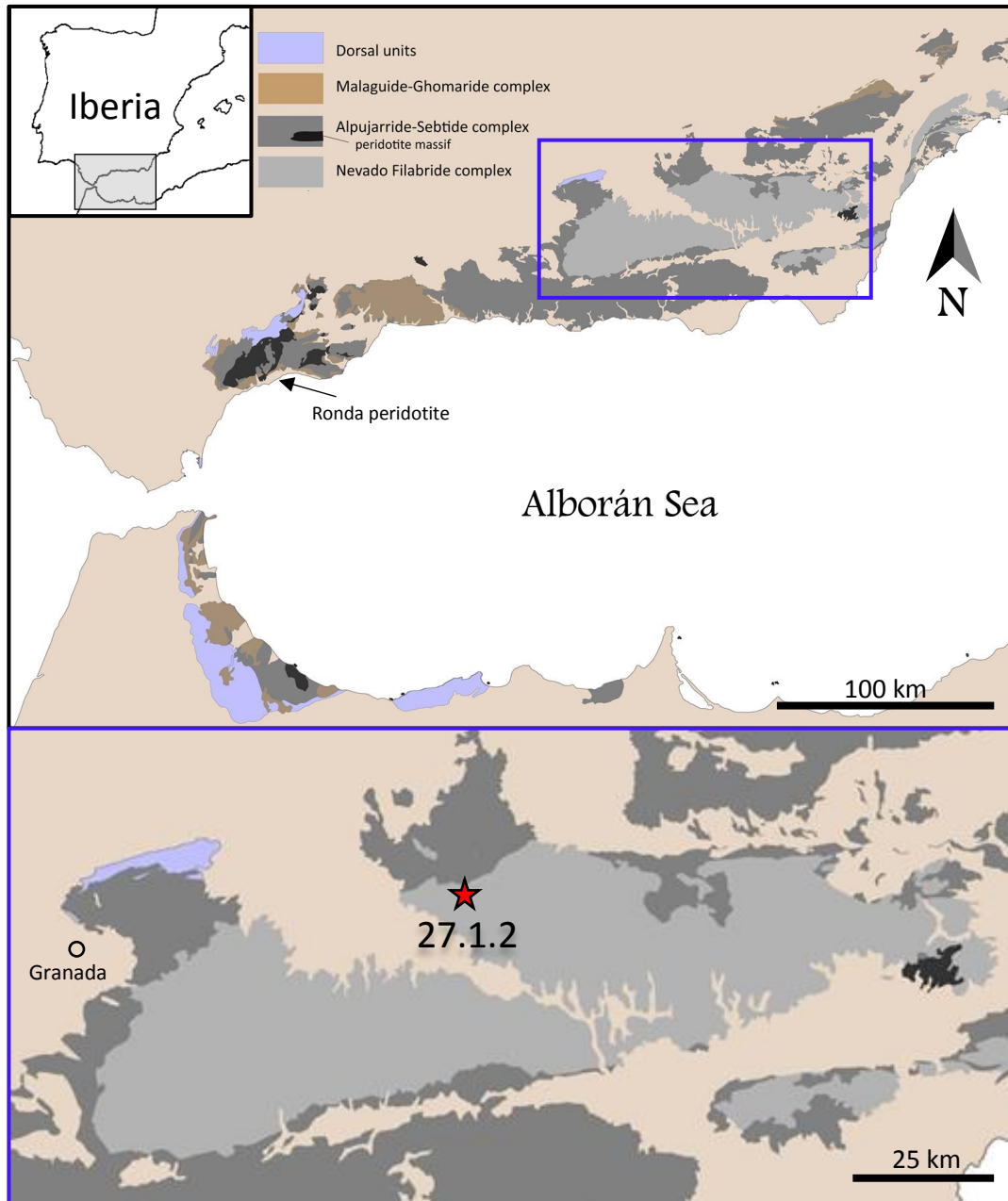


Figure 3.2.1 Geologic map of Betic Cordillera and the Nevado-Filabride Complex. Red star denotes the location of sample 27.1.2. Latitude -2.82784° , Longitude 37.30270° .

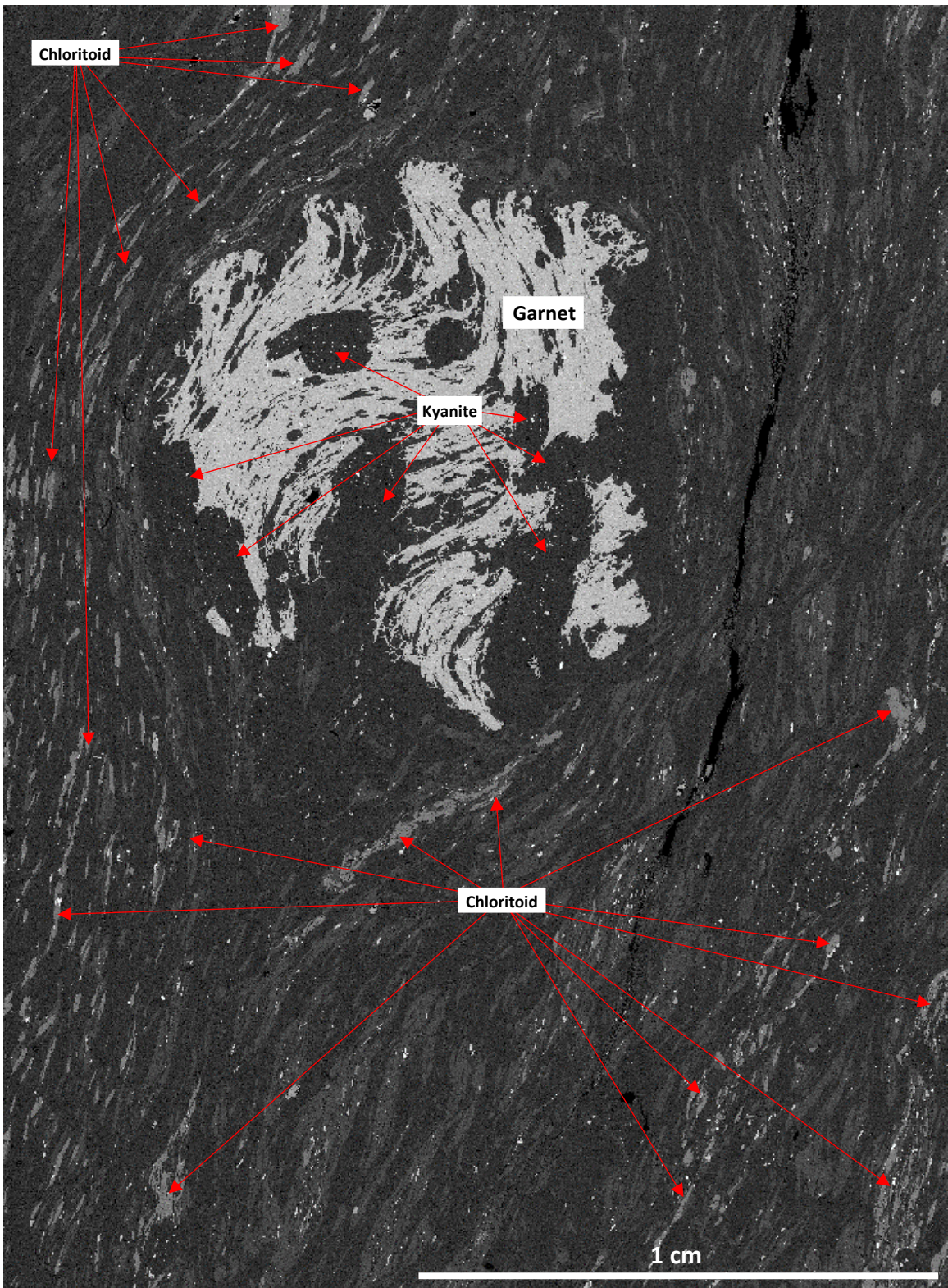


Figure 3.2.1 BSE image of sample 27.1.2. Large spiral garnets with abundant kyanite, muscovite, quartz inclusions. The matrix is dominated by chloritoid, muscovite, quartz, rutile, and minor amounts of apatite, zircon, and allanite.

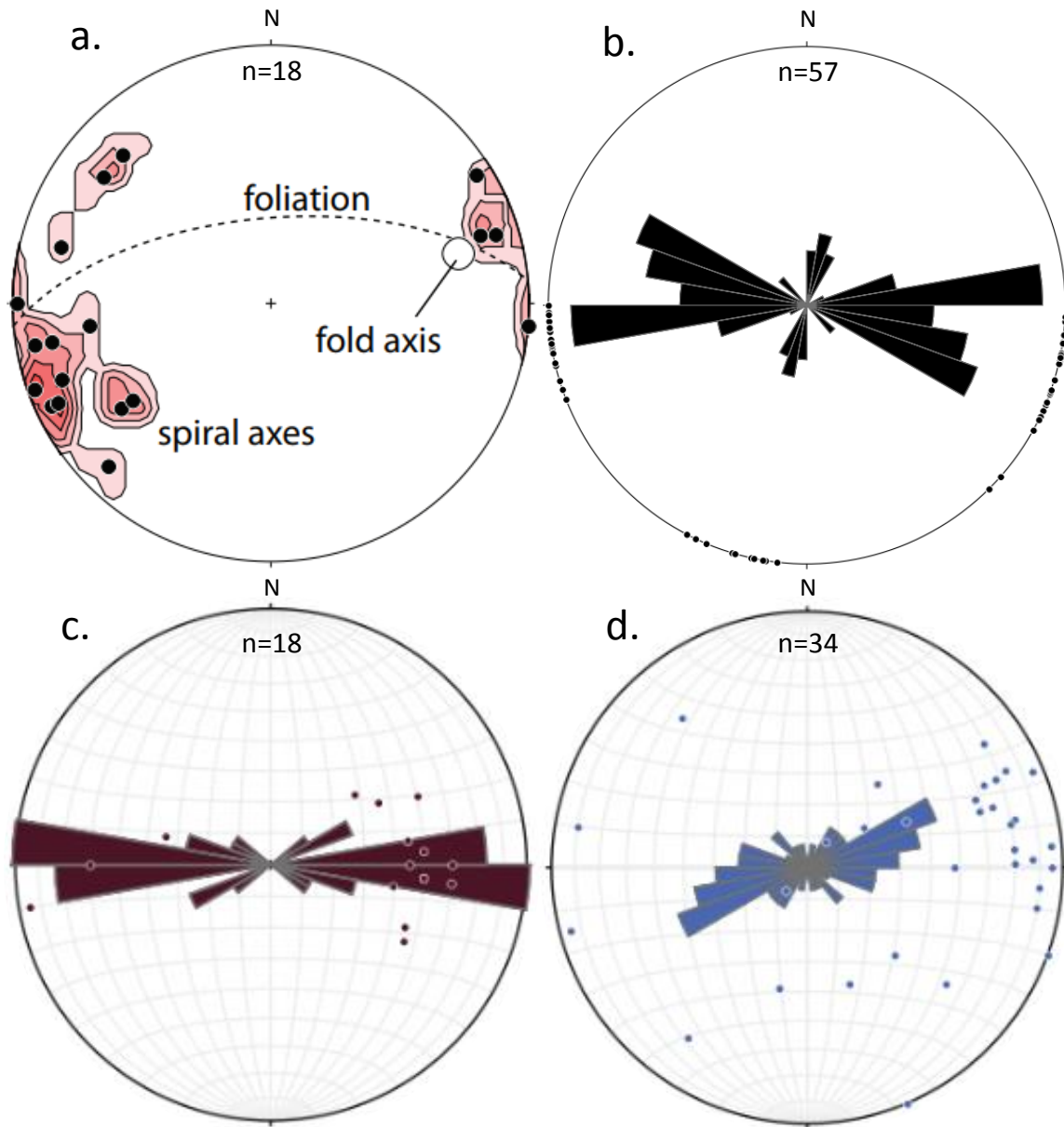


Figure 3.3.2 Summary of microstructural and macrostructural orientations. (a.) Plot of XRT data from sample 46.8.1. Black dots denote spiral garnet axes, open circle denote fold axes measured in the outcrop. (b.) Strike of vertical truncations from garnet porphyroblasts measured from sample 27.1.2. (c.) Orientation of meter-scale fold axes in the study area surrounding 27.1.2 (d.) orientation of stretching and/or crenulation lineations from study area.

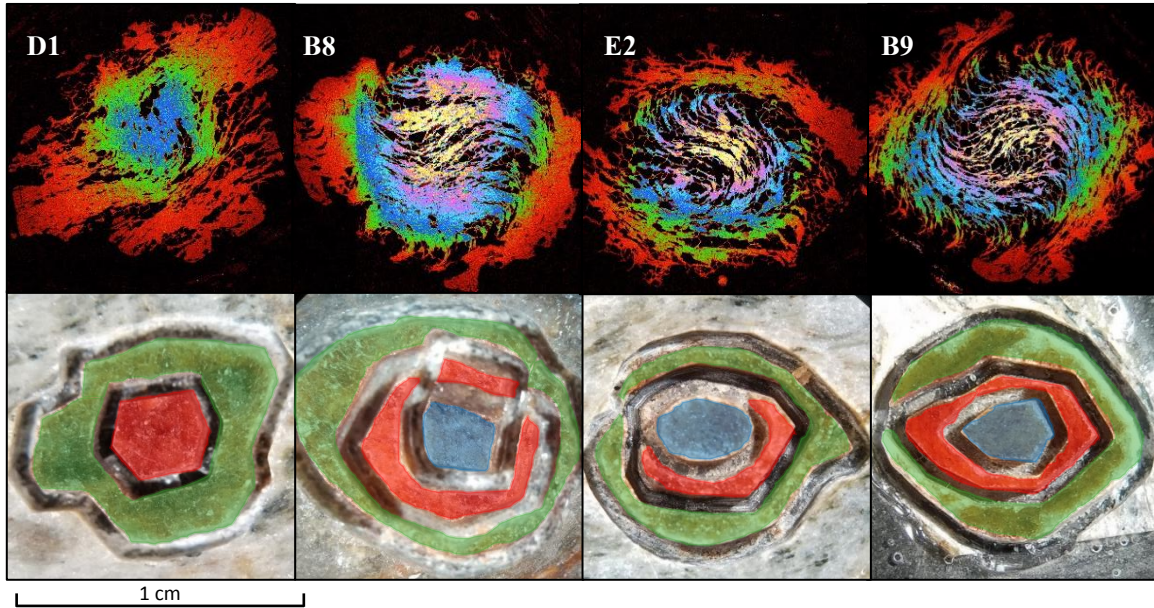


Figure 3.4.1 false color manganese concentration maps used to determine garnet growth zones for micro-drilling (top). Microprobe analysis completed at University of Granada. Photos of four garnets after micro-drilling, cores; blue, medians; red, and rims; green (bottom).

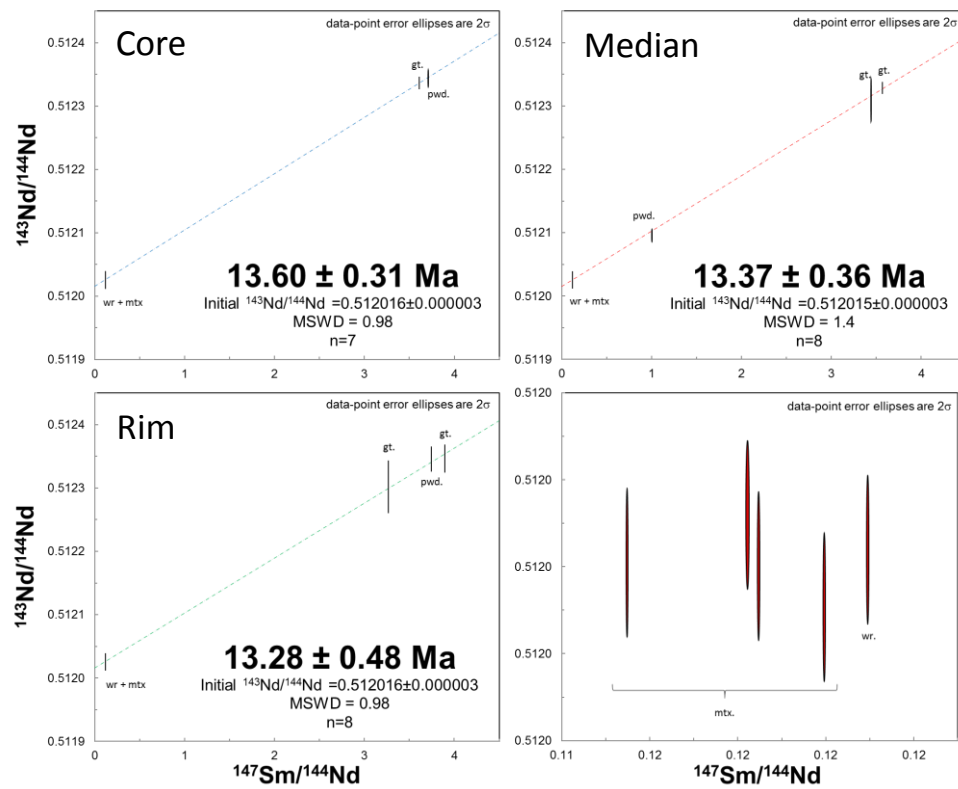


Figure 3.5.1 Sm-Nd isochrons for garnet zones from sample 27.1.2. MSWD = mean square of weighted deviates.

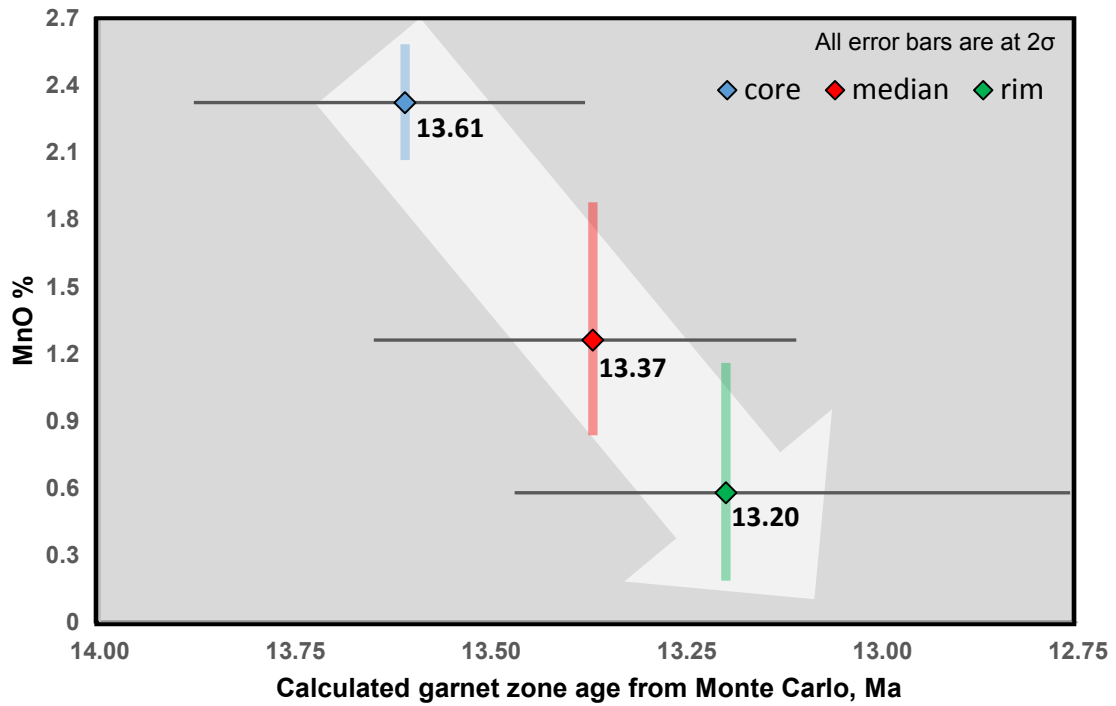


Figure 3.6.1 Calculated Sm-Nd ages and error bars from garnet zones. Shaded regions represent range in MnO% for each zone. Garnet zone ages and error bars were calculated from Monte Carlo simulation using 64,000 iterations from input values of individual Sm-Nd isochron ages for each zone.

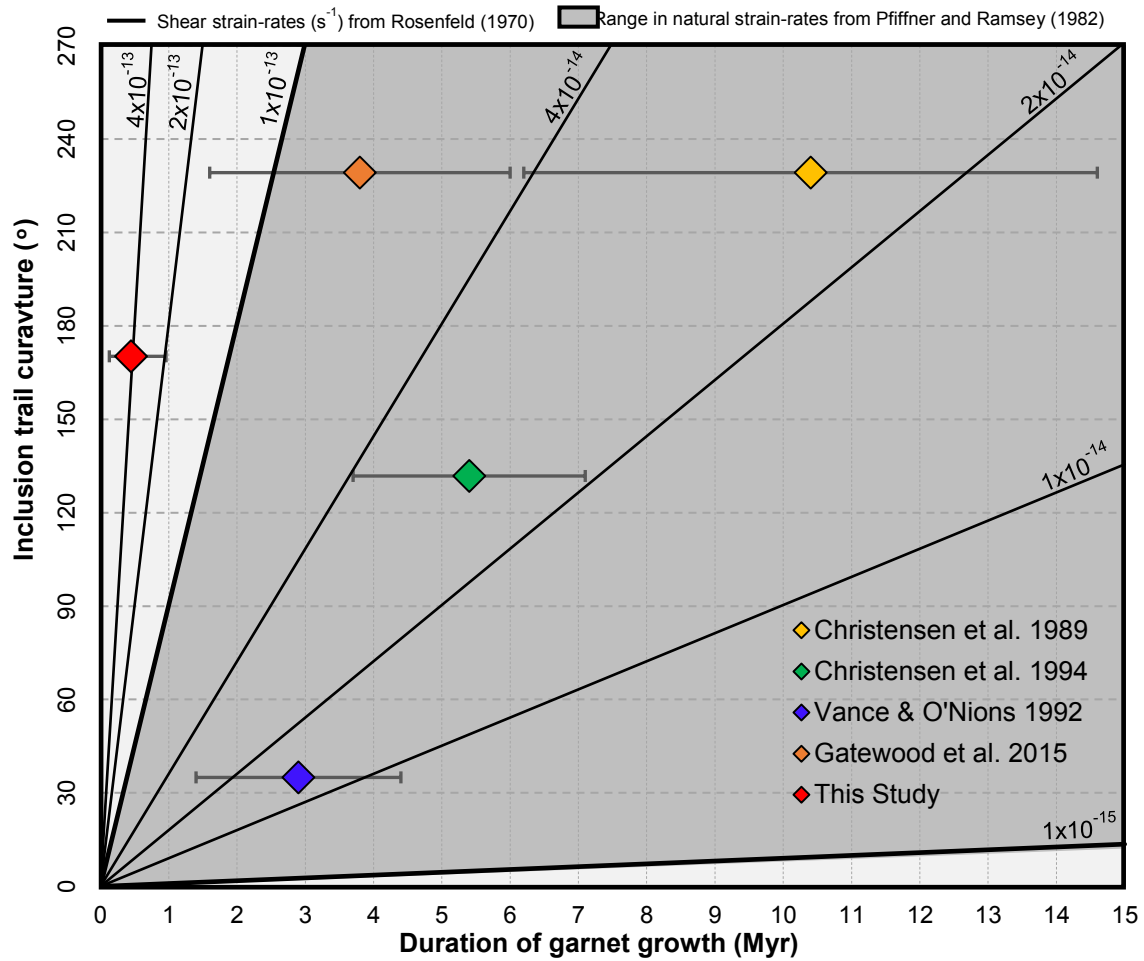


Figure 3.6.2 A comparison of inclusion trail curvature and geochronology from this study with other notable spiral garnet chronology studies. Strain-rate lines calculated using the model of Rosenfeld (1970), where shear strain rate = $2 \times$ apparent garnet rotation in radians (ω) over duration of garnet growth. Orange diamond applies garnet chronology from Gatewood et al. (2015) to inclusion trail curvature from Christensen et al. (1989).

a.



b.

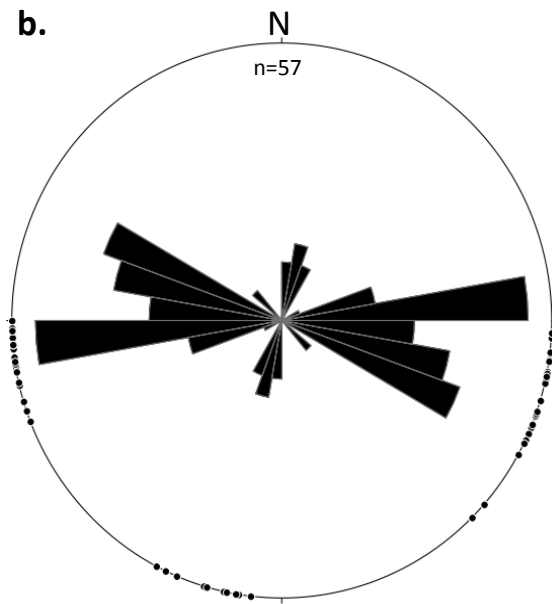


Figure 3.9.1 (a.) Inclusion trails sketches garnet prophyroblasts from sample 27.1.2. Dashed lines denote truncation surfaces. (b.) Rose diagram showing preferred orientation of truncation surfaces from garnets from 27.1.2.

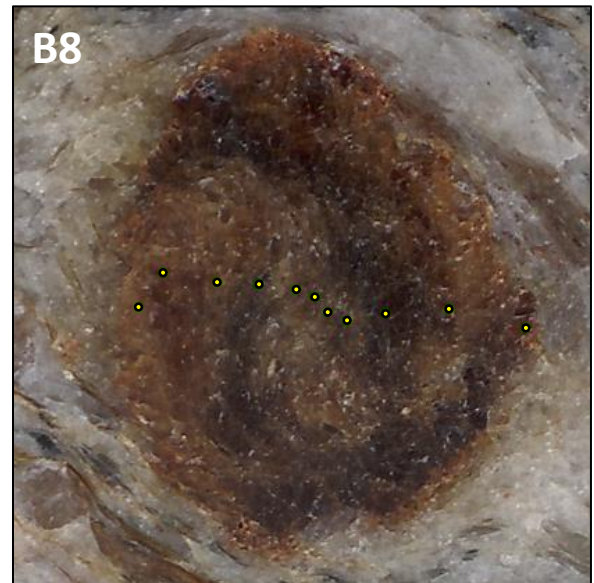
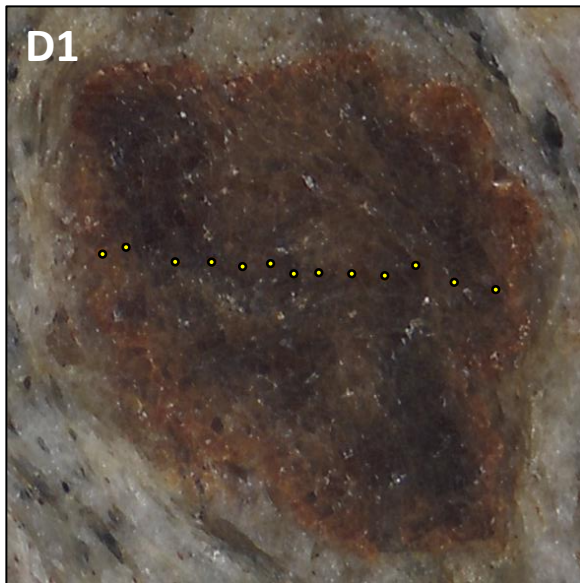
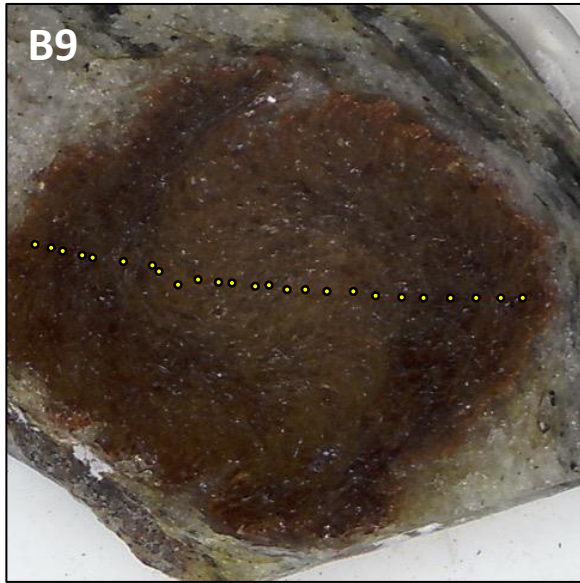


Figure 3.9.2 Yellow dots denote location of point analysis from electron microprobe

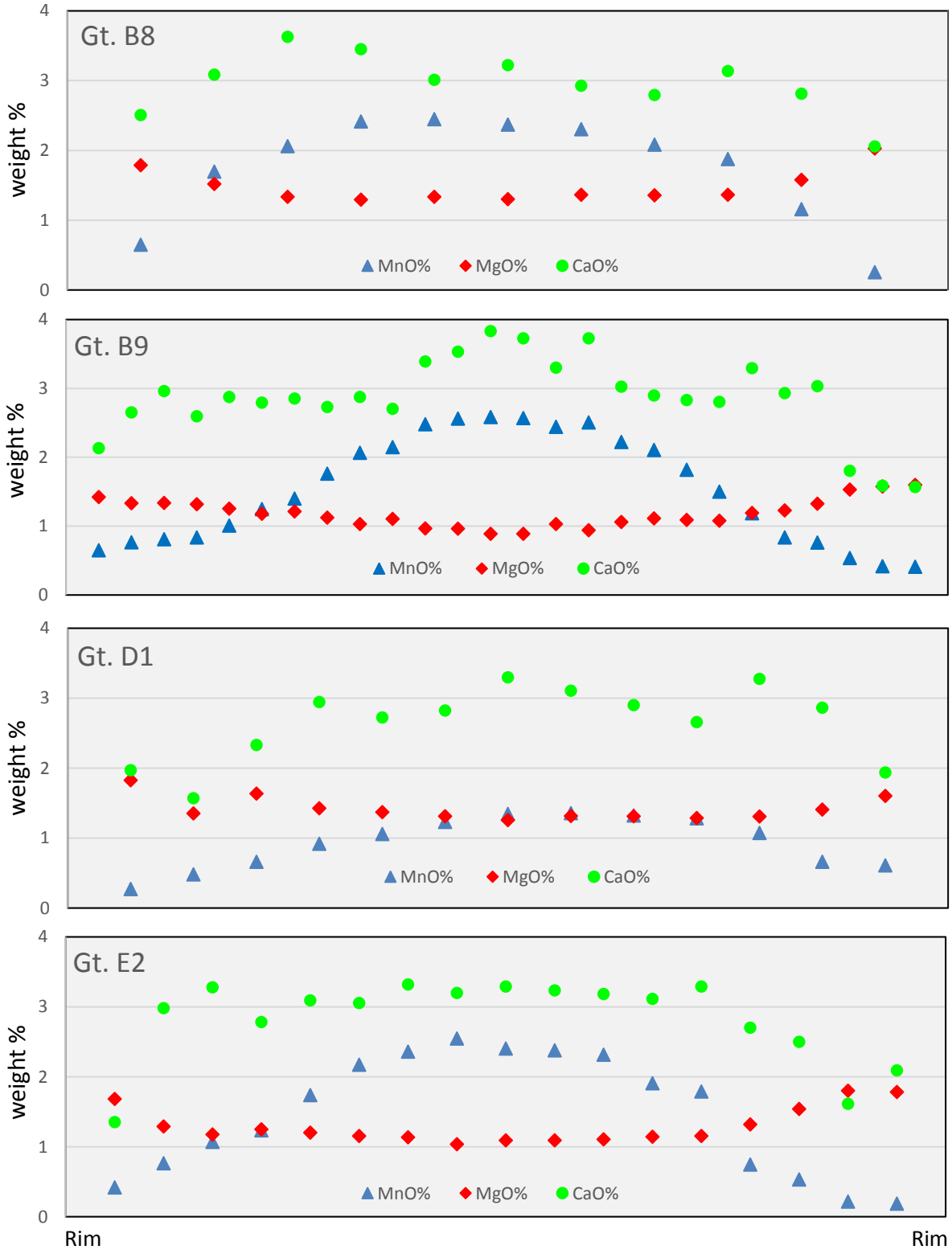


Figure 3.9.3 Weight % of MnO, MgO, and CaO from point analyses across transects of garnets B8, B9, D1, and E2. Location of point analyses are shown in figure 3.9.2.

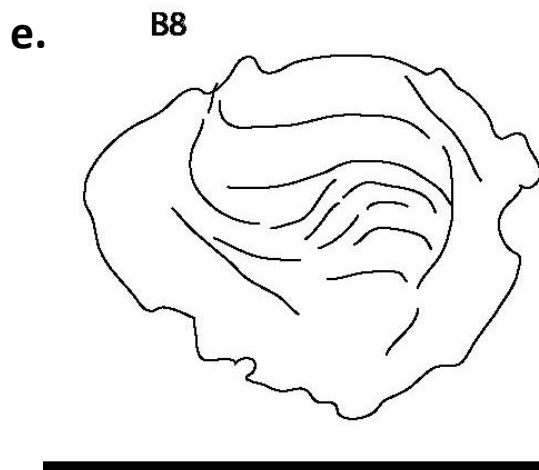
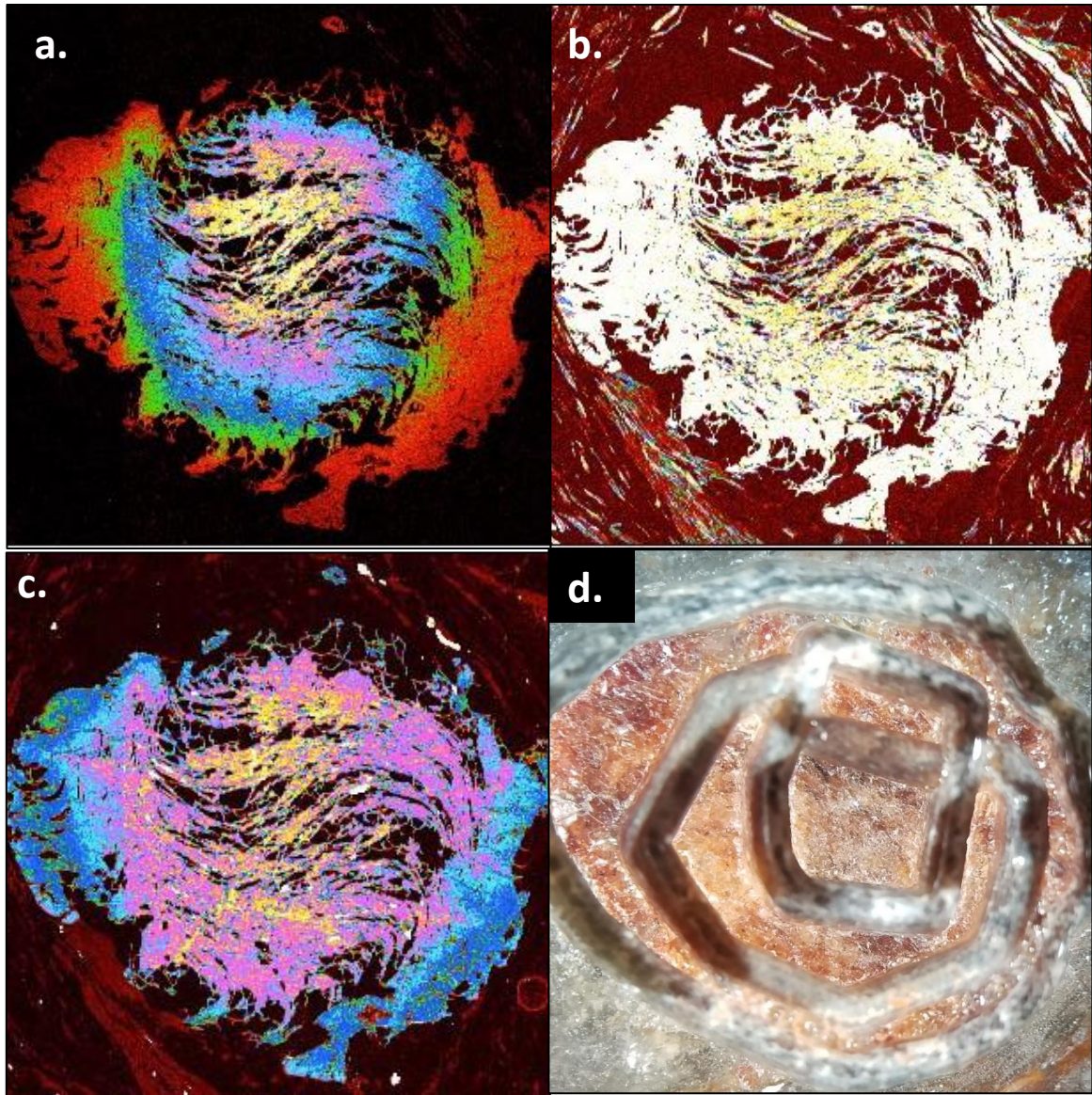


Figure 3.9.4 Chemical maps of (a) Mn, (b) Mg, and (c) Ca zonation for garnet B8. (d) Photo of drilled zones from garnet B8. (e) Sketch of inclusion trail orientation.

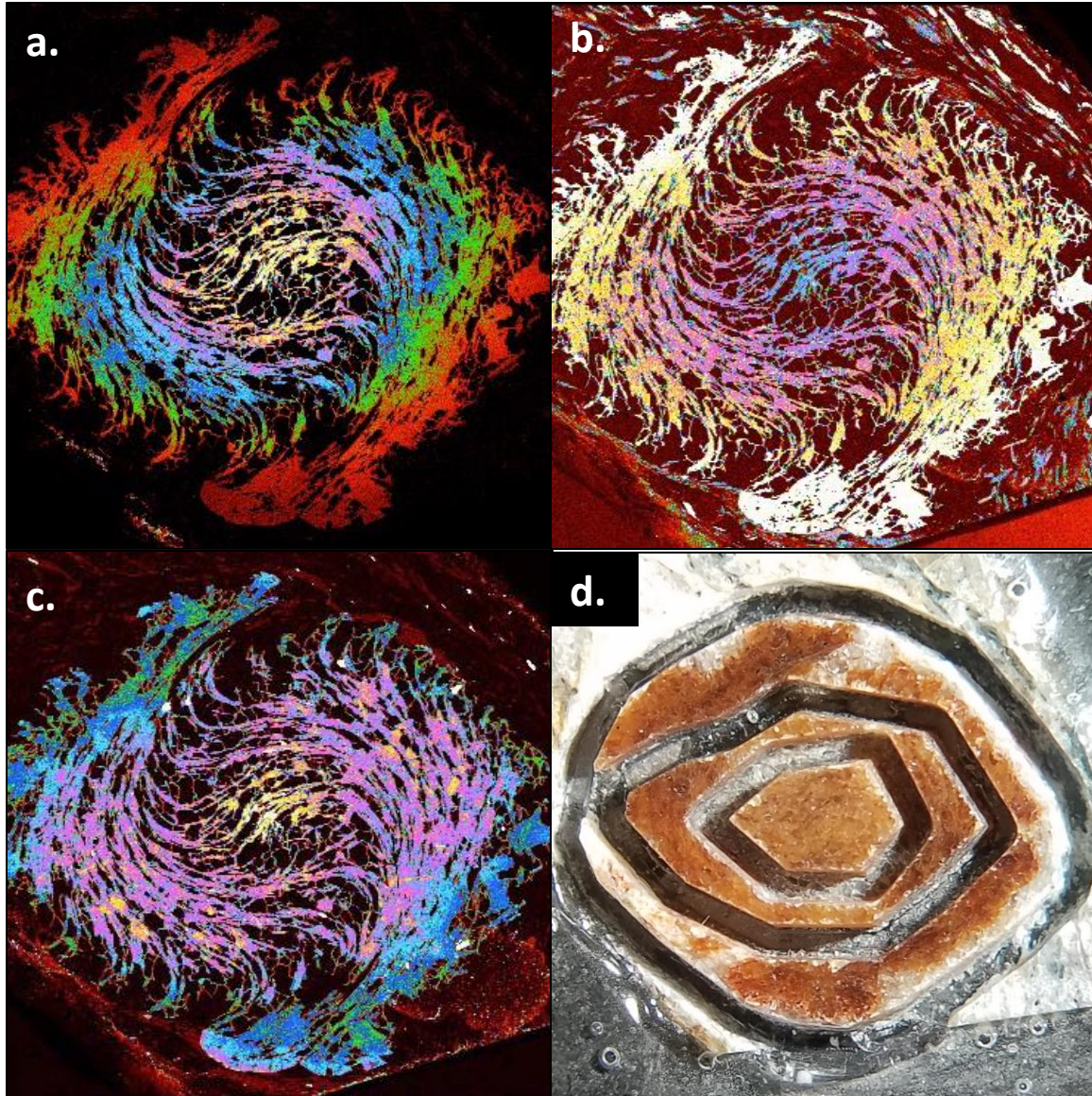
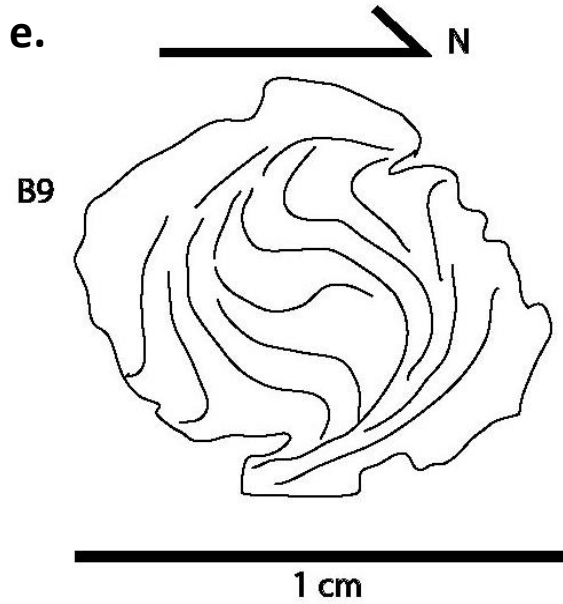


Figure 3.9.5 Chemical maps of (a) Mn, (b) Mg, and (c) Ca zonation for Garnet B9. (d) Photo of drilled zones from garnet B9. (e) Sketch of inclusion trail orientation.



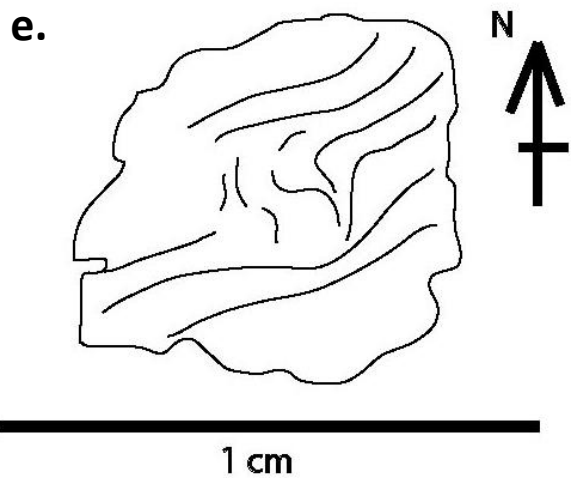
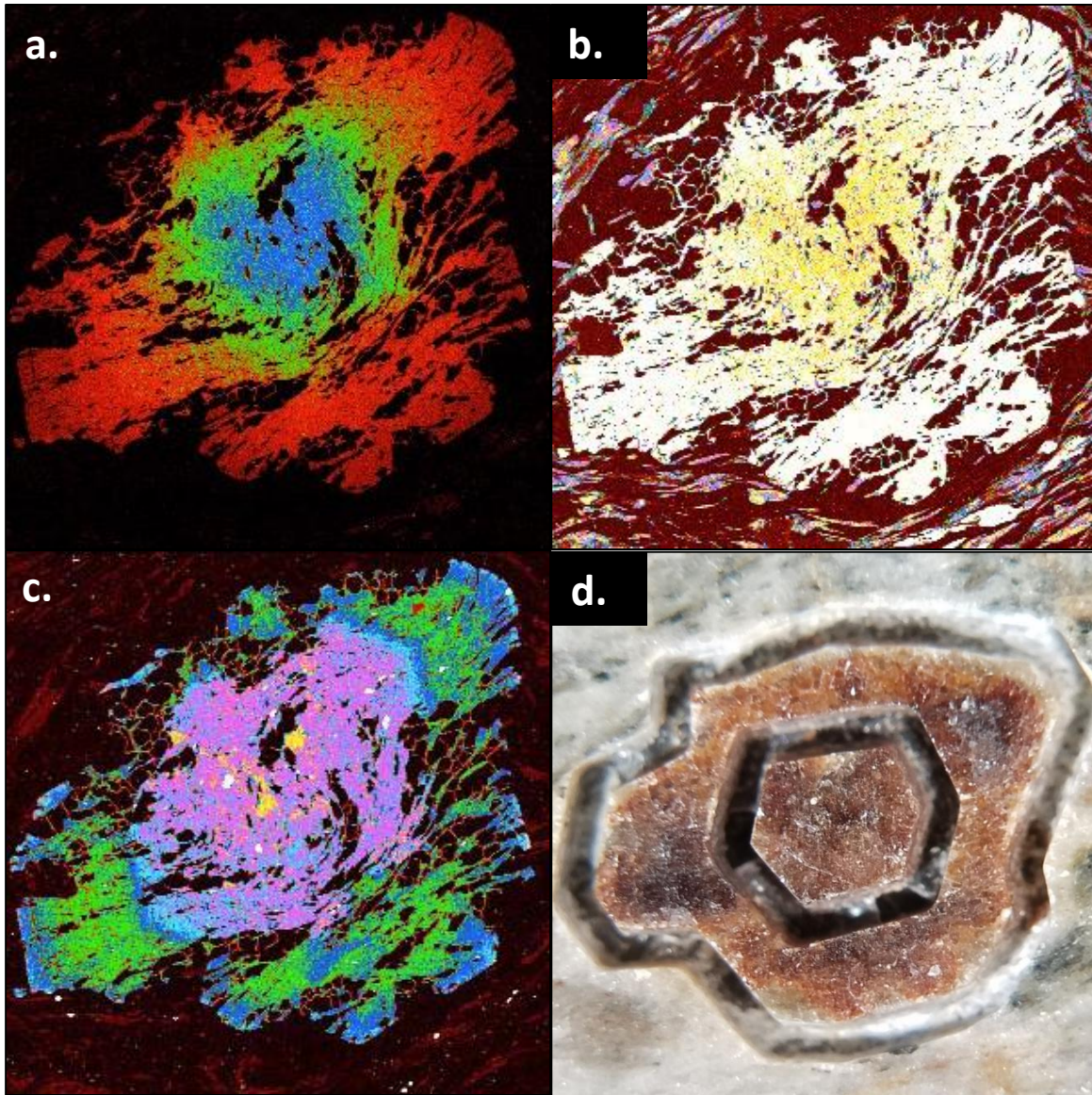
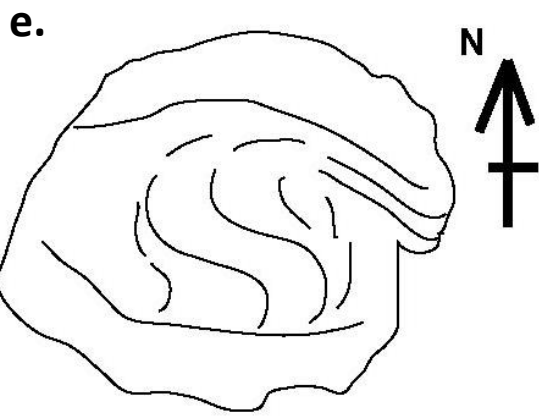
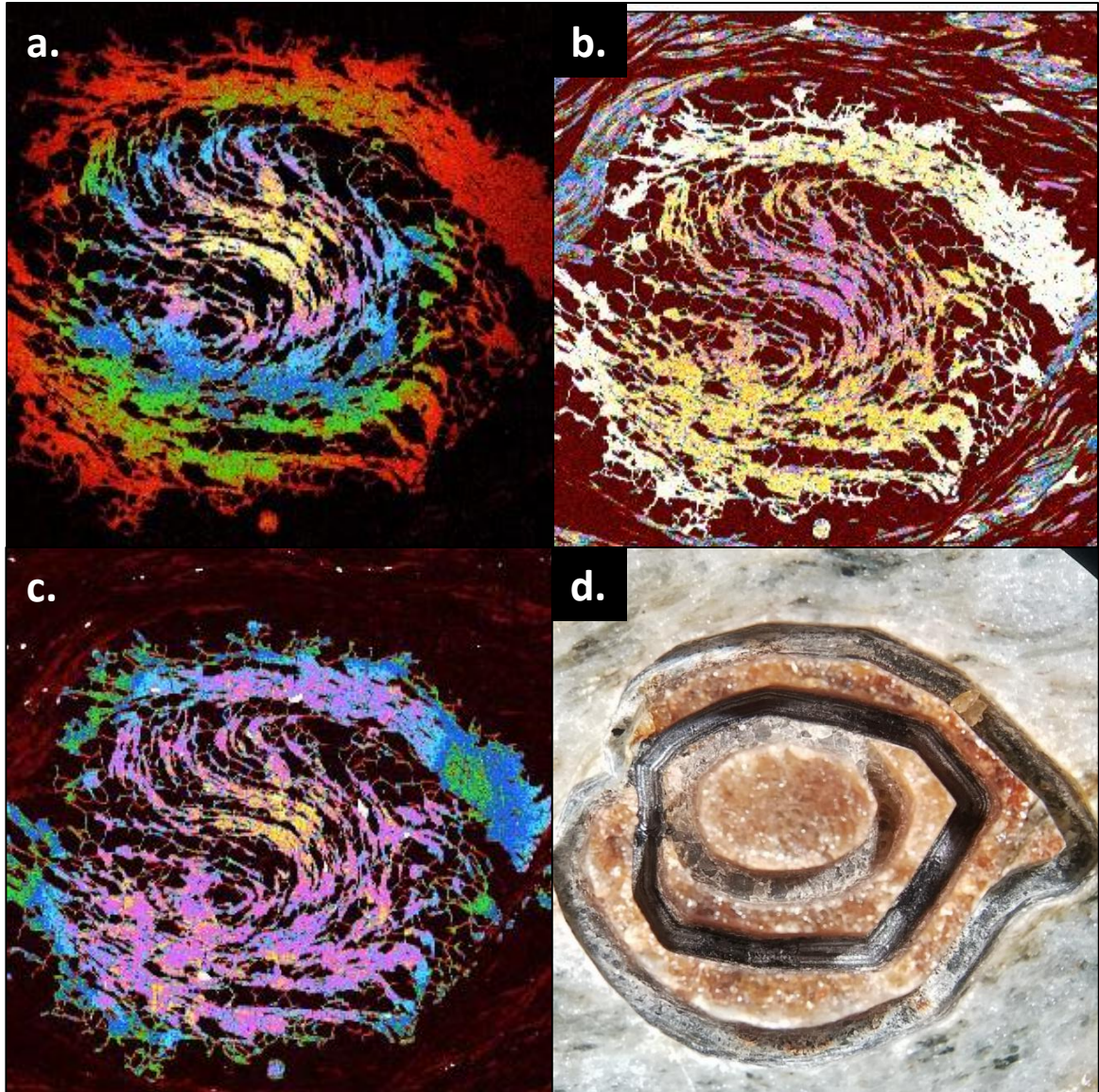


Figure 3.9.6 Chemical maps of (a) Mn, (b) Mg, and (c) Ca zonation for Garnet D1. (d) Photo of drilled zones from garnet B9. (e) Sketch of inclusion trail orientation.



1 cm

Figure 3.9.7 Chemical maps of Garnet E2 (a) Mn, (b) Mg, and (c) Ca zonation. Photo of drilled zones from garnet B9 (d). Sketch of inclusion trail orientation (e).

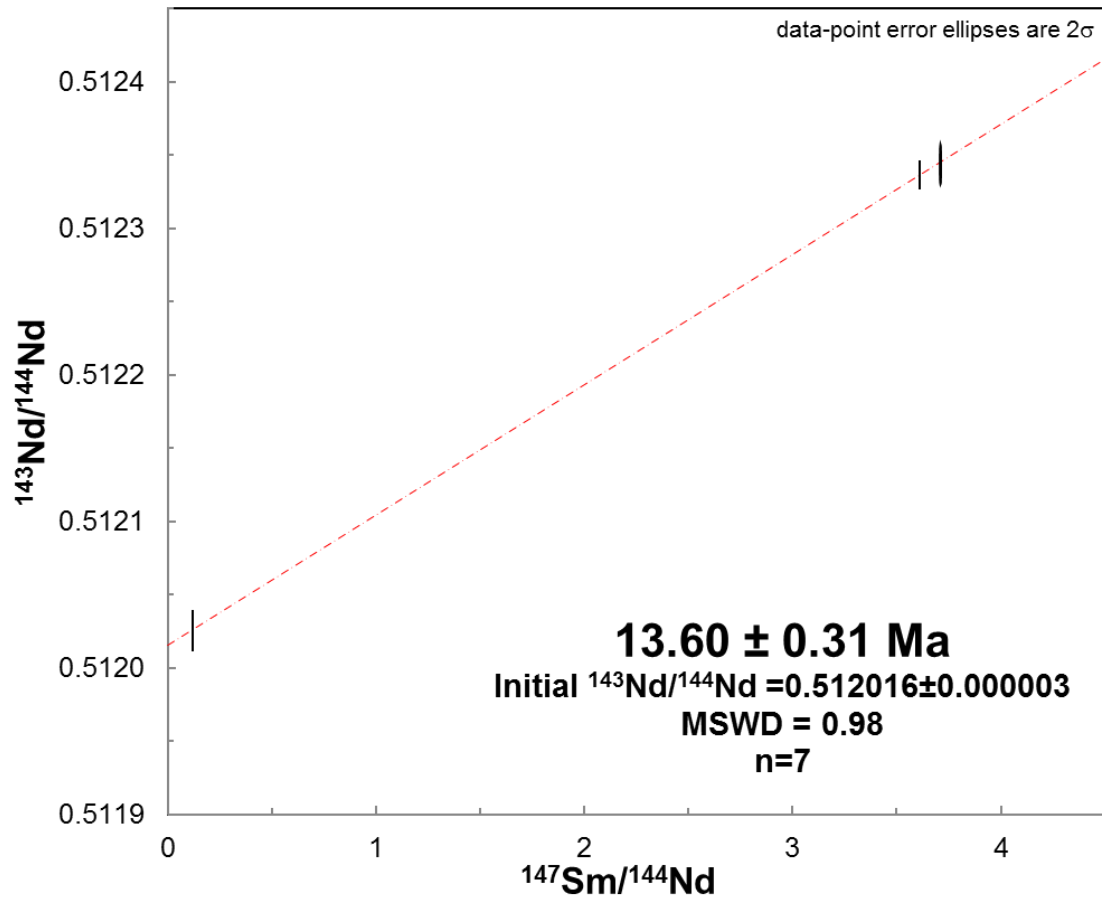


Figure 3.9.8 seven-point isochron of all analyzed data for combined core (zone 1) from garnets B8, B9, and E2.

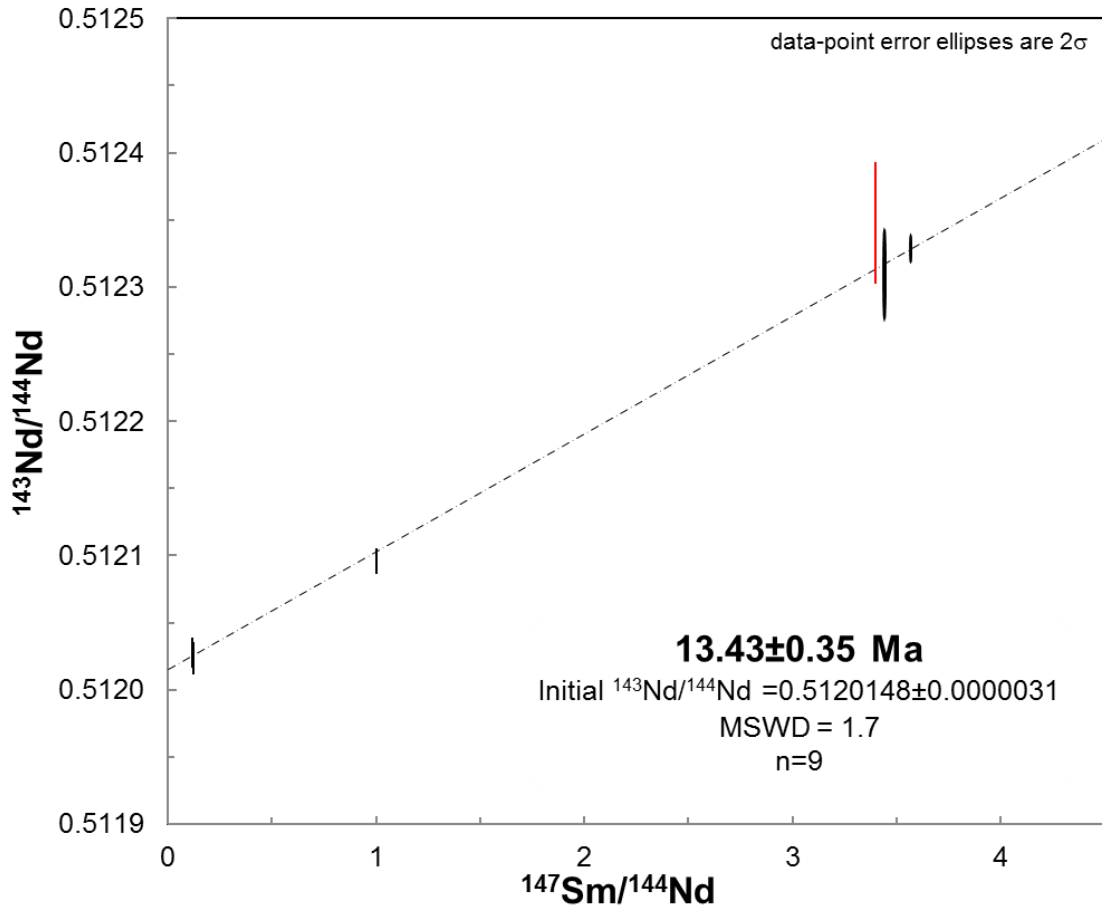


Figure 3.9.9 nine-point isochron of all analyzed data for median zones from garnets B8, B9, D1, and E2. Red data points denote rejected data.

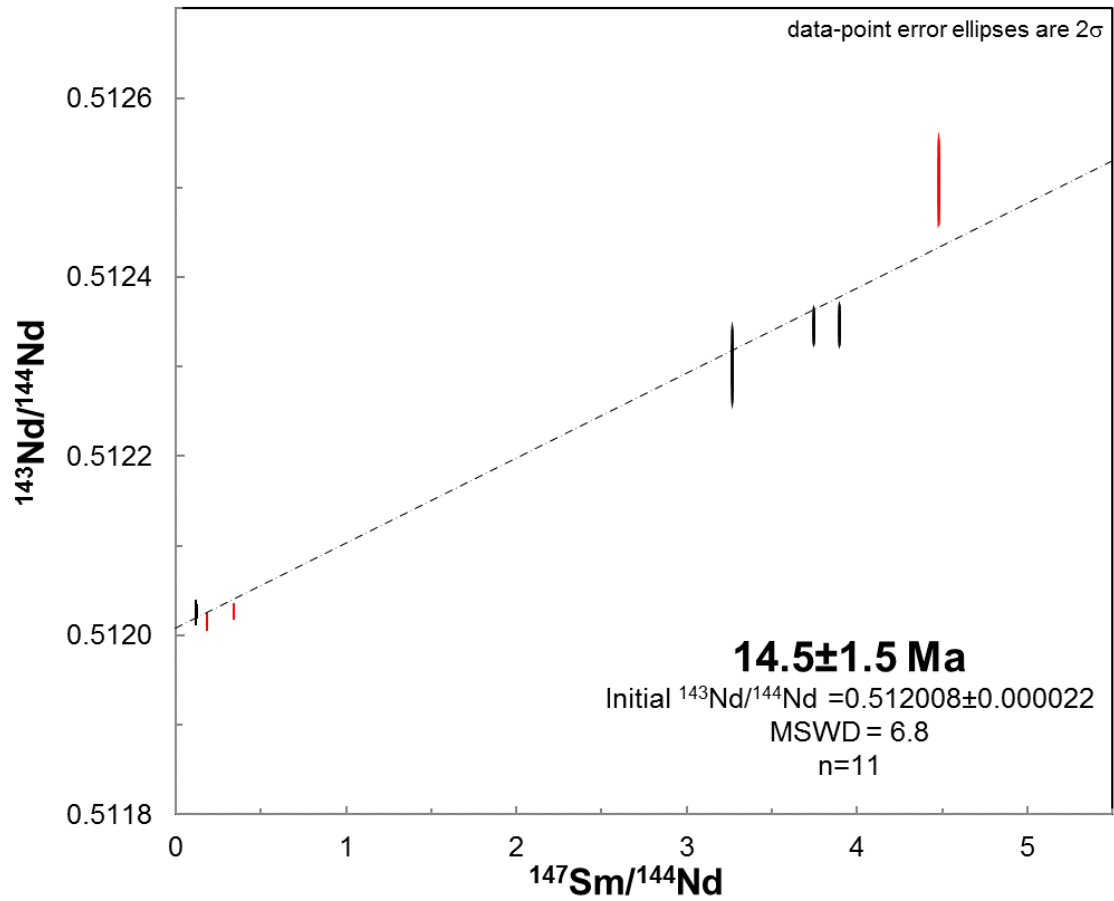


Figure 3.9.10 eleven-point isochron of all analyzed data for garnet rims (zone 3) from garnets B8, B9, D1, and E2. Red data points denote rejected data.

6.0 BIBLIOGRAPHY

- Aerden, D. G. A. M., 1995. Porphyroblast non-rotation during crustal extension in the Variscan Lys-Caillaouas Massif, Pyrenees. *Journal of Structural Geology*, 17, 709-725.
- Aerden, D.G., 2003. Preferred orientation of planar microstructures determined via statistical best-fit of measured intersection-lines: the 'FitPitch' computer program. *Journal of Structural Geology*, 25(6), 923 – 934.
- Aerden, D.G.A.M., 2004. Correlating deformations in the Iberian Massif (Variscan belt) using porphyroblasts; implications for the development of the Ibero-Armorican Arc. *Journal of Structural Geology*, 26, 177 – 196.
- Aerden, D. G. A. M., 2005. Comment on “Reference frame, angular momentum, and porphyroblast rotation” by Diazhi Jiang and Paul F. Williams. *Journal of Structural Geology* (27) 1128 – 1133.
- Aerden, D., and Sayab, M., 2008. From Adria-to Africa-driven orogenesis: Evidence from porphyroblasts in the Betic Cordillera, Spain. *Journal of Structural Geology*, 30(10), 1272 – 1287.
- Aerden, D. G. A. M., Mohammad, S., Bouybaouene, M. L., 2010 Conjugate-shear folding: A model for the relationship between foliations, folds and shear zones. *Journal of Structural Geology*, 32, 1030 – 1045.
- Aerden, D. G. A. M., Bell, T. H., Puga, E., Sayab, M., Lozano, J. A., and de Federico, A. D., 2013. Multi-stage mountain building vs. relative plate motions in the Betic Cordillera deduced from integrated microstructural and petrological analysis of porphyroblast inclusion trails. *Tectonophysics*, 537, 188 – 206.
- Augier, R., Agard, P., Monié, P., Jolivet, L., Robin, C., and Booth-Rea, G., 2005. Exhumation, doming and slab retreat in the Betic Cordillera (SE Spain): in situ $^{40}\text{Ar}/^{39}\text{Ar}$ ages and P–T–d–t paths for the Nevado-Filabride complex. *Journal of Metamorphic Geology*, 23(5), 357 – 381.
- Bakker, H. E., Jong, K., Helmers, H., and Biermann, C., 1989. The geodynamic evolution of the Internal Zone of the Betic Cordilleras (south-east Spain): a model based on structural analysis and geothermobarometry. *Journal of Metamorphic Geology*, 7(3), 359 – 381.
- Baxter, E. F., DePaolo, D. J., 2004. Can metamorphic reactions proceed faster than bulk strain?. *Contrib Mineral Petrol*, 146, 657 – 670.
- Baxter, E. F., Scherer, E. E., 2013. Garent Geochronology: Timekeeper of Tectonometamorphic Processes. *Elements*, 9, 433 – 438.

- Baxter, E. F., Caddick, M. J., Dragovic, B. 2017. Garnet: A Rock-Forming Mineral Petrochronometer. Chapter 15 Reviews in Mineralogy and Geochemistry, 83, 469 – 533.
- Bell, T. H., Rubenach, M. J., 1980. Crenulation cleavage development – evidence for progressive bulk inhomogeneous shortening from “millipede” microstructures in the Robertson River Metamorphics. *Tectonophysics*, 68, 9 – 15.
- Bell, T. H., 1981. Foliation development; the contribution, geometry and significance of progressive bulk inhomogeneous shortening. *Tectonophysics*, 75, 273 – 296.
- Bell, T. H., 1985. Deformation partitioning and porphyroblast rotation in metamorphic rocks: a radical reinterpretation. *Journal of Metamorphic Geology*, 3, 109 – 118.
- Bell, T. H. and Johnson, S. E., 1989. Porphyroblast inclusion trails: the key to orogenesis. *Journal of Metamorphic Geology*, 7, 279 – 310.
- Bell, T. H., Forde, A., and Hayward, N., 1992. Do smoothly curving, spiral-shaped inclusion trails signify porphyroblast rotation? *Geology*, 20(1), 59 – 62.
- Bell, T.H., Forde, A., Wang, J., 1995. A new indicator of movement direction during orogenesis: measurement technique and application to the Alps. *Terra Nova* 7, 500 – 508.
- Bell, T. H., Hickey, K. A. and Upton, J. G., 1998. Distinguishing and correlating multiple phases of metamorphism across a multiply deformed region using the axes of spiral, staircase and sigmoidal inclusion trails in garnet, *Journal of Metamorphic Geology*, 16, 767 – 794.
- Bell, T. H., Ham, A. P., and Kim, H. S., 2004. Partitioning of deformation along an orogen and its effects on porphyroblast growth during orogenesis. *Journal of Structural Geology* 26, 825 – 845.
- Bell, T. H. and Kim, H. S., 2004. Preservation of Acadian deformation and metamorphism through intense Alleghenian shearing. *Journal of Metamorphic Geology*, 26, 1591 – 1613.
- Bell, T. H. and Newman, R., 2006. Appalachian orogenesis: The role of repeated gravitational collapse, Butler R., and Mazzoli, S., eds., *Styles of continental compression: Geological Society of America Special Paper 414*, 95 – 118.
- Bell, T. H. and Bruce, M. D., 2007. Progressive deformation partitioning and deformation history: Evidence from millipede structures. *Journal of Structural Geology*, 29, 18 – 35.

- Bell, T. H. and Sapkota, J., 2012. Episodic gravitational collapse and migration of the mountain chain during orogenic roll-on in the Himalayas. *Journal of Metamorphic Geology*, 30, 651 – 666.
- Berg, C. A., Carlson, W. D., Connelly, J. N., 2013. Strain rates at high temporal resolution from curved inclusion trails in garnet, Passo del Sole, Central Swiss Alps. *Journal of Metamorphic Geology*, 31, 243 – 262.
- Berndt, T., Ruiz-Martínez, V. C., Chalouan, A., 2015. New constraints on the evolution of the Gibraltar Arc from palaeomagnetic data of the Ceuta and Beni Bousera peridotites (Rif, northern Africa). *Journal of Geodynamics*, 84, 19 – 39.
- Biermeier, C Stuwe, K., 2003. Strain-rate from snowball garnet. *Journal of Metamorphic Geology*, 21, 253 – 268.
- Bons, P. D., Jessell, M. W., Griera, A, 2009, Porphyroblast rotation versus nonrotation: Conflict resolution! : COMMENT. *Geology*, 37(2), 182 – 182.
- Bowring, J. F., McLean, M. N., and Bowring, S. A., 2011. Engineering cyber infrastructure for U-Pb geochronology: Tripoli and U-Pb_Redux, *Geochem. Geophys. Geosyst.*, doi:10.1029/2010GC003478, in press.
- Bufom, E. and Udías, A., 1991. Focal mechanisms of earthquakes in the Gulf of Cadiz, South Spain and Alboran Sea. In: Mezcuá, J. and Udías, A. (eds), *Seismicity, Seismotectonics and Seismic Risk of the Ibero-Maghrebian Region*, Instituto Geográfico Nacional Monograph, 8, 29 – 40.
- Carlson, W. D., 2011. Porphyroblast crystallization: linking processes, kinematics, and microstructures. *International Geology Review*, 53(3-4), 406 – 445.
- Christensen, J. N., Rosenfeld, J. L., DePaolo, D. J., 1989. Rates of Tectonometamorphic Processes from Rubidium and Strontium Isotopes in Garnet. *Science*, 244, 1465 – 1469.
- Christensen, J. N., Selverstone, J., Rosenfeld, J. L., DePaolo, D. J., 1994. Correlation by Rb-Sr geochronology of garnet growth histories from different structural levels within the Tauern Window, eastern Alps. *Contrib Mineral Petrol*, 118, 1 – 12.
- Cifelli, F., Mattei, M., Porreca, M., 2008. New paleomagnetic data from oligocene-upper Miocene sediments in the Rif chain (northern Morocco): insights on the Neogene tectonic evolution of the Gibraltar Arc. *J. Geophys. Res.: Solid Earth (1978–2012)* 113 (B2).
- Cihan, M., Evins, P., Lisowiec, N., Blake, K., 2006. Time constraints on deformation and metamorphism from EPMA dating of monazite in the Proterozoic Robertson River Metamorphics, NE Australia. *Precambrian res*, 145, 1 – 23.

- Dragovic, B., Samanta, L. M., Baxter, E. F., Selverstone, J. 2012. Using garnet to constrain the duration and rate of water-releasing metamorphic reactions during subduction: An example from Sifnos, Greece. *Chemical Geology*, 314 – 317, 9 – 22.
- Dragovic, B., Baxter, E. F., Caddick, M. J. 2015. Pulsed dehydration and garnet growth during subduction revealed by zoned garnet geochronology and thermodynamic modeling, Sifnos, Greece. *Earth and Planetary Science Letters*, 413, 111 – 122.
- Fay B., Bell, T. H. Hobbs, B. E., 2008. Porphyroblast rotation versus nonrotation: conflict resolution! *Geology*, 36, 307 – 310.
- Fay B., Bell, T. H. Hobbs, B. E., 2009. Porphyroblast rotation versus nonrotation: conflict resolution!: Reply. *Geology*, 37, 188.
- Handy, M. R., Schmid, S. M., Bousquet, R., Kissling, E., and Bernoulli, D. (2010). Reconciling - plate-tectonic reconstructions of Alpine Thethys with geological-geophysical record of spreading and subduction in the Alps. *Earth-Science Reviews*, 102(3), 121 – 158.
- Harvey, J., Baxter, E. F., 2009. An improved method for TIMS high precision neodymium isotope analysis of very small aliquots (1–10 ng). *Chemical Geology*, 258, 251 – 257.
- Hayward, N., 1990. Determination of early fold axis orientations in multiply deformed rocks using porphyroblasts inclusion trails. *Tectonophysics*, 179(3), 353 – 369.
- Hickey, K.A., Bell, T.H., 1999. Behavior of rigid objects during deformation and metamorphism: a test using schists from the Bolton syncline, Connecticut, USA. *Journal of Metamorphic Geology* 17, 211 – 228.
- Huddleston-Holmes, C. R., Ketcham, R. A., 2010. An X-ray computed tomography study of inclusion trail orientations in multiple porphyroblasts from a single sample. *Tectonophysics*, 480, 305 – 320.
- Gaidies, F., Pattison, D. R. M., de Capitani, C., 2011. Toward a quantitative model of metamorphic nucleation and growth. *Contribution to Mineralogy and Petrology*, 162(5), 975 – 993.
- Gatewood, M. P., Dragovic, B., Stowell, H. H., Baxter, E.F, Hirsch, D. M., Bloom, R. 2015. Evaluating chemical equilibrium in metamorphic rocks using major element and Sm–Nd isotopic age zoning in garnet, Townshend Dam, Vermont, USA. *Chemical Geology*, 401, 151 – 168.
- Gómez-Pugnaire, M.T., Rubatto, D., Fernández-Soler, J. M., Jabaloy-Sanchez, A., López Sánchez-Vizcaino, V., Gonzalez-Lodeiro, F., Galindo-Zaldivar, J., Padron-Navarta, J. A., 2012. Late Variscan magmatism in the Nevado–Filabride Complex:

- U–Pb geochronologic evidence for the pre-Mesozoic nature of the deepest Betic complex (SE Spain). *Lithos*, 146, 93 – 111.
- Griera, A., Llorens, M. G., Gomez-Rivas, E., Bons, P. D., Jessell, M. W., 2013. Numerical modelling of porphyroblast and porphyroblast rotation in anisotropic rocks. *Tectonophysics*, 587, 4 – 29.
- Jeffery, G. B., 1922. The motion of ellipsoidal particales immersed in a viscous fluid. *Proceedings of the Royal Society of London, Series A*, 102, 191 – 179.
- Jiang, D. and Williams, P. F., 2004. Reference frame, angular momentum, and porphyroblast rotation. *Journal of Structural Geology*, 26, 2211 - 2224.
- Johnson, S. E., 1993a. Testing models for the development of spiral-shaped inclusion trails in garnet porphyroblasts: to rotate or not to rotate, that is the question. *Journal of Metamorphic Geology*, 11, 635 – 659.
- Johnson, S. E., 1993b. Unravelling the spirals: a serial thin-section study and three-dimensional computer-aided reconstruction of spiral-shaped inclusion trails in garnet porphyroblasts. *Journal of Metamorphic Geology*, 11, 621 – 634.
- Johnson, C., Harbury, N., Hurford, A. J., 1997. The role of extension in the Miocene denudation of the Nevado-Filabride complex, Betic Cordillera (SE Spain), *Tectonics*, 16(2), 189 – 204.
- Johnson, S.E. and Williams, M.L., 1998. Determining finite longitudinal strains from oppositely-concave microfolds in and around porphyroblasts: a new quantitative method. *Journal of Structural Geology*, 20, 1521 – 1530.
- Johnson, S. E., 1999. Porphyroblast microstructures: A review of current and future trends. *American Mineralogist*, 84, 1711 – 1726.
- Johnson, S. E., Dupee, M. E., Guidotti, C. V., 2006. Porphyroblast rotation during crenulation cleavage development: an example from aureole of the Mooselookmeguntic pluton, Maine, USA. *Journal of Metamorphic Geology*, 24, 55 – 73.
- Johnson, S. E., 2009. Porphyroblast rotation and strain localization: Debate settled! *Geology*, 37(7), 663 – 666.
- Kim, H. S., Bell, T. H., 2005. Combining compositional zoning and foliation intersection axes (FIAs) in garnet to quantitatively determine early P-T-t paths in multiply deformed and metamorphosed schists: north-central Massachusetts, USA. *Contrib. Mineral. Petrol.* 149, 141 – 163.

- Kirchner, K. L., Behr, W. M., Loewy, S., Stockli, D. F., 2016. Early Miocene subduction in the western Mediterranean: Constraints from Rb-Sr multimineral isochron geochronology. AGU Publications, 1842 – 1860.
- Li, B., Massonne, H. J., 2018. Two Tertiary metamorphic events recognized in high-pressure metapelites of the Nevado-Filabride Complex (Betic Cordillera, S Spain). *Journal of Metamorph Geology*, 1 – 28.
- Ludwig, K. R. 2003. User's manual for Isoplot 3.00: a geochronological toolkit for Microsoft Excel (No. 4). Kenneth R. Ludwig.
- Macchiavelli, C., Vergés, J., Schettino, A., Fernández, M., Turco, E., Casciello, E., 2017. A new southern North Atlantic isochron map: Insights into the drift of the Iberian plate since the Late Cretaceous. *Journal of Geophysical Research: Solid Earth*, 122, 9603. 10.1002/2017JB014769–9626.
- Martinez-Martinez, J. M., Soto, J. I., and Balanya, J. C., 2002 Orthogonal folding of extensional detachments: structure and origin of the Sierra Nevada elongated dome (Betics, SE Spain), *Tectonics*, 21, doi: 10.1029/2001TC001283.
- Mattei, M., Cifelli, F., Rojas, I.M., Crespo Blanc, A., Comas, M., Faccenna, C., Porreca, M., 2006. Neogene tectonic evolution of the Gibraltar Arc: new paleomagnetic constrains from the Betic chain. *Earth Planet. Sci. Lett.* 250 (3), 522 – 540.
- Monie, P., Zaldivar, J. G., Lodeiro, F. G., Goffe, B., Jabaloy, A. 1991. $^{40}\text{Ar}/^{39}\text{Ar}$ geochronology of Alpine tectonism in the Betic Cordilleras (southern Spain), *J. Geol. Soc. London*, 148(2), 289-297.
- Müller, W., Aerden., D. A. G. M., Halliday, A. N., 2000. Isotopic Dating of Strain Fringe Increments: Duration and Rates of Deformation in Shear Zones. *Science*, 288, 2195 – 2198.
- Passchier, C. W., Trouw, R. A. J., Zwart, H. J., Vissar, R. L. M. 1992. Porphyroblast rotation: *eppur si muove*?. *Journal of Metamorphic Geology*, 10, 283 – 294.
- Passchier, C. W. and Trouw, R. A. J., 2005. *Microtectonics* 2nd Ed. Springer Verlag, Berlin, pp. 289.
- Patriat, P., Achache, J., 1984. India–Eurasia collision chronology has implications for crustal shortening and driving mechanism of plates. *Nature*, 311, 615 – 621.
- Pattison, D. R. M., de Capitani, C., Gaidies, F., 2011. Petrological consequences of variations in metamorphic reaction affinity. *Journal of Metamorphic Geology*, 29(9), 953 – 977.

- Peach, B. N., Gunn, W., Clough, C. T., Hinxman, L. W., Crampton, C. B., Anderson, E. M. and Flett, J. S. 1912. The geology of Ben Wyvis, Carn Chuinneag, Inchbae and the surrounding country, including Garve, Evanton, Alness and Kincardine (explanation of sheet 93): Mem. Geol. Surv., Scotland, p. 1-189.
- Pfiffner, O. A., Ramsey, J. G., 1982, Constraints on geological strain rates: arguments from finite strain rates of naturally deformed rocks. *J Geophys Res*, 87, 311 – 321.
- Platt, J., Whitehouse, M., Kelley, S., Carter, A., Hollick, L. 2003. Simultaneous extensional and exhumation across the Alboran basin: implications for the cause of late orogenic extension. *Geology*, 31(3), 251 – 254.
- Platt, J. P., Kelley, S. P., Carter, A., Orozco, M. 2005. Timing of tectonic events in the Alpujarride Complex, Betic Cordillera, southern Spain. *Journal of the Geological Society*, London, 162, 451 – 462.
- Platt, J. P., Anckziewicz, R., Soto, J. I., Kelley, S. P., Thirwall, M. 2006. Early Miocene continental subduction and rapid exhumation in the western Mediterranean. *Geology*, 34(11), 981 – 984.
- Platt, J.P., Behr, W.M., Johannesen, K., Williams, J.R., 2013. The Betic–Rif Arc and its orogenic hinterland: a review. *Ann. Rev. Earth Planet. Sci.* 41, 313 – 357.
- Pollington, A. D., Baxter, E. F., 2010. High resolution Sm–Nd garnet geochronology reveals the uneven pace of tectonometamorphic processes. *Earth and Planetary Science Letters*, 293, 63 – 71.
- Pollington, A. D., Baxter, E. F., 2011. High precision microsampling and preparation of zoned garnet porphyroblasts for Sm–Nd geochronology. *Chemical Geology*, 281, 270 – 282.
- Puga, E., De Federico, A.D., Nieto, J.M. 2002. Tectonostratigraphic Subdivision and Petrological Characterization of the Deepest Complexes of the Betic Zone: A Review. *Geodinamica Acta* 15, 1, 23 – 43.
- Ramsey, J. G. 1962. The geometry and mechanisms of formation of ‘similar’ type fold. *Journal of Geology*, 70, 309 – 327.
- Robyr, M., Carlson, W. D., Passchier, C., Vonlanthen, P. (2009) Microstructural, chemical and textural records during growth of snowball garnet. *Journal of Metamorphic Geology*, 27, 423 – 437.
- Rosenfeld, J. 1968. Garnet rotations due to major Paleozoic deformations in Southeast Vermont. In: *Studies of Appalachian Geology* (ed. E. A. Zen), pp. 185 – 202.
- Rosenfeld, J. 1970 Rotated garnets in metamorphic rocks. *Geological Society of America Special paper*, 129.

- Rubatto, D., Regis, D., Hermann, J., Boston, K., Engi, M., Beltrando, M., and McAlpine, S., 2011, Yo-yo subduction recorded by accessory minerals in the Italian Western Alps, *Nature Geoscience*, 4, 338 – 442.
- Ruiz-Fuentes, A., Aerden, D. G. A. M., 2018, Transposition of foliations and superposition of lineations during polyphase deformation in the Nevado-Filabride complex: tectonic implications. *International Journal of Earth Science*, 107, 1975 – 1988.
- Sayab, M. 2005, N-S shortening during orogenesis within the Mt Isa Inlier (NW Queensland, Australia): The preservation of early W-E trending foliations in porphyroblasts revealed by independent 3D measurement techniques. *Journal of Structural Geology*, 21, 1445 – 1468.
- Sayab, M., Shah, S. Z., Aerden, D. G., 2016, Metamorphic record of the NW Himalayan orogeny between the Indian plate-Kohistan Ladakh Arc and Asia: Revelations from foliation axis (FIA) controlled P-T-t-d paths. *Tectonophysics*, 671, 110 – 126.
- Schettino, A., Turco, E., 2011, Tectonic history of the western Tethys since the Late Triassic. *GSA Bulletin*, 123(1/2), 89 – 105.
- Schmidt, A., Pourteau, A., Candan, O., Oberhansli, R., 2015, Lu-Hf geochronology on cm-sized garnets using microsampling: New constraints on garnet growth rates and duration of metamorphism during continental collision (Menderes Massif, Turkey). *Earth and Planetary Science Letters*, 432, 24 – 35.
- Schoneveld, C., 1977, A study of some typical inclusion patterns in strongly paracrystalline-rotated garnets. *Tectonophysics*, 39, 453 – 471.
- Schoneveld, C., 1979, The geometry and the Significance of Inclusion patterns in Syntectonic Porphyroblasts 125 p. Ph.D. Dissertation, University of Leiden.
- Shah, S. Z., Sayab, M., Aerden, D., 2011. Foliation intersection axes preserved in garnet porphyroblasts from the Swat area, NW Himalayas: a record of successive crustal shortening directions between Indian Plate and Kohistan-Ladakh Island Arc. *Tectonophysics* 509, 14 – 32.
- Stallard, A. and Hickey, K., 2001. Shear zone vs folding origin for spiral inclusion trails in the Canton Schist. *Journal of Structural Geology*, 23, 1845 – 1864.
- Stewart, E. M., 2015. CHAPTER TWO: Exploring the Tectonic Significance of Porphyroblast Inclusion Trails via Sm/Nd Garnet Geochronology in the Betic Cordillera, Spain. Unpublished Master's Thesis, p. 29 – 57.
- Teyssier, C., Tikoff, B., Markley, M., 1995, Oblique plate motion and continental tectonics, *Geology*, 23(5), 447 – 450.

- Tikoff B. and Fossen, B., 1999, Three-dimensional reference deformations and strain facies, *Journal of Structural Geology*, 21, 1497 – 1512.
- Thompson, J. B. 1950. A gneiss dome in southeastern Vermont: Ph.D. thesis, Massachusetts Inst. of Tech., 1 – 149.
- Trouw, R. A. J., Tavares, F. M., Robyr, M. 2008. Rotated garnets: a mechanism to explain the high frequency of inclusion trail curvature angles around 90° and 180°. *Journal of Structural Geology*, 30, 1024 – 1033.
- Vance, D. and O’Nions, R. K., 1992. Prograde and retrograde thermal histories from the central Swiss Alps. *Earth and Planetary Science Letters*, 114, 113 – 129.
- Verges, J., Sabat, F., 1999. Constraints on the Neogene Mediterranean kinematic evolution along a 1000 km transect from Iberia to Africa. *Geological Society London Special Publications*, 145(1), 63 – 80.
- Viete, D. R., Hacker, B. R., Allen, M. B., Seward, G. G. E., Tobin, M. J., Kelley, C. S., Cinque, G., Duckworth, A. R. 2018. Metamorphic records of multiple seismic cycles during subduction. *Science Advances*, 4, 1 – 13.
- Villalain, J., Osete, M., Vegas, R., Garcí a-Due nas, V., Heller, F., 1996. The Neogene remagnetization in the western Betics: a brief comment on the reliability paleomagnetic directions. *Geol. Soc. Lond. Spl. Publ.* 105 (1), 33 – 41.
- Villasante-Marcos, V., Osete, M., Gervilla, F., Garcia-Duenas, V., 2003. Paleo-magnetic study of the ronda peridotites (Betic Cordillera, Southern Spain). *Tectonophysics* 377 (1), 119 – 141.
- Welch, P., 2003. Microprobe dating of monazite in relation to porphyroblast growth and thermodynamic modelling P-T paths for rocks affected by prolonged orogenesis. Unpublished Ph.D. Thesis, James Cook University.
- Wendt, I., Carl, C., 1991. The statistical distribution of the mean squared weighted deviation. *Chemical Geology*, 86, 275 – 285.
- Whitney, D. L., 1996, Garnets as open systems during regional metamorphism. *Geology*, 24(2), 147 – 150.
- Williams, J. R. and Platt, J. P., 2018. A new structural and kinematic framework for the Alborán Domain (Betic–Rif arc, western Mediterranean orogenic system). *Journal of the Geological Society*, 175, 465 – 496

APPENDIX A: Blanks and Standards

This appendix contains the data from all three-column and full procedural Nd blanks run during this study, as well as the internal and long-term external precision on all Ames NdO and Sm standards analyzed.

Table A.1 Summary of Nd blanks, date denotes day of MLA columns

Blank name	$^{143}\text{Nd}/^{144}\text{Nd}$	± 2 S.E.	$^{150}\text{Nd}/^{144}\text{Nd}$	Spike weight (mg)	Blank weight (pg)
Full procedural blank 7/09/18	0.516436	0.0043	42.15443	2.02	2.34
Full procedural blank 2/13/19	0.515238	0.1452	13.36975	1.84	9.75
3 column blank 11/5/18	0.512462	n/a	46.34550	2.14	2.65
3 column blank 11/14/18	0.516762	0.0790	20.51711	1.91	5.93
3 column blank 4/12/18	0.507289	1.0553	26.75746	1.67	3.71
3 column blank 6/26/18	0.515622	0.0697	16.21449	1.75	7.21
3 column blank 1/31/19	0.504298	0.4294	26.26115	0.97	2.41
3 column blank 1/17/19	0.549700	3.06	34.97636	1.85	3.28
3 column blank 2/13/19	0.515970	0.2857	12.61753	1.80	10.16
Average	0.517086	0.6411	26.57931	1.79	4.47

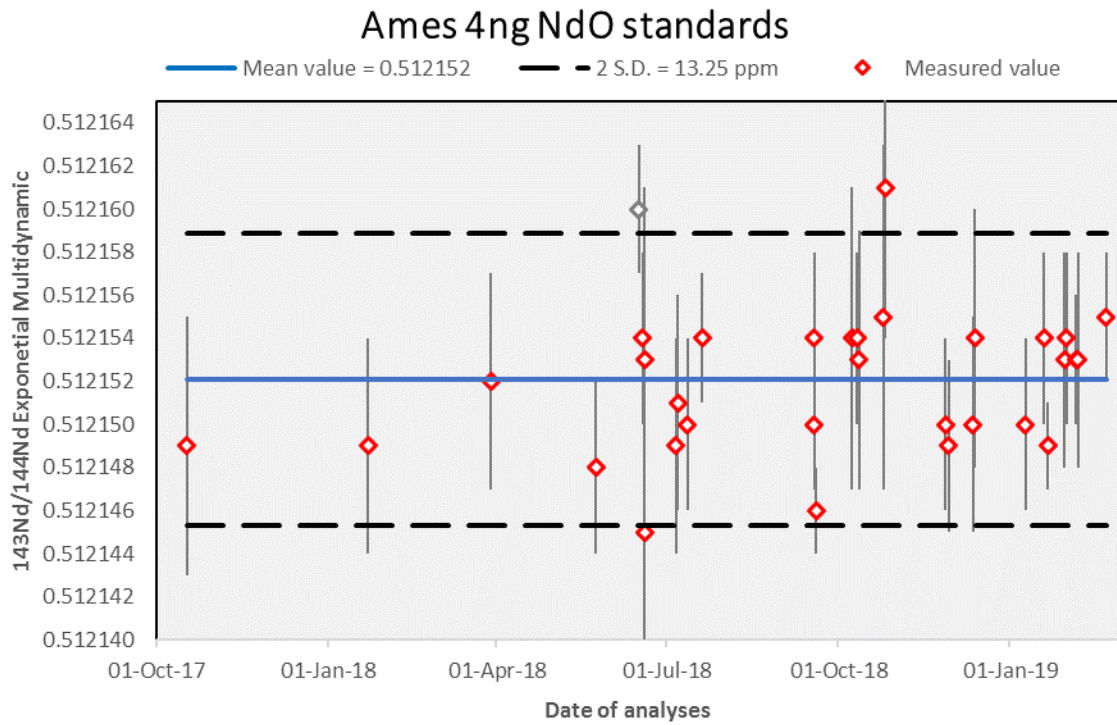


Figure A.1 All Ames 4ng NdO standards run by the author during this study.

Table A.2 Summary of Isotopic data for all Ames 4ng NdO Standards run by the author during this study

Date of Analysis	$^{142}\text{Nd}/^{144}\text{Nd}$ Exp. MD.	$^{142}\text{Nd}/^{144}\text{Nd}$ 2 S.E.	$^{143}\text{Nd}/^{144}\text{Nd}$ Exp. MD.	$^{143}\text{Nd}/^{144}\text{Nd}$ 2 S.E.	$^{145}\text{Nd}/^{144}\text{Nd}$ Exp. MD.	$^{145}\text{Nd}/^{144}\text{Nd}$ 2 S.E.	$^{148}\text{Nd}/^{144}\text{Nd}$ Exp. Seq. 2	$^{148}\text{Nd}/^{144}\text{Nd}$ 2 S.E.	$^{150}\text{Nd}/\text{Nd}^{144}$ Exp. Seq. 3	$^{150}\text{Nd}/^{144}\text{Nd}$ 2 S.E.
10/17/17	1.141840	0.000019	0.512149	0.000006	0.348409	0.000004	0.241577	0.000004	0.236506	0.000008
01/22/18	1.141853	0.000016	0.512149	0.000005	0.348413	0.000003	0.241556	0.000005	0.236483	0.000006
03/29/18	1.141851	0.000014	0.512152	0.000005	0.348405	0.000004	0.241562	0.000006	0.236493	0.000006
05/24/18	1.141840	0.000013	0.512148	0.000004	0.348411	0.000003	0.241556	0.000003	0.236506	0.000005
06/16/18	1.141856	0.000011	0.512160	0.000003	0.348404	0.000002	0.241569	0.000004	0.236489	0.000005
06/18/18	1.141860	0.000012	0.512154	0.000004	0.348404	0.000002	0.241575	0.000003	0.236496	0.000004
06/19/18	1.141826	0.000021	0.512145	0.000006	0.348409	0.000003	0.241569	0.000005	0.236495	0.000009
06/19/18	1.141881	0.000023	0.512153	0.000008	0.348401	0.000004	0.241598	0.000006	0.236486	0.000012
07/06/18	1.141824	0.000017	0.512149	0.000005	0.348404	0.000003	0.241568	0.000005	0.236518	0.000008
07/07/18	1.141838	0.000016	0.512151	0.000005	0.348402	0.000003	0.241568	0.000004	0.236502	0.000007
07/12/18	1.141857	0.000013	0.512150	0.000004	0.348402	0.000003	0.241557	0.000004	0.236492	0.000007
07/20/18	1.141835	0.000010	0.512154	0.000003	0.348406	0.000002	0.241565	0.000004	0.236488	0.000005
09/18/18	1.141882	0.000011	0.512154	0.000004	0.348399	0.000002	0.241562	0.000003	0.236481	0.000005
09/18/18	1.141847	0.000010	0.512150	0.000003	0.348405	0.000002	0.241566	0.000003	0.236486	0.000004
09/19/18	1.141845	0.000011	0.512146	0.000002	0.348407	0.000002	0.241564	0.000005	0.236482	0.000006
10/08/18	1.141872	0.000019	0.512154	0.000007	0.348398	0.000004	0.241551	0.000007	0.236484	0.000007
10/11/18	1.141845	0.000011	0.512154	0.000004	0.348408	0.000002	0.241550	0.000003	0.236483	0.000005
10/12/18	1.141857	0.000023	0.512153	0.000006	0.348405	0.000003	0.241551	0.000005	0.236496	0.000009
10/25/18	1.141897	0.000052	0.512155	0.000008	0.348392	0.000006	0.241557	0.000007	0.236493	0.000013
10/26/18	1.141886	0.000022	0.512161	0.000007	0.348400	0.000004	0.241578	0.000005	0.236476	0.000010
11/27/18	1.141836	0.000014	0.512150	0.000004	0.348406	0.000003	0.241585	0.000003	0.236536	0.000008
11/29/18	1.141825	0.000015	0.512149	0.000004	0.348405	0.000002	0.241569	0.000004	0.236506	0.000006
12/12/18	1.141838	0.000012	0.512150	0.000005	0.348403	0.000003	0.241553	0.000004	0.236484	0.000006
12/13/18	1.141854	0.000015	0.512154	0.000006	0.348408	0.000003	0.241567	0.000004	0.236495	0.000005
01/09/19	1.141865	0.000010	0.512150	0.000004	0.348406	0.000002	0.241561	0.000003	0.236482	0.000004
01/19/19	1.141848	0.000013	0.512154	0.000004	0.348403	0.000002	0.241563	0.000003	0.236495	0.000005
01/21/19	1.141844	0.000010	0.512149	0.000002	0.348406	0.000002	0.241559	0.000003	0.236493	0.000006
01/30/19	1.141862	0.000021	0.512153	0.000005	0.348403	0.000004	0.241538	0.000006	0.236496	0.000008
01/31/19	1.141872	0.000012	0.512154	0.000004	0.348401	0.000003	0.241558	0.000004	0.236480	0.000005
02/05/19	1.141849	0.000009	0.512153	0.000003	0.348407	0.000002	0.241570	0.000003	0.236499	0.000004
02/06/19	1.141826	0.000021	0.512153	0.000005	0.348407	0.000003	0.241555	0.000004	0.236508	0.000007
02/21/19	1.141861	0.000011	0.512155	0.000003	0.348409	0.000002	0.241596	0.000004	0.236527	0.000005
02/22/19	1.141855	0.000020	0.512153	0.000005	0.348409	0.000003	0.241599	0.000004	0.236505	0.000012
External Value	1.141852	± 31.75 ppm	0.512152	± 13.24 ppm	0.348405	± 23.58 ppm	0.241566	± 114.28 ppm	0.236495	± 114.35 ppm

*Exp. MD. = Exponential Multidynamic corrected to $^{146}\text{Nd}/^{144}\text{Nd}$ value of 0.7216

Ames 20ng Sm Standards

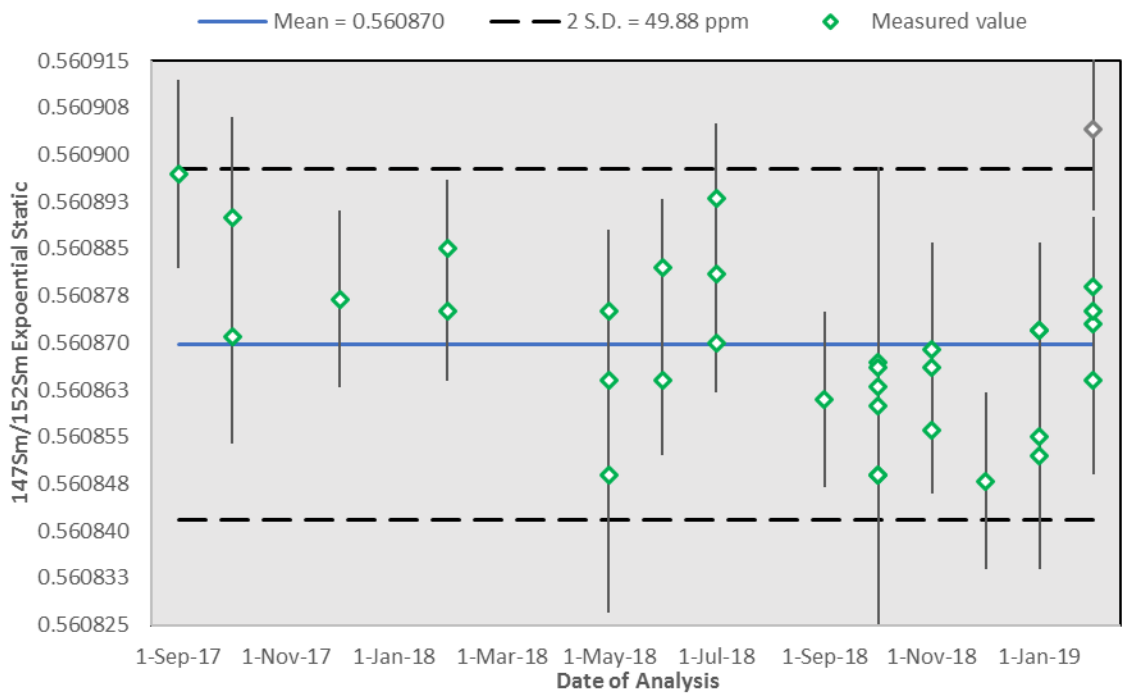


Figure A.2 All Ames 20ng Sm standards run by the author during this study.

Table A.3 Summary of Isotopic ratios for all Ames 20ng Sm Standards run by the author during this study.

Date of Analysis	144/152 norm.	144/152 2 S.E.	147/152 norm.	147/152 2 S.E.	148/152 norm.	148/152 2 S.E.	150/152 norm.	150/152 2 S.E.	154/152 norm.	154/152 2 S.E.
09/12/17	0.115025	0.000006	0.560897	0.000015	0.420493	0.000010	0.275999	0.000012	0.850755	0.000017
10/17/17	0.114999	0.000008	0.560890	0.000016	0.420474	0.000011	0.276018	0.000006	0.850720	0.000029
10/17/17	0.115002	0.000006	0.560871	0.000017	0.420485	0.000010	0.276004	0.000006	0.850748	0.000016
12/01/17	0.115008	0.000005	0.560877	0.000014	0.420463	0.000010	0.276014	0.000005	0.850744	0.000015
02/16/18	0.114994	0.000004	0.560875	0.000011	0.420472	0.000007	0.276018	0.000005	0.850741	0.000012
02/27/18	0.115002	0.000005	0.560885	0.000011	0.420487	0.000008	0.276018	0.000004	0.850733	0.000011
05/01/18	0.115002	0.000009	0.560849	0.000022	0.420459	0.000015	0.275982	0.000009	0.850763	0.000025
05/22/18	0.114983	0.000010	0.560864	0.000022	0.420460	0.000015	0.276013	0.000012	0.850780	0.000028
05/23/18	0.114991	0.000005	0.560875	0.000013	0.420471	0.000008	0.276012	0.000005	0.850760	0.000014
06/15/18	0.115010	0.000005	0.560882	0.000011	0.420482	0.000007	0.276012	0.000005	0.850733	0.000012
06/16/18	0.115006	0.000005	0.560864	0.000012	0.420468	0.000008	0.276011	0.000004	0.850765	0.000014
07/07/18	0.115017	0.000005	0.560881	0.000012	0.420473	0.000008	0.276009	0.000006	0.850719	0.000015
07/11/18	0.115011	0.000003	0.560870	0.000008	0.420467	0.000006	0.276012	0.000004	0.850744	0.000010
07/12/18	0.115021	0.000005	0.560893	0.000012	0.420481	0.000008	0.276013	0.000005	0.850725	0.000013
09/06/18	0.114994	0.000005	0.560861	0.000014	0.420453	0.000009	0.276007	0.000006	0.850743	0.000015
10/01/18	0.115015	0.000010	0.560867	0.000023	0.420455	0.000015	0.276015	0.000012	0.850727	0.000025
10/02/18	0.114991	0.000010	0.560849	0.000025	0.420473	0.000015	0.276018	0.000010	0.850745	0.000028
10/04/18	0.115000	0.000008	0.560863	0.000019	0.420458	0.000011	0.276006	0.000008	0.850750	0.000021
10/08/18	0.114997	0.000003	0.560860	0.000008	0.420455	0.000005	0.276013	0.000003	0.850763	0.000010
10/24/18	0.114964	0.000017	0.560866	0.000032	0.420425	0.000022	0.276005	0.000015	0.850744	0.000039
10/24/18	0.114988	0.000006	0.560849	0.000011	0.420456	0.000007	0.276010	0.000006	0.850745	0.000015
11/12/18	0.115005	0.000005	0.560869	0.000011	0.420462	0.000007	0.276013	0.000004	0.850731	0.000013
11/29/18	0.115009	0.000004	0.560856	0.000009	0.420474	0.000007	0.276011	0.000004	0.850769	0.000012
11/30/18	0.114995	0.000009	0.560866	0.000020	0.420449	0.000014	0.275996	0.000009	0.850683	0.000025
12/13/18	0.115026	0.000000	0.560848	0.000014	0.420465	0.000009	0.276002	0.000006	0.850753	0.000016
01/10/19	0.115001	0.000003	0.560855	0.000005	0.420457	0.000004	0.276012	0.000003	0.850733	0.000008
01/21/19	0.115024	0.000006	0.560872	0.000014	0.420472	0.000009	0.276015	0.000006	0.850699	0.000014
01/22/19	0.115010	0.000004	0.560872	0.000009	0.420466	0.000007	0.276024	0.000004	0.850756	0.000014
01/31/19	0.115000	0.000008	0.560852	0.000018	0.420447	0.000011	0.275997	0.000009	0.850744	0.000019
02/01/19	0.115025	0.000007	0.560873	0.000017	0.420454	0.000012	0.276020	0.000006	0.850731	0.000020
02/06/19	0.115011	0.000007	0.560864	0.000015	0.420466	0.000010	0.276017	0.000006	0.850747	0.000018
02/07/19	0.115014	0.000006	0.560875	0.000012	0.420458	0.000008	0.276012	0.000005	0.850719	0.000017
02/20/19	0.115013	0.000006	0.560904	0.000013	0.420477	0.000009	0.275990	0.000006	0.850771	0.000017
02/20/19	0.115004	0.000004	0.560879	0.000009	0.420481	0.000007	0.276001	0.000004	0.850788	0.000012
External Value	0.115004	± 233.55 ppm	0.560870	± 50.31 ppm	0.420466	± 63.78 ppm	0.276009	± 64.58 ppm	0.850743	± 47.87 ppm

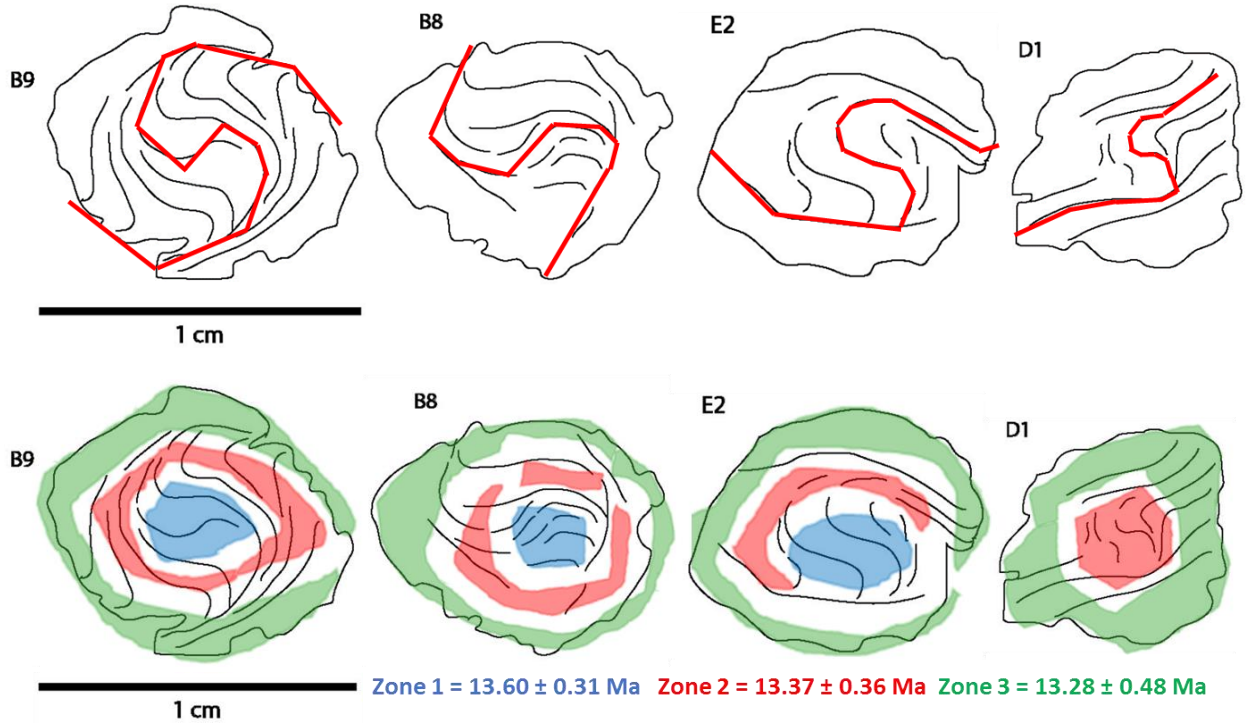
*All values ran in static mode and normalized to $^{149}\text{Sm}/^{152}\text{Sm}$ ratio of 0.516860

APPENDIX B: Location of every sample analyzed during this study

Sample Name	Region	Metamorphic Complex	Latitude (°)	Longitude (°)	Description
A7	Betic Cordillera Spain	Alpujárride	36°45'15.04"	-3°39'13.28"	Graphitic micaschist
B5	Rif Cordillera Morocco	Sebtide	35°55'00.20"	-5°22'08.33"	Graphitic micaschist
F8	Rif Cordillera Morocco	Sebtide	35°23'24.29"	-5° 00'26.74"	Graphitic micaschist
F16	Rif Cordillera Morocco	Sebtide	35°19'02.91"	-4°58'45.99"	Graph-rich micaschist
MT8	Rif Cordillera Morocco	Sebtide	35°10'45.08"	-4°50'43'10"	Graphitic micaschist
27.1.2	Betic Cordillera Spain	Nevado-Filabride	37°18'09.73"	-2°49'40.23"	Quartz-rich micaschist
27.2.1	Betic Cordillera Spain	Nevado-Filabride	37°18'14.32"	-2°49'46.15"	Quartz-rich micaschist
53.10.1	Betic Cordillera Spain	Nevado-Filabride	36°56'44.78"	-3°26'47.92"	Graph-rich micaschist

APPENDIX C: Strain-rate calculations for spiral garnets from sample 27.1.2

Average apparent rotations from garnets B8, B9, D1, and E2 \approx 170°



$$\sim 170 \text{ degrees apparent rotation} * \frac{\pi}{180} = \mathbf{2.6971 \text{ radians}}$$

Shear Strain = 2 x radians (Jeffery, 1922; Rosenfeld, 1970)

$$\text{Shear Strain} = 2 \times 2.6971 = \mathbf{5.9341}$$

garnet growth duration from 27.1.2 = 450,000^{+510,000}_{-320,000} years (see page 45)

$$\text{Shear Strain - rate} = \frac{2 \times \text{radians}}{\text{duration}} ; \text{Shear Strain - rate} = \frac{5.9341}{450,000^{\pm 510,000}_{-320,000}}$$

$$\text{Mean Strain - rate (s}^{-1}\text{)} = \frac{5.9341}{450,000 \text{ yr}} \times \frac{1 \text{ yr}}{31,536,000 \text{ sec}} = \mathbf{4.18 \times 10^{-13}}$$

$$\text{Lower Strain - rate (s}^{-1}\text{)} = \frac{5.9341}{960,000 \text{ yr}} \times \frac{1 \text{ yr}}{31,536,000 \text{ sec}} = \mathbf{1.96 \times 10^{-13}}$$

$$\text{Upper Strain - rate (s}^{-1}\text{)} = \frac{5.9341}{130,000 \text{ yr}} \times \frac{1 \text{ yr}}{31,536,000 \text{ sec}} = \mathbf{1.45 \times 10^{-12}}$$

$$\text{Calculated Shear Strain - rate} = \mathbf{4.2^{+10.9}_{-2.4} \times 10^{-14} \text{ s}^{-1}}$$

APPENDIX D: Nd Data Reduction Sheets

This appendix contains Nd data reduction sheets for every sample mentioned in the above chapters. Note each page corresponds to one analyzed separate from a given sample. Samples appear in alphabetical followed by numerical order, with a sub order of whole rock, garnet, garnet leachate, garnet powder, and garnet powder leachate.

Full Sample Name: **A7 WR AQ1**
 Date of TIMS analysis: **<enter!>** Position #: **19**
 estimated Nd load (ng): **<enter!>**

Rspike Values Nd {SmNd 0.15 A spike, 6-12-08 calib}

142/144	143/144	145/144	146/144	148/144	150/144	[Nd150]
0.830433	0.494001	0.436936	0.885201	0.740574	198.371260	0.125778
						nm/g

Wt Sample (g)= **0.0009164** g
 Wt Spike (g)= **0.30729** g

Mass Spectrometer Information:

Number of cycles measured:	111	
Number of cycles used:	101	
	start	average (from
Filament Current range: from	3.77	3.77
		Amps
Beam intensity range: from	1.072	1.834
		Volts 144Nd.160
Temperature range: from	1553	1640
		° C

Final Ratio Data:

Interference Values (oxide corrected; informational only... not used in this sheet)

Ce140/Nd144 **0.00127**
 Pr141/Nd144 **0.003366**
 Sm149/Nd144 **1.792E-05**

for Ratios & %1SE: use grand mean oxygen corr, interference corr, exp normalized values

	142/144	143/144	145/144	146/144	148/144	150/144
Ratios	1.1416345	0.5121821	0.3486089	0.7219	0.24316205	1.0441914
%StdErr	0.0004448	0.0002574	0.0003737	0	0.0007066	0.0008464
<i>for comparison only</i>	142/144	143/144	145/144	146/144	148/144	150/144
DePaolo 88, p.14, ln. B'	1.141854	na	0.348416	0.721882	0.241572	na

FINAL DATA TO REPORT:

	142/144	143/144	145/144	146/144	148/144	150/144	150t/144s
Ratios	1.141839	0.512017	0.348409	0.721900	0.241568	0.236478	1.227178
± 2 S.E.	0.000010	0.000003	0.000003	0.000000	0.000003	0.000004	0.000021

Epsilon143= -12.12 using (143/144)chur= 0.512638
 ± 0.05 (Hamilton et al. 1983)

linked from Sm sheet

[Sm147]= 5.867071 nm/g ± 0.000495	[Nd144]= 51.75500 nm/g ± 0.00188
[Sm]= 5.882369 ppm ± 0.000496	[Nd]= 31.38810 ppm ± 0.00114
TOT ng Sm= 5.3908946	TOT ng Nd= 28.7656102
Sm147/Nd144= 0.113362 ± 2 S.E. 0.000010 ± 2RSE % 0%	

Full Sample Name: **A7 WR AQ2**
 Date of TIMS analysis: **3/29/2018** Position #: **3**
 estimated Nd load (ng): **7**

Rspike Values Nd {SmNd 0.15 A spike, 6-12-08 calib}						
142/144	143/144	145/144	146/144	148/144	150/144	[Nd150]
0.830433	0.494001	0.436936	0.885201	0.740574	198.371260	0.125778
						nm/g

Wt Sample (g)= **0.0009942** g
 Wt Spike (g)= **0.33819** g

Mass Spectrometer Information:

Number of cycles measured: **96**
 Number of cycles used: **90**

	start	average (from	
Filament Current range: from	3.65	<enter!>	Amps
Beam intensity range: from	0.40187	0.84354	Volts 144Nd.160
Temperature range: from	1500	1630	° C

Final Ratio Data:

Interference Values (oxide corrected; informational only... not used in this sheet)

Ce140/Nd144 **0.004133**
 Pr141/Nd144 **0.004777**
 Sm149/Nd144 **1.719E-05**

for Ratios & %1SE: use grand mean oxygen corr, interference corr, exp normalized values

	142/144	143/144	145/144	146/144	148/144	150/144
Ratios	1.1416411	0.512192	0.3485995	0.7219	0.2431824	1.0565463
%StdErr	0.0021671	0.0009609	0.0008632	0	0.00105737	0.0019733

for comparison only	142/144	143/144	145/144	146/144	148/144	150/144
DePaolo 88, p.14, ln. B':	1.141854	na	0.348416	0.721882	0.241572	na

FINAL DATA TO REPORT:								146/144 set to 0.7219	
	142/144	143/144	145/144	146/144	148/144	150/144	150t/144s		
Ratios	1.141849	0.512024	0.348396	0.721900	0.241564	0.236478	1.208563		
± 2 S.E.	0.000049	0.000010	0.000006	0.000000	0.000005	0.000009	0.000048		
				Epsilon143=	-11.97	using (143/144)chur=		0.512638	
				±	0.19	(Hamilton et al. 1983)			
<i>linked from Sm sheet</i>									
[Sm147]=	5.881570 nm/g			[Nd144]=	51.71057 nm/g				
	± 0.000613				± 0.00262				
[Sm]=	5.896906 ppm			[Nd]=	31.36115 ppm				
	± 0.000615				± 0.00159				
TOT ng Sm=	5.8624583			TOT ng Nd=	31.1779539				
				Sm147/Nd144=	0.113740				
				± 2 S.E.	0.000013				
				± 2RSE %	0%				

Full Sample Name: **A7 Gt A AQ1**
 Date of TIMS analysis: **3/24/2018**
 estimated Nd load (ng): **4**

Position #: **10**

Rspike Values Nd {SmNd 1.0 A spike, 6-12-08 calib}

142/144	143/144	145/144	146/144	148/144	150/144	[Nd150]
0.830433	0.494001	0.436936	0.885201	0.740574	198.371260	0.049114

nm/g

Wt Sample (g)= **0.0051954** g
 Wt Spike (g)= **0.07426** g

Mass Spectrometer Information:

Number of cycles measured:	177	
Number of cycles used:	163	
	start	average (from
Filament Current range: from	3.8	4
Beam intensity range: from	0.182	0.156
Temperature range: from	1513	1567

Amps
Volts 144Nd.160
° C

Final Ratio Data:

Interference Values (oxide corrected; informational only... not used in this sheet)

Ce140/Nd144 **0.0192299**
 Pr141/Nd144 **0.0064565**
 Sm149/Nd144 **3.099E-05**

for Ratios & %1SE: use grand mean oxygen corr, interference corr, exp normalized values

	142/144	143/144	145/144	146/144	148/144	150/144
Ratios	1.1417818	0.5123245	0.3484904	0.7219	0.24239665	0.6492623
%StdErr	0.0014356	0.0013	0.0012011	0	0.00355649	0.0033261

<i>for comparison only</i>	142/144	143/144	145/144	146/144	148/144	150/144
DePaolo 88, p.14, ln. B:	1.141854	na	0.348416	0.721882	0.241572	na

FINAL DATA TO REPORT:

146/144 set to 0.7219

	142/144	143/144	145/144	146/144	148/144	150/144	150t/144s
Ratios	1.141886	0.512241	0.348388	0.721900	0.241582	0.236478	2.409332
± 2 S.E.	0.000033	0.000013	0.000008	0.000000	0.000017	0.000016	0.000160

Epsilon143= -7.75 using (143/144)chur= 0.512638
 ± 0.26 (Hamilton et al. 1983)

linked from Sm sheet

[Sm147]= 3.200909 nm/g
 ± 0.001207

[Nd144]= 1.69135 nm/g
 ± 0.00015

[Sm]= 3.209255 ppm
 ± 0.001210

[Nd]= 1.02576 ppm
 ± 0.00009

TOT ng Sm= 16.673483

TOT ng Nd= 5.32927587

Sm147/Nd144= 1.892517
 ± 2 S.E. 0.000734
 ± 2RSE % 0%

Full Sample Name: **A7 Gt. A AQ2**
 Date of TIMS analysis: **5/1/2018** Position #: **5**
 estimated Nd load (ng): **4**

Rspike Values Nd {SmNd 1.0 A spike, 6-12-08 calib}						
142/144	143/144	145/144	146/144	148/144	150/144	[Nd150]
0.830433	0.494001	0.436936	0.885201	0.740574	198.371260	0.049114
						nm/g

Wt Sample (g)= **0.0050656** g
 Wt Spike (g)= **0.20038** g

Mass Spectrometer Information:

Number of cycles measured:	88		
Number of cycles used:	79		
		average	
	start	(from	
Filament Current range: from	3.48	3.58	Amps
Beam intensity range: from	0.168	0.126	Volts 144Nd.160
Temperature range: from	1587	1620	° C

Final Ratio Data:

Interference Values (oxide corrected; informational only... not used in this sheet)

Ce140/Nd144 **0.0273977**
 Pr141/Nd144 **0.0127667**
 Sm149/Nd144 **0.0001047**

for Ratios & %1SE: use grand mean oxygen corr, interference corr, exp normalized values

	142/144	143/144	145/144	146/144	148/144	150/144
Ratios	1.141686	0.512480	3.49E-01	0.7219	2.44E-01	1.38E+00
%StdErr	0.0020101	0.0024035	0.002678	0	0.0055281	0.0041058

for comparison only	142/144	143/144	145/144	146/144	148/144	150/144
DePaolo 88, p.14, ln. B'	1.141854	na	0.348416	0.721882	0.241572	na

FINAL DATA TO REPORT:

146/144 set to 0.7219

	142/144	143/144	145/144	146/144	148/144	150/144	150t/144s
Ratios	1.141976	0.512247	0.348419	0.721900	0.241585	0.236478	0.865719
± 2 S.E.	0.000046	0.000025	0.000019	0.000000	0.000027	0.000019	0.000071

Epsilon143= -7.62 using (143/144)chur= 0.512638
 ± 0.48 (Hamilton et al. 1983)

linked from Sm sheet

[Sm147]= 3.183993 nm/g [Nd144]= 1.68192 nm/g
 ± 0.000455 ± 0.00014

[Sm]= 3.192294 ppm [Nd]= 1.02004 ppm
 ± 0.000456 ± 0.00009

TOT ng Sm= 16.170886 TOT ng Nd= 5.16711106

Sm147/Nd144= **1.893075**
 ± 2 S.E. **0.000315**
 ± 2RSE % **0%**

Full Sample Name: **A7 Gt. A leach3 AQ1**
 Date of TIMS analysis: **3/22/2018** Position #: **5**
 estimated Nd load (ng): **4**

Rspike Values Nd {SmNd 1.0 A spike, 6-12-08 calib}						
142/144	143/144	145/144	146/144	148/144	150/144	[Nd150]
0.830433	0.494001	0.436936	0.885201	0.740574	198.371260	0.049114
						nm/g

Wt Sample (g)= **0.0035953** g
 Wt Spike (g)= **0.09202** g

Mass Spectrometer Information:

Number of cycles measured:	81	
Number of cycles used:	75	
	start	average (from
Filament Current range: from	3.3	3.3
		Amps
Beam intensity range: from	0.036	0.101
		Volts 144Nd.160
Temperature range: from	1647	1680
		° C

Final Ratio Data:

Interference Values (oxide corrected; informational only... not used in this sheet)
 Ce140/Nd144 **0.0131406**
 Pr141/Nd144 **0.0021257**
 Sm149/Nd144 **0.0001115**

for Ratios & %ISE: use grand mean oxygen corr, interference corr, exp normalized values

	142/144	143/144	145/144	146/144	148/144	150/144
Ratios	1.1419239	0.5122297	0.3484753	0.7219	0.24238964	0.6698389
%StdErr	0.0046524	0.0027667	0.0027301	0	0.00590015	0.0102372

for comparison only	142/144	143/144	145/144	146/144	148/144	150/144
DePaolo 88, p.14, ln. B'	1.141854	na	0.348416	0.721882	0.241572	na

FINAL DATA TO REPORT:

	142/144	143/144	145/144	146/144	148/144	150/144	150t/144s
Ratios	1.142033	0.512141	0.348368	0.721900	0.241534	0.236478	2.294534
± 2 S.E.	0.000106	0.000028	0.000019	0.000000	0.000029	0.000048	0.000470

Epsilon143= **-9.69** using (143/144)chur= **0.512638**
 ± **0.55** (Hamilton et al. 1983)

linked from Sm sheet

[Sm147]= 2.614046 nm/g ± 0.000459
 [Nd144]= 2.88436 nm/g ± 0.00062

[Sm]= 2.620862 ppm ± 0.000460
 [Nd]= 1.74929 ppm ± 0.00037

TOT ng Sm= 9.4227066 TOT ng Nd= 6.28916945

Sm147/Nd144= **0.906284**
 ± 2 S.E. **0.000250**
 ± 2RSE % **0%**

Full Sample Name: **A7 gt leach3 alq2**
 Date of TIMS analysis: **1/25/2018** Position #: **5**
 estimated Nd load (ng): **4**

Rspike Values Nd {SmNd 1.0 A spike, 6-12-08 calib}						
142/144	143/144	145/144	146/144	148/144	150/144	[Nd150]
0.830433	0.494001	0.436936	0.885201	0.740574	198.371260	0.049114
						nm/g

Wt Sample (g)= **0.0066547** g
 Wt Spike (g)= **0.29353** g

Mass Spectrometer Information:

Number of cycles measured:	97	
Number of cycles used:	89	
	start	average (from
Filament Current range: from	3.1	3.3
		Amps
Beam intensity range: from	0.338	0.33
		Volts 144Nd.160
Temperature range: from	1527	1619
		° C

Final Ratio Data:

Interference Values (oxide corrected; informational only... not used in this sheet)

Ce140/Nd144 **0.0081875**
 Pr141/Nd144 **0.0049258**
 Sm149/Nd144 **8.556E-05**

for Ratios & %1SE: use grand mean oxygen corr, interference corr, exp normalized values

	142/144	143/144	145/144	146/144	148/144	150/144
Ratios	1.1416879	0.5122873	0.3485962	0.7219	0.84343243	0.9867871
%StdErr	0.001435	0.0010786	0.0009207	0	0.0020169	0.0031158
for comparison only	142/144	143/144	145/144	146/144	148/144	150/144
DePaolo 88, p.14, ln. B':	1.141854	na	0.348416	0.721882	0.241572	na

FINAL DATA TO REPORT:

	142/144	143/144	145/144	146/144	148/144	150/144	150t/144s
Ratios	1.141878	0.512134	0.348410	0.721900	0.845271	0.236478	1.321711
± 2 S.E.	0.000033	0.000011	0.000006	0.000000	0.000034	0.000015	0.000082

Epsilon143= -9.83 using (143/144)chur= 0.512638
 ± 0.22 (Hamilton et al. 1983)

linked from Sm sheet

[Sm147]= 2.595348 nm/g [Nd144]= 2.86327 nm/g
 ± 0.000262 ± 0.00020

[Sm]= 2.602115 ppm [Nd]= 1.73650 ppm
 ± 0.000263 ± 0.00012

TOT ng Sm= 17.316372 TOT ng Nd= 11.5559489

Sm147/Nd144= **0.906427**
 ± 2 S.E. **0.000112**
 ± 2RSE % **0%**

Full Sample Name: **A7 gt powder1**
 Date of TIMS analysis: **3/22/2018** Position #: **11**
 estimated Nd load (ng): **4**

Rspike Values Nd {SmNd 1.0 A spike, 6-12-08 calib}						
142/144	143/144	145/144	146/144	148/144	150/144	[Nd150]
0.830433	0.494001	0.436936	0.885201	0.740574	198.371260	0.049114
						nm/g

Wt Sample (g)= **0.0027888** g
 Wt Spike (g)= **0.09802** g

Mass Spectrometer Information:

Number of cycles measured: **51**
 Number of cycles used: **44**

	start	average (from	
Filament Current range: from	3.1	<enter!>	Amps
Beam intensity range: from	0.0403	0.052357	Volts 144Nd.160
Temperature range: from	1553	1618	° C

Final Ratio Data:

Interference Values (oxide corrected; informational only... not used in this sheet)
 Ce140/Nd144 **0.2913522**
 Pr141/Nd144 **0.033985**
 Sm149/Nd144 **0.0007068**

for Ratios & %ISE: use grand mean oxygen corr, interference corr, exp normalized values

	142/144	143/144	145/144	146/144	148/144	150/144
Ratios	1.1416283	0.5128207	0.3488982	0.7219	0.24540379	2.202579
%StdErr	0.0076581	0.0044219	0.0045407	0	0.01619582	0.0718792

for comparison only	142/144	143/144	145/144	146/144	148/144	150/144
DePaolo 88, p.14, ln. B'	1.141854	na	0.348416	0.721882	0.241572	na

FINAL DATA TO REPORT:

	142/144	143/144	145/144	146/144	148/144	150/144	150t/144s
Ratios	1.142134	0.512421	0.348409	0.721900	0.241518	0.236478	0.499184
± 2 S.E.	0.000175	0.000045	0.000032	0.000000	0.000078	0.000340	0.000718

Epsilon143= -4.24 using (143/144)chur= 0.512638
 ± 0.88 (Hamilton et al. 1983)

linked from Sm sheet

[Sm147]= 2.309643 nm/g [Nd144]= 0.86171 nm/g
 ± 0.000265 ± 0.00124

[Sm]= 2.315665 ppm [Nd]= 0.52261 ppm
 ± 0.000266 ± 0.00075

TOT ng Sm= 6.4579188 TOT ng Nd= 1.45744302

Sm147/Nd144= 2.680296
 ± 2 S.E. 0.003866
 ± 2RSE % 0%

Full Sample Name: **A7 Gt pwd AQ2**
 Date of TIMS analysis: **4/30/2018** Position #: **14**
 estimated Nd load (ng): **2**

Rspike Values Nd {SmNd 1.0 A spike, 6-12-08 calib}

142/144	143/144	145/144	146/144	148/144	150/144	[Nd150]
0.830433	0.494001	0.436936	0.885201	0.740574	198.371260	0.049114
						nm/g

Wt Sample (g)= **0.0049312** g
 Wt Spike (g)= **0.12371** g

Mass Spectrometer Information:

Number of cycles measured: **120**
 Number of cycles used: **113**

	start	average (from	
Filament Current range: from	3.25	3.5	Amps
Beam intensity range: from	0.185	0.101	Volts 144Nd.16O
Temperature range: from	1567	1647	° C

Final Ratio Data:

Interference Values (oxide corrected; informational only... not used in this sheet)
 Ce140/Nd144 **0.046083**
 Pr141/Nd144 **0.0056989**
 Sm149/Nd144 **0.0001736**

for Ratios & %1SE: use grand mean oxygen corr, interference corr, exp normalized values

	142/144	143/144	145/144	146/144	148/144	150/144
Ratios	1.1415846	0.5126787	0.3487825	0.7219	0.24445193	1.6817515
%StdErr	0.0029871	0.0017433	0.0026864	0	0.00917484	0.005257
<i>for comparison only</i>	142/144	143/144	145/144	146/144	148/144	150/144
DePaolo 88, p.14, ln. B':	1.141854	na	0.348416	0.721882	0.241572	na

FINAL DATA TO REPORT:				146/144 set to 0.7219			
	142/144	143/144	145/144	146/144	148/144	150/144	150t/144s
Ratios	1.141954	0.512385	0.348424	0.721900	0.241598	0.236478	0.682110
± 2 S.E.	0.000068	0.000018	0.000019	0.000000	0.000044	0.000025	0.000072
Epsilon143=				-4.94	using (143/144)chur=		0.512638
				± 0.35	(Hamilton et al. 1983)		
<i>linked from Sm sheet</i>							
[Sm147]=	2.290559	nm/g	[Nd144]=	0.84045	nm/g		
	± 0.000358			± 0.00009			
[Sm]=	2.296531	ppm	[Nd]=	0.50971	ppm		
	± 0.000359			± 0.00005			
TOT ng Sm=	11.324658		TOT ng Nd=	2.51348396			
	Sm147/Nd144=	2.725403					
	± 2 S.E.	0.000515					
	± 2RSE %	0%					

Full Sample Name: **A7 gt pwd leach2 AQ1**
 Date of TIMS analysis: **4/23/2018** Position #: **2**
 estimated Nd load (ng): **4**

Rspike Values Nd {SmNd 1.0 A spike, 6-12-08 calib}						
142/144	143/144	145/144	146/144	148/144	150/144	[Nd150]
0.830433	0.494001	0.436936	0.885201	0.740574	198.371260	0.049114
						nm/g

Wt Sample (g)= **0.00317** g
 Wt Spike (g)= **0.11821** g

Mass Spectrometer Information:

Number of cycles measured:	129		
Number of cycles used:	122		
	start	average (from	
Filament Current range: from	3.3	3.4	Amps
Beam intensity range: from	0.123	0.177	Volts 144Nd.160
Temperature range: from	1560	1627	° C

Final Ratio Data:

Interference Values (oxide corrected; informational only... not used in this sheet)

Ce140/Nd144 **0.0259093**
 Pr141/Nd144 **0.0121841**
 Sm149/Nd144 **0.0006132**

for Ratios & %ISE: use grand mean oxygen corr, interference corr, exp normalized values

	142/144	143/144	145/144	146/144	148/144	150/144
Ratios	1.14159	0.5125189	0.3487281	0.7219	0.24416377	1.5749801
%StdErr	0.0018732	0.0012619	0.0014386	0	0.00280788	0.0032047

for comparison only	142/144	143/144	145/144	146/144	148/144	150/144
DePaolo 88, p.14, ln. B':	1.141854	na	0.348416	0.721882	0.241572	na

FINAL DATA TO REPORT:

146/144 set to 0.7219

	142/144	143/144	145/144	146/144	148/144	150/144	150t/144s
Ratios	1.141931	0.512246	0.348396	0.721900	0.241520	0.236478	0.737194
± 2 S.E.	0.000043	0.000013	0.000010	0.000000	0.000014	0.000015	0.000047

Epsilon143= -7.65 using (143/144)chur= 0.512638
 ± 0.25 (Hamilton et al. 1983)

linked from Sm sheet

[Sm147]= 2.245455 nm/g [Nd144]= 1.35016 nm/g
 ± 0.000239 ± 0.00009

[Sm]= 2.251310 ppm [Nd]= 0.81884 ppm
 ± 0.000240 ± 0.00005

TOT ng Sm= 7.136594 TOT ng Nd= 2.59568971

Sm147/Nd144= 1.663106
 ± 2 S.E. 0.000209
 ± 2RSE % 0%

Full Sample Name: **B5 WR1 aq1**
 Date of TIMS analysis: **7/5/2018** Position #: **13**
 estimated Nd load (ng): **45**

Rspike Values Nd {SmNd 0.15 A spike, 6-12-08 calib}

142/144	143/144	145/144	146/144	148/144	150/144	[Nd150]
0.830433	0.494001	0.436936	0.885201	0.740574	198.371260	0.125778

nm/g

Wt Sample (g)= **0.0013954** g
 Wt Spike (g)= **0.4576** g

Mass Spectrometer Information:

Number of cycles measured: **161**
 Number of cycles used: **143**

	start	average (from)	
Filament Current range: from	3.675	3.675	Amps
Beam intensity range: from	1.77	2.27	Volts 144Nd.160
Temperature range: from	1540	1587	° C

Final Ratio Data:

Interference Values (oxide corrected; informational only... not used in this sheet)
 Ce140/Nd144 **4.554E-05**
 Pr141/Nd144 **0.0002716**
 Sm149/Nd144 **1.19E-05**

for Ratios & %1SE: use grand mean oxygen corr, interference corr, exp normalized values

	142/144	143/144	145/144	146/144	148/144	150/144
Ratios	1.1417044	0.5121187	0.3485495	0.7219	0.24265411	0.7871428
%StdErr	0.0007871	0.0004164	0.0002638	0	0.00046475	0.0006023
<i>for comparison only</i>	142/144	143/144	145/144	146/144	148/144	150/144
DePaolo 88, p.14, ln. B:	1.141854	na	0.348416	0.721882	0.241572	na

FINAL DATA TO REPORT:								146/144 set to 0.7219	
	142/144	143/144	145/144	146/144	148/144	150/144	150t/144s		
Ratios	1.141843	0.512006	0.348413	0.721900	0.241567	0.236478	1.803953		
± 2 S.E.	0.000018	0.000004	0.000002	0.000000	0.000002	0.000003	0.000022		
				Epsilon143=	-12.33	using (143/144)chur=		0.512638	
				±	0.08	(Hamilton et al. 1983)			
<i>linked from Sm sheet</i>									
[Sm147]=	8.613935	nm/g	[Nd144]=	74.40515	nm/g				
	± 0.001013			± 0.00363					
[Sm]=	8.636395	ppm	[Nd]=	45.12484	ppm				
	± 0.001016			± 0.00220					
TOT ng Sm=	12.051623		TOT ng Nd=	62.9692752					
		Sm147/Nd144=	0.115771						
		± 2 S.E.	0.000015						
		± 2RSE %	0%						

Full Sample Name: **B5 Gt. A aq1**
 Date of TIMS analysis: **7/5/2018**
 estimated Nd load (ng): **4**

Position #: **14**

Rspike Values Nd {SmNd 1.0 A spike, 6-12-08 calib}						
142/144	143/144	145/144	146/144	148/144	150/144	[Nd150]
0.830433	0.494001	0.436936	0.885201	0.740574	198.371260	0.049114
						nm/g

Wt Sample (g)= **0.0033621** g
 Wt Spike (g)= **0.12355** g

Mass Spectrometer Information:

Number of cycles measured:	81	
Number of cycles used:	75	
	start	average (from
Filament Current range: from	3.7	3.7
Beam intensity range: from	0.0308	0.053
Temperature range: from	1573	1595
		Amps
		Volts 144Nd.160
		° C

Final Ratio Data:

Interference Values (oxide corrected; informational only... not used in this sheet)

Ce140/Nd144 **0.025654**
 Pr141/Nd144 **0.0116722**
 Sm149/Nd144 **0.0013285**

for Ratios & %1SE: use grand mean oxygen corr, interference corr, exp normalized values

	142/144	143/144	145/144	146/144	148/144	150/144
Ratios	1.140582	0.5133472	0.3496193	0.7219	0.25122957	5.1190938
%StdErr	0.0047855	0.0037794	0.0034901	0	0.00739172	0.0108108
for comparison only	142/144	143/144	145/144	146/144	148/144	150/144
DePaolo 88, p.14, ln. B'	1.141854	na	0.348416	0.721882	0.241572	na

FINAL DATA TO REPORT:

146/144 set to 0.7219

	142/144	143/144	145/144	146/144	148/144	150/144	150t/144s
Ratios	1.141873	0.512344	0.348393	0.721900	0.241554	0.236478	0.195964
± 2 S.E.	0.000109	0.000039	0.000024	0.000000	0.000036	0.000051	0.000042

Epsilon143= -5.73 using (143/144)chur= 0.512638
 ± 0.76 (Hamilton et al. 1983)

linked from Sm sheet

[Sm147]= 0.768965 nm/g [Nd144]= 0.35368 nm/g
 ± 0.000048 ± 0.00008

[Sm]= 0.770970 ppm [Nd]= 0.21450 ppm
 ± 0.000048 ± 0.00005

TOT ng Sm= 2.5920634 TOT ng Nd= 0.72116769

Sm147/Nd144= 2.174158
 ± 2 S.E. 0.000489
 ± 2RSE % 0%

Full Sample Name: **B5 Gt. A leach1**
 Date of TIMS analysis: **9/18/2018** Position #: **7**
 estimated Nd load (ng): **2**

Rspike Values Nd {SmNd 1.0 A spike, 6-12-08 calib}						
142/144	143/144	145/144	146/144	148/144	150/144	[Nd150]
0.830433	0.494001	0.436936	0.885201	0.740574	198.371260	0.049114
						nm/g

Wt Sample (g)= **0.00667** g
 Wt Spike (g)= **0.08241** g

Mass Spectrometer Information:

Number of cycles measured: **49**
 Number of cycles used: **30**

	start	average (from	
Filament Current range: from	3.7	3.7	Amps
Beam intensity range: from	0.0818	0.0688	Volts 144Nd.160
Temperature range: from	1560	1633	° C

Final Ratio Data:

Interference Values (oxide corrected; informational only... not used in this sheet)
 Ce140/Nd144 **0.0296182**
 Pr141/Nd144 **0.013758**
 Sm149/Nd144 **0.000724**

for Ratios & %1SE: use grand mean oxygen corr, interference corr, exp normalized values

	142/144	143/144	145/144	146/144	148/144	150/144
Ratios	1.1412928	0.5122187	0.3486977	0.7219	0.24310996	1.0648901
%StdErr	0.0074023	0.00412	0.0046174	0	0.01010375	0.0109061
<i>for comparison only</i>	142/144	143/144	145/144	146/144	148/144	150/144
DePaolo 88, p.14, ln. B'	1.141854	na	0.348416	0.721882	0.241572	na

FINAL DATA TO REPORT:

146/144 set to 0.7219

	142/144	143/144	145/144	146/144	148/144	150/144	150t/144s
Ratios	1.141501	0.512049	0.348493	0.721900	0.241474	0.236478	1.196305
± 2 S.E.	0.000169	0.000042	0.000032	0.000000	0.000049	0.000052	0.000261

Epsilon143= **-11.48** using (143/144)chur= **0.512638**
 ± **0.82** (Hamilton et al. 1983)

linked from Sm sheet

[Sm147]= **0.534118** nm/g
 ± **0.000170**

[Nd144]= **0.72594** nm/g
 ± **0.00016**

[Sm]= **0.535511** ppm
 ± **0.000170**

[Nd]= **0.44026** ppm
 ± **0.00010**

TOT ng Sm= **3.5718568**

TOT ng Nd= **2.93655824**

Sm147/Nd144= **0.735762**
 ± 2 S.E. **0.000285**
 ± 2RSE % **0%**

Full Sample Name: **B5 Gt. B**
 Date of TIMS analysis: **10/25/2018**
 estimated Nd load (ng): **2**

Position #: **5**

Rspike Values Nd {SmNd 1.0 A spike, 6-12-08 calib}

142/144	143/144	145/144	146/144	148/144	150/144	[Nd150]
0.830433	0.494001	0.436936	0.885201	0.740574	198.371260	0.049114 nm/g

Wt Sample (g)= **0.0072** g
 Wt Spike (g)= **0.04037** g

Mass Spectrometer Information:

Number of cycles measured:	37		
Number of cycles used:	34		
	start	average (from	
Filament Current range: from	3.5	3.5	Amps
Beam intensity range: from	0.0444	0.0466	Volts 144Nd.160
Temperature range: from	1587	1647	° C

Final Ratio Data:

Interference Values (oxide corrected; informational only... not used in this sheet)

Ce140/Nd144 **0.20537**
 Pr141/Nd144 **0.01249**
 Sm149/Nd144 **0.0155398**

for Ratios & %1SE: use grand mean oxygen corr, interference corr, exp normalized values

	142/144	143/144	145/144	146/144	148/144	150/144
Ratios	1.1416425	0.5123254	0.3484862	0.7219	0.24316717	1.01305
%StdErr	0.001233	0.0123441	0.0076232	0	0.01313929	0.016

<i>for comparison only</i>	142/144	143/144	145/144	146/144	148/144	150/144
DePaolo 88, p.14, ln. B':	1.141854	na	0.348416	0.721882	0.241572	na

FINAL DATA TO REPORT:

146/144 set to 0.7219

	142/144	143/144	145/144	146/144	148/144	150/144	150t/144s
Ratios	1.141839	0.512167	0.348293	0.721900	0.241635	0.236478	1.276727
± 2 S.E.	0.000028	0.000126	0.000053	0.000000	0.000063	0.000076	0.000409

Epsilon143= **-9.19** using (143/144)chur= **0.512638**
 ± **2.47** (Hamilton et al. 1983)

linked from Sm sheet

[Sm147]= 0.738076 nm/g
 ± 0.000164

[Nd144]= 0.35158 nm/g
 ± 0.00011

[Sm]= 0.740000 ppm
 ± 0.000164

[Nd]= 0.21323 ppm
 ± 0.00007

TOT ng Sm= 5.3280026

TOT ng Nd= 1.53523012

Sm147/Nd144= **2.099291**
 ± 2 S.E. **0.000820**
 ± 2RSE % **0%**

B5 gt pwd1 aq1

Full Sample Name: **B5 Gt pwd AQ1**
 Date of TIMS analysis: **7/5/2018** Position #: **14**
 estimated Nd load (ng): **4**

Rspike Values Nd {SmNd 1.0 A spike, 6-12-08 calib}						
142/144	143/144	145/144	146/144	148/144	150/144	[Nd150]
0.830433	0.494001	0.436936	0.885201	0.740574	198.371260	0.049114
						nm/g

Wt Sample (g)= **0.0025357** g
 Wt Spike (g)= **0.09786** g

Mass Spectrometer Information:

Number of cycles measured:	103		
Number of cycles used:	95		
	start	average (from	
Filament Current range: from	3.1	3.1	Amps
Beam intensity range: from	0.217	0.156	Volts 144Nd.160
Temperature range: from	1580	1627	° C

Final Ratio Data:

Interference Values (oxide corrected; informational only... not used in this sheet)
 Ce140/Nd144 **0.00817**
 Pr141/Nd144 **0.00199**
 Sm149/Nd144 **0.000339**

for Ratios & %1SE: use grand mean oxygen corr, interference corr, exp normalized values

	142/144	143/144	145/144	146/144	148/144	150/144
Ratios	1.1416363	0.512417	0.3488116	0.7219	0.24461398	1.7847356
%StdErr	0.0017151	0.0013654	0.0019479	0	0.00440834	0.0034891
<i>for comparison only</i>	142/144	143/144	145/144	146/144	148/144	150/144
DePaolo 88, p.14, ln. B'	1.141854	na	0.348416	0.721882	0.241572	na

FINAL DATA TO REPORT:

	142/144	143/144	145/144	146/144	148/144	150/144	150t/144s
Ratios	1.142032	0.512100	0.348427	0.721900	0.241556	0.236478	0.636178
± 2 S.E.	0.000039	0.000014	0.000014	0.000000	0.000021	0.000017	0.000044

Epsilon143= -10.49 using (143/144)chur= 0.512638
 ± 0.27 (Hamilton et al. 1983)

linked from Sm sheet

[Sm147]= 0.739159 nm/g ± 0.000056
 [Nd144]= 1.20584 nm/g ± 0.00009

[Sm]= 0.741086 ppm ± 0.000056
 [Nd]= 0.73131 ppm ± 0.00005

TOT ng Sm= 1.8791725 TOT ng Nd= 1.85438868

Sm147/Nd144= 0.612982
 ± 2 S.E. 0.000064
 ± 2RSE % 0%

Full Sample Name: **F8 WR1**
 Date of TIMS analysis: **9/19/2018**
 estimated Nd load (ng): **45**

Position #: **3**

Rspike Values Nd {SmNd 0.15 A spike, 6-12-08 calib}

142/144	143/144	145/144	146/144	148/144	150/144	[Nd150]
0.830433	0.494001	0.436936	0.885201	0.740574	198.371260	0.125778 nm/g

Wt Sample (g)= **0.0013947** g
 Wt Spike (g)= **0.44371** g

Mass Spectrometer Information:

Number of cycles measured: **61**
 Number of cycles used: **45**

	start	average (from	
Filament Current range: from	3.47	3.47	Amps
Beam intensity range: from	0.742	2.148	Volts 144Nd.160
Temperature range: from	1560	1605	° C

Final Ratio Data:

Interference Values (oxide corrected; informational only... not used in this sheet)

Ce140/Nd144 **0.00508**
 Pr141/Nd144 **0.00404**
 Sm149/Nd144 **0.0000195**

for Ratios & %1SE: use grand mean oxygen corr, interference corr, exp normalized values

	142/144	143/144	145/144	146/144	148/144	150/144
Ratios	1.1416502	0.5120733	0.3485796	0.7219	0.24290565	0.9130632
%StdErr	0.0011672	0.0005151	0.0004533	0	0.0007878	0.0021461
<i>for comparison only</i>	142/144	143/144	145/144	146/144	148/144	150/144
DePaolo 88, p.14, ln. B'	1.141854	na	0.348416	0.721882	0.241572	na

FINAL DATA TO REPORT:

146/144 set to 0.7219

	142/144	143/144	145/144	146/144	148/144	150/144	150t/144s
Ratios	1.141821	0.511935	0.348412	0.721900	0.241570	0.236478	1.466649
± 2 S.E.	0.000027	0.000005	0.000003	0.000000	0.000004	0.000010	0.000063

Epsilon143= -13.72 using (143/144)chur= 0.512638
 ± 0.10 (Hamilton et al. 1983)

linked from Sm sheet

[Sm147]= 6.825829 nm/g
 ± 0.000689

[Nd144]= 58.68801 nm/g
 ± 0.00338

[Sm]= 6.843627 ppm

[Nd]= 35.59279 ppm

± 0.000691

± 0.00205

TOT ng Sm= 9.5448063

TOT ng Nd= 49.6412656

Sm147/Nd144= 0.116307

± 2 S.E. **0.000014**

± 2RSE % **0%**

Full Sample Name: **8 Gt. Alpha**
 Date of TIMS analysis: **1/1/2019**
 estimated Nd load (ng): **4**

Position #: **12**

Rspike Values Nd {SmNd 1.0 A spike, 6-12-08 calib}

142/144	143/144	145/144	146/144	148/144	150/144	[Nd150]
0.830433	0.494001	0.436936	0.885201	0.740574	198.371260	0.049114
						nm/g

Wt Sample (g)= **0.01756** g
 Wt Spike (g)= **0.09155** g

Mass Spectrometer Information:

Number of cycles measured: **145**
 Number of cycles used: **90**

	start	average (from	
Filament Current range: from	3.4	3.65	Amps
Beam intensity range: from	0.132	0.428	Volts 144Nd.160
Temperature range: from	1560	1633	° C

Final Ratio Data:

Interference Values (oxide corrected; informational only... not used in this sheet)

Ce140/Nd144 **0.0245022**
 Pr141/Nd144 **0.0269143**
 Sm149/Nd144 **0.0002085**

for Ratios & %1SE: use grand mean oxygen corr, interference corr, exp normalized values

	142/144	143/144	145/144	146/144	148/144	150/144
Ratios	1.1417071	0.5122952	0.3485887	0.7219	0.243104	1.0097163
%StdErr	0.001009	0.0007681	0.000961	0	0.002296	0.002619

<i>for comparison only</i>	142/144	143/144	145/144	146/144	148/144	150/144
DePaolo 88, p.14, ln. B':	1.141854	na	0.348416	0.721882	0.241572	na

FINAL DATA TO REPORT:

146/144 set to 0.7219

	142/144	143/144	145/144	146/144	148/144	150/144	150t/144s
Ratios	1.141903	0.512137	0.348397	0.721900	0.241578	0.236478	1.282268
± 2 S.E.	0.000023	0.000008	0.000007	0.000000	0.000011	0.000012	0.000067

Epsilon143= **-9.77** using (143/144)chur= **0.512638**
 ± **0.15** (Hamilton et al. 1983)

linked from Sm sheet

[Sm147]= **0.425587** nm/g
 ± **0.000066**

[Nd144]= **0.32833** nm/g
 ± **0.00002**

[Sm]= **0.426696** ppm
 ± **0.000066**

[Nd]= **0.19913** ppm
 ± **0.00001**

TOT ng Sm= **7.4927854**

TOT ng Nd= **3.49666279**

Sm147/Nd144= **1.296198**
 ± 2 S.E. **0.000217**
 ± 2RSE % **0%**

Full Sample Name: **F8 Gt. CI**
 Date of TIMS analysis: **10/25/2018**
 estimated Nd load (ng): **4**

Position #: **6**

Rspike Values Nd {SmNd 1.0 A spike, 6-12-08 calib}						
142/144	143/144	145/144	146/144	148/144	150/144	[Nd150]
0.830433	0.494001	0.436936	0.885201	0.740574	198.371260	0.049114
						nm/g

Wt Sample (g)= **0.00881** g
 Wt Spike (g)= **0.07023** g

Mass Spectrometer Information:

Number of cycles measured: **97**
 Number of cycles used: **88**

	start	average (from	
Filament Current range: from	3.48	3.48	Amps
Beam intensity range: from	0.045	0.1058	Volts 144Nd.160
Temperature range: from	1527	1580	°C

Final Ratio Data:

Interference Values (oxide corrected; informational only... not used in this sheet)

Ce140/Nd144 **0.050991**
 Pr141/Nd144 **0.010933**
 Sm149/Nd144 **0.001056**

for Ratios & %ISE: use grand mean oxygen corr, interference corr, exp normalized values

	142/144	143/144	145/144	146/144	148/144	150/144
Ratios	1.1414789	0.5125763	0.3488196	0.7219	0.2445416	1.7872764
%StdErr	0.0035534	0.0023918	0.0031058	0	0.0096264	0.0077101

for comparison only	142/144	143/144	145/144	146/144	148/144	150/144
DePaolo 88, p.14, ln. B':	1.141854	na	0.348416	0.721882	0.241572	na

FINAL DATA TO REPORT:

146/144 set to 0.7219

	142/144	143/144	145/144	146/144	148/144	150/144	150t/144s
Ratios	1.141875	0.512260	0.348434	0.721900	0.241477	0.236478	0.635122
± 2 S.E.	0.000081	0.000025	0.000022	0.000000	0.000046	0.000036	0.000098

Epsilon143= -7.37 using (143/144)chur= 0.512638
 ± 0.48 (Hamilton et al. 1983)

linked from Sm sheet

[Sm147]= 0.376171 nm/g
 ± 0.001138

[Nd144]= 0.24866 nm/g
 ± 0.00004

[Sm]= 0.377152 ppm
 ± 0.001141

[Nd]= 0.15081 ppm
 ± 0.00002

TOT ng Sm= 3.3227113

TOT ng Nd= 1.32860737

Sm147/Nd144= 1.512787
 ± 2 S.E. 0.004582
 ± 2RSE % 0%

Full Sample Name: **F8 gt Cl 1ch2**
 Date of TIMS analysis: **11/12/2019**
 estimated Nd load (ng): **2**

Position #: **4**

Rspike Values Nd {SmNd 1.0 A spike, 6-12-08 calib}

142/144	143/144	145/144	146/144	148/144	150/144	[Nd150]
0.830433	0.494001	0.436936	0.885201	0.740574	198.371260	0.049114

nm/g

Wt Sample (g) = **0.00423** g
 Wt Spike (g) = **0.04228** g

Mass Spectrometer Information:

Number of cycles measured: **81**
 Number of cycles used: **76**

	start	average (from	
Filament Current range: from	3.65	3.65	Amps
Beam intensity range: from	0.084	0.181	Volts 144Nd.16O
Temperature range: from	1547	1633	° C

Final Ratio Data:

Interference Values (oxide corrected; informational only... not used in this sheet)

Ce140/Nd144 **0.076398**
 Pr141/Nd144 **0.0597469**
 Sm149/Nd144 **0.000179**

for Ratios & %1SE: use grand mean oxygen corr, interference corr, exp normalized values

	142/144	143/144	145/144	146/144	148/144	150/144
Ratios	1.1415399	0.51239315	0.348789	0.7219	0.24449077	1.7263776
%StdErr	0.002658	0.00204365	0.0023474	0	0.0071226	0.0049977
for comparison only	142/144	143/144	145/144	146/144	148/144	150/144
DePaolo 88, p.14, ln. B':	1.141854	na	0.348416	0.721882	0.241572	na

FINAL DATA TO REPORT:

146/144 set to 0.7219

	142/144	143/144	145/144	146/144	148/144	150/144	150t/144s
Ratios	1.141920	0.512088	0.348419	0.721900	0.241548	0.236478	0.661427
± 2 S.E.	0.000061	0.000021	0.000016	0.000000	0.000034	0.000024	0.000066

Epsilon143 = -10.72 using (143/144)chur = 0.512638
 ± 0.41 (Hamilton et al. 1983)

linked from Sm sheet

[Sm147] = 0.360638 nm/g
 ± 0.000051

[Nd144] = 0.32470 nm/g
 ± 0.00003

[Sm] = 0.361578 ppm

[Nd] = 0.19692 ppm

± 0.000051

± 0.00002

TOT ng Sm = 1.5294745

TOT ng Nd = 0.83297811

Sm147/Nd144 = 1.110684

± 2 S.E. 0.000194

± 2RSE % 0%

Full Sample Name: **F8 gt. Dr**
 Date of TIMS analysis: **10/25/2018**
 estimated Nd load (ng): **1**

Position #: **7**

Rspike Values Nd {SmNd 1.0 A spike, 6-12-08 calib}						
142/144	143/144	145/144	146/144	148/144	150/144	[Nd150]
0.830433	0.494001	0.436936	0.885201	0.740574	198.371260	0.049114
nm/g						

Wt Sample (g)= **0.00315** g
 Wt Spike (g)= **0.04103** g

Mass Spectrometer Information:

Number of cycles measured: **105**
 Number of cycles used: **98**

	start	average (from	
Filament Current range: from	3.45	3.45	Amps
Beam intensity range: from	0.044	0.0427	Volts 144Nd.160
Temperature range: from	1540	1627	°C

Final Ratio Data:

Interference Values (oxide corrected; informational only... not used in this sheet)

Ce140/Nd144 **0.1382232**
 Pr141/Nd144 **0.0250394**
 Sm149/Nd144 **0.0004314**

for Ratios & %1SE: use grand mean oxygen corr, interference corr, exp normalized values

	142/144	143/144	145/144	146/144	148/144	150/144
Ratios	1.141322	0.5128285	0.3490061	0.7219	0.24730495	3.0943498
%StdErr	0.0064082	0.0041406	0.0054919	0	0.0149823	0.0119798

for comparison only	142/144	143/144	145/144	146/144	148/144	150/144
DePaolo 88, p.14, ln. B'	1.141854	na	0.348416	0.721882	0.241572	na

FINAL DATA TO REPORT:

146/144 set to 0.7219

	142/144	143/144	145/144	146/144	148/144	150/144	150t/144s
Ratios	1.142064	0.512243	0.348291	0.721900	0.241655	0.236478	0.340786
± 2 S.E.	0.000146	0.000042	0.000038	0.000000	0.000072	0.000057	0.000082

Epsilon143= -7.70 using (143/144)chur= 0.512638
 ± 0.83 (Hamilton et al. 1983)

linked from Sm sheet

[Sm147]= 0.397455 nm/g
 ± 0.000037

[Nd144]= 0.21801 nm/g
 ± 0.00005

[Sm]= 0.398491 ppm
 ± 0.000037

[Nd]= 0.13222 ppm
 ± 0.00003

TOT ng Sm= 1.255247

TOT ng Nd= 0.41648531

Sm147/Nd144= 1.823103
 ± 2 S.E. 0.000468
 ± 2RSE % 0%

Full Sample Name: **F16 wr1 AQ3**
 Date of TIMS analysis: **2/10/2018**
 estimated Nd load (ng): **4**

Position #: **5**

Rspike Values Nd {SmNd 0.15 A spike, 6-12-08 calib}

142/144	143/144	145/144	146/144	148/144	150/144	[Nd150]
0.830433	0.494001	0.436936	0.885201	0.740574	198.371260	0.125778 nm/g

Wt Sample (g)= **0.0010269** g

Wt Spike (g)= **0.36068** g

Mass Spectrometer Information:

Number of cycles measured:	225		
Number of cycles used:	207		
		average	
	start	(from	
Filament Current range: from	3.35	3.525	Amps
Beam intensity range: from	0.441	1.089	Volts 144Nd.160
Temperature range: from	1533	1593	° C

Final Ratio Data:

Interference Values (oxide corrected; informational only... not used in this sheet)

Ce140/Nd144	0.0051809
Pr141/Nd144	0.0060123
Sm149/Nd144	1.302E-05

for Ratios & %1SE: use grand mean oxygen corr, interference corr, exp normalized values

	142/144	143/144	145/144	146/144	148/144	150/144
Ratios	1.1416511	0.5121482	0.3485831	0.7219	0.24294038	0.947079
%StdErr	0.0006165	0.0005233	0.0004895	0	0.00964726	0.0012834
<i>for comparison only</i>	142/144	143/144	145/144	146/144	148/144	150/144
DePaolo 88, p.14, ln. B':	1.141854	na	0.348416	0.721882	0.241572	na

FINAL DATA TO REPORT:

146/144 set to 0.7219

	142/144	143/144	145/144	146/144	148/144	150/144	150t/144s
Ratios	1.141831	0.512003	0.348407	0.721900	0.241538	0.236478	1.396038
± 2 S.E.	0.000014	0.000005	0.000003	0.000000	0.000047	0.000006	0.000036

Epsilon143= -12.39 using (143/144)chur= 0.512638
 ± 0.10 (Hamilton et al. 1983)

linked from Sm sheet

[Sm147]= 7.368313 nm/g
 ± 0.000713

[Nd144]= 61.67454 nm/g
 ± 0.00276

[Sm]= 7.387525 ppm
 ± 0.000715

[Nd]= 37.40404 ppm
 ± 0.00167

TOT ng Sm= 7.5860791

TOT ng Nd= 38.4093492

Sm147/Nd144= 0.119471
 ± 2 S.E. 0.000013
 ± 2RSE % 0%

Full Sample Name: **F16 Gt. C**
 Date of TIMS analysis: **1/22/2018**
 estimated Nd load (ng): **0.5**

Position #: **7**

Rspike Values Nd {SmNd 1.0 A spike, 6-12-08 calib}

142/144	143/144	145/144	146/144	148/144	150/144	[Nd150]
0.830433	0.494001	0.436936	0.885201	0.740574	198.371260	0.049114
						nm/g

Wt Sample (g)= **0.00075** g
 Wt Spike (g)= **0.00972** g

Mass Spectrometer Information:

Number of cycles measured:	42		
Number of cycles used:	40		
	start	average (from	
Filament Current range: from	3.95	4.05	Amps
Beam intensity range: from	0.603	0.75	Volts 144Nd.160
Temperature range: from	1553	1595	° C

Final Ratio Data:

Interference Values (oxide corrected; informational only... not used in this sheet)

Ce140/Nd144 **0.1268572**
 Pr141/Nd144 **0.0863969**
 Sm149/Nd144 **0.0002739**

for Ratios & %1SE: use grand mean oxygen corr, interference corr, exp normalized values

	142/144	143/144	145/144	146/144	148/144	150/144
Ratios	1.1422097	0.512340	0.348444	0.7219	0.24232789	0.5847749
%StdErr	0.0069519	0.0068914	0.0038069	0	0.00840924	0.0201023

<i>for comparison only</i>	142/144	143/144	145/144	146/144	148/144	150/144
DePaolo 88, p.14, ln. B'	1.141854	na	0.348416	0.721882	0.241572	na

FINAL DATA TO REPORT:

146/144 set to 0.7219

	142/144	143/144	145/144	146/144	148/144	150/144	150t/144s
Ratios	1.142298	0.512269	0.348358	0.721900	0.241641	0.236478	2.856980
± 2 S.E.	0.000159	0.000071	0.000027	0.000000	0.000041	0.000095	0.001149

Epsilon143= **-7.20** using (143/144)chur= **0.512638**
 ± **1.38** (Hamilton et al. 1983)

linked from Sm sheet

[Sm147]= **2.812593** nm/g
 ± 0.001065

[Nd144]= **1.81851** nm/g
 ± **0.00074**

[Sm]= **2.819926** ppm
 ± 0.001068

[Nd]= **1.10288** ppm
 ± **0.00045**

TOT ng Sm= **2.1149446**

TOT ng Nd= **0.82716116**

Sm147/Nd144= **1.546645**
 ± 2 S.E. **0.000862**
 ± 2RSE % **0%**

Full Sample Name: **F16 Gt D leach alq1**
 Date of TIMS analysis: **2/10/2018** Position #: **6**
 estimated Nd load (ng): **4**

Rspike Values Nd {SmNd 1.0 A spike, 6-12-08 calib}

142/144	143/144	145/144	146/144	148/144	150/144	[Nd150]
0.830433	0.494001	0.436936	0.885201	0.740574	198.371260	0.049114
						nm/g

Wt Sample (g)= **0.0040562** g
 Wt Spike (g)= **0.12495** g

Mass Spectrometer Information:

Number of cycles measured: **92**
 Number of cycles used: **86**

	start	average (from	
Filament Current range: from	3.35	3.5	Amps
Beam intensity range: from	0.182	0.436	Volts 144Nd.160
Temperature range: from	1533	1653	° C

Final Ratio Data:

Interference Values (oxide corrected; informational only... not used in this sheet)

Ce140/Nd144 **0.0397253**
 Pr141/Nd144 **0.0096208**
 Sm149/Nd144 **0.000165**

for Ratios & %ISE: use grand mean oxygen corr, interference corr, exp normalized values

	142/144	143/144	145/144	146/144	148/144	150/144
Ratios	1.1414887	0.5126695	0.3488414	0.7219	0.24489664	1.943648
%StdErr	0.0015096	0.0011159	0.0012612	0	0.00241947	0.0026535
<i>for comparison only</i>	142/144	143/144	145/144	146/144	148/144	2
DePaolo 88, p.14, ln. B':	1.141854	na	0.348416	0.721882	0.241572	na

FINAL DATA TO REPORT:

146/144 set to 0.7219

	142/144	143/144	145/144	146/144	148/144	150/144	150t/144s
Ratios	1.141926	0.512322	0.348417	0.721900	0.241524	0.236478	0.576175
± 2 S.E.	0.000034	0.000011	0.000009	0.000000	0.000012	0.000013	0.000031

Epsilon143= -6.17 using (143/144)chur= 0.512638
 ± 0.22 (Hamilton et al. 1983)

linked from Sm sheet

[Sm147]= 1.747927 nm/g [Nd144]= 0.87171 nm/g
 ± 0.000180 ± 0.00005

[Sm]= 1.752484 ppm [Nd]= 0.52867 ppm
 ± 0.000180 ± 0.00003

TOT ng Sm= 7.1085021 TOT ng Nd= 2.14440693

Sm147/Nd144= 2.005177
 ± 2 S.E. 0.000234
 ± 2RSE % 0%

Full Sample Name: **F16 Gt pwd AQ1**
 Date of TIMS analysis: **1/25/2018** Position #: **5**
 estimated Nd load (ng): **4**

Rspike Values Nd {SmNd 1.0 A spike, 6-12-08 calib}

142/144	143/144	145/144	146/144	148/144	150/144	[Nd150]
0.830433	0.494001	0.436936	0.885201	0.740574	198.371260	0.049114

nm/g

Wt Sample (g)= **0.0046502** g
 Wt Spike (g)= **0.12312** g

Mass Spectrometer Information:

Number of cycles measured:	103		
Number of cycles used:	90		
	start	average (from	
Filament Current range: from	3.45	3.55	Amps
Beam intensity range: from	0.12	0.47	Volts 144Nd.160
Temperature range: from	1553	1586	° C

Final Ratio Data:

Interference Values (oxide corrected; informational only... not used in this sheet)

Ce140/Nd144 **0.0452567**
 Pr141/Nd144 **0.0204213**
 Sm149/Nd144 **9.542E-05**

for Ratios & %ISE: use grand mean oxygen corr, interference corr, exp normalized values

	142/144	143/144	145/144	146/144	148/144	150/144
Ratios	1.1415782	0.512591	0.3487188	0.7219	0.24414988	1.556136
%StdErr	0.0012396	0.0007722	0.001049	0	0.00200553	0.0022671
<i>for comparison only</i>	142/144	143/144	145/144	146/144	148/144	150/144
DePaolo 88, p.14, ln. B'	1.141854	na	0.348416	0.721882	0.241572	na

FINAL DATA TO REPORT:

146/144 set to 0.7219

	142/144	143/144	145/144	146/144	148/144	150/144	150t/144s
Ratios	1.141914	0.512322	0.348391	0.721900	0.241544	0.236478	0.747841
± 2 S.E.	0.000028	0.000008	0.000007	0.000000	0.000010	0.000011	0.000034

Epsilon143= -6.16 using (143/144)chur= 0.512638
 ± 0.15 (Hamilton et al. 1983)

linked from Sm sheet

[Sm147]= 2.043993 nm/g [Nd144]= 0.97245 nm/g
 ± 0.000273 ± 0.00005

[Sm]= 2.049322 ppm [Nd]= 0.58977 ppm
 ± 0.000274 ± 0.00003

TOT ng Sm= 9.5298153 TOT ng Nd= 2.74255104

Sm147/Nd144= 2.101898
 ± 2 S.E. 0.000300
 ± 2RSE % 0%

Full Sample Name: **F16 Gt pwd leach AQ1**
 Date of TIMS analysis: **2/10/2018** Position #: **4**
 estimated Nd load (ng): **4**

Rspike Values Nd {SmNd 1.0 A spike, 6-12-08 calib}						
142/144	143/144	145/144	146/144	148/144	150/144	[Nd150]
0.830433	0.494001	0.436936	0.885201	0.740574	198.371260	0.049114
						nm/g

Wt Sample (g)= **0.0057758** g
 Wt Spike (g)= **0.18108** g

Mass Spectrometer Information:

Number of cycles measured:	145	
Number of cycles used:	137	
	start	average (from
Filament Current range: from	3.4	3.45
		Amps
Beam intensity range: from	0.15	<enter!>
		Volts 144Nd.160
Temperature range: from	1533	16
		° C

Final Ratio Data:

Interference Values (oxide corrected; informational only... not used in this sheet)
 Ce140/Nd144 **0.0157266**
 Pr141/Nd144 **0.0150251**
 Sm149/Nd144 **9.623E-05**

for Ratios & %ISE: use grand mean oxygen corr, interference corr, exp normalized values

	142/144	143/144	145/144	146/144	148/144	150/144
Ratios	1.1415669	0.5124147	0.3486759	0.7219	0.24358589	1.2713626
%StdErr	0.0011009	0.0010134	0.0009313	0	0.00248931	0.001795

for comparison only	142/144	143/144	145/144	146/144	148/144	150/144
DePaolo 88, p.14, ln. B'	1.141854	na	0.348416	0.721882	0.241572	na

FINAL DATA TO REPORT:

146/144 set to 0.7219

	142/144	143/144	145/144	146/144	148/144	150/144	150t/144s
Ratios	1.141829	0.512204	0.348419	0.721900	0.241543	0.236478	0.955947
± 2 S.E.	0.000025	0.000010	0.000006	0.000000	0.000012	0.000008	0.000034

Epsilon143= **-8.47** using (143/144)chur= **0.512638**
 ± **0.20** (Hamilton et al. 1983)

linked from Sm sheet

[Sm147]= 2.029718 nm/g ± 0.000231	[Nd144]= 1.47195 nm/g ± 0.00006
[Sm]= 2.035010 ppm ± 0.000232	[Nd]= 0.89270 ppm ± 0.00004
TOT ng Sm= 11.75389	TOT ng Nd= 5.15609334
Sm147/Nd144= 1.378931 ± 2 S.E. 0.000168 ± 2RSE % 0%	

Full Sample Name: **MT8 WR2**
 Date of TIMS analysis: **4/2/2018**
 estimated Nd load (ng): **30**

Position #: **19**

Rspike Values Nd {SmNd 0.15 A spike, 6-12-08 calib}

142/144	143/144	145/144	146/144	148/144	150/144	[Nd150]
0.830433	0.494001	0.436936	0.885201	0.740574	198.371260	0.125778
						nm/g

Wt Sample (g)= **0.000921** g
 Wt Spike (g)= **0.30798** g

Mass Spectrometer Information:

Number of cycles measured:	130	
Number of cycles used:	122	
	start	average (from
Filament Current range: from	3.53	3.53
		Amps
Beam intensity range: from	0.435	0.234
		Volts 144Nd.160
Temperature range: from	1540	1587
		° C

Final Ratio Data:

Interference Values (oxide corrected; informational only... not used in this sheet)

Ce140/Nd144 **0.0271183**
 Pr141/Nd144 **0.02907**
 Sm149/Nd144 **0.0000554**

for Ratios & %ISE: use grand mean oxygen corr, interference corr, exp normalized values

	142/144	143/144	145/144	146/144	148/144	150/144
Ratios	1.14E+00	0.5135975	3.50E-01	0.7219	2.57E-01	7.9003778
%StdErr	0.001423	0.001294	0.001098	0	0.002219	0.0023892

<i>for comparison only</i>	142/144	143/144	145/144	146/144	148/144	150/144
DePaolo 88, p.14, ln. B'	1.141854	na	0.348416	0.721882	0.241572	na

FINAL DATA TO REPORT:

146/144 set to 0.7219

	142/144	143/144	145/144	146/144	148/144	150/144	150t/144s
Ratios	1.141831	0.511999	0.348419	0.721900	0.241571	0.236476	0.121775
± 2 S.E.	0.000032	0.000013	0.000008	0.000000	0.000011	0.000011	0.000006

Epsilon143= -12.47 using (143/144)chur= 0.512638
 ± 0.26 (Hamilton et al. 1983)

linked from Sm sheet

[Sm147]= 0.838601 nm/g [Nd144]= 5.12182 nm/g
 ± 0.000531 ± 0.00025

[Sm]= 0.840787 ppm [Nd]= 3.10625 ppm

± 0.000533 ± 0.00015

TOT ng Sm= 0.7743669 TOT ng Nd= 2.86086456

Sm147/Nd144= 0.163731
 ± 2 S.E. 0.000104
 ± 2RSE % 0%

Full Sample Name: **MT8 WR 4**
 Date of TIMS analysis: **9/19/2018**
 estimated Nd load (ng): **20**

Position #: **4**

Rspike Values Nd {SmNd 0.15 A spike, 6-12-08 calib}						
142/144	143/144	145/144	146/144	148/144	150/144	[Nd150]
0.830433	0.494001	0.436936	0.885201	0.740574	198.371260	0.125778
						nm/g

Wt Sample (g)= **0.0102934** g
 Wt Spike (g)= **0.33732** g

Mass Spectrometer Information:

Number of cycles measured:	97		
Number of cycles used:	87		
		average (from	
Filament Current range: from	3.25	3.25	Amps
Beam intensity range: from	0.775	1.16	Volts 144Nd.160
Temperature range: from	1560	1575	° C

Final Ratio Data:

Interference Values (oxide corrected; informational only... not used in this sheet)

Ce140/Nd144 **0.0021671**
 Pr141/Nd144 **0.0055302**
 Sm149/Nd144 **1.982E-05**

for Ratios & %1SE: use grand mean oxygen corr, interference corr, exp normalized values

	142/144	143/144	145/144	146/144	148/144	150/144
Ratios	1.1416106	0.5121554	0.3486032	0.7219	0.24312266	1.0299539
%StdErr	0.0007528	0.0004594	0.000447	0	0.000937	0.001139
for comparison only	142/144	143/144	145/144	146/144	148/144	150/144
DePaolo 88, p.14, ln. B'	1.141854	na	0.348416	0.721882	0.241572	na

FINAL DATA TO REPORT:

	142/144	143/144	145/144	146/144	148/144	150/144	150t/144s
Ratios	1.141811	0.511993	0.348407	0.721900	0.241556	0.236478	1.249349
± 2 S.E.	0.000017	0.000005	0.000003	0.000000	0.000005	0.000005	0.000028
				Epsilon143=	-12.58	using (143/144)chur=	0.512638
				±	0.09	(Hamilton et al. 1983)	
<i>linked from Sm sheet</i>							
[Sm147]=	0.800352	nm/g		[Nd144]=	5.14960	nm/g	
	± 0.000089				± 0.00021		
[Sm]=	0.802439	ppm		[Nd]=	3.12310	ppm	
	± 0.000089				± 0.00012		
TOT ng Sm=	8.2598012			TOT ng Nd=	32.1472149		
		Sm147/Nd144=	0.155420				
		± 2 S.E.	0.000018				
		± 2RSE %	0%				

Full Sample Name: **MT8 Gt A AQ1**
 Date of TIMS analysis: **3/24/2018** Position #: **13**
 estimated Nd load (ng): **4**

Rspike Values Nd {SmNd 1.0 A spike, 6-12-08 calib}

142/144	143/144	145/144	146/144	148/144	150/144	[Nd150]
0.830433	0.494001	0.436936	0.885201	0.740574	198.371260	0.049114

nm/g

Wt Sample (g)= **0.0053461** g
 Wt Spike (g)= **0.12805** g

Mass Spectrometer Information:

Number of cycles measured:	97	
Number of cycles used:	88	
	start	average (from
Filament Current range: from	3.52	3.55
		Amps
Beam intensity range: from	<enter!>	0.11709
		Volts 144Nd.160
Temperature range: from	1527	1557
		° C

Final Ratio Data:

Interference Values (oxide corrected; informational only... not used in this sheet)

Ce140/Nd144 **0.0480965**
 Pr141/Nd144 **0.0199128**
 Sm149/Nd144 **7.703E-05**

for Ratios & %ISE: use grand mean oxygen corr, interference corr, exp normalized values

	142/144	143/144	145/144	146/144	148/144	150/144
Ratios	1.1412964	0.5125583	0.3489352	0.7219	0.24559165	2.2861149
%StdErr	0.0026392	0.0020479	0.002237	0	0.00502453	0.0057648

for comparison only

	142/144	143/144	145/144	146/144	148/144	150/144
DePaolo 88, p.14, ln. B'	1.141854	na	0.348416	0.721882	0.241572	na

FINAL DATA TO REPORT:

146/144 set to 0.7219

	142/144	143/144	145/144	146/144	148/144	150/144	150t/144s
Ratios	1.141822	0.512139	0.348425	0.721900	0.241541	0.236478	0.478495
± 2 S.E.	0.000060	0.000021	0.000016	0.000000	0.000024	0.000027	0.000055

Epsilon143= -9.74 using (143/144)chur= 0.512638
 ± 0.41 (Hamilton et al. 1983)

linked from Sm sheet

[Sm147]= 0.537826 nm/g ± 0.000058	[Nd144]= 0.56289 nm/g ± 0.00007
[Sm]= 0.539228 ppm ± 0.000058	[Nd]= 0.34138 ppm ± 0.00004
TOT ng Sm= 2.8827791	TOT ng Nd= 1.82504477
Sm147/Nd144= 0.955476 ± 2 S.E. 0.000152 ± 2RSE % 0%	

Full Sample Name: **MT8 Gt. A AQ2**
 Date of TIMS analysis: **5/24/2018** Position #: **3**
 estimated Nd load (ng): **4**

Rspike Values Nd {SmNd 1.0 A spike, 6-12-08 calib}

142/144	143/144	145/144	146/144	148/144	150/144	[Nd150]
0.830433	0.494001	0.436936	0.885201	0.740574	198.371260	0.049114
						nm/g

Wt Sample (g)= **0.0093939** g
 Wt Spike (g)= **0.08238** g

Mass Spectrometer Information:

Number of cycles measured:	129		
Number of cycles used:	118		
	start	average (from	
Filament Current range: from	3.45	3.67	Amps
Beam intensity range: from	0.12	0.117	Volts 144Nd.160
Temperature range: from	1587	1660	° C

Final Ratio Data:

Interference Values (oxide corrected; informational only... not used in this sheet)

Ce140/Nd144 **0.0421035**
 Pr141/Nd144 **0.0229795**
 Sm149/Nd144 **0.000136**

for Ratios & %ISE: use grand mean oxygen corr, interference corr, exp normalized values

	142/144	143/144	145/144	146/144	148/144	150/144
Ratios	1.1415967	0.5122701	0.3486071	0.7219	0.24300992	1.0063767
%StdErr	0.0022574	0.0018897	0.0017978	0	0.00345069	0.0044092
<i>for comparison only</i>	142/144	143/144	145/144	146/144	148/144	150/144
DePaolo 88, p.14, ln. B'	1.141854	na	0.348416	0.721882	0.241572	na

FINAL DATA TO REPORT:

146/144 set to 0.7219

	142/144	143/144	145/144	146/144	148/144	150/144	150t/144s
Ratios	1.141791	0.512113	0.348416	0.721900	0.241490	0.236478	1.287867
± 2 S.E.	0.000052	0.000019	0.000013	0.000000	0.000017	0.000021	0.000114

Epsilon143= -10.24 using (143/144)chur= 0.512638
 ± 0.38 (Hamilton et al. 1983)

linked from Sm sheet

[Sm147]= 0.527151 nm/g [Nd144]= 0.55469 nm/g
 ± 0.000057 ± 0.00005

[Sm]= 0.528525 ppm [Nd]= 0.33641 ppm
 ± 0.000057 ± 0.00003

TOT ng Sm= 4.9649048 TOT ng Nd= 3.16016169

Sm147/Nd144= 0.950350
 ± 2 S.E. 0.000137
 ± 2RSE % 0%

Full Sample Name: **MT8 gt leach3 alq2**
 Date of TIMS analysis: **5/24/2018** Position #: **4**
 estimated Nd load (ng): **9**

Rspike Values Nd {SmNd 1.0 A spike, 6-12-08 calib}						
142/144	143/144	145/144	146/144	148/144	150/144	[Nd150]
0.830433	0.494001	0.436936	0.885201	0.740574	198.371260	0.049114
						nm/g

Wt Sample (g)= **0.0146885** g
 Wt Spike (g)= **0.157** g

Mass Spectrometer Information:

Number of cycles measured:	103		
Number of cycles used:	90		
	start	average (from	
Filament Current range: from	3.5	3.7	Amps
Beam intensity range: from	0.176	0.189	Volts 144Nd.160
Temperature range: from	1540	1588	° C

Final Ratio Data:

Interference Values (oxide corrected; informational only... not used in this sheet)

Ce140/Nd144 **0.0200352**
 Pr141/Nd144 **0.0100129**
 Sm149/Nd144 **0.0000498**

for Ratios & %ISE: use grand mean oxygen corr, interference corr, exp normalized values

	142/144	143/144	145/144	146/144	148/144	150/144
Ratios	1.1417352	0.5121791	0.3485134	0.7219	0.24254048	0.7376082
%StdErr	0.0015515	0.0009982	0.0010527	0	0.00189957	0.0027019
<i>for comparison only</i>	142/144	143/144	145/144	146/144	148/144	150/144
DePaolo 88, p.14, ln. B'	1.141854	na	0.348416	0.721882	0.241572	na

FINAL DATA TO REPORT:

	142/144	143/144	145/144	146/144	148/144	150/144	150t/144s
Ratios	1.141862	0.512077	0.348389	0.721900	0.241552	0.236478	1.983098
± 2 S.E.	0.000035	0.000010	0.000007	0.000000	0.000009	0.000013	0.000107

Epsilon143= **-10.95** using (143/144)chur= **0.512638**
 ± **0.20** (Hamilton et al. 1983)

linked from Sm sheet

[Sm147]= 0.509714 nm/g [Nd144]= 1.04105 nm/g
 ± 0.000069 ± 0.00008

[Sm]= 0.511043 ppm [Nd]= 0.63137 ppm
 ± 0.000069 ± 0.00005

TOT ng Sm= 7.5064717 TOT ng Nd= 9.27386012

Sm147/Nd144= **0.489618**
 ± 2 S.E. **0.000076**
 ± 2RSE % **0%**

Full Sample Name: **MT8 Gt UC**
 Date of TIMS analysis: **1/25/2018** Position #: **5**
 estimated Nd load (ng): **4**

Rspike Values Nd {SmNd 1.0 A spike, 6-12-08 calib}						
142/144	143/144	145/144	146/144	148/144	150/144	[Nd150]
0.830433	0.494001	0.436936	0.885201	0.740574	198.371260	0.049114
						nm/g

Wt Sample (g)= **0.02545** g
 Wt Spike (g)= **0.070865** g

Mass Spectrometer Information:

Number of cycles measured:	102	
Number of cycles used:	94	
	start	average (from
Filament Current range: from	3.53	3.56
Beam intensity range: from	0.156	0.244
Temperature range: from	1593	1633
		Amps
		Volts 144Nd.160
		° C

Final Ratio Data:

Interference Values (oxide corrected; informational only... not used in this sheet)

Ce140/Nd144 **0.0025981**
 Pr141/Nd144 **0.0015652**
 Sm149/Nd144 **0.0001758**

for Ratios & %ISE: use grand mean oxygen corr, interference corr, exp normalized values

	142/144	143/144	145/144	146/144	148/144	150/144
Ratios	1.14E+00	5.12E-01	3.48E-01	0.7219	2.42E-01	4.25E-01
%StdErr	0.001642	0.0011978	0.001068	0	0.002345	0.0035876

for comparison only	142/144	143/144	145/144	146/144	148/144	150/144
DePaolo 88, p.14, ln. B'	1.141854	na	0.348416	0.721882	0.241572	na

FINAL DATA TO REPORT:

146/144 set to 0.7219

	142/144	143/144	145/144	146/144	148/144	150/144	150t/144s
Ratios	1.141847	0.512151	0.348387	0.721900	0.241571	0.236478	5.291360
± 2 S.E.	0.000037	0.000012	0.000007	0.000000	0.000011	0.000017	0.000380

Epsilon143= -9.51 using (143/144)chur= 0.512638
 ± 0.24 (Hamilton et al. 1983)

linked from Sm sheet

[Sm147]= 0.767954 nm/g [Nd144]= 0.72363 nm/g
 ± 0.000355 ± 0.00011

[Sm]= 0.769957 ppm [Nd]= 0.43886 ppm
 ± 0.000356 ± 0.00007

TOT ng Sm= 19.595393 TOT ng Nd= 11.1690372

Sm147/Nd144= 1.061256
 ± 2 S.E. 0.000518
 ± 2RSE % 0%

Full Sample Name: **MT8 gt UC leach2**
 Date of TIMS analysis: **9/18/2018** Position #: **6**
 estimated Nd load (ng): **4**

Rspike Values Nd {SmNd 1.0 A spike, 6-12-08 calib}						
142/144	143/144	145/144	146/144	148/144	150/144	[Nd150]
0.830433	0.494001	0.436936	0.885201	0.740574	198.371260	0.049114
						nm/g

Wt Sample (g)= **0.00706** g
 Wt Spike (g)= **0.08224** g

Mass Spectrometer Information:

Number of cycles measured:	97	
Number of cycles used:	89	
	start	average (from
Filament Current range: from	3.42	3.42
		Amps
Beam intensity range: from	0.505	0.545
		Volts 144Nd.160
Temperature range: from	1533	1593
		° C

Final Ratio Data:

Interference Values (oxide corrected; informational only... not used in this sheet)
 Ce140/Nd144 **0.0082161**
 Pr141/Nd144 **0.002166**
 Sm149/Nd144 **9.747E-05**

for Ratios & %ISE: use grand mean oxygen corr, interference corr, exp normalized values

	142/144	143/144	145/144	146/144	148/144	150/144
Ratios	1.1417779	0.5121862	0.3485116	0.7219	0.24240971	0.6680923
%StdErr	0.0009637	0.0007582	0.0053839	0	0.0010423	0.002013
for comparison only	142/144	143/144	145/144	146/144	148/144	150/144
DePaolo 88, p.14, ln. B'	1.141854	na	0.348416	0.721882	0.241572	na

FINAL DATA TO REPORT:

		142/144	143/144	145/144	146/144	148/144	150/144	150t/144s
Ratios		1.141887	0.512098	0.348405	0.721900	0.241558	0.236478	2.303853
± 2 S.E.		0.000022	0.000008	0.000038	0.000000	0.000005	0.000010	0.000093
Epsilon143=					-10.53	using (143/144)chur=		0.512638
±					0.15	(Hamilton et al. 1983)		
linked from Sm sheet								
[Sm147]=	0.981297	nm/g			[Nd144]=	1.31807	nm/g	
	± 0.000149					±	0.00010	
[Sm]=	0.983856	ppm			[Nd]=	0.79937	ppm	
	± 0.000150					±	0.00006	
TOT ng Sm=	6.9460229				TOT ng Nd=	5.6435769		
					Sm147/Nd144=	0.744498		
					± 2 S.E.	0.000126		
					± 2RSE %	0%		

Full Sample Name: **MT8 garnet powd**
 Date of TIMS analysis: **3/24/2018** Position #: **14**
 estimated Nd load (ng): **4**

Rspike Values Nd {SmNd 1.0 A spike, 6-12-08 calib}						
142/144	143/144	145/144	146/144	148/144	150/144	[Nd150]
0.830433	0.494001	0.436936	0.885201	0.740574	198.371260	0.049114
						nm/g

Wt Sample (g)= **0.0024673** g
 Wt Spike (g)= **0.1188** g

Mass Spectrometer Information:

Number of cycles measured:	52		
Number of cycles used:	49		
	start	average (from	
Filament Current range: from	3.475	3.475	Amps
Beam intensity range: from	0.02	0.01	Volts 144Nd.160
Temperature range: from	1573	1580	° C

Final Ratio Data:

Interference Values (oxide corrected; informational only... not used in this sheet)

Ce140/Nd144 **0.3320309**
 Pr141/Nd144 **0.0478033**
 Sm149/Nd144 **0.0007705**

for Ratios & %ISE: use grand mean oxygen corr, interference corr, exp normalized values

	142/144	143/144	145/144	146/144	148/144	150/144
Ratios	1.1400879	0.5134961	0.3504799	0.7219	0.25574487	7.6064731
%StdErr	0.0128067	0.0095656	0.010157	0	0.02950267	0.0238252
for comparison only	142/144	143/144	145/144	146/144	148/144	150/144
DePaolo 88, p.14, ln. B'	1.141854	na	0.348416	0.721882	0.241572	na

FINAL DATA TO REPORT:

	142/144	143/144	145/144	146/144	148/144	150/144	150t/144s
Ratios	1.142096	0.511958	0.348624	0.721900	0.241078	0.236476	0.126969
± 2 S.E.	0.000293	0.000098	0.000071	0.000000	0.000142	0.000113	0.000061

Epsilon143= **-13.26** using (143/144)chur= **0.512638**
 ± **1.91** (Hamilton et al. 1983)

linked from Sm sheet

[Sm147]= 0.407340 nm/g ± 0.000037	[Nd144]= 0.30026 nm/g ± 0.00014
[Sm]= 0.408402 ppm ± 0.000037	[Nd]= 0.18210 ppm ± 0.00009
TOT ng Sm= 1.0076363	TOT ng Nd= 0.44929416
Sm147/Nd144= 1.356609 ± 2 S.E. 0.000658 ± 2RSE % 0%	

MT8 garnet powder AQ2

Full Sample Name: **MT8 Gt pwd AQ2**
 Date of TIMS analysis: **4/30/2018** Position #: **15**
 estimated Nd load (ng): **2**

Rspike Values Nd {SmNd 1.0 A spike, 6-12-08 calib}						
142/144	143/144	145/144	146/144	148/144	150/144	[Nd150]
0.830433	0.494001	0.436936	0.885201	0.740574	198.371260	0.049114
						nm/g

Wt Sample (g)= **0.0112727** g
 Wt Spike (g)= **0.06506** g

Mass Spectrometer Information:

Number of cycles measured:	128		
Number of cycles used:	120		
		average	
	start	(from	
Filament Current range: from	3.55	3.8	Amps
Beam intensity range: from	0.11	0.2307	Volts 144Nd.160
Temperature range: from	1527	1589	° C

Final Ratio Data:

Interference Values (oxide corrected; informational only... not used in this sheet)
 Ce140/Nd144 **0.048199**
 Pr141/Nd144 **0.0194786**
 Sm149/Nd144 **0.0001484**

for Ratios & %ISE: use grand mean oxygen corr, interference corr, exp normalized values

	142/144	143/144	145/144	146/144	148/144	150/144
Ratios	1.1416473	0.5124067	0.3486561	0.7219	0.24345825	1.2006259
%StdErr	0.0016268	0.0009812	0.0011805	0	0.00320449	0.0035027
<i>for comparison only</i>	142/144	143/144	145/144	146/144	148/144	150/144
DePaolo 88, p.14, ln. B'	1.141854	na	0.348416	0.721882	0.241572	na

FINAL DATA TO REPORT:

	142/144	143/144	145/144	146/144	148/144	150/144	150t/144s
Ratios	1.141892	0.512210	0.348417	0.721900	0.241555	0.236478	1.026700
± 2 S.E.	0.000037	0.000010	0.000008	0.000000	0.000015	0.000017	0.000072

Epsilon143= -8.34 using (143/144)chur= 0.512638
 ± 0.20 (Hamilton et al. 1983)

linked from Sm sheet

[Sm147]= 0.400779 nm/g ± 0.000062	[Nd144]= 0.29103 nm/g ± 0.00002
[Sm]= 0.401824 ppm ± 0.000063	[Nd]= 0.17650 ppm ± 0.00001
TOT ng Sm= 4.5296552	TOT ng Nd= 1.98963836
Sm147/Nd144= 1.377123 ± 2 S.E. 0.000238 ± 2RSE % 0%	

Full Sample Name: **MT8 Gt UC pwd**
 Date of TIMS analysis: **6/19/2018** Position #: **9**
 estimated Nd load (ng): **4**

Rspike Values Nd {SmNd 1.0 A spike, 6-12-08 calib}						
142/144	143/144	145/144	146/144	148/144	150/144	[Nd150]
0.830433	0.494001	0.436936	0.885201	0.740574	198.371260	0.049114
						nm/g

Wt Sample (g)= **0.01587** g
 Wt Spike (g)= **0.05972** g

Mass Spectrometer Information:

Number of cycles measured:	65	
Number of cycles used:	60	
	start	average (from
Filament Current range: from	3.5	3.5
Beam intensity range: from	0.869	1.463
Temperature range: from	1580	1616
		Amps
		Volts 144Nd.160
		° C

Final Ratio Data:

Interference Values (oxide corrected; informational only... not used in this sheet)
 Ce140/Nd144 **0.0015**
 Pr141/Nd144 **0.00112**
 Sm149/Nd144 **0.000628**

for Ratios & %1SE: use grand mean oxygen corr, interference corr, exp normalized values

	142/144	143/144	145/144	146/144	148/144	150/144
Ratios	1.1418012	0.512147	0.348463	0.7219	0.2419977	0.4489186
%StdErr	0.0007968	0.0006304	0.00047	0	0.001107	0.0012101
for comparison only	142/144	143/144	145/144	146/144	148/144	150/144
DePaolo 88, p.14, ln. B'	1.141854	na	0.348416	0.721882	0.241572	na

FINAL DATA TO REPORT:

		146/144 set to 0.7219					
	142/144	143/144	145/144	146/144	148/144	150/144	150t/144s
Ratios	1.141855	0.512104	0.348410	0.721900	0.241579	0.236478	4.689412
± 2 S.E.	0.000018	0.000006	0.000003	0.000000	0.000005	0.000006	0.000113
		Epsilon143=		-10.42	using (143/144)chur=		0.512638
		±		0.13	(Hamilton et al. 1983)		
<i>linked from Sm sheet</i>							
[Sm147]=	0.711021	nm/g		[Nd144]=	0.86669	nm/g	
	± 0.000226				± 0.00011		
[Sm]=	0.712875	ppm		[Nd]=	0.52563	ppm	
	± 0.000226				± 0.00007		
TOT ng Sm=	11.31332			TOT ng Nd=	8.34170502		
		Sm147/Nd144=	0.820384				
		± 2 S.E.	0.000280				
		± 2RSE %	0%				

Full Sample Name: **27.2.1 whole rock 1**
 Date of TIMS analysis: **6/16/2018** Position #: **3**
 estimated Nd load (ng): **45**

Rspike Values Nd {SmNd 0.15 A spike, 6-12-08 calib}

142/144	143/144	145/144	146/144	148/144	150/144	[Nd150]
0.830433	0.494001	0.436936	0.885201	0.740574	198.371260	0.125778

nm/g

Wt Sample (g)= **0.0014397** g
 Wt Spike (g)= **0.43864** g

Mass Spectrometer Information:

Number of cycles measured:	96		
Number of cycles used:	89		
	start	average (from	
Filament Current range: from	3.325	3.325	Amps
Beam intensity range: from	1.308	1.92057	Volts 144Nd.160
Temperature range: from	1567	1600	° C

Final Ratio Data:

Interference Values (oxide corrected; informational only... not used in this sheet)

Ce140/Nd144 **0.0008173**
 Pr141/Nd144 **0.0033591**
 Sm149/Nd144 **1.491E-05**

for Ratios & %1SE: use grand mean oxygen corr, interference corr, exp normalized values

	142/144	143/144	145/144	146/144	148/144	150/144
Ratios	1.1417141	0.512129	0.348545	0.7219	0.24265825	0.7850463
%StdErr	0.0005581	0.0003078	0.000281	0	0.00057191	0.0010124

<i>for comparison only</i>	142/144	143/144	145/144	146/144	148/144	150/144
DePaolo 88, p.14, ln. B':	1.141854	na	0.348416	0.721882	0.241572	na

FINAL DATA TO REPORT:

146/144 set to 0.7219

	142/144	143/144	145/144	146/144	148/144	150/144	150t/144s
Ratios	1.141853	0.512017	0.348409	0.721900	0.241576	0.236478	1.810879
± 2 S.E.	0.000013	0.000003	0.000002	0.000000	0.000003	0.000005	0.000037

Epsilon143= -12.12 using (143/144)chur= 0.512638
 ± 0.06 (Hamilton et al. 1983)

linked from Sm sheet

[Sm147]= 8.175546 nm/g [Nd144]= 69.39780 nm/g
 ± 0.000975 ± 0.00358

[Sm]= 8.196863 ppm [Nd]= 42.08801 ppm

± 0.000977 ± 0.00217

TOT ng Sm= 11.800613 TOT ng Nd= 60.5920015

Sm147/Nd144= **0.117807**
 ± 2 S.E. **0.000015**
 ± 2RSE % **0%**

Full Sample Name: 27.2.1 WR2
 Date of TIMS analysis: 6/18/2018
 estimated Nd load (ng): 45

Position #: 4

Rspike Values Nd {SmNd 0.15 A spike, 6-12-08 calib}

142/144	143/144	145/144	146/144	148/144	150/144	[Nd150]
0.830433	0.494001	0.436936	0.885201	0.740574	198.371260	0.125778

nm/g

Wt Sample (g)= 0.0012902 g
 Wt Spike (g)= 0.3858 g

Mass Spectrometer Information:

Number of cycles measured:	132		
Number of cycles used:	120		
	start	average (from)	
Filament Current range: from	3.65	3.65	Amps
Beam intensity range: from	0.924	1.06	Volts 144Nd.160
Temperature range: from	1567	1599	° C

Final Ratio Data:

Interference Values (oxide corrected; informational only... not used in this sheet)

Ce140/Nd144 0.0006908
 Pr141/Nd144 0.0022096
 Sm149/Nd144 1.584E-05

for Ratios & %1SE: use grand mean oxygen corr, interference corr, exp normalized values

	142/144	143/144	145/144	146/144	148/144	150/144
Ratios	1.1416755	0.5121105	0.3485342	0.7219	0.24256449	0.735021
%StdErr	0.0008043	0.0004299	0.0003699	0	0.00084883	0.0008395

for comparison only	142/144	143/144	145/144	146/144	148/144	150/144
DePaolo 88, p.14, ln. B:	1.141854	na	0.348416	0.721882	0.241572	na

FINAL DATA TO REPORT:

146/144 set to 0.7219

	142/144	143/144	145/144	146/144	148/144	150/144	150t/144s
Ratios	1.141801	0.512009	0.348411	0.721900	0.241581	0.236478	1.993433
± 2 S.E.	0.000018	0.000004	0.000003	0.000000	0.000004	0.000004	0.000033

Epsilon143= -12.28 using (143/144)chur= 0.512638
 ± 0.09 (Hamilton et al. 1983)

linked from Sm sheet

[Sm147]= 8.805517 nm/g
 ± 0.001174

[Nd144]= 74.97686 nm/g
 ± 0.00411

[Sm]= 8.828476 ppm
 ± 0.001177

[Nd]= 45.47156 ppm
 ± 0.00249

TOT ng Sm= 11.390096

TOT ng Nd= 58.6653307

Sm147/Nd144= 0.117443
 ± 2 S.E. 0.000017
 ± 2RSE % 0%

Full Sample Name: **27.2.1 Gt sep A**
 Date of TIMS analysis: **6/16/2018**
 estimated Nd load (ng): **4**

Position #: **5**

Rspike Values Nd {SmNd 1.0 A spike, 6-12-08 calib}

142/144	143/144	145/144	146/144	148/144	150/144	[Nd150]
0.830433	0.494001	0.436936	0.885201	0.740574	198.371260	0.049114

nm/g

Wt Sample (g)= **0.01842** g
 Wt Spike (g)= **0.27191** g

Mass Spectrometer Information:

Number of cycles measured:	65	
Number of cycles used:	60	
	start	average (from
Filament Current range: from	3.77	3.77
		Amps
Beam intensity range: from	1.4115	4.0697
		Volts 144Nd.160
Temperature range: from	1553	1660
		° C

Final Ratio Data:

Interference Values (oxide corrected; informational only... not used in this sheet)

Ce140/Nd144 **0.0045193**
 Pr141/Nd144 **0.014678**
 Sm149/Nd144 **0.0000287**

for Ratios & %1SE: use grand mean oxygen corr, interference corr, exp normalized values

	142/144	143/144	145/144	146/144	148/144	150/144
Ratios	1.1418423	0.512068	0.3484337	0.7219	0.241769	0.332569
%StdErr	0.000867	0.0003396	0.0036676	0	0.009179	0.0009504

<i>for comparison only</i>	142/144	143/144	145/144	146/144	148/144	150/144
DePaolo 88, p.14, ln. B':	1.141854	na	0.348416	0.721882	0.241572	na

FINAL DATA TO REPORT:

146/144 set to 0.7219

	142/144	143/144	145/144	146/144	148/144	150/144	150t/144s
Ratios	1.141866	0.512048	0.348410	0.721900	0.241579	0.236478	10.377671
± 2 S.E.	0.000020	0.000003	0.000026	0.000000	0.000044	0.000004	0.000197

Epsilon143= **-11.50** using (143/144)chur= **0.512638**
 ± **0.07** (Hamilton et al. 1983)

linked from Sm sheet

[Sm147]= 3.012312 nm/g
 ± 0.001031

[Nd144]= 7.52384 nm/g
 ± 0.00204

[Sm]= 3.020166 ppm
 ± 0.001033

[Nd]= 4.56302 ppm
 ± 0.00124

TOT ng Sm= 55.631464

TOT ng Nd= 84.0507733

Sm147/Nd144= **0.400369**
 ± 2 S.E. **0.000175**
 ± 2RSE % **0%**

Full Sample Name: **27.2.1 gt. A leach**
 Date of TIMS analysis: **5/25/2018** Position #: **5**
 estimated Nd load (ng): **4**

Rspike Values Nd {SmNd 1.0 A spike, 6-12-08 calib}						
142/144	143/144	145/144	146/144	148/144	150/144	[Nd150]
0.830433	0.494001	0.436936	0.885201	0.740574	198.371260	0.049114
						nm/g

Wt Sample (g)= **0.00767** g
 Wt Spike (g)= **0.1717** g

Mass Spectrometer Information:

Number of cycles measured:	33	
Number of cycles used:	32	
	start	average (from
Filament Current range: from	3.6	3.6
Beam intensity range: from	1.064	2.3265
Temperature range: from	1580	1620
		Amps
		Volts 144Nd.160
		° C

Final Ratio Data:

Interference Values (oxide corrected; informational only... not used in this sheet)
 Ce140/Nd144 **0.0056567**
 Pr141/Nd144 **0.0106802**
 Sm149/Nd144 **0.0000217**

for Ratios & %ISE: use grand mean oxygen corr, interference corr, exp normalized values

	142/144	143/144	145/144	146/144	148/144	150/144
Ratios	1.1418248	0.5120148	0.3484205	0.7219	0.2416473	0.267219
%StdErr	0.002037	0.0010352	0.0006463	0	0.00066161	0.0017539

for comparison only	142/144	143/144	145/144	146/144	148/144	150/144
DePaolo 88, p.14, ln. B':	1.141854	na	0.348416	0.721882	0.241572	na

FINAL DATA TO REPORT:							146/144 set to 0.7219	
	142/144	143/144	145/144	146/144	148/144	150/144	150t/144s	
Ratios	1.141833	0.512009	0.348413	0.721900	0.241587	0.236478	32.456683	
± 2 S.E.	0.000047	0.000011	0.000005	0.000000	0.000003	0.000008	0.001139	

Epsilon143= -12.28 using (143/144)chur= 0.512638
 ± 0.21 (Hamilton et al. 1983)

linked from Sm sheet

[Sm147]= 5.580721 nm/g [Nd144]= 35.68478 nm/g
 ± 0.002330 ± 0.03025

[Sm]= 5.595272 ppm [Nd]= 21.64192 ppm
 ± 0.002336 ± 0.01834

TOT ng Sm= 42.915739 TOT ng Nd= 165.993495

Sm147/Nd144= 0.156389
 ± 2 S.E. 0.000148
 ± 2RSE % 0%

Full Sample Name: **27.2.1 Gt. B**
 Date of TIMS analysis: **11/28/2018**
 estimated Nd load (ng): **4**

Position #: **14**

Rspike Values Nd (SmNd 1.0 A spike, 6-12-08 calib)

142/144	143/144	145/144	146/144	148/144	150/144	[Nd150]
0.830433	0.494001	0.436936	0.885201	0.740574	198.371260	0.049114 nm/g

Wt Sample (g)= **0.00904** g
 Wt Spike (g)= **0.08693** g

Mass Spectrometer Information:

Number of cycles measured: **106**
 Number of cycles used: **94**

	start	average (from	Amps
Filament Current range: from	3.5	3.5	
Beam intensity range: from	0.0182	0.032285	Volts 144Nd.160
Temperature range: from	1567	1647	° C

Final Ratio Data:

Interference Values (oxide corrected; informational only... not used in this sheet)

Ce140/Nd144 **0.3581536**
 Pr141/Nd144 **0.0989678**
 Sm149/Nd144 **0.0003697**

for Ratios & %ISE: use grand mean oxygen corr, interference corr, exp normalized values

	142/144	143/144	145/144	146/144	148/144	150/144
Ratios	1.1421053	0.51230879	0.3483605	0.7219	0.24254289	0.730732
%StdErr	0.0012396	0.0055842	0.0080155	0	0.0112134	0.01398
<i>for comparison only</i>	142/144	143/144	145/144	146/144	148/144	150/144
DePaolo 88, p.14, ln. B':	1.141854	na	0.348416	0.721882	0.241572	na

FINAL DATA TO REPORT:

146/144 set to 0.7219

	142/144	143/144	145/144	146/144	148/144	150/144	150t/144s
Ratios	1.142231	0.512208	0.348238	0.721900	0.241568	0.236478	2.010805
± 2 S.E.	0.000028	0.000057	0.000056	0.000000	0.000054	0.000066	0.000562

Epsilon143= **-8.38** using (143/144)chur= **0.512638**
 ± **1.12** (Hamilton et al. 1983)

linked from Sm sheet

[Sm147]= **1.662145** nm/g
 ± **0.001192**

[Nd144]= **0.94968** nm/g
 ± **0.00027**

[Sm]= **1.666479** ppm
 ± **0.001195**

[Nd]= **0.57595** ppm
 ± **0.00016**

TOT ng Sm= **15.064971**

TOT ng Nd= **5.20662462**

Sm147/Nd144= **1.750225**
 ± 2 S.E. **0.001350**
 ± 2RSE % **0%**

Full Sample Name: **27.2.1 Gt. B lch3**
 Date of TIMS analysis: **11/27/2018**
 estimated Nd load (ng): **2.5**

Position #: **13**

Rspike Values Nd {SmNd 1.0 A spike, 6-12-08 calib}

142/144	143/144	145/144	146/144	148/144	150/144	[Nd150]
0.830433	0.494001	0.436936	0.885201	0.740574	198.371260	0.049114

nm/g

Wt Sample (g)= **0.00544** g
 Wt Spike (g)= **0.1033** g

Mass Spectrometer Information:

Number of cycles measured: **161**
 Number of cycles used: **144**

	start	average (from	
Filament Current range: from	3.4	3.4	Amps
Beam intensity range: from	0.91	0.1748	Volts 144Nd.160
Temperature range: from	1560	1587	° C

Final Ratio Data:

Interference Values (oxide corrected; informational only... not used in this sheet)

Ce140/Nd144 **0.0293**
 Pr141/Nd144 **0.0244**
 Sm149/Nd144 **0.000123**

for Ratios & %ISE: use grand mean oxygen corr, interference corr, exp normalized values

	142/144	143/144	145/144	146/144	148/144	150/144
Ratios	1.1414766	0.51243832	0.348696	0.7219	0.24397013	1.4506093
%StdErr	0.0018179	0.00117868	0.0012859	0	0.00277546	0.0028212
<i>for comparison only</i>	142/144	143/144	145/144	146/144	148/144	150/144
DePaolo 88, p.14, ln. B':	1.141854	na	0.348416	0.721882	0.241572	na

FINAL DATA TO REPORT:

146/144 set to 0.7219

	142/144	143/144	145/144	146/144	148/144	150/144	150t/144s
Ratios	1.141785	0.512191	0.348395	0.721900	0.241573	0.236478	0.813573
± 2 S.E.	0.000042	0.000012	0.000009	0.000000	0.000013	0.000013	0.000046

Epsilon143= **-8.73** using (143/144)chur= **0.512638**
 ± **0.24** (Hamilton et al. 1983)

linked from Sm sheet

[Sm147]= **1.595625** nm/g
 ± 0.000229

[Nd144]= **0.75876** nm/g
 ± **0.00005**

[Sm]= **1.599785** ppm
 ± 0.000230

[Nd]= **0.46017** ppm
 ± **0.00003**

TOT ng Sm= **8.7028319**

TOT ng Nd= **2.50330239**

Sm147/Nd144= **2.102950**
 ± 2 S.E. **0.000328**
 ± 2RSE % **0%**

Full Sample Name: **27.2.1 Gt. D**
 Date of TIMS analysis: **11/28/2018**
 estimated Nd load (ng): **4**

Position #: **14**

Rspike Values Nd {SmNd 1.0 A spike, 6-12-08 calib}

142/144	143/144	145/144	146/144	148/144	150/144	[Nd150]
0.830433	0.494001	0.436936	0.885201	0.740574	198.371260	0.049114
						nm/g

Wt Sample (g)= **0.00627** g
 Wt Spike (g)= **0.08267** g

Mass Spectrometer Information:

Number of cycles measured: **97**
 Number of cycles used: **60**

	start	average (from)	
Filament Current range: from	3.45	3.5	Amps
Beam intensity range: from	0.128	0.176	Volts 144Nd.160
Temperature range: from	1552	1620	° C

Final Ratio Data:

Interference Values (oxide corrected; informational only... not used in this sheet)

Ce140/Nd144 **0.0104807**
 Pr141/Nd144 **0.0135205**
 Sm149/Nd144 **4.281E-05**

for Ratios & %1SE: use grand mean oxygen corr, interference corr, exp normalized values

	142/144	143/144	145/144	146/144	148/144	150/144
Ratios	1.141669	0.51219527	0.3485022	0.7219	0.24234441	0.6148861
%StdErr	0.0029057	0.001681836	0.0017394	0	0.0045826	0.0063762
<i>for comparison only</i>	142/144	143/144	145/144	146/144	148/144	150/144
DePaolo 88, p.14, ln. B'	1.141854	na	0.348416	0.721882	0.241572	na

FINAL DATA TO REPORT:

146/144 set to 0.7219

	142/144	143/144	145/144	146/144	148/144	150/144	150t/144s
Ratios	1.141764	0.512118	0.348408	0.721900	0.241598	0.236478	2.628971
± 2 S.E.	0.000066	0.000017	0.000012	0.000000	0.000022	0.000030	0.000335

Epsilon143= **-10.14** using (143/144)chur= **0.512638**
 ± **0.34** (Hamilton et al. 1983)

linked from Sm sheet

[Sm147]= 2.552485 nm/g
 ± 0.000829

[Nd144]= 1.70243 nm/g
 ± 0.00025

[Sm]= 2.559140 ppm
 ± 0.000831

[Nd]= 1.03248 ppm
 ± 0.00015

TOT ng Sm= 16.045811

TOT ng Nd= 6.47366699

Sm147/Nd144= **1.499316**
 ± 2 S.E. **0.000533**
 ± 2RSE % **0%**

Full Sample Name: **27.2.1 Gt. E (UC)**
 Date of TIMS analysis: **11/28/2018**
 estimated Nd load (ng): **4**

Position #: **15****Rspike Values Nd {SmNd 1.0 A spike, 6-12-08 calib}**

142/144	143/144	145/144	146/144	148/144	150/144	[Nd150]
0.830433	0.494001	0.436936	0.885201	0.740574	198.371260	0.049114 nm/g

Wt Sample (g)= **0.00734** gWt Spike (g)= **0.09342** g

Mass Spectrometer Information:

Number of cycles measured: **154**Number of cycles used: **139**

	start	average (from	
Filament Current range: from	3.4	3.4	Amps
Beam intensity range: from	0.397	0.3172	Volts 144Nd.160
Temperature range: from	1560	1620	° C

Final Ratio Data:

Interference Values (oxide corrected; informational only... not used in this sheet)

Ce140/Nd144 **0.011622**Pr141/Nd144 **0.0068099**Sm149/Nd144 **5.926E-05***for Ratios & %ISE: use grand mean oxygen corr, interference corr, exp normalized values*

	142/144	143/144	145/144	146/144	148/144	150/144
Ratios	1.1417194	0.51221717	0.3485241	0.7219	0.24244589	0.6777109
%StdErr	0.0013013	0.000734134	0.0071043	0	0.00163251	0.001829

<i>for comparison only</i>	142/144	143/144	145/144	146/144	148/144	150/144
DePaolo 88, p.14, ln. B':	1.141854	na	0.348416	0.721882	0.241572	na

FINAL DATA TO REPORT:**146/144 set to 0.7219**

	142/144	143/144	145/144	146/144	148/144	150/144	150t/144s
Ratios	1.141831	0.512127	0.348415	0.721900	0.241575	0.236478	2.253447
± 2 S.E.	0.000030	0.000008	0.000050	0.000000	0.000008	0.000009	0.000082

Epsilon143= **-9.96** using (143/144)chur= **0.512638**
 ± **0.15** (Hamilton et al. 1983)

linked from Sm sheet

[Sm147]= **2.254829** nm/g
 ± **0.000967**

[Nd144]= **1.40862** nm/g
 ± **0.00010**

[Sm]= **2.260709** ppm[Nd]= **0.85429** ppm± **0.000969**± **0.00006**TOT ng Sm= **16.593601**TOT ng Nd= **6.27052345**Sm147/Nd144= **1.600732**± 2 S.E. **0.000695**± 2RSE % **0%**

Full Sample Name: **27.2.1 gt pwd2**
 Date of TIMS analysis: **7/13/2018** Position #: **10**
 estimated Nd load (ng): **4**

Rspike Values Nd {SmNd 1.0 A spike, 6-12-08 calib}

142/144	143/144	145/144	146/144	148/144	150/144	[Nd150]
0.830433	0.494001	0.436936	0.885201	0.740574	198.371260	0.049114
						nm/g

Wt Sample (g)= **0.00886** g
 Wt Spike (g)= **0.26052** g

Mass Spectrometer Information:

Number of cycles measured:	49	
Number of cycles used:	45	
		average (from
Filament Current range: from	3.76	3.76 Amps
Beam intensity range: from	0.429	0.283 Volts 144Nd.160
Temperature range: from	1413	1440 °C

Final Ratio Data:

Interference Values (oxide corrected; informational only... not used in this sheet)
 Ce140/Nd144 **0.0019484**
 Pr141/Nd144 **0.0016759**
 Sm149/Nd144 **9.455E-05**

for Ratios & %1SE: use grand mean oxygen corr, interference corr, exp normalized values

	142/144	143/144	145/144	146/144	148/144	150/144
Ratios	1.1418509	0.5121033	0.348464	0.7219	0.24213391	0.5566402
%StdErr	0.0021713	0.0016121	0.0009774	0	0.00393191	0.0045528

for comparison only

	142/144	143/144	145/144	146/144	148/144	150/144
DePaolo 88, p.14, ln. B'	1.141854	na	0.348416	0.721882	0.241572	na

FINAL DATA TO REPORT:

146/144 set to 0.7219

	142/144	143/144	145/144	146/144	148/144	150/144	150t/144s
Ratios	1.141932	0.512038	0.348385	0.721900	0.241502	0.236478	3.108781
± 2 S.E.	0.000050	0.000017	0.000007	0.000000	0.000019	0.000022	0.000283

Epsilon143= -11.71 using (143/144)chur= 0.512638
 ± 0.32 (Hamilton et al. 1983)

linked from Sm sheet

[Sm147]= 1.366585 nm/g [Nd144]= 4.48954 nm/g
 ± 0.000120 ± 0.00055

[Sm]= 1.370149 ppm [Nd]= 2.72279 ppm
 ± 0.000120 ± 0.00033

TOT ng Sm= 12.139517 TOT ng Nd= 24.1239206

Sm147/Nd144= 0.304393
 ± 2 S.E. 0.000046
 ± 2RSE % 0%

Full Sample Name: **27.2.1 Gt pwd 3 aq1**
 Date of TIMS analysis: **7/10/2018** Position #: **11**
 estimated Nd load (ng): **4**

Rspike Values Nd {SmNd 1.0 A spike, 6-12-08 calib}

142/144	143/144	145/144	146/144	148/144	150/144	[Nd150]
0.830433	0.494001	0.436936	0.885201	0.740574	198.371260	0.049114

nm/g

Wt Sample (g)= **0.0063681** g
 Wt Spike (g)= **0.25932** g

Mass Spectrometer Information:

Number of cycles measured:	65	
Number of cycles used:	60	
		average (from
Filament Current range: from	3.58	3.7 Amps
Beam intensity range: from	0.25272	0.722117 Volts 144Nd.16O
Temperature range: from	1567	1593 °C

Final Ratio Data:

Interference Values (oxide corrected; informational only... not used in this sheet)

Ce140/Nd144 **0.0011852**
 Pr141/Nd144 **0.0017431**
 Sm149/Nd144 **0.0000315**

for Ratios & %1SE: use grand mean oxygen corr, interference corr, exp normalized values

	142/144	143/144	145/144	146/144	148/144	150/144
Ratios	1.1417628	0.512070	0.3484557	0.7219	0.241966	0.44635
%StdErr	0.0010334	0.0006588	0.0005596	0	0.00138118	0.0020301

for comparison only

	142/144	143/144	145/144	146/144	148/144	150/144
DePaolo 88, p.14, ln. B':	1.141854	na	0.348416	0.721882	0.241572	na

FINAL DATA TO REPORT:

146/144 set to 0.7219

	142/144	143/144	145/144	146/144	148/144	150/144	150t/144s
Ratios	1.141816	0.512027	0.348404	0.721900	0.241552	0.236478	4.746907
± 2 S.E.	0.000024	0.000007	0.000004	0.000000	0.000007	0.000010	0.000193

Epsilon143= **-11.91** using (143/144)chur= **0.512638**
 ± **0.13** (Hamilton et al. 1983)

linked from Sm sheet

[Sm147]= 2.846900 nm/g [Nd144]= 9.49382 nm/g
 ± 0.000337 ± 0.00124

[Sm]= 2.854323 ppm [Nd]= 5.75776 ppm
 ± 0.000338 ± 0.00075

TOT ng Sm= 18.176615 TOT ng Nd= 36.6659892

Sm147/Nd144= **0.299869**
 ± 2 S.E. **0.000053**
 ± 2RSE % **0%**

Full Sample Name: **53.10 WR Aq1**
 Date of TIMS analysis: **12/12/2018**
 estimated Nd load (ng): **20**

Position #: **3**

Rspike Values Nd {SmNd 0.15 A spike, 6-12-08 calib}

142/144	143/144	145/144	146/144	148/144	150/144	[Nd150]
0.830433	0.494001	0.436936	0.885201	0.740574	198.371260	0.125778

nm/g

Wt Sample (g)= **0.0013812** g
 Wt Spike (g)= **0.4566** g

Mass Spectrometer Information:

Number of cycles measured:	97		
Number of cycles used:	77		
		average	
	start	(from	
Filament Current range: from	3.5	3.5	Amps
Beam intensity range: from	0.52	1.047	Volts 144Nd.16O
Temperature range: from	1540	1613	° C

Final Ratio Data:

Interference Values (oxide corrected; informational only... not used in this sheet)

Ce140/Nd144 **0.0023645**
 Pr141/Nd144 **0.0320187**
 Sm149/Nd144 **2.55E-05**

for Ratios & %1SE: use grand mean oxygen corr, interference corr, exp normalized values

	142/144	143/144	145/144	146/144	148/144	150/144
Ratios	1.1416928	0.51213019	0.3485542	0.7219	0.24277618	0.8468832
%StdErr	0.0011741	0.00076287	0.0007086	0	0.00125695	0.0011755
<i>for comparison only</i>	142/144	143/144	145/144	146/144	148/144	150/144
DePaolo 88, p.14, ln. B':	1.141854	na	0.348416	0.721882	0.241572	na

FINAL DATA TO REPORT:

146/144 set to 0.7219

	142/144	143/144	145/144	146/144	148/144	150/144	150t/144s
Ratios	1.141847	0.512005	0.348403	0.721900	0.241572	0.236478	1.626575
± 2 S.E.	0.000027	0.000008	0.000005	0.000000	0.000006	0.000006	0.000038

Epsilon143= -12.34 using (143/144)chur= 0.512638
 ± 0.15 (Hamilton et al. 1983)

linked from Sm sheet

[Sm147]= 8.130353 nm/g
 ± 0.000892

[Nd144]= 67.63296 nm/g
 ± 0.00329

[Sm]= 8.15151 ppm

[Nd]= 41.01768 ppm

± 0.000894

± 0.00200

TOT ng Sm= 11.258923

TOT ng Nd= 56.6536189

Sm147/Nd144= 0.120213

± 2 S.E. 0.000014

± 2RSE % 0%

Full Sample Name: **53.10 Gt. A**
 Date of TIMS analysis: **11/26/2018**
 estimated Nd load (ng): **4**

Position #: **16**

Rspike Values Nd {SmNd 1.0 A spike, 6-12-08 calib}

142/144	143/144	145/144	146/144	148/144	150/144	[Nd150]
0.830433	0.494001	0.436936	0.885201	0.740574	198.371260	0.049114
						nm/g

Wt Sample (g)= **0.0081** g
 Wt Spike (g)= **0.08267** g

Mass Spectrometer Information:

Number of cycles measured: **171**
 Number of cycles used: **159**

	start	average (from	
Filament Current range: from	3.6	3.7	Amps
Beam intensity range: from	0.235	0.566	Volts 144Nd.160
Temperature range: from	1547	1613	°C

Final Ratio Data:

Interference Values (oxide corrected; informational only... not used in this sheet)

Ce140/Nd144 **0.008091**
 Pr141/Nd144 **0.0168019**
 Sm149/Nd144 **3.362E-05**

for Ratios & %1SE: use grand mean oxygen corr, interference corr, exp normalized values

	142/144	143/144	145/144	146/144	148/144	150/144
Ratios	1.1415782	0.5121247	0.3487188	0.7219	0.24414988	0.4846263
%StdErr	0.0012396	0.0005738	0.001049	0	0.00200553	0.0022671
<i>for comparison only</i>	142/144	143/144	145/144	146/144	148/144	150/144
DePaolo 88, p.14, ln. B':	1.141854	na	0.348416	0.721882	0.241572	na

FINAL DATA TO REPORT:

146/144 set to 0.7219

	142/144	143/144	145/144	146/144	148/144	150/144	150t/144s
Ratios	1.141640	0.512074	0.348658	0.721900	0.243664	0.236478	4.013410
± 2 S.E.	0.000028	0.000006	0.000007	0.000000	0.000010	0.000011	0.000182

Epsilon143= **-11.00** using (143/144)chur= **0.512638**
 ± **0.11** (Hamilton et al. 1983)

linked from Sm sheet

[Sm147]= 1.177966 nm/g
 ± 0.000249

[Nd144]= 2.01178 nm/g
 ± 0.00023

[Sm]= 1.181038 ppm
 ± 0.000250

[Nd]= 1.22009 ppm
 ± 0.00014

TOT ng Sm= 9.5664062

TOT ng Nd= 9.88275596

Sm147/Nd144= **0.585535**
 ± 2 S.E. **0.000141**
 ± 2RSE % **0%**

Full Sample Name: **53.10 Gt. B**
 Date of TIMS analysis: **1/9/2019**
 estimated Nd load (ng): **4**

Position #: **13**

Rspike Values Nd {SmNd 1.0 A spike, 6-12-08 calib}						
142/144	143/144	145/144	146/144	148/144	150/144	[Nd150]
0.830433	0.494001	0.436936	0.885201	0.740574	198.371260	0.049114
						nm/g

Wt Sample (g)= **0.01001** g
 Wt Spike (g)= **0.25905** g

Mass Spectrometer Information:

Number of cycles measured:	120		
Number of cycles used:	113		
		start	average (from
Filament Current range: from	3.5	3.5	Amps
Beam intensity range: from	0.217	0.819	Volts 144Nd.160
Temperature range: from	1500	1587	° C

Final Ratio Data:

Interference Values (oxide corrected; informational only... not used in this sheet)

Ce140/Nd144 **0.01262**
 Pr141/Nd144 **0.0224115**
 Sm149/Nd144 **0.0002163**

for Ratios & %ISE: use grand mean oxygen corr, interference corr, exp normalized values

	142/144	143/144	145/144	146/144	148/144	150/144
Ratios	1.141641	0.5122216	0.3485849	0.7219	0.24290949	0.9260893
%StdErr	0.000925	0.0005103	0.0005509	0	0.001208	0.001248
for comparison only	142/144	143/144	145/144	146/144	148/144	150/144
DePaolo 88, p.14, ln. B'	1.141854	na	0.348416	0.721882	0.241572	na

FINAL DATA TO REPORT:

	142/144	143/144	145/144	146/144	148/144	150/144	150t/144s
Ratios	1.141815	0.512081	0.348414	0.721900	0.241548	0.236478	1.438786
± 2 S.E.	0.000021	0.000005	0.000004	0.000000	0.000006	0.000006	0.000036

Epsilon143= -10.87 using (143/144)chur= 0.512638
 ± 0.10 (Hamilton et al. 1983)

linked from Sm sheet

[Sm147]= 1.157462 nm/g
 ± 0.000094

[Nd144]= 1.82873 nm/g
 ± 0.00008

[Sm]= 1.160480 ppm
 ± 0.000094

[Nd]= 1.10908 ppm
 ± 0.00005

TOT ng Sm= 11.616407

TOT ng Nd= 11.1018771

Sm147/Nd144= 0.632932
 ± 2 S.E. 0.000059
 ± 2RSE % 0%

Full Sample Name: **53.10. Gt. C**
 Date of TIMS analysis: **1/19/2019**
 estimated Nd load (ng): **4**

Position #: **3**

Rspike Values Nd {SmNd 1.0 A spike, 6-12-08 calib}						
142/144	143/144	145/144	146/144	148/144	150/144	[Nd150]
0.830433	0.494001	0.436936	0.885201	0.740574	198.371260	0.049114
nm/g						

Wt Sample (g)= **0.00403** g
 Wt Spike (g)= **0.06392** g

Mass Spectrometer Information:

Number of cycles measured:	129		
Number of cycles used:	119		
		start	average (from
Filament Current range: from		3.35	3.47
			Amps
Beam intensity range: from		0.075	0.419
			Volts 144Nd.160
Temperature range: from		1527	1607
			° C

Final Ratio Data:

Interference Values (oxide corrected; informational only... not used in this sheet)

Ce140/Nd144 **0.0289927**
 Pr141/Nd144 **0.0178715**
 Sm149/Nd144 **0.0001264**

for Ratios & %1SE: use grand mean oxygen corr, interference corr, exp normalized values

	142/144	143/144	145/144	146/144	148/144	150/144
Ratios	1.1517525	0.5121553	0.3485014	0.7219	0.2422869	0.6106749
%StdErr	0.0009585	0.0010177	0.0008351	0	0.001925	0.0022182
for comparison only	142/144	143/144	145/144	146/144	148/144	150/144
DePaolo 88, p.14, ln. B':	1.141854	na	0.348416	0.721882	0.241572	na

FINAL DATA TO REPORT:

146/144 set to 0.7219

	142/144	143/144	145/144	146/144	148/144	150/144	150t/144s
Ratios	1.151861	0.512079	0.348409	0.721900	0.241549	0.236478	2.658652
± 2 S.E.	0.000022	0.000010	0.000006	0.000000	0.000009	0.000010	0.000118

Epsilon143= -10.91 using (143/144)chur= 0.512638
 ± 0.20 (Hamilton et al. 1983)

linked from Sm sheet

[Sm147]= 1.545881 nm/g
 ± 0.000259

[Nd144]= 2.07108 nm/g
 ± 0.00017

[Sm]= 1.549912 ppm
 ± 0.000260

[Nd]= 1.25606 ppm
 ± 0.00010

TOT ng Sm= 6.2461457

TOT ng Nd= 5.06191577

Sm147/Nd144= 0.746413
 ± 2 S.E. 0.000140
 ± 2RSE % 0%

Full Sample Name: **53.10 Gt pwd1**
 Date of TIMS analysis: **11/28/2018**
 estimated Nd load (ng): **4**

Position #: **17**

Rspike Values Nd {SmNd 1.0 A spike, 6-12-08 calib}

142/144	143/144	145/144	146/144	148/144	150/144	[Nd150]
0.830433	0.494001	0.436936	0.885201	0.740574	198.371260	0.049114 nm/g

Wt Sample (g)= **0.00408** g
 Wt Spike (g)= **0.05021** g

Mass Spectrometer Information:

Number of cycles measured:	240	
Number of cycles used:	225	
		average (from
Filament Current range: from	3.4	3.8 Amps
Beam intensity range: from	0.0624	0.0829799 Volts 144Nd.16O
Temperature range: from	1560	1633 °C

Final Ratio Data:

Interference Values (oxide corrected; informational only... not used in this sheet)

Ce140/Nd144 **0.0536846**
 Pr141/Nd144 **0.0192039**
 Sm149/Nd144 **0.0001625**

for Ratios & %1SE: use grand mean oxygen corr, interference corr, exp normalized values

	142/144	143/144	145/144	146/144	148/144	150/144
Ratios	1.1416513	0.512225	0.3485599	0.7219	0.24269391	0.8135982
%StdErr	0.0025923	0.002253	0.001049	0	0.00200553	0.0022671
<i>for comparison only</i>	142/144	143/144	145/144	146/144	148/144	150/144
DePaolo 88, p.14, ln. B':	1.141854	na	0.348416	0.721882	0.241572	na

FINAL DATA TO REPORT:

146/144 set to 0.7219

	142/144	143/144	145/144	146/144	148/144	150/144	150t/144s
Ratios	1.141797	0.512107	0.348417	0.721900	0.241555	0.236478	1.720873
± 2 S.E.	0.000059	0.000023	0.000007	0.000000	0.000010	0.000011	0.000078

Epsilon143= -10.35 using (143/144)chur= 0.512638
 ± 0.45 (Hamilton et al. 1983)

linked from Sm sheet

[Sm147]= 1.241338 nm/g
 ± 0.000438

[Nd144]= 1.04012 nm/g
 ± 0.00007

[Sm]= 1.244574 ppm
 ± 0.000439

[Nd]= 0.63081 ppm
 ± 0.00004

TOT ng Sm= 5.0778633

TOT ng Nd= 2.57368651

Sm147/Nd144= 1.193458
 ± 2 S.E. 0.000428
 ± 2RSE % 0%

Full Sample Name: **53.10 gt pwd2**
 Date of TIMS analysis: **1/10/2019**
 estimated Nd load (ng): **2**

Position #: **14**

Rspike Values Nd {SmNd 1.0 A spike, 6-12-08 calib}

142/144	143/144	145/144	146/144	148/144	150/144	[Nd150]
0.830433	0.494001	0.436936	0.885201	0.740574	198.371260	0.049114
						nm/g

Wt Sample (g)= **0.00369** g
 Wt Spike (g)= **0.0581** g

Mass Spectrometer Information:

Number of cycles measured: **240**
 Number of cycles used: **122**

	start	average (from	
Filament Current range: from	3.26	3.4	Amps
Beam intensity range: from	0.091	0.260261	Volts 144Nd.16O
Temperature range: from	1553	1600	° C

Final Ratio Data:

Interference Values (oxide corrected; informational only... not used in this sheet)

Ce140/Nd144 **0.0357816**
 Pr141/Nd144 **0.034608**
 Sm149/Nd144 **1.012E-05**

for Ratios & %1SE: use grand mean oxygen corr, interference corr, exp normalized values

	142/144	143/144	145/144	146/144	148/144	150/144
Ratios	1.1417377	0.512245	0.3485632	0.7219	0.242834	0.8677465
%StdErr	0.0015246	0.0012049	0.0012133	0	0.00289144	0.0022838
<i>for comparison only</i>	142/144	143/144	145/144	146/144	148/144	150/144
DePaolo 88, p.14, ln. B':	1.141854	na	0.348416	0.721882	0.241572	na

FINAL DATA TO REPORT:

146/144 set to 0.7219

	142/144	143/144	145/144	146/144	148/144	150/144	150t/144s
Ratios	1.141897	0.512116	0.348407	0.721900	0.241588	0.236478	1.572539
± 2 S.E.	0.000035	0.000012	0.000008	0.000000	0.000014	0.000011	0.000072

Epsilon143= **-10.18** using (143/144)chur= **0.512638**
 ± **0.24** (Hamilton et al. 1983)

linked from Sm sheet

[Sm147]= 1.121880 nm/g
 ± 0.000156

[Nd144]= 1.21606 nm/g
 ± 0.00007

[Sm]= 1.124805 ppm
 ± 0.000157

[Nd]= 0.73751 ppm
 ± 0.00005

TOT ng Sm= 4.1505301

TOT ng Nd= 2.72141155

Sm147/Nd144= **0.922553**
 ± 2 S.E. **0.000140**
 ± 2RSE % **0%**

Full Sample Name: **27.1.2 WR AQ1**
 Date of TIMS analysis: **11/6/2017** Position #: **2**
 estimated Nd load (ng): **4**

Rspike Values Nd {SmNd 0.15 A spike, 6-12-08 calib}						
142/144	143/144	145/144	146/144	148/144	150/144	[Nd150]
0.830433	0.494001	0.436936	0.885201	0.740574	198.371260	0.125778
						nm/g

Wt Sample (g)= **0.0003023** g
 Wt Spike (g)= **0.10248** g

Mass Spectrometer Information:

Number of cycles measured: **47**
 Number of cycles used: **44**

	start	average (from	
Filament Current range: from	3.425	<enter!>	Amps
Beam intensity range: from	600	<enter!>	Volts 144Nd.160
Temperature range: from	1516	<enter!>	° C

Final Ratio Data:

Interference Values (oxide corrected; informational only... not used in this sheet)
 Ce140/Nd144 **0.0019376**
 Pr141/Nd144 **0.0038437**
 Sm149/Nd144 **8.951E-05**

for Ratios & %ISE: use grand mean oxygen corr, interference corr, exp normalized values

	142/144	143/144	145/144	146/144	148/144	150/144
Ratios	1.1416205	0.5121503	0.3485925	0.7219	0.02430362	0.9871466
%StdErr	0.0020156	0.0020597	0.0027895	0	0.00589611	0.0041699
<i>for comparison only</i>	142/144	143/144	145/144	146/144	148/144	150/144
DePaolo 88, p.14, ln. B'	1.141854	na	0.348416	0.721882	0.241572	na

FINAL DATA TO REPORT:

	142/144	143/144	145/144	146/144	148/144	150/144	150t/144s
Ratios	1.141810	0.511997	0.348406	0.721900	0.021612	0.236478	1.321074
± 2 S.E.	0.000046	0.000021	0.000019	0.000000	0.000003	0.000020	0.000110

Epsilon143= -12.51 using (143/144)chur= 0.512638
 ± 0.41 (Hamilton et al. 1983)

linked from Sm sheet

[Sm147]= 6.552519 nm/g ± 0.004946	[Nd144]= 56.33383 nm/g ± 0.00509
[Sm]= 6.569604 ppm ± 0.004959	[Nd]= 34.16504 ppm ± 0.00309
TOT ng Sm= 1.9858251	TOT ng Nd= 10.3272282
Sm147/Nd144= 0.116316 ± 2 S.E. 0.000088 ± 2RSE % 0%	

Full Sample Name: **27.1.2 Gt. A**
 Date of TIMS analysis: **12/12/2017**
 estimated Nd load (ng): **4**

Position #: **11**

Rspike Values Nd {SmNd 1.0 A spike, 6-12-08 calib}

142/144	143/144	145/144	146/144	148/144	150/144	[Nd150]
0.830433	0.494001	0.436936	0.885201	0.740574	198.371260	0.049114 nm/g

Wt Sample (g)= **0.0053122** g
 Wt Spike (g)= **0.15311** g

Mass Spectrometer Information:

Number of cycles measured:	85		
Number of cycles used:	76		
		average	
	start	(from	
Filament Current range: from	3.58	3.67	Amps
Beam intensity range: from	0.75	0.685	Volts 144Nd.160
Temperature range: from	1513	1607	° C

Final Ratio Data:

Interference Values (oxide corrected; informational only... not used in this sheet)

Ce140/Nd144 **0.0065744**
 Pr141/Nd144 **0.002637**
 Sm149/Nd144 **5.329E-05**

for Ratios & %1SE: use grand mean oxygen corr, interference corr, exp normalized values

	142/144	143/144	145/144	146/144	148/144	150/144
Ratios	1.1416695	0.51233003	0.3485822	0.7219	0.24287092	0.9088313
%StdErr	0.0011456	0.00064007	0.0006186	0	0.00169047	0.0014023
<i>for comparison only</i>	142/144	143/144	145/144	146/144	148/144	150/144
DePaolo 88, p.14, ln. B':	1.141854	na	0.348416	0.721882	0.241572	na

FINAL DATA TO REPORT:

146/144 set to 0.7219

	142/144	143/144	145/144	146/144	148/144	150/144	150t/144s
Ratios	1.141839	0.512193	0.348416	0.721900	0.241544	0.236478	1.475933
± 2 S.E.	0.000026	0.000007	0.000004	0.000000	0.000008	0.000007	0.000041

Epsilon143= -8.68 using (143/144)chur= 0.512638
 ± 0.13 (Hamilton et al. 1983)

linked from Sm sheet

[Sm147]= 4.418466 nm/g
 ± 0.001147

[Nd144]= 2.08931 nm/g
 ± 0.00010

[Sm]= 4.429986 ppm
 ± 0.001150

[Nd]= 1.26711 ppm
 ± 0.00006

TOT ng Sm= 23.532832

TOT ng Nd= 6.73111236

Sm147/Nd144= 2.114799
 ± 2 S.E. 0.000558
 ± 2RSE % 0%

Full Sample Name: **27.1.2 Gt. B**
 Date of TIMS analysis: **11/9/2017**
 estimated Nd load (ng): **4**

Position #: **12**

Rspike Values Nd {SmNd 1.0 A spike, 6-12-08 calib}

142/144	143/144	145/144	146/144	148/144	150/144	[Nd150]
0.830433	0.494001	0.436936	0.885201	0.740574	198.371260	0.049114
						nm/g

Wt Sample (g)= **0.010544** g
 Wt Spike (g)= **0.18682** g

Mass Spectrometer Information:

Number of cycles measured:	68		
Number of cycles used:	62		
		average	
	start	(from	
Filament Current range: from	3.43	3.44	Amps
Beam intensity range: from	1.056	0.765	Volts 144Nd.160
Temperature range: from	1532	1607	° C

Final Ratio Data:

Interference Values (oxide corrected; informational only... not used in this sheet)

Ce140/Nd144 **0.0039859**
 Pr141/Nd144 **0.001219**
 Sm149/Nd144 **8.783E-05**

for Ratios & %ISE: use grand mean oxygen corr, interference corr, exp normalized values

	142/144	143/144	145/144	146/144	148/144	150/144
Ratios	1.1417507	0.5122296	0.3485234	0.7219	0.24247992	0.7182674
%StdErr	0.0007593	0.000859	0.0006477		0.00144219	0.0014382

<i>for comparison only</i>	142/144	143/144	145/144	146/144	148/144	150/144
DePaolo 88, p.14, ln. B':	1.141854	na	0.348416	0.721882	0.241572	na

FINAL DATA TO REPORT:

146/144 set to 0.7219

	142/144	143/144	145/144	146/144	148/144	150/144	150t/144s
Ratios	1.141872	0.512131	0.348404	0.721900	0.241529	0.236478	2.063045
± 2 S.E.	0.000017	0.000009	0.000005	0.000000	0.000007	0.000007	0.000059

Epsilon143= -9.88 using (143/144)chur= 0.512638
 ± 0.17 (Hamilton et al. 1983)

linked from Sm sheet

[Sm147]= 2.624023 nm/g [Nd144]= 1.79527 nm/g
 ± 0.003175 ± 0.00011

[Sm]= 2.630865 ppm [Nd]= 1.08879 ppm

± 0.003184 ± 0.00007

TOT ng Sm= 27.739903 TOT ng Nd= 11.4801816

Sm147/Nd144= 1.461632

± 2 S.E. 0.001771

± 2RSE % 0%

Full Sample Name: **27.1.2 Gt. C**
 Date of TIMS analysis: **11/9/2017**
 estimated Nd load (ng): **4**

Position #: **3**

Rspike Values Nd (SmNd 1.0 A spike, 6-12-08 calib)

142/144	143/144	145/144	146/144	148/144	150/144	[Nd150]
0.830433	0.494001	0.436936	0.885201	0.740574	198.371260	0.049114
						nm/g

Wt Sample (g)= **0.0058643** g
 Wt Spike (g)= **0.15272** g

Mass Spectrometer Information:

Number of cycles measured:	161		
Number of cycles used:	143		
		average	
	start	(from	
Filament Current range: from	3.48	3.67	Amps
Beam intensity range: from	0.172	0.147	Volts 144Nd.160
Temperature range: from	1533	1600	° C

Final Ratio Data:

Interference Values (oxide corrected; informational only... not used in this sheet)

Ce140/Nd144	0
Pr141/Nd144	0
Sm149/Nd144	0

for Ratios & %1SE: use grand mean oxygen corr, interference corr, exp normalized values

	142/144	143/144	145/144	146/144	148/144	150/144
Ratios	1.1416085	0.51213576	0.3485087	0.7219	0.24232736	0.6307435
%StdErr	0.0014289	0.00117885	0.0012931	0	0.00432414	0.0039078
<i>for comparison only</i>	142/144	143/144	145/144	146/144	148/144	150/144
DePaolo 88, p.14, ln. B':	1.141854	na	0.348416	0.721882	0.241572	na

FINAL DATA TO REPORT:

146/144 set to 0.7219

	142/144	143/144	145/144	146/144	148/144	150/144	150t/144s
Ratios	1.141708	0.512055	0.348411	0.721900	0.241549	0.236478	2.522895
± 2 S.E.	0.000033	0.000012	0.000009	0.000000	0.000021	0.000018	0.000197

Epsilon143= **-11.37** using (143/144)chur= **0.512638**
 ± **0.24** (Hamilton et al. 1983)

linked from Sm sheet

[Sm147]= 3.458247 nm/g
 ± 0.000790

[Nd144]= 3.22686 nm/g
 ± 0.00033

[Sm]= 3.467264 ppm
 ± 0.000792

[Nd]= 1.95701 ppm
 ± 0.00020

TOT ng Sm= 20.333234

TOT ng Nd= 11.4765588

Sm147/Nd144= **1.071708**
 ± 2 S.E. **0.000268**
 ± 2RSE % **0%**

Full Sample Name: **27.1.2 gt pwd aq1**
 Date of TIMS analysis: **11/8/2017** Position #: **3**
 estimated Nd load (ng): **4**

Rspike Values Nd {SmNd 1.0 A spike, 6-12-08 calib}

142/144	143/144	145/144	146/144	148/144	150/144	[Nd150]
0.830433	0.494001	0.436936	0.885201	0.740574	198.371260	0.049114
						nm/g

Wt Sample (g)= **0.0053383** g
 Wt Spike (g)= **0.020714** g

Mass Spectrometer Information:

Number of cycles measured:	96	
Number of cycles used:	88	
	start	average (from
Filament Current range: from	3.6	3.6
		Amps
Beam intensity range: from	1.019	0.749
		Volts 144Nd.160
Temperature range: from	1500	1573
		° C

Final Ratio Data:

Interference Values (oxide corrected; informational only... not used in this sheet)

Ce140/Nd144 **0.0003339**
 Pr141/Nd144 **0.0009263**
 Sm149/Nd144 **4.121E-05**

for Ratios & %ISE: use grand mean oxygen corr, interference corr, exp normalized values

	142/144	143/144	145/144	146/144	148/144	150/144
Ratios	1.1417753	0.5120911	0.3484759	0.7219	0.24209597	0.5113876
%StdErr	0.0007719	0.0004909	0.0005129	0	0.00132804	0.0018205
<i>for comparison only</i>	142/144	143/144	145/144	146/144	148/144	150/144
DePaolo 88, p.14, ln. B'	1.141854	na	0.348416	0.721882	0.241572	na

FINAL DATA TO REPORT:

146/144 set to 0.7219

	142/144	143/144	145/144	146/144	148/144	150/144	150t/144s
Ratios	1.141844	0.512035	0.348408	0.721900	0.241554	0.236478	3.621901
± 2 S.E.	0.000018	0.000005	0.000004	0.000000	0.000006	0.000009	0.000132

Epsilon143= -11.76 using (143/144)chur= 0.512638
 ± 0.10 (Hamilton et al. 1983)

linked from Sm sheet

[Sm147]= 0.231661 nm/g
 ± 0.000025

[Nd144]= 0.69025 nm/g
 ± 0.00007

[Sm]= 0.232265 ppm
 ± 0.000025

[Nd]= 0.41862 ppm
 ± 0.00004

TOT ng Sm= 1.2398906

TOT ng Nd= 2.23468931

Sm147/Nd144= 0.335620
 ± 2 S.E. 0.000049
 ± 2RSE % 0%

Full Sample Name: **B6 Matrix**
 Date of TIMS analysis: **7/6/2018**
 estimated Nd load (ng): **45**

Position #: **18**

Rspike Values Nd {SmNd 0.15 A spike, 6-12-08 calib}						
142/144	143/144	145/144	146/144	148/144	150/144	[Nd150]
0.830433	0.494001	0.436936	0.885201	0.740574	198.371260	0.125778
						nm/g

Wt Sample (g)= **0.0010255** g
 Wt Spike (g)= **0.34037** g

Mass Spectrometer Information:

Number of cycles measured:	177	
Number of cycles used:	162	
	start	average (from
Filament Current range: from	3.7	3.7
		Amps
Beam intensity range: from	0.6816	1.0125
		Volts 144Nd.160
Temperature range: from	1580	1602
		° C

Final Ratio Data:

Interference Values (oxide corrected; informational only... not used in this sheet)

Ce140/Nd144 **0.0007428**
 Pr141/Nd144 **0.0011258**
 Sm149/Nd144 **2.09E-05**

for Ratios & %1SE: use grand mean oxygen corr, interference corr, exp normalized values

	142/144	143/144	145/144	146/144	148/144	150/144
Ratios	1.1416484	0.5121577	0.3485693	0.7219	0.24281915	0.8735136
%StdErr	0.0004859	0.0003183	0.0002551	0	0.00063267	0.0008722

for comparison only	142/144	143/144	145/144	146/144	148/144	150/144
DePaolo 88, p.14, ln. B'	1.141854	na	0.348416	0.721882	0.241572	na

FINAL DATA TO REPORT:

146/144 set to 0.7219

	142/144	143/144	145/144	146/144	148/144	150/144	150t/144s
Ratios	1.141809	0.512027	0.348411	0.721900	0.241562	0.236478	1.558227
± 2 S.E.	0.000011	0.000003	0.000002	0.000000	0.000003	0.000004	0.000027

Epsilon143= -11.91 using (143/144)chur= 0.512638
 ± 0.06 (Hamilton et al. 1983)

linked from Sm sheet

[Sm147]= 7.642081 nm/g [Nd144]= 65.05368 nm/g
 ± 0.000779 ± 0.00289

[Sm]= 7.662007 ppm [Nd]= 39.45341 ppm

± 0.000781 ± 0.00175

TOT ng Sm= 7.8570129 TOT ng Nd= 40.4575358

Sm147/Nd144= 0.117473
 ± 2 S.E. 0.000013
 ± 2RSE % 0%

Full Sample Name: **B8 matrix**
 Date of TIMS analysis: **1/30/2019**
 estimated Nd load (ng): **20**

Position #: **4**

Rspike Values Nd {SmNd 0.15 A spike, 6-12-08 calib}

142/144	143/144	145/144	146/144	148/144	150/144	[Nd150]
0.830433	0.494001	0.436936	0.885201	0.740574	198.371260	0.125778 nm/g

Wt Sample (g)= **0.0014979** g
 Wt Spike (g)= **0.54247** g

Mass Spectrometer Information:

Number of cycles measured:	65		
Number of cycles used:	56		
	start	average (from	
Filament Current range: from	3.7	3.7	Amps
Beam intensity range: from	0.547	2.909	Volts 144Nd.16O
Temperature range: from	1460	1660	° C

Final Ratio Data:

Interference Values (oxide corrected; informational only... not used in this sheet)

Ce140/Nd144 **0.0070171**
 Pr141/Nd144 **0.0269904**
 Sm149/Nd144 **1.591E-05**

for Ratios & %1SE: use grand mean oxygen corr, interference corr, exp normalized values

	142/144	143/144	145/144	146/144	148/144	150/144
Ratios	1.1416563	0.5121665	0.3485902	0.7219	0.24298045	0.9509222
%StdErr	0.0012655	0.000673	0.0004495	0	0.00102955	0.0008166
<i>for comparison only</i>	142/144	143/144	145/144	146/144	148/144	150/144
DePaolo 88, p.14, ln. B':	1.141854	na	0.348416	0.721882	0.241572	na

FINAL DATA TO REPORT:

146/144 set to 0.7219

	142/144	143/144	145/144	146/144	148/144	150/144	150t/144s
Ratios	1.141837	0.512020	0.348413	0.721900	0.241570	0.236478	1.388483
± 2 S.E.	0.000029	0.000007	0.000003	0.000000	0.000005	0.000004	0.000023

Epsilon143= -12.05 using (143/144)chur= 0.512638
 ± 0.13 (Hamilton et al. 1983)

linked from Sm sheet

[Sm147]= 7.397478 nm/g
 ± 0.000738

[Nd144]= 63.24889 nm/g
 ± 0.00252

[Sm]= 7.416766 ppm
 ± 0.000740

[Nd]= 38.35885 ppm
 ± 0.00153

TOT ng Sm= 11.109205

TOT ng Nd= 57.455813

Sm147/Nd144= 0.116958
 ± 2 S.E. 0.000013
 ± 2RSE % 0%

Full Sample Name: **B9 matrix**
 Date of TIMS analysis: **1/30/2019**
 estimated Nd load (ng): **25**

Position #: **5**

Rspike Values Nd {SmNd 0.15 A spike, 6-12-08 calib}						
142/144	143/144	145/144	146/144	148/144	150/144	[Nd150]
0.830433	0.494001	0.436936	0.885201	0.740574	198.371260	0.125778
						nm/g

Wt Sample (g)= **0.0015716** g
 Wt Spike (g)= **0.57007** g

Mass Spectrometer Information:

Number of cycles measured:	150		
Number of cycles used:	136		
	start	average (from)	
Filament Current range: from	3.53	3.64	Amps
Beam intensity range: from	0.091	1.061	Volts 14Nd.16O
Temperature range: from	1460	1593	° C

Final Ratio Data:

Interference Values (oxide corrected; informational only... not used in this sheet)
 Ce140/Nd144 **0.0094552**
 Pr141/Nd144 **0.0314239**
 Sm149/Nd144 **1.539E-05**

for Ratios & %ISE: use grand mean oxygen corr, interference corr, exp normalized values

	142/144	143/144	145/144	146/144	148/144	150/144
Ratios	1.1416349	0.5122108	0.3486416	0.7219	0.243363	1.1423079
%StdErr	0.0011161	0.0006198	0.0005969	0	0.0014358	0.0013906
for comparison only	142/144	143/144	145/144	146/144	148/144	150/144
DePaolo 88, p.14, ln. B'	1.141854	na	0.348416	0.721882	0.241572	na

FINAL DATA TO REPORT:

	142/144	143/144	145/144	146/144	148/144	150/144	150t/144s
Ratios	1.141864	0.512025	0.348417	0.721900	0.241575	0.236478	1.093342
± 2 S.E.	0.000025	0.000006	0.000004	0.000000	0.000007	0.000007	0.000030

Epsilon143= -11.95 using (143/144)chur= 0.512638
 ± 0.12 (Hamilton et al. 1983)

linked from Sm sheet

[Sm147]= 5.717433 nm/g ± 0.000416	[Nd144]= 49.88359 nm/g ± 0.00199
[Sm]= 5.732340 ppm ± 0.000418	[Nd]= 30.25313 ppm ± 0.00121
TOT ng Sm= 9.0087244	TOT ng Nd= 47.544654
Sm147/Nd144= 0.114616 ± 2 S.E. 0.000010 ± 2RSE % 0%	

Full Sample Name: **D1 matrix**
 Date of TIMS analysis: **1/30/2019**
 estimated Nd load (ng): **25**

Position #: **6**

Rspike Values Nd {SmNd 0.15 A spike, 6-12-08 calib}

142/144	143/144	145/144	146/144	148/144	150/144	[Nd150]
0.830433	0.494001	0.436936	0.885201	0.740574	198.371260	0.125778
						nm/g

Wt Sample (g)= **0.0016017** g
 Wt Spike (g)= **0.56753** g

Mass Spectrometer Information:

Number of cycles measured:	145		
Number of cycles used:	133		
		average	
	start	(from	
Filament Current range: from	3.33	3.54	Amps
Beam intensity range: from	0.409	1.009	Volts 144Nd.160
Temperature range: from	1527	1593	° C

Final Ratio Data:

Interference Values (oxide corrected; informational only... not used in this sheet)

Ce140/Nd144 **0.003617**
 Pr141/Nd144 **0.017917**
 Sm149/Nd144 **1.434E-05**

for Ratios & %1SE: use grand mean oxygen corr, interference corr, exp normalized values

	142/144	143/144	145/144	146/144	148/144	150/144
Ratios	1.1417215	0.5121464	0.3485489	0.7219	0.24269692	0.8831471
%StdErr	0.0005075	0.0004077	0.0004341	0	0.00095	0.0008621
<i>for comparison only</i>	142/144	143/144	145/144	146/144	148/144	150/144
DePaolo 88, p.14, ln. B'	1.141854	na	0.348416	0.721882	0.241572	na

FINAL DATA TO REPORT:

146/144 set to 0.7219

	142/144	143/144	145/144	146/144	148/144	150/144	150t/144s
Ratios	1.141885	0.512014	0.348389	0.721900	0.241420	0.236478	1.534888
± 2 S.E.	0.000012	0.000004	0.000003	0.000000	0.000005	0.000004	0.000026

Epsilon143= -12.17 using (143/144)chur= 0.512638
 ± 0.08 (Hamilton et al. 1983)

linked from Sm sheet

[Sm147]= 9.082792 nm/g
 ± 0.001052

[Nd144]= 68.40522 nm/g
 ± 0.00299

[Sm]= 9.106474 ppm
 ± 0.001054

[Nd]= 41.48603 ppm
 ± 0.00182

TOT ng Sm= 14.58584

TOT ng Nd= 66.4481803

Sm147/Nd144= 0.132779
 ± 2 S.E. 0.000016
 ± 2RSE % 0%

Full Sample Name: **E2 matrix**
 Date of TIMS analysis: **1/31/2019**
 estimated Nd load (ng): **25**

Position #: **7**

Rspike Values Nd {SmNd 0.15 A spike, 6-12-08 calib}

142/144	143/144	145/144	146/144	148/144	150/144	[Nd150]
0.830433	0.494001	0.436936	0.885201	0.740574	198.371260	0.125778
						nm/g

Wt Sample (g)= **0.0015582** g
 Wt Spike (g)= **0.5574** g

Mass Spectrometer Information:

Number of cycles measured:	209		
Number of cycles used:	198		
	start	average (from	
Filament Current range: from	3.15	3.45	Amps
Beam intensity range: from	0.142	0.913	Volts 144Nd.160
Temperature range: from	1520	1593	° C

Final Ratio Data:

Interference Values (oxide corrected; informational only... not used in this sheet)

Ce140/Nd144 **0.004645**
 Pr141/Nd144 **0.0285506**
 Sm149/Nd144 **1.993E-05**

for Ratios & %1SE: use grand mean oxygen corr, interference corr, exp normalized values

	142/144	143/144	145/144	146/144	148/144	150/144
Ratios	1.1416126	0.5122049	0.3486237	0.7219	0.24329526	1.1152388
%StdErr	0.0008472	0.0005218	0.000474	0	0.0011881	0.0016149
<i>for comparison only</i>	142/144	143/144	145/144	146/144	148/144	150/144
DePaolo 88, p.14, ln. B'	1.141854	na	0.348416	0.721882	0.241572	na

FINAL DATA TO REPORT:

146/144 set to 0.7219

	142/144	143/144	145/144	146/144	148/144	150/144	150t/144s
Ratios	1.141835	0.512025	0.348406	0.721900	0.241561	0.236478	1.127280
± 2 S.E.	0.000019	0.000005	0.000003	0.000000	0.000006	0.000008	0.000036

Epsilon143= -11.96 using (143/144)chur= 0.512638
 ± 0.10 (Hamilton et al. 1983)

linked from Sm sheet

[Sm147]= 5.892345 nm/g
 ± 0.000592

[Nd144]= 50.71885 nm/g
 ± 0.00222

[Sm]= 5.907708 ppm
 ± 0.000593

[Nd]= 30.75970 ppm
 ± 0.00135

TOT ng Sm= 9.2056274

TOT ng Nd= 47.9309936

Sm147/Nd144= 0.116177
 ± 2 S.E. 0.000013
 ± 2RSE % 0%

Full Sample Name: **Gt B6 zone 4 1mg test**
 Date of TIMS analysis: **7/6/2018** Position #: **16**
 estimated Nd load (ng): **4**

Rspike Values Nd {SmNd 1.0 A spike, 6-12-08 calib}						
142/144	143/144	145/144	146/144	148/144	150/144	[Nd150]
0.830433	0.494001	0.436936	0.885201	0.740574	198.371260	0.049114
						nm/g

Wt Sample (g)= **0.00137** g
 Wt Spike (g)= **0.04293** g

Mass Spectrometer Information:

Number of cycles measured:	100	
Number of cycles used:	91	
	start	average (from
Filament Current range: from	3.62	3.62
Beam intensity range: from	0.481	0.51316
Temperature range: from	1580	1606
		Amps
		Volts 144Nd.160
		° C

Final Ratio Data:

Interference Values (oxide corrected; informational only... not used in this sheet)
 Ce140/Nd144 **0.005349**
 Pr141/Nd144 **0.0011917**
 Sm149/Nd144 **0.0000988**

for Ratios & %1SE: use grand mean oxygen corr, interference corr, exp normalized values

	142/144	143/144	145/144	146/144	148/144	150/144
Ratios	1.1417949	0.512118	0.3484913	0.7219	0.24224017	0.5862885
%StdErr	0.0011246	0.0007131	0.0007731	0	0.00155996	0.0017472

for comparison only	142/144	143/144	145/144	146/144	148/144	150/144
DePaolo 88, p.14, ln. B'	1.141854	na	0.348416	0.721882	0.241572	na

FINAL DATA TO REPORT:

	142/144	143/144	145/144	146/144	148/144	150/144	150t/144s
Ratios	1.141883	0.512047	0.348405	0.721900	0.241550	0.236478	2.844582
± 2 S.E.	0.000026	0.000007	0.000005	0.000000	0.000008	0.000008	0.000099

Epsilon143= -11.54 using (143/144)chur= 0.512638
 ± 0.14 (Hamilton et al. 1983)

linked from Sm sheet

[Sm147]= 1.553158 nm/g [Nd144]= 4.37787 nm/g
 ± 0.000136 ± 0.00036

[Sm]= 1.557207 ppm [Nd]= 2.65507 ppm
 ± 0.000136 ± 0.00022

TOT ng Sm= 2.133374 TOT ng Nd= 3.63744093

Sm147/Nd144= **0.354775**
 ± 2 S.E. **0.000043**
 ± 2RSE % **0%**

Full Sample Name: **Gt. B6 zone4 pwd 1mg test**
 Date of TIMS analysis: **7/6/2018** Position #: **17**
 estimated Nd load (ng): **4**

Rspike Values Nd {SmNd 1.0 A spike, 6-12-08 calib}						
142/144	143/144	145/144	146/144	148/144	150/144	[Nd150]
0.830433	0.494001	0.436936	0.885201	0.740574	198.371260	0.049114
						nm/g

Wt Sample (g)= **0.0011** g
 Wt Spike (g)= **0.04566** g

Mass Spectrometer Information:

Number of cycles measured:	129	
Number of cycles used:	121	
	start	average (from
Filament Current range: from	3.6	3.65
Beam intensity range: from	1.0953	0.9094
Temperature range: from	1573	1603
		Amps
		Volts 144Nd.160
		° C

Final Ratio Data:

Interference Values (oxide corrected; informational only... not used in this sheet)

Ce140/Nd144 **0.0012672**
 Pr141/Nd144 **0.0030394**
 Sm149/Nd144 **2.185E-05**

for Ratios & %ISE: use grand mean oxygen corr, interference corr, exp normalized values

	142/144	143/144	145/144	146/144	148/144	150/144
Ratios	1.1418317	0.512054	0.3484264	0.7219	0.24172801	0.3198808
%StdErr	0.0006323	0.0003953	0.0004771	0	0.00103261	0.0012984
for comparison only	142/144	143/144	145/144	146/144	148/144	150/144
DePaolo 88, p.14, ln. B'	1.141854	na	0.348416	0.721882	0.241572	na

FINAL DATA TO REPORT:

146/144 set to 0.7219

	142/144	143/144	145/144	146/144	148/144	150/144	150t/144s
Ratios	1.141853	0.512037	0.348406	0.721900	0.241564	0.236478	11.957720
± 2 S.E.	0.000014	0.000004	0.000003	0.000000	0.000005	0.000006	0.000311

Epsilon143= -11.72 using (143/144)chur= 0.512638
 ± 0.08 (Hamilton et al. 1983)

linked from Sm sheet

[Sm147]= 5.066389 nm/g
 ± 0.001052

[Nd144]= 24.37786 nm/g
 ± 0.00763

[Sm]= 5.079599 ppm
 ± 0.001055

[Nd]= 14.78455 ppm
 ± 0.00463

TOT ng Sm= 5.587559

TOT ng Nd= 16.2630097

Sm147/Nd144= 0.207827
 ± 2 S.E. 0.000078
 ± 2RSE % 0%

Full Sample Name: **B8B9E2 zone 1 gt**
 Date of TIMS analysis: **2/21/2019** Position #: **10**
 estimated Nd load (ng): **2**

Rspike Values Nd {SmNd 1.0 A spike, 6-12-08 calib}						
142/144	143/144	145/144	146/144	148/144	150/144	[Nd150]
0.830433	0.494001	0.436936	0.885201	0.740574	198.371260	0.049114
						nm/g

Wt Sample (g) = **0.00626** g
 Wt Spike (g) = **0.0762** g

Mass Spectrometer Information:

Number of cycles measured:	159		
Number of cycles used:	105		
	start	average (from)	
Filament Current range: from	3.66	3.84	Amps
Beam intensity range: from	0.267	0.439	Volts 144Nd.160
Temperature range: from	1507	1640	° C

Final Ratio Data:

Interference Values (oxide corrected; informational only... not used in this sheet)
 Ce140/Nd144 **0.0282076**
 Pr141/Nd144 **0.0231913**
 Sm149/Nd144 **0.0001294**

for Ratios & %ISE: use grand mean oxygen corr, interference corr, exp normalized values

	142/144	143/144	145/144	146/144	148/144	150/144
Ratios	1.1416655	0.5125017	0.3486146	0.7219	0.24322839	1.0487061
%StdErr	0.0012168	0.0008216	0.0006799	0	0.00214565	0.001639
for comparison only	142/144	143/144	145/144	146/144	148/144	150/144
DePaolo 88, p.14, ln. B'	1.141854	na	0.348416	0.721882	0.241572	na

FINAL DATA TO REPORT:

	142/144	143/144	145/144	146/144	148/144	150/144	150t/144s
Ratios	1.141871	0.512337	0.348413	0.721900	0.241626	0.236478	1.220310
± 2 S.E.	0.000028	0.000008	0.000005	0.000000	0.000010	0.000008	0.000040

Epsilon143 = -5.88 using (143/144)chur = 0.512638
 ± 0.16 (Hamilton et al. 1983)

linked from Sm sheet

[Sm147] = 2.632449 nm/g [Nd144] = 0.72955 nm/g
 ± 0.000956 ± 0.00003

[Sm] = 2.639313 ppm [Nd] = 0.44245 ppm
 ± 0.000958 ± 0.00002

TOT ng Sm = 16.522098 TOT ng Nd = 2.76975808

Sm147/Nd144 = 3.608321
 ± 2 S.E. 0.001321
 ± 2RSE % 0%

Full Sample Name: **9E2 zone1 pwd**
 Date of TIMS analysis: **1/21/2019** Position #: **7**
 estimated Nd load (ng): **2**

Rspike Values Nd {SmNd 1.0 A spike, 6-12-08 calib}						
142/144	143/144	145/144	146/144	148/144	150/144	[Nd150]
0.830433	0.494001	0.436936	0.885201	0.740574	198.371260	0.049114
						nm/g

Wt Sample (g) = **0.005** g
 Wt Spike (g) = **0.07192** g

Mass Spectrometer Information:

Number of cycles measured: **240**
 Number of cycles used: **225**

	start	average (from	
Filament Current range: from	1492	1610	Amps
Beam intensity range: from	0.021	0.1481	Volts 144Nd.160
Temperature range: from	1492	1607	° C

Final Ratio Data:

Interference Values (oxide corrected; informational only... not used in this sheet)

Ce140/Nd144 **0.0610688**
 Pr141/Nd144 **0.0095846**
 Sm149/Nd144 **0.0001428**

for Ratios & %1SE: use grand mean oxygen corr, interference corr, exp normalized values

	142/144	143/144	145/144	146/144	148/144	150/144
Ratios	1.141610	0.5125743	0.34867	0.7219	0.2437951	1.3690329
%StdErr	0.0019342	0.0010442	0.0010306	0	0.00278016	0.0030909

for comparison only	142/144	143/144	145/144	146/144	148/144	150/144
DePaolo 88, p.14, ln. B'	1.141854	na	0.348416	0.721882	0.241572	na

FINAL DATA TO REPORT:

146/144 set to 0.7219

	142/144	143/144	145/144	146/144	148/144	150/144	150t/144s
Ratios	1.141898	0.512344	0.348389	0.721900	0.241559	0.236478	0.872780
± 2 S.E.	0.000044	0.000011	0.000007	0.000000	0.000013	0.000015	0.000054

Epsilon143 = -5.73 using (143/144)chur = 0.512638
 ± 0.21 (Hamilton et al. 1983)

linked from Sm sheet

[Sm147] = 2.285998 nm/g [Nd144] = 0.61658 nm/g
 ± 0.000648 ± 0.00004

[Sm] = 2.291959 ppm [Nd] = 0.37394 ppm
 ± 0.000650 ± 0.00002

TOT ng Sm = 11.459793 TOT ng Nd = 1.86969685

Sm147/Nd144 = 3.707553
 ± 2 S.E. 0.001079
 ± 2RSE % 0%

Full Sample Name: **B8B9E2 zone 2 Gt**
 Date of TIMS analysis: **2/21/2019** Position #: **11**
 estimated Nd load (ng): **3**

Rspike Values Nd {SmNd 1.0 A spike, 6-12-08 calib}

142/144	143/144	145/144	146/144	148/144	150/144	[Nd150]
0.830433	0.494001	0.436936	0.885201	0.740574	198.371260	0.049114
						nm/g

Wt Sample (g)= **0.00625** g
 Wt Spike (g)= **0.0768** g

Mass Spectrometer Information:

Number of cycles measured:	81		
Number of cycles used:	56		
	start	average (from	
Filament Current range: from	3.2	3.2	Amps
Beam intensity range: from	0.327	0.799	Volts 144Nd.160
Temperature range: from	1520	1647	° C

Final Ratio Data:

Interference Values (oxide corrected; informational only... not used in this sheet)

Ce140/Nd144 **0.0239716**
 Pr141/Nd144 **0.0195967**
 Sm149/Nd144 **0.0002357**

for Ratios & %1SE: use grand mean oxygen corr, interference corr, exp normalized values

	142/144	143/144	145/144	146/144	148/144	150/144
Ratios	1.1416849	0.5124667	0.3485872	0.7219	0.24291781	0.9143262
%StdErr	0.0092395	0.0007766	0.0005081	0	0.00154367	0.001546
<i>for comparison only</i>	142/144	143/144	145/144	146/144	148/144	150/144
DePaolo 88, p.14, ln. B'	1.141854	na	0.348416	0.721882	0.241572	na

FINAL DATA TO REPORT:

146/144 set to 0.7219

	142/144	143/144	145/144	146/144	148/144	150/144	150t/144s
Ratios	1.141856	0.512329	0.348419	0.721900	0.241580	0.236478	1.463900
± 2 S.E.	0.000211	0.000008	0.000004	0.000000	0.000007	0.000007	0.000045

Epsilon143= -6.03 using (143/144)chur= 0.512638
 ± 0.16 (Hamilton et al. 1983)

linked from Sm sheet

[Sm147]= 3.151229 nm/g
 ± 0.001358

[Nd144]= 0.88348 nm/g
 ± 0.00004

[Sm]= 3.159445 ppm
 ± 0.001361

[Nd]= 0.53581 ppm
 ± 0.00003

TOT ng Sm= 19.746533

TOT ng Nd= 3.3488007

Sm147/Nd144= 3.566838
 ± 2 S.E. 0.001547
 ± 2RSE % 0%

Full Sample Name: **DE2_zone2_pwd**
 Date of TIMS analysis: **1/21/2019**
 estimated Nd load (ng): **4**

Position #: **8**

Rspike Values Nd {SmNd 1.0 A spike, 6-12-08 calib}

142/144	143/144	145/144	146/144	148/144	150/144	[Nd150]
0.830433	0.494001	0.436936	0.885201	0.740574	198.371260	0.049114
						nm/g

Wt Sample (g)= **0.00525** g
 Wt Spike (g)= **0.0716** g

Mass Spectrometer Information:

Number of cycles measured: **145**
 Number of cycles used: **137**

	start	average (from	
Filament Current range: from	3.47	3.6	Amps
Beam intensity range: from	0.132	0.766	Volts 144Nd.160
Temperature range: from	1531	1620	° C

Final Ratio Data:

Interference Values (oxide corrected; informational only... not used in this sheet)

Ce140/Nd144 **0.0144386**
 Pr141/Nd144 **0.0133888**
 Sm149/Nd144 **3.297E-05**

for Ratios & %ISE: use grand mean oxygen corr, interference corr, exp normalized values

	142/144	143/144	145/144	146/144	148/144	150/144
Ratios	1.1418045	0.5121377	0.3484615	0.7219	0.24195497	0.4405065
%StdErr	0.0008009	0.0005533	0.000532	0	0.00123349	0.001623

<i>for comparison only</i>	142/144	143/144	145/144	146/144	148/144	150/144
DePaolo 88, p.14, ln. B':	1.141854	na	0.348416	0.721882	0.241572	na

FINAL DATA TO REPORT:

146/144 set to 0.7219

	142/144	143/144	145/144	146/144	148/144	150/144	150t/144s
Ratios	1.141856	0.512096	0.348411	0.721900	0.241552	0.236478	4.883103
± 2 S.E.	0.000018	0.000006	0.000004	0.000000	0.000006	0.000008	0.000159

Epsilon143= **-10.57** using (143/144)chur= **0.512638**
 ± **0.11** (Hamilton et al. 1983)

linked from Sm sheet

[Sm147]= 3.274846 nm/g [Nd144]= 3.27080 nm/g
 ± 0.001318 ± 0.00043

[Sm]= 3.283385 ppm [Nd]= 1.98366 ppm

± 0.001322 ± 0.00026

TOT ng Sm= 17.237769 TOT ng Nd= 10.4141902

Sm147/Nd144= **1.001238**
 ± 2 S.E. **0.000424**
 ± 2RSE % **0%**

Full Sample Name: **B8E2 Zone 3 gt**
 Date of TIMS analysis: **2/5/2019**
 estimated Nd load (ng): **4**

Position #: **3**

Rspike Values Nd {SmNd 1.0 A spike, 6-12-08 calib}						
142/144	143/144	145/144	146/144	148/144	150/144	[Nd150]
0.830433	0.494001	0.436936	0.885201	0.740574	198.371260	0.049114
						nm/g

Wt Sample (g)= **0.00827** g
 Wt Spike (g)= **0.10412** g

Mass Spectrometer Information:

Number of cycles measured: **33**
 Number of cycles used: **16**

	start	average (from	
Filament Current range: from	3.55	355	Amps
Beam intensity range: from	0.377	0.384	Volts 144Nd.160
Temperature range: from	1527	1613	° C

Final Ratio Data:

Interference Values (oxide corrected; informational only... not used in this sheet)

Ce140/Nd144 **0.015781**
 Pr141/Nd144 **0.0138339**
 Sm149/Nd144 **0.0004775**

for Ratios & %1SE: use grand mean oxygen corr, interference corr, exp normalized values

	142/144	143/144	145/144	146/144	148/144	150/144
Ratios	1.1416179	0.512480	0.3486155	0.7219	0.24325347	1.1132004
%StdErr	0.0041627	0.0032953	0.0023909	0	0.00538641	0.0094107
for comparison only	142/144	143/144	145/144	146/144	148/144	150/144
DePaolo 88, p.14, ln. B'	1.141854	na	0.348416	0.721882	0.241572	na

FINAL DATA TO REPORT:

146/144 set to 0.7219

	142/144	143/144	145/144	146/144	148/144	150/144	150t/144s
Ratios	1.141969	0.512302	0.348396	0.721900	0.241491	0.236478	1.129921
± 2 S.E. #VALUE!		0.000034	0.000016	0.000000	0.000019	0.000045	0.000213

Epsilon143= -6.56 using (143/144)chur= 0.512638
 ± 0.66 (Hamilton et al. 1983)

linked from Sm sheet

[Sm147]= 2.280892 nm/g [Nd144]= 0.69868 nm/g
 ± 0.000695 ± 0.00013

[Sm]= 2.286839 ppm [Nd]= 0.42373 ppm
 ± 0.000696 ± 0.00008

TOT ng Sm= 18.91216 TOT ng Nd= 3.50428174

Sm147/Nd144= 3.264554
 ± 2 S.E. 0.001173
 ± 2RSE % 0%

Full Sample Name: **B9 Gt Zone3**
 Date of TIMS analysis: **2/5/2019** Position #: **4**
 estimated Nd load (ng): **2**

Rspike Values Nd {SmNd 1.0 A spike, 6-12-08 calib}

142/144	143/144	145/144	146/144	148/144	150/144	[Nd150]
0.830433	0.494001	0.436936	0.885201	0.740574	198.371260	0.049114
						nm/g

Wt Sample (g)= **0.00646** g
 Wt Spike (g)= **0.08167** g

Mass Spectrometer Information:

Number of cycles measured: **141**
 Number of cycles used: **55**

	start	average (from	
Filament Current range: from	3.68	3.68	Amps
Beam intensity range: from	0.076	0.098	Volts 144Nd.160
Temperature range: from	1447	1633	° C

Final Ratio Data:

Interference Values (oxide corrected; informational only... not used in this sheet)

Ce140/Nd144 **0.057636**
 Pr141/Nd144 **0.050096**
 Sm149/Nd144 **0.0002419**

for Ratios & %1SE: use grand mean oxygen corr, interference corr, exp normalized values

	142/144	143/144	145/144	146/144	148/144	150/144
Ratios	1.1412349	0.512858	0.3488973	0.7219	0.24513514	2.048736
%StdErr	0.0046038	0.003649	0.0040822	0	0.007642	0.0120186
<i>for comparison only</i>	142/144	143/144	145/144	146/144	148/144	150/144
DePaolo 88, p.14, ln. B'	1.141854	na	0.348416	0.721882	0.241572	na

FINAL DATA TO REPORT:

146/144 set to 0.7219

	142/144	143/144	145/144	146/144	148/144	150/144	150t/144s
Ratios	1.141697	0.512490	0.348447	0.721900	0.241554	0.236478	0.542275
± 2 S.E.	0.000105	0.000037	0.000028	0.000000	0.000037	0.000057	0.000130

Epsilon143= -2.88 using (143/144)chur= 0.512638
 ± 0.73 (Hamilton et al. 1983)

linked from Sm sheet

[Sm147]= 1.507474 nm/g
 ± 0.000325

[Nd144]= 0.33671 nm/g
 ± 0.00008

[Sm]= 1.511404 ppm
 ± 0.000326

[Nd]= 0.20420 ppm
 ± 0.00005

TOT ng Sm= 9.7636726

TOT ng Nd= 1.31916425

Sm147/Nd144= 4.477093
 ± 2 S.E. **0.001446**
 ± 2RSE % **0%**

D1_core_gt

Full Sample Name: **D1 gt. core**
 Date of TIMS analysis: **2/5/2019**
 estimated Nd load (ng): **2**

Position #: **5**

Rspike Values Nd {SmNd 1.0 A spike, 6-12-08 calib}						
142/144	143/144	145/144	146/144	148/144	150/144	[Nd150]
0.830433	0.494001	0.436936	0.885201	0.740574	198.371260	0.049114 nm/g

Wt Sample (g)= **0.00583** g
 Wt Spike (g)= **0.0453** g

Mass Spectrometer Information:

Number of cycles measured:	100		
Number of cycles used:	92		
	start	average (from	
Filament Current range: from	3.4	3.4	Amps
Beam intensity range: from	0.114	0.0795	Volts 144Nd.160
Temperature range: from	1547	1620	° C

Final Ratio Data:

Interference Values (oxide corrected; informational only... not used in this sheet)
 Ce140/Nd144 **0.0153837**
 Pr141/Nd144 **0.022908**
 Sm149/Nd144 **0.000539**

for Ratios & %1SE: use grand mean oxygen corr, interference corr, exp normalized values

	142/144	143/144	145/144	146/144	148/144	150/144
Ratios	1.1417461	0.5123848	0.3485016	0.7219	0.24232091	0.605345
%StdErr	0.0044385	0.0025947	0.0026732	0	0.00600797	0.007433
<i>for comparison only</i>	142/144	143/144	145/144	146/144	148/144	150/144
DePaolo 88, p.14, ln. B':	1.141854	na	0.348416	0.721882	0.241572	na

FINAL DATA TO REPORT:

	142/144	143/144	145/144	146/144	148/144	150/144	150t/144s
Ratios	1.141839	0.512310	0.348410	0.721900	0.241593	0.236478	2.697189
± 2 S.E.	0.000101	0.000027	0.000019	0.000000	0.000029	0.000035	0.000401

Epsilon143= -6.40 using (143/144)chur= 0.512638
 ± 0.52 (Hamilton et al. 1983)

linked from Sm sheet

[Sm147]= 3.541985 nm/g
 ± 0.002711

[Nd144]= 1.02931 nm/g
 ± 0.00017

[Sm]= 3.551221 ppm
 ± 0.002718

[Nd]= 0.62425 ppm
 ± 0.00010

TOT ng Sm= 20.703617

TOT ng Nd= 3.63937075

Sm147/Nd144= 3.441135
 ± 2 S.E. 0.002694
 ± 2RSE % 0%

Full Sample Name: **D1 core pwd**
 Date of TIMS analysis: **1/20/2019** Position #: **5**
 estimated Nd load (ng): **2**

Rspike Values Nd {SmNd 1.0 A spike, 6-12-08 calib}						
142/144	143/144	145/144	146/144	148/144	150/144	[Nd150]
0.830433	0.494001	0.436936	0.885201	0.740574	198.371260	0.049114
						nm/g

Wt Sample (g)= **0.00387** g
 Wt Spike (g)= **0.0513** g

Mass Spectrometer Information:

Number of cycles measured: **157**
 Number of cycles used: **137**

	start	average (from	
Filament Current range: from	3.45	3.5	Amps
Beam intensity range: from	0.011	0.047	Volts 144Nd.160
Temperature range: from	1533	1687	° C

Final Ratio Data:

Interference Values (oxide corrected; informational only... not used in this sheet)

Ce140/Nd144 **0.130616**
 Pr141/Nd144 **0.0370668**
 Sm149/Nd144 **0.0001534**

for Ratios & %1SE: use grand mean oxygen corr, interference corr, exp normalized values

	142/144	143/144	145/144	146/144	148/144	150/144
Ratios	1.1415218	0.5126533	0.3487262	0.7219	0.24442309	1.7371989
%StdErr	0.0047352	0.0035771	0.0031416	0	0.0078078	0.0091229
for comparison only	142/144	143/144	145/144	146/144	148/144	150/144
DePaolo 88, p.14, ln. B':	1.141854	na	0.348416	0.721882	0.241572	na

FINAL DATA TO REPORT:

146/144 set to 0.7219

	142/144	143/144	145/144	146/144	148/144	150/144	150t/144s
Ratios	1.141905	0.512348	0.348353	0.721900	0.241458	0.236478	0.656597
± 2 S.E.	0.000108	0.000037	0.000022	0.000000	0.000038	0.000043	0.000120

Epsilon143= -5.66 using (143/144)chur= 0.512638
 ± 0.72 (Hamilton et al. 1983)

linked from Sm sheet

[Sm147]= 1.380867 nm/g [Nd144]= 0.42747 nm/g
 ± #VALUE! ± 0.00008

[Sm]= 1.384467 ppm [Nd]= 0.25925 ppm
 ± #VALUE! ± 0.00005

TOT ng Sm= 5.3578879 TOT ng Nd= 1.00330471

Sm147/Nd144= 3.230298
 ± 2 S.E. #VALUE!
 ± 2RSE % #VALUE!

D1_rim_gt

Full Sample Name: **D1 Gt rim**
 Date of TIMS analysis: **2/6/2019** Position #: **6**
 estimated Nd load (ng): **4**

Rspike Values Nd {SmNd 1.0 A spike, 6-12-08 calib}						
142/144	143/144	145/144	146/144	148/144	150/144	[Nd150]
0.830433	0.494001	0.436936	0.885201	0.740574	198.371260	0.049114
						nm/g

Wt Sample (g)= **0.00917** g
 Wt Spike (g)= **0.09447** g

Mass Spectrometer Information:

Number of cycles measured: **192**
 Number of cycles used: **167**

	start	average (from	
Filament Current range: from	3.5	3.64	Amps
Beam intensity range: from	0.063	0.0783	Volts 144Nd.16O
Temperature range: from	1560	1693	° C

Final Ratio Data:

Interference Values (oxide corrected; informational only... not used in this sheet)

Ce140/Nd144 **0.042564**
 Pr141/Nd144 **0.0204076**
 Sm149/Nd144 **0.000403**

for Ratios & %ISE: use grand mean oxygen corr, interference corr, exp normalized values

	142/144	143/144	145/144	146/144	148/144	150/144
Ratios	1.1415791	0.5125671	0.3486738	0.7219	0.2438029	1.3172369
%StdErr	<enter!>	0.0018377	0.0024959	0	0.0065484	0.005345
for comparison only	142/144	143/144	145/144	146/144	148/144	150/144
DePaolo 88, p.14, ln. B'	1.141854	na	0.348416	0.721882	0.241572	na

FINAL DATA TO REPORT:

	142/144	143/144	145/144	146/144	148/144	150/144	150t/144s
Ratios	1.141853	0.512347	0.348406	0.721900	0.241670	0.236478	0.915012
± 2 S.E. #VALUE!		0.000019	0.000017	0.000000	0.000032	0.000025	0.000098

Epsilon143= -5.67 using (143/144)chur= 0.512638
 ± 0.37 (Hamilton et al. 1983)

linked from Sm sheet

[Sm147]= 1.803238 nm/g [Nd144]= 0.46297 nm/g
 ± 0.000530 ± 0.00005

[Sm]= 1.807939 ppm [Nd]= 0.28078 ppm
 ± 0.000531 ± 0.00003

TOT ng Sm= 16.578805 TOT ng Nd= 2.57476492

Sm147/Nd144= **3.894910**
 ± 2 S.E. **0.001221**
 ± 2RSE % **0%**

Full Sample Name: **t. D1 rim pwd**
 Date of TIMS analysis: **1/19/2019**
 estimated Nd load (ng): **2**

Position #: **4**

Rspike Values Nd {SmNd 1.0 A spike, 6-12-08 calib}						
142/144	143/144	145/144	146/144	148/144	150/144	[Nd150]
0.830433	0.494001	0.436936	0.885201	0.740574	198.371260	0.049114
						nm/g

Wt Sample (g)= **0.00434** g
 Wt Spike (g)= **0.05734** g

Mass Spectrometer Information:

Number of cycles measured: **240**
 Number of cycles used: **183**

	start	average (from)	
Filament Current range: from	3.2	3.5	Amps
Beam intensity range: from	0.0403	0.1069	Volts 144Nd.160
Temperature range: from	1553	1667	°C

Final Ratio Data:

Interference Values (oxide corrected; informational only... not used in this sheet)

Ce140/Nd144 **0.0650387**
 Pr141/Nd144 **0.0155016**
 Sm149/Nd144 **0.0001719**

for Ratios & %1SE: use grand mean oxygen corr, interference corr, exp normalized values

	142/144	143/144	145/144	146/144	148/144	150/144
Ratios	1.1416393	0.512530	0.348653	0.7219	0.24334573	1.1441452
%StdErr	0.0022187	0.0016028	0.0016241	0	0.00316999	0.0045106

for comparison only	142/144	143/144	145/144	146/144	148/144	150/144
DePaolo 88, p.14, ln. B':	1.141854	na	0.348416	0.721882	0.241572	na

FINAL DATA TO REPORT:

146/144 set to 0.7219

	142/144	143/144	145/144	146/144	148/144	150/144	150t/144s
Ratios	1.141869	0.512346	0.348428	0.721900	0.241554	0.236478	1.091112
± 2 S.E.	0.000051	0.000016	0.000011	0.000000	0.000015	0.000021	0.000098

Epsilon143= **-5.70** using (143/144)chur= **0.512638**
 ± **0.32** (Hamilton et al. 1983)

linked from Sm sheet

[Sm147]= 2.650602 nm/g [Nd144]= 0.70801 nm/g
 ± 0.000896 ± 0.00007

[Sm]= 2.657514 ppm [Nd]= 0.42939 ppm
 ± 0.000899 ± 0.00004

TOT ng Sm= 11.533609 TOT ng Nd= 1.86356053

Sm147/Nd144= **3.743721**
 ± 2 S.E. **0.001315**
 ± 2RSE % **0%**

Full Sample Name: **B8E2 Zone3 pwd rim**
 Date of TIMS analysis: **1/21/2019** Position #: **<enter!>**
 estimated Nd load (ng): **4**

Rspike Values Nd {SmNd 1.0 A spike, 6-12-08 calib}						
142/144	143/144	145/144	146/144	148/144	150/144	[Nd150]
0.830433	0.494001	0.436936	0.885201	0.740574	198.371260	0.049114

nm/g

Wt Sample (g)= **0.00529** g
 Wt Spike (g)= **0.07151** g

Mass Spectrometer Information:

Number of cycles measured:	133		
Number of cycles used:	117		
		average	
	start	(from	
Filament Current range: from	3.2	3.45	Amps
Beam intensity range: from	0.5	1.019	Volts 144Nd.160
Temperature range: from	1527	1613	° C

Final Ratio Data:

Interference Values (oxide corrected; informational only... not used in this sheet)
 Ce140/Nd144 **0.011936**
 Pr141/Nd144 **0.0193139**
 Sm149/Nd144 **1.847E-05**

for Ratios & %1SE: use grand mean oxygen corr, interference corr, exp normalized values

	142/144	143/144	145/144	146/144	148/144	150/144
Ratios	1.141777	0.512044	0.3484248	0.7219	0.2416981	0.3074947
%StdErr	0.0006505	0.0003739	0.0004041	0	0.00094341	0.0010083
<i>for comparison only</i>	142/144	143/144	145/144	146/144	148/144	150/144
DePaolo 88, p.14, ln. B':	1.141854	na	0.348416	0.721882	0.241572	na

FINAL DATA TO REPORT:							
146/144 set to 0.7219							
	142/144	143/144	145/144	146/144	148/144	150/144	150t/144s
Ratios	1.141795	0.512029	0.348407	0.721900	0.241558	0.236478	14.044743
± 2 S.E.	0.000015	0.000004	0.000003	0.000000	0.000005	0.000005	0.000283
Epsilon143=				-11.87	using (143/144)chur=		
±				0.07	(Hamilton et al. 1983)		
<i>linked from Sm sheet</i>							
[Sm147]=	3.119722 nm/g			[Nd144]=	9.32457 nm/g		
±	0.001224			±	0.00342		
[Sm]=	3.127857 ppm			[Nd]=	5.65512 ppm		
±	0.001228			±	0.00208		
TOT ng Sm=	16.546362			TOT ng Nd=	29.915565		
Sm147/Nd144=				0.334570			
± 2 S.E.				0.000180			
± 2RSE %				0%			